Geometrical Properties of Strip Produced by Plasto-Hydrodynamic Drawing

by

Mark Richard Stokes

A thesis submitted in partial fulfilment of the
requirements of
Sheffield Hallam University
for the degree of Doctor of Philosophy

November 1994

Collaborating Organisation: Davy Mckee Ltd

Acknowledgements

The author gratefully acknowledges the guidance and support given by Professor G.R. Symmons and Dr R. Crampton throughout the course of this work.

The technical assistance offered by Mr R Teasdale and his staff was greatly appreciated and in particular thanks go to Messrs R Wilkinson, M Muldownie, R Sidebottom and R Tingle for their co-operation during the duration of this work.

Declaration

The author declares that no part of this work has been submitted in support of another degree or qualification to this or any other establishment. The author further declares that he has not been a registered candidate or enrolled student for another award of Sheffield Hallam University or professional institution during the course of the research programme.

M R Stokes

Abstract

The Shape Control of Plasto-Hydrodynamically produced Wide Strip

M.R. Stokes

A detailed investigation is carried out for the novel process of Plasto-hydrodynamically produced wide strip. In this process the conventional die is replaced by a pressure head with a rectangular hole. The internal geometry of the hole is shaped such that a convergent fluid flow is produced. This flow causes the production of hydrodynamic forces within the pressure head, namely hydrodynamic pressure and surface shear stresses. These forces are of sufficient magnitude that plastic deformation is induced within the working material.

An in-depth theoretical analysis has been undertaken to establish the relevance of the geometrical parameters of the pressure head for the control of deformation performance. An extensive study of the solution algorithm for this type of plasto-hydrodynamic problem is made and modifications introduced to improve the dynamic response of the model. A new non-Newtonian model of the process has been developed using a power law type constitutive equation for the fluid behaviour. The modifications to the solution algorithm were also included in this new model.

The plasto-hydrodynamic models developed during this work were subjected to numerical optimisation. The non-linear pattern search algorithm was utilised for this purpose. Correlations between the optimum geometrical form for the pressure head and process velocity were established. A study was made of the effect of varying the non-Newtonian parameters and the optimum pressure head geometry.

A Computational Fluid Dynamic (CFD) analysis was made of the Hydrostatic assumption. This assumption allows major simplifications during the derivation of the models of the process. Its validity is established along with the impact of side leakage on the pressure field.

An experimental programme was undertaken to provide data to establish a correlation between the predictions of process performance and an analysis of the output form of the strip produced by the process. The material used for the study was commercially available soft copper strip. The maximum reduction in area produced was 12% approximately.

Contents

Nomenclature

t	Thickness of the strip
W	Width of the strip
L	Land length in pressure head
h	Gap between strip and pressure head land face
V	Velocity
P	Hydrodynamic pressure
$\partial p/\partial x$	Pressure gradient
Pm	Hydrodynamic pressure at the step
τ	Shear stress
σ	direct stress
Q	Volumetric flow rate
X_I	Point of initial yielding
K	i) Power Law consistency constant
	ii) Strain hardening constant
n	i) Power Law consistency index
	ii) Strain hardening index
$\dot{\gamma}$	Shear rate
μ	absolute viscosity
PRA	Percentage Reduction in Area
PRW	Percentage Reduction in Width
PRT	Percentage Reduction in Thickness
m	Aspect ratio of the strip
A	Constant of integration
B	Constant of integration
C	Arbitary constant

η_o	Arbitary constant
R	Residual
T	Temperature
ϕ	Redundant shear strain
G	Hessian matrix
M	Merit function

Superscripts and Subscripts

1	Inlet land
2	Outlet land
3	Edge face of strip
x	Axial direction
y	Direction through strip thickness
z	Direction across strip width
i	i_{th} node
i1	i_{th} + 1 node
y	Yield
yo	Original yield
T	Transposed matrix
ϵ	Plastic strain
sy	yield stress in shear
g	glass transition
*	arbitary point
o	arbitary point

CHAPTER 1

1.0 Introduction

1.1 The Drawing Process

In the drawing process the workpiece is pulled or drawn through a convergent die. The shape of the die at the exit determines the final cross-section of the workpiece be this circular or rectangular. The technique of drawing or rather wire drawing is known to date back to ancient Egypt.

During the drawing process extreme pressure conditions are generated causing metal to metal contact and thus friction and die wear. Effective lubrication is required to reduce the coefficient of friction with its associated reduction in the force and power requirements of the process. Boundary lubrication is the dominant regime in the drawing process.

1.2 Strip Drawing

The work carried out specifically on the drawing of rectangular strip will now be reviewed.

Various experimental and theoretical studies have been made with a plane strain arrangement or assumption. Fukui *et al* (1) used a parallel die and tapered plug arrangement to determine the friction coefficient directly during the strip drawing process. With this apparatus various process variables were examined such as lubricant type, drawing speed, strip material, and surface finish of both the die and work material on the coefficient of friction. The results obtained demonstrated that:

i) Increasing drawing velocity results in a reduction in the coefficient of friction for low viscosity lubricants or poor lubricity,

ii) The surface finish of the die/work material greatly influenced the value of the coefficient of friction, with a decrease observed with increasing roughness of the work material and with smoother die finish.

Lancaster and Rowe (2) studied the effect of lubrication on strip drawing using wedge shaped dies. The study consisted of two distinct parts. Firstly, an evaluation of a soft solid lubricant that could be carried through the die with the work material. It was found that the lubricant film thickness was dependent upon the grade of lubricant, surface roughness of the specimen and the geometrical configuration of the dies. The volume of the lubricant being carried through the dies was found to be strongly dependent on the die angle. Secondly, a comparison of experimentally measured coefficient of friction and drawing stress was made with existing drawing theories (3,4,5).

Kudo *et al* (6) carried out drawing tests with sheets of copper and aluminium to investigate friction and lubrication in the cold forming process. Experiments were performed at velocities ranging from 0.2 to 3000 mm/s using different types of lubricants, with tangential and normal loads at the die/material interface being measured separately. Published results show the dependence of the coefficient of friction on the reduction, velocity and lubricant.

Wilson and Cazeault (7) investigated the effect of various combinations of lubricant, die-angle, reduction and velocity on the friction conditions in strip drawing using a split die arrangement. They concluded from their results that friction was highly sensitive to the die geometry but velocity had little effect.

Rao *et al* (8) investigated the plane-strain strip drawing process using transparent sapphire dies. The use of transparent dies enabled the interface

displacements to be observed directly and the relative velocities determined. A reference collection of experimental data for such parameters as die angle, velocity, back tension, interface friction and interface velocity values was utilised. Interface velocity measurements were used to provide boundary condition information at the tool/workpiece interface. This data was then utilised in various theoretical models, to calculate an accurate value of the coefficient of friction rather than an assumed value. A numerical analysis was then given (9) with the numerical predictions being compared with the experimental data of (8).

The economic viability of industrial processes demands the use of high speed drawing techniques; the attention of researchers had been concentrated on the drawing of various metallic sections at high velocities. To this end Parsons *et al* (10) presented a paper on the feasibility of high speed impact drawing. A theoretical analysis of the process was given, which considered the mechanics of the deformation of the bar and the impact dynamics for the process.

Experimental analysis of the high speed drawing of both rectangular and tubular sections was performed by Baxter (11). A substantial portion of this work related to the drawing of rectangular sections at high velocities through wedge shaped dies. Hydrodynamic lubrication was seen to be present in the process at high velocities and a theoretical expression was developed to evaluate the film thickness in the presence of such a regime.

Extended experiments were made by Devenpeck and Rigo (12), using an apparatus which essentially was a combination of a laboratory rolling mill and a custom die-block. Test lengths of 1.5 km were produced. The material used was tin plated steel strip. Various lubricants were used to study the effect of different parameters such as velocity, reduction, cumulative length of strip on the coefficient

of friction and wear.

1.3 Hydrodynamic Lubrication in Deformation Processes

The wear problems created as a consequence of boundary lubrication present in the drawing process stimulated various researchers to consider the possibility of promoting full fluid film lubrication (FFFL) as the optimum solution to the reduction of friction and wear within the die.

Christopherson and Naylor (13) performed one of the initial studies in the promotion of FFFL but with respect to wire drawing. A pressure tube was mounted on the input side of the die; which was characterised by two properties. Firstly, the clearance between the wire and the internal bore of the tube was small so as to maximise the hydrodynamic processes. Secondly, the tube was long allowing the build-up of large pressures prior to the die which provides the convergent flow required for hydrodynamics. Oil was the drawing lubricant. Experimental results demonstrated that hydrodynamic conditions were generated in the die under the imposed conditions. A theoretical analysis, assuming isothermal conditions, of the pressure tube was given. This analysis was developed further with the introduction of a deformation zone, by Tattersal (14) and by Osterle and Dixon (15).

Cheng (16) performed a plasto-hydrodynamic analysis of strip rolling incorporating thermal, plasticity and lubricant derived phenomena.

Bedi (17) produced an analysis assuming total hydrodynamic lubrication for the drawing of wire through a conical die, from which the hydrodynamic film thickness and coefficient of friction could be evaluated.

An elasto-plasto-hydrodynamic analysis was presented by Bloor *et al* (18)

for the lubrication of strip drawing through wedge shaped dies, with the process phenomena being analysed both on entry and exit of the die. It was concluded from this analysis that the film thicknesses calculated could be sustained by the drawing process.

As a continuation of the work presented by Bloor *et al* (18), Dowson *et al* (19) using modified geometry presented an elasto-plasto-hydrodynamic analysis of the lubrication in the wire drawing process.

An experimental programme of high speed drawing tests was carried out by Lancaster (20) to determine the possibility of establishing hydrodynamic lubrication using conventional dies as opposed to pressure tubes or compound dies. The experiments were performed using aluminium (hard and soft) and low carbon steel bars with drawing speeds up to 30 m/s. The drawing lubricants used were Polyglycols and Lanoline. The results obtained indicated that a high drawing velocity alone is insufficient for the development of hydrodynamic films. However, hydrodynamic films can be generated but are dependent upon the lubricant, the material properties and die angle.

Avitzur (21) subsequently discussed and specified the required conditions to maintain separation between the die and workpiece.

Kudo *et al* (22) performed an experimental study on cold sheet drawing through wedge shaped dies to investigate plasto-hydrodynamic lubrication in forming processes. The average coefficient of friction, the lubricant film thickness and interface temperatures were calculated from a thermal rigid-plasto-hydrodynamic analysis of the process.

Various research workers (Wilson and Mahdavian (23), Dow *et al* (24), Mahdavian and Wilson (25)) have presented theoretical analyses for the

hydrodynamic lubrication of rolling and drawing through conventional dies including thermal effects.

1.4 The Development of Plasto-hydrodynamic Die-less Drawing

For FFFL to be the dominant regime in the drawing process the lubricant must exhibit the following viscosity characteristics:

i) the fluid viscosity should provide for laminar flow within any entry pressure tube,

ii) adhesion of the lubricant to the work material should be maintained at all times.

The requirement for the above characteristics has led recently to the testing of alternative lubricants to those currently in use. Symmons *et al* (26,27) introduced the use of polymer melts during drawing as a lubricating agent. Small scale testing of the coating properties of polymer melts when used in the application has also been performed.

The lubricant properties of polymer melts was studied by Crampton (28) by varying the following process variables: polymer melt temperature, drawing velocity and wire material. The system used for the study was essentially the same as the apparatus of Christopherson, with the exception that the lubricating agent was a polymer melt. Various analytical solutions (29,30) were presented for the process in this form; they accounted for the physical phenomena of non-Newtonian flow characteristics, strain hardening and strain rate sensitivity of the work material. The experimental results of (28) demonstrated that plastic deformation of the wire had occurred in the pressure tube prior to the die. Therefore, the function of the die was reduced to acting as a seal. Furthermore, it was postulated that the die could

be replaced with a conical unit in which the smallest bore size would be larger than the entry wire diameter and when used in conjunction with a polymer melt permanent deformation would be achieved. Hashmi, Symmons and Parvinmehr (31-33) then used a unit with a stepped bore such that the smallest bore size was larger than the entry diameter of the wire, which produced a reduction in the wire diameter. From these findings an innovative metal forming process was investigated and patented as 'Plasto-hydrodynamic Die-less drawing'.

In this process the working medium is pulled through a melt chamber containing polymer melt then into the stepped bore reduction unit. The stepped bore reduction unit is so constructed that the smallest bore is larger than the entry size of the working medium and also the larger of the two bore sizes which produce the step is placed on the entry side of the unit. The adherence of the polymer to the surface of the working material draws the polymer into the reduction unit, hence filling the clearances between the stepped bore and the working material. The convergent flow so created gives rise to hydrodynamically generated pressures and shear stresses. The shear stresses induce a cumulative back stress in the working medium as it moves along the reduction unit. At some point the combination of the back stress and the applied hydrodynamic pressure exceeds the yield stress of the material, and deformation begins. The benefit of this arrangement is that die wear is completely eliminated as no metal to metal contact takes place. Various analytical and numerical solutions for the process have been presented:

i) Hashmi and Symmons (34-35) for a solid continuum through a conical orifice filled with a viscous fluid,

ii) Parvinmehr *et al* (36) produced a non-Newtonian analysis for the process including strain hardening, strain rate sensitivity of the work

material and a limiting or critical shear stress for the viscous medium,

iii) the process was extended to tube sinking by Panwher *et al* (37) with positive results, an analytical solution for this implementation assuming a Newtonian fluid was presented. Later the analysis was modified to include non-Newtonian fluid characteristics (Panwher (38)).

Other non-linear effects in the fluid behaviour are the sensitivity to pressure and temperature. Symmons *et al* (39-41) presented various analyses for die-less wire drawing including these phenomena, the objective of which was to isolate the effect of temperature and pressure on the fluid and thus the performance of the process as a whole.

The process was then applied to the reduction of rectangular strip by Memon (42). The configuration of the stepped bore was modified to that of a stepped slot; only the width faces of the unit were stepped, the gaps on the edge faces being set to a similar magnitude as that of the width face gaps. The assumption required for this configuration is that the hydrodynamically produced pressure is propagated equally around the cross section at any point.

Memon (42) performed an in-depth study of this new application of the concept: his objectives were:

i) to assess the effects of the reduction unit geometry on the pressure distribution, drawing stress and the overall drawing performance,

ii) to assess the effects of drawing velocity and polymer melt temperature on the overall drawing performance,

iii) to develop a mathematical model for the prediction of various parameters involved in the process such as pressure distribution,

initiation of yielding, product size and the drawing stress,

iv) to examine the correlation between experimental and theoretical results,

v) to assess the feasibility of the process in comparison with the conventional process.

The process proved to be successful in this application, with percentage reductions in area in the order of 20%. The modelling of the process was reported by Symmons *et al* (43-45). During this period various reports have been made on the continuing development of the process for wire drawing and coating - Symmons *et al* (46-47), Hashmi *et al* (48) and Panhwar *et al* (49).

1.5 The Aim and Objectives of the Current Investigation

The aim of the investigation is to determine and assess the deformed shape and reduction of rectangular wide strip using a plasto-hydrodynamic drawing process. Deformed shape is defined as:

'the distribution of thickness across the width face of the strip and the overall reduction in sectional area'.

Furthermore the term 'Shape control' in the context of this work shall be defined as:

'the accurate prediction of the reduction in cross-sectional area'.

To achieve the stated aim the following objectives have been identified:

i) to analyse the system and produce a predictive mathematical model, taking into account the relevant physical phenomena,

ii) to examine in detail all major assumptions in the analysis and their validity,

iii) to develop the ability to optimise the internal geometry of the stepped bore reduction unit for a specified process velocity as a necessary precursor to an economic viability analysis of the process,

iv) to perform experimental trials of a stepped bore reduction unit using material of an aspect ratio larger than previously used (ie 16:1),

v) to establish the deformed shape of the material produced by the process and compare this with that of the feed stock supplied to the process,

vi) to compare experimental results with the predictions of the numerical model.

CHAPTER 2

2.0 Properties of Experimental Materials

2.1 Rheology of Polymer Melts

The Newtonian fluids familiar to engineering practitioners will be seen to be merely one of many different types of possible fluid behaviour. The working fluid for this study is a polymer melt, which exhibits non-Newtonian flow characteristics. When a polymer flows, molecules of the melt are subjected to a sliding or shearing action. The resistance to this flow is dependent upon the forces or entanglements present at the molecular level and the flexibility inherent in the molecular chains of the polymer. The magnitude of these phenomena may be altered by various environmental factors and the initial choice of polymer which specifies the form of the molecular chain. A brief outline of the established theory for these factors is now given.

2.1.1 Fluid Classification

Fluids may be separated into two main groups:

i) Time-independent fluids, in which the shear rate (s^{-1}) is an arbitrary function of the applied shear stress.

ii) Time-dependent fluids, in which the shear rate / shear stress function is dependent upon its shear history.

These groups are considered separately below.

2.1.1.1 Time-independent Fluids

The shear rate / shear strain relationship for time independent fluids is given below for the general case.

$$\dot{\gamma} = f(\tau) \qquad (2.1)$$

Various flow curves are possible, but four standard forms are defined in rheology texts. These are:

i) Newtonian fluids; where the shear strain / shear stress relationship is a constant; this is the simplest of all possible relationships,

ii) Pseudoplastic fluids; where the shear rate increases at a more than linear rate with an increase in shear stress; sometimes referred to as shear thinning,

iii) Dilatant fluids; are the opposite of pseudoplastic, where the shear rate increases at a less than linear rate with an increase in shear stress sometimes referred to as shear thickening, and

iv) Bingham body; a highly idealised material where it is assumed that a distinct yield stress is observed after which a constant ratio of shear rate / shear stress (ie.Newtonian) is observed.

These basic forms are given graphically in Figure 2.1. Various oils, emulsions, suspensions, slurries and pastes can exhibit any one or other of the characteristics given above, however, the majority of polymer melts are pseudoplastic in their behaviour.

2.1.1.2 Time-dependent Fluids

There are various materials whose viscosity changes with both the rate and time of shearing. This may be a reversible process in that the viscosity will recover to its initial state if left for a sufficiently long time. Some material processes,

for example the mastication of rubber, cause irreversible changes due to modification of the molecular structure. Fluids which exhibit this decrease in shear stress with the duration of an applied constant shear strain rate are classified as Thixotropic. A more strict definition is sometimes used where the change must also be reversible. The opposite of Thixotropic behaviour is negative thixotropy or Rheopectic behaviour, where at any given shear rate the shear stress increases and reaches an asymptotic maximum value. The time dependent nature of the fluid viscosity can be demonstrated by the use of a rotary viscometer, in which the fluid is cycled from rest to some maximum shear rate and returned to rest. A plot of shear stress against shear rate then reveals a hysteresis loop, the direction of which specifies thixotropic or rheopectic behaviour, as shown in Figure 2.2.

2.1.2 Shear Rate Dependent Fluid Behaviour

2.1.2.1 Pseudoplastic Behaviour

Pseudoplastic properties may result from a number of phenomena. Two of the most significant are thought to be:

i) Asymmetric particles or molecules are randomly oriented and/or extremely entangled initially. Under shear motion the particles (or molecules) are oriented and points of entanglement are reduced. At extreme shear rates the orientation may become total and at this point the fluid behaviour may become near-Newtonian.

ii) Extremely solvated particles / molecules may be present in the fluid. Given an increase in the shear rate, solvated layers could be sheared away causing the effective size of the particles / molecules

to be reduced, resulting in decreased interaction of the particles / molecules and a consequent reduction in apparent viscosity.

A variety of mathematical models have been proposed in order to describe the behaviour of pseudoplastic materials. They have been derived from consideration of molecular structure, of differing levels of complexity, or are of a completely empirical basis. Skelland (50) reviewed these equations, concluding that the mathematics involved in obtaining a solution for anything other than the most simple of problems in most cases did not justify the effort involved. The equation which has obtained a measure of success in real applications is the power law equation. The form of this equation is given below.

$$\tau = K(\dot{\gamma})^n \qquad (2.2)$$

2.1.2.2 Dilatant Behaviour

The inverse of pseudoplastic behaviour is dilatant behaviour. Materials with dilatant characteristics demonstrate an increase in viscosity with increasing shear rate. A classical definition of dilatancy is that of increasing volume with increasing shear rate, but the former definition is now the most commonly used. Dilatant characteristics are commonly demonstrated by highly concentrated suspensions, in particular PVC pastes. The most successful model used for dilatant behaviour is also the power law equation (Equation 2.2) as stated previously. It is the value of n, the power law index, which determines which type of behaviour is modelled. Dilatant behaviour is produced with an index greater than one. A power law index of one is equivalent to Newtonian flow

characteristics. Power law indices less than one produce pseudoplastic characteristics.

An overall view of the fluid classification structure discussed in this and the previous sections, is given in Figure 2.3.

2.1.3 Temperature Dependent Fluid Behaviour

The dependence of viscosity upon temperature is widely known. For Newtonian fluids it is well established that the viscosity temperature relationship may be described by an Arrhenius equation of the form:-

$$\mu = Ae^{E/RT} \tag{2.3}$$

where A is a constant, E is the activation energy, R is the universal gas constant and T is temperature. It has already been stated that polymer melts are pseudoplastic in nature; to account for variations found from Equation 2.3 a second empirical equation is often used:-

$$\mu = ae^{-bT} \tag{2.4}$$

where both a and b are constants. In practice plots of log μ against log T for experimental data are curved rather than linear in form. Various attempts have been made to obtain a fundamental explanation for the differences in the temperature / viscosity relationship between different polymers, the most successful of which is the 'free volume theory'. The free volume theory suggests that at some critical temperature T_o (approximately 52°C below the measured glass transition temperature T_g) there is no 'free volume' between the molecules.

The free volume is postulated to increase linearly with temperature such that at the T_g the free volume has a value f_g. The expansion coefficient α_f is defined by the expression below.

$$f = f_g + \alpha_f(T - T_g) \tag{2.5}$$

It has been postulated that f_g has a constant or universal value of 0.025 and α_f has a constant or universal value of 0.48.

Williams, Landel and Ferry (51) proposed from Equation 2.4 that the viscosity μ of a melt at some temperature T can be related to that at an arbitrary temperature T_a by the equation.

$$\log\frac{\mu}{\mu_a} = -\frac{C_1^a(T - T_a)}{C_2^a + T - T_a} \tag{2.6}$$

Substitution of T_g for the arbitrary reference temperature yields

$$\log\frac{\mu}{\mu_g} = -\frac{C_1^g(T - T_g)}{C_2^g + T - T_g} \tag{2.7}$$

where,

$$C_1^g = \frac{1}{2.303 f_g} = 17.44 \tag{2.8}$$

and

$$C_1^g = \frac{1}{2.303 C_1^g \alpha_f} = 51.6 \qquad (2.9)$$

have been postulated as universal constants. These equations are generally known as the WLF (Williams, Landel & Ferry) equations. Small deviations from these equations can be found for various polymer melts. However, experimental values for the constants which would yield more accurate results can be determined for a particular polymer.

2.1.4 Pressure Sensitivity of Polymer Flow

A capillary rheometer consists of a melt chamber with a capillary fixed in one end. A piston is used to force the polymer melt from the chamber. The accurate measurement of the pressure generated in the melt chamber due to the capillary, coupled with the flow rate calculated from the piston speed, enables the shear rate and shear stress to be computed, hence forming the characteristic flow curve of the polymer melt. The fundamental basis upon which this type of rheometer relies is the pressure difference created across the length of the capillary. The question as to whether or not the absolute pressure at which this difference occurs has an influence on the melt viscosity, will now be addressed.

The WLF equations discussed previously make use of the free volume surrounding a molecule as a dependent variable in the relationship of viscosity and temperature. Since an increase in pressure will decrease the distance between particles or molecules (and hence free volume) it might be expected that an increase in pressure will lead to a corresponding increase in viscosity. Westover (52) performed the first investigation in this area using a double piston rheometer.

With this apparatus it is possible to establish flow environments such as those shown schematically in Figure 2.4 (it should be noted that only the first case may be developed with a conventional rheometer). It was found in the case of polystyrene that increasing the pressure from 13.7 MPa to 172 MPa raised the apparent viscosity of the melt by 2 orders of magnitude.

Capillary based techniques suffer from the disadvantage that the applied shear stress is calculated from the force applied to cause the pressure difference which will be effected by the presence of friction between the moving parts, hence producing an unavoidable source of error. Semjonov (53) originally, and later Cogswell (54), used a pressurised Couette-Hatschek viscometer which does not suffer from this problem. With this type of apparatus inner and outer concentric cylinders are used, and the void between them is filled with polymer melt at a controlled pressure. The inner cylinder is held stationary while the outer is rotated thus shearing the melt. The torque induced on the inner cylinder due to viscous drag is then measured and interpreted as a shear stress.

Cogswell's (54) results demonstrated that the flow curves for a given melt at varying temperature and pressures were superimposable by a shift at constant stress. A reasonable approximation is possible if it is assumed that the change in $\log(\mu)$ is linearly proportional to the temperature or pressure change. It then follows that the effect of temperature on viscosity could be equated to the effect of pressure on viscosity through a coefficient $-(\Delta T/\Delta P)_{\mu}$. The value of this constant was found to be reasonably constant with polymer type, given in Table 2.1. It may also be concluded that a polymer which is sensitive to changes in temperature will also be sensitive to changes in pressure.

Table 2.1 - Temperature-Pressure coefficients at constant viscosity, entropy and volume ($^{\circ}C/Nm^{-2}$); after Cogswell (54)

Polymer	$-(\Delta t/\Delta p)_{\mu} \times 10^{-7}$	$(\Delta t/\Delta p)_S \times 10^{-7}$	$(\Delta t/\Delta p)_V \times 10^{-7}$
PVC	3.1	1.1	16
Nylon 66	3.2	1.2	11
Poly(methyl methacrylate)	3.3	1.2	13
Polystyrene	4.0	1.5	13
Polyethylene (high-density)	4.2	1.5	13
Acetal copolymer	5.1	1.4	14
Polyethylene (low density)	5.3	1.6	16
Silicone polymer	6.7	1.9	9
Polypropylene	8.6	2.2	19

2.2 The Working Fluid

A proprietary grade of Nylon 12 was used as the working fluid throughout the duration of this project. The precise grade was Grilamid L25 which is manufactured by EMS-CHEMIE AG and supplied by EMS-GRILON Ltd, their British subsidiary. Grilamid L25 is an extrusion grade polymer; a typical application is the extrusion of rigid tubes. Its flow data was supplied by the manufacturers in the form of flow curves for the polymer at three different temperatures, see Figure 2.5. This grade of polymer was selected based on two important properties after consultation with the manufacturers. Firstly, due to its tolerance of extreme shear conditions. No quantifiable data was available as a basis for this decision. A qualitative appraisal was made, based on the experience of the company in high shear applications. Secondly, the high viscosity of the fluid in the projected operational shear rate range (3000-5000 s^{-1}) on the apparatus.

2.3 Strain Hardening Characteristics of the Strip Material

The stress-strain characteristics of the strip material were investigated by performing a number of uniaxial tensile tests. The test samples were fitted with post yield strain gauges for use into the plastic strain range. The resultant stress-strain data was fitted to a 'power law' type expression to describe the material behaviour, as given below.

$$\sigma_y = \sigma_{yo} + K\varepsilon^n \qquad (2.10)$$

where,

σ_{yo} = initial yield stress
K = strain hardening constant
n = strain hardening index

Three batches of material were used during the tests, the values obtained for each batch are given below,

Material 1

σ_{yo} = 74.58 MPa
K = 585.215 MPa
n = 0.659983

Material 2

σ_{yo} = 88.49 MPa
K = 497.262 MPa
n = 0.595859

Material 3

σ_{yo} = 72.1749 MPa
K = 702.21 MPa
n = 0.713081

The true stress / true plastic strain curves for this data in given in Figures 2.6, 2.7 and 2.8 respectively.

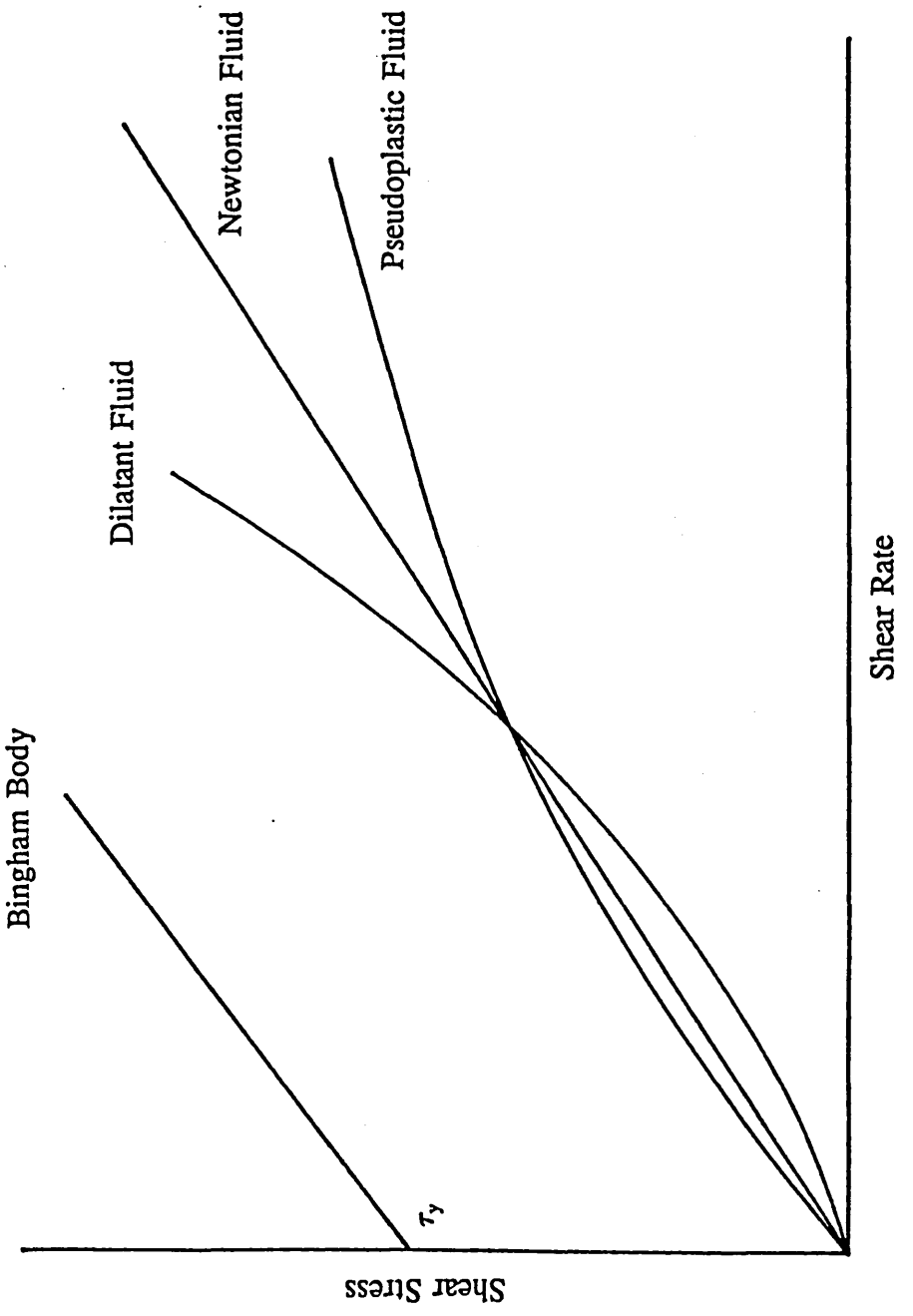

Figure 2.1 - Shear Stress / Shear Rate curves for the four standard Rheological forms

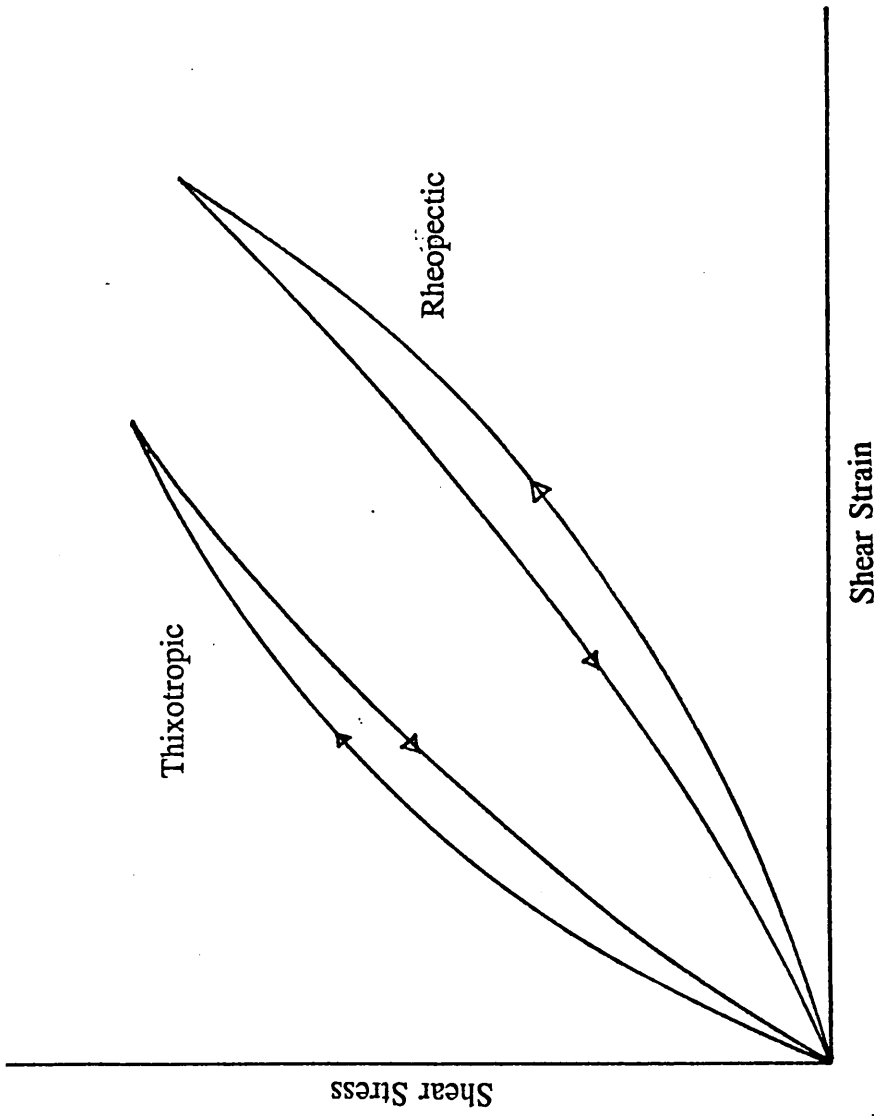

Figure 2.2 - Thixotropic and Rheopetic hysteresis loops

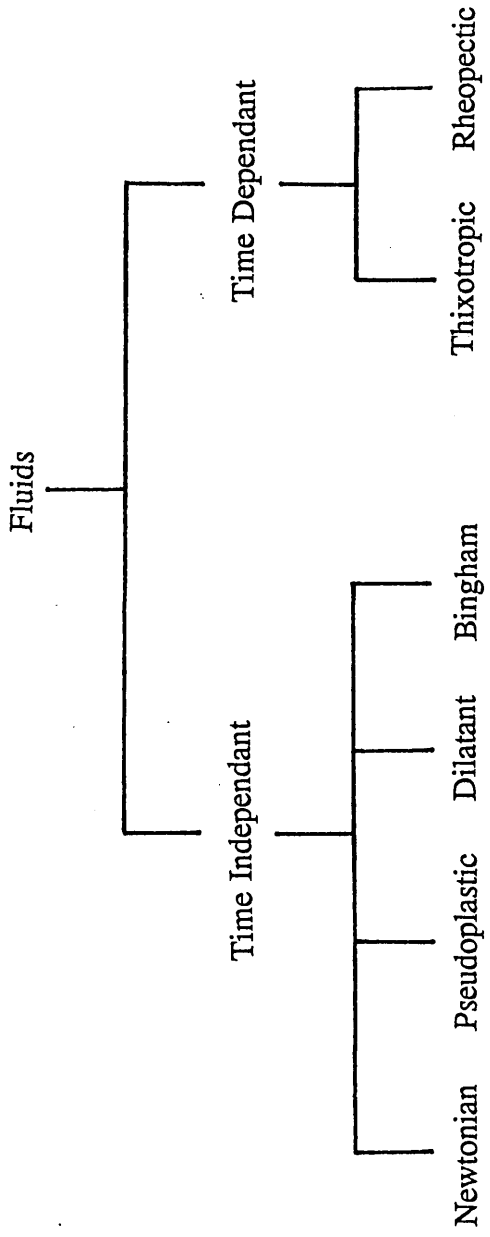

Figure 2.3 - Schematic of possible fluid classifications

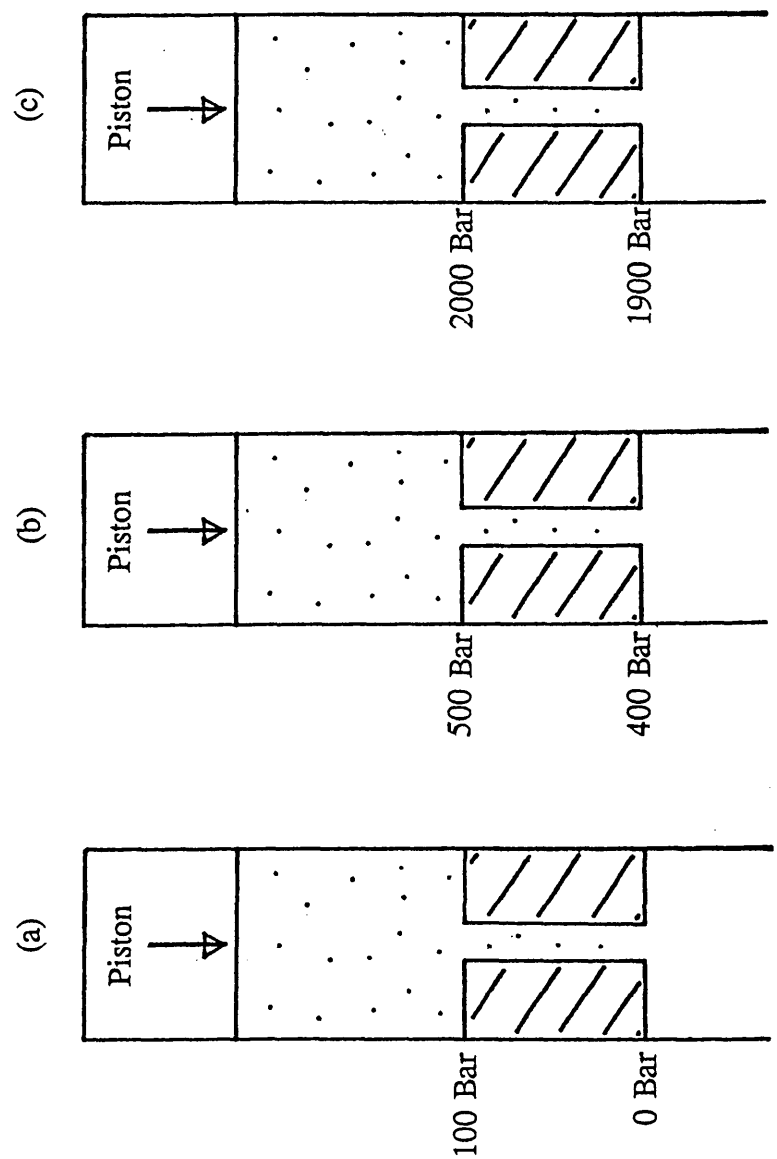

Figure 2.4 - Equivalent pressure drops at various absolute pressures

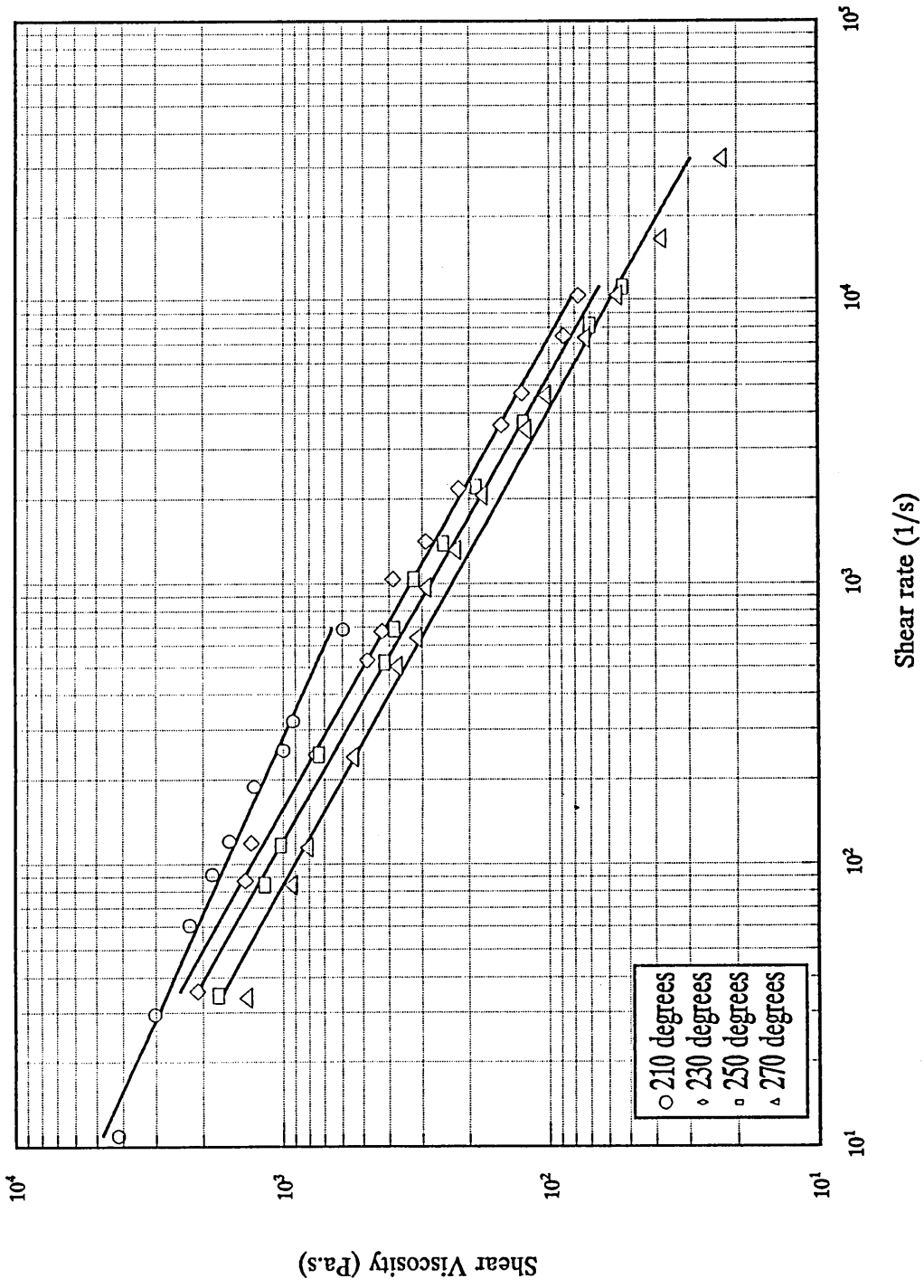

Figure 2.5 - Viscosity / Shear rate curves for Grilamid L25

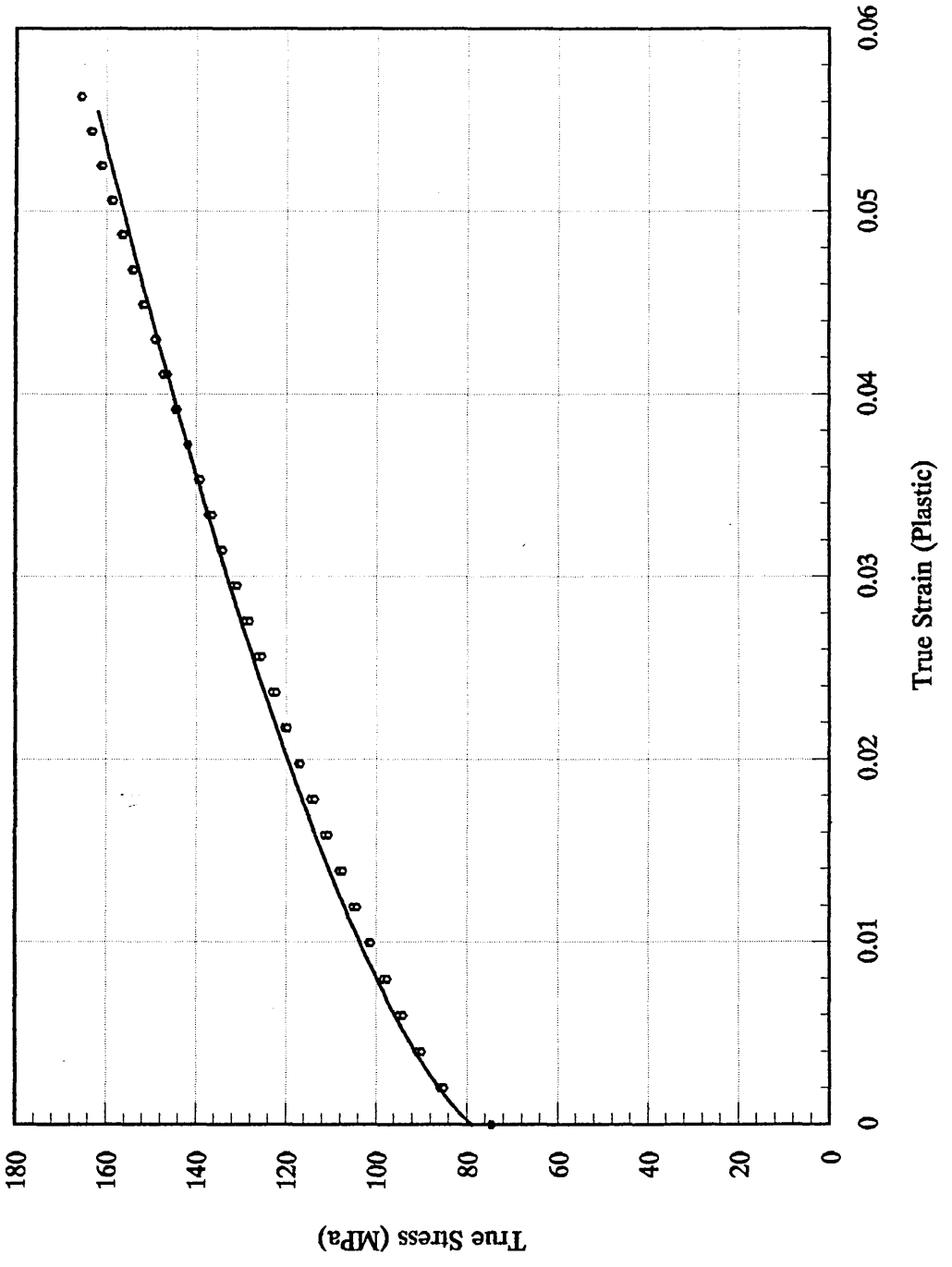

Figure 2.6 - The yield characteristics of the copper strip (batch 1)

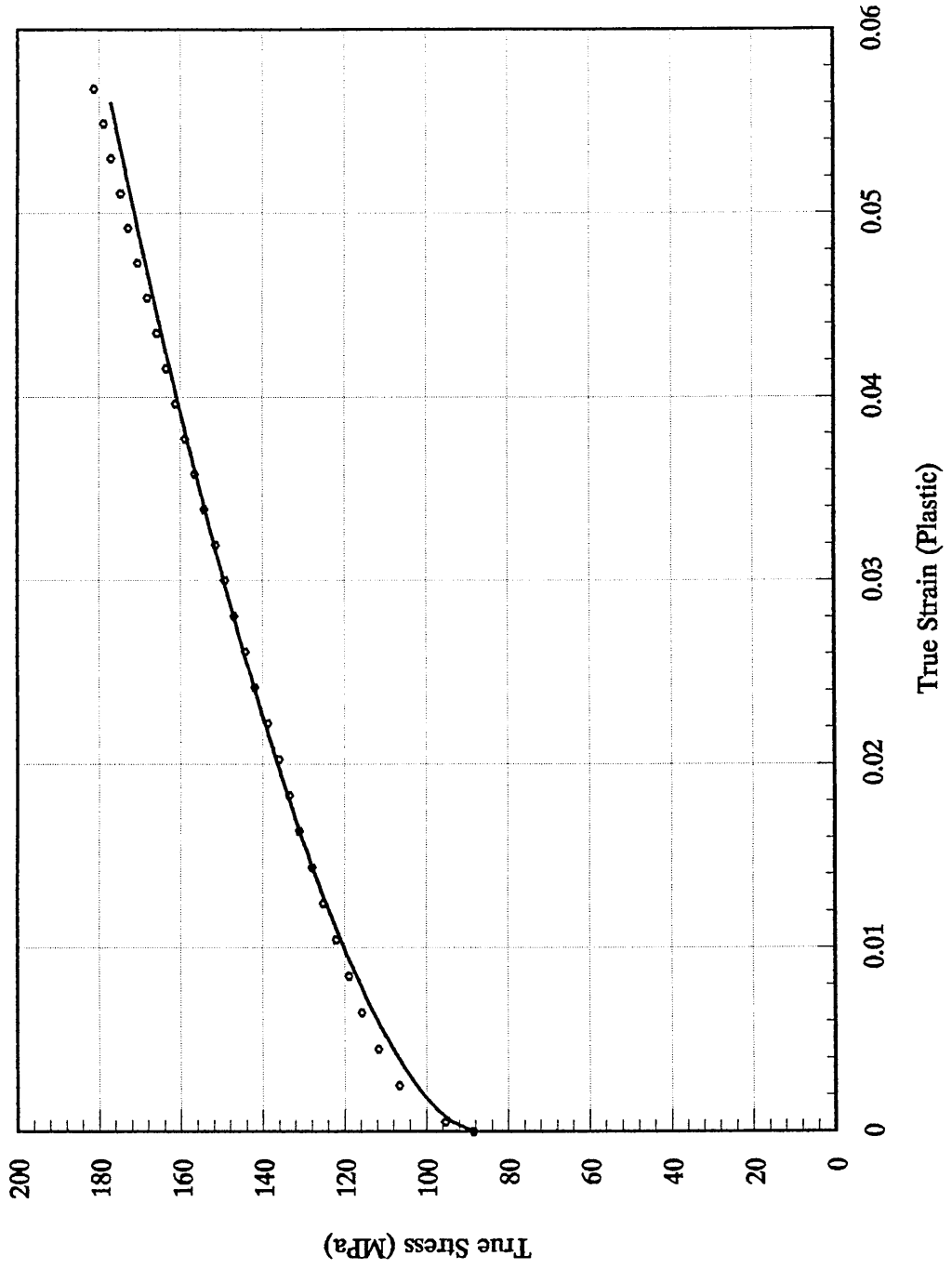

Figure 2.7 - The yield characteristics of the copper strip (batch 2)

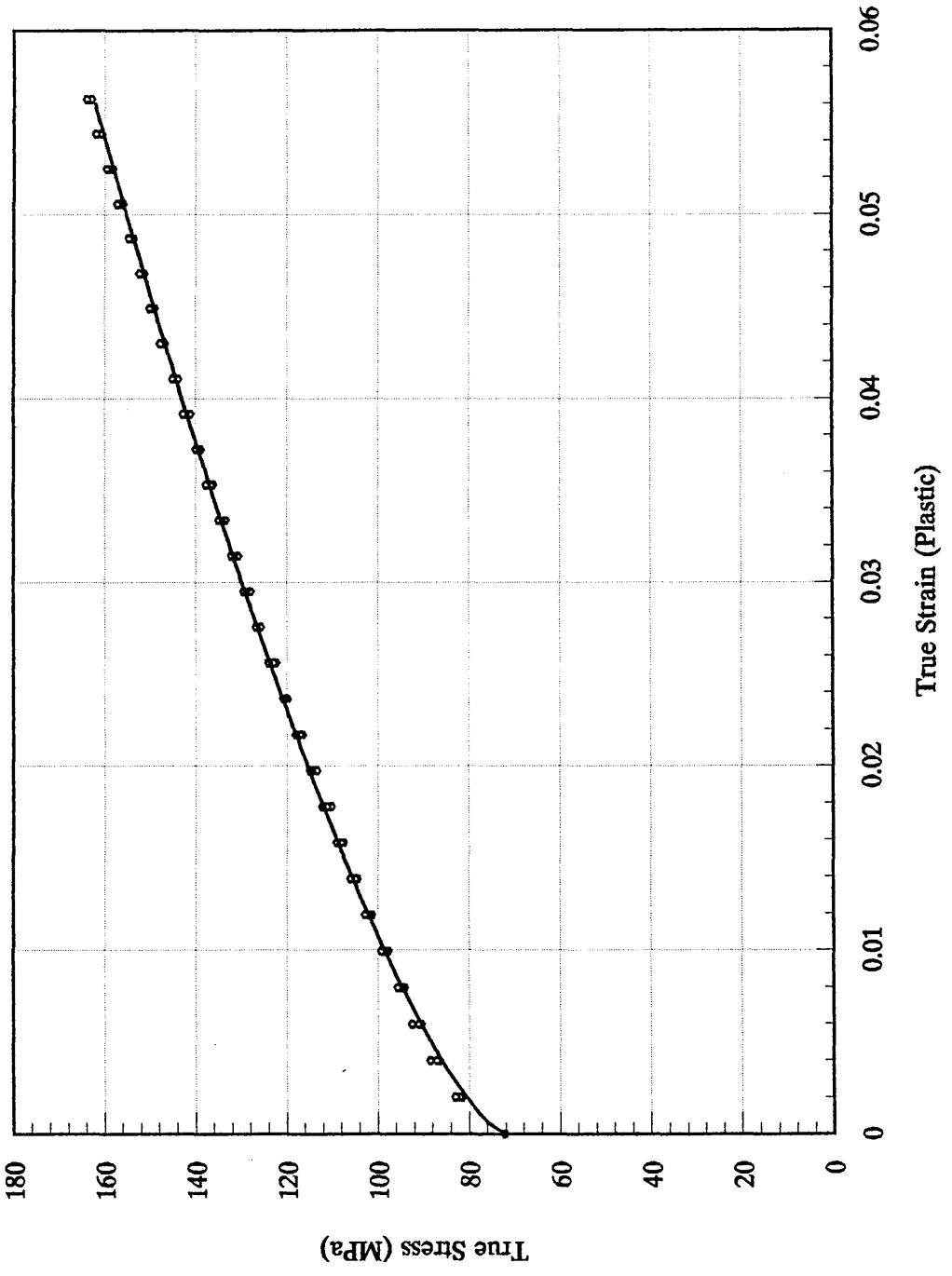

Figure 2.8 - The yield characteristics of the copper strip (batch 3)

CHAPTER 3

3.0 Experimental test apparatus design specification

3.1 General description

Previous work by Memon (42) on hydrodynamic strip drawing was mainly at an aspect ratio of 8:1 (width/thickness : 12.7mm/1.59mm). With this in mind the aspect ratio range of the apparatus for the current body of work was set at 32-16:1.

The prime mover is a Marshall Richards Barco chain driven draw bench with a stated load capacity of 40 kN. This is fitted with a variable speed transmission with a velocity range of 0.1 to 0.5 m/s. A rail guided unit fitted with a dog clamp is drawn over the bench length by a spring loaded hook. The hook is disengaged from the chain drive at the end of the draw stroke by two ramps lifting the hook from the chain. The plasto-hydrodynamic pressure unit is mounted at the head of the draw bench. Only the draw bench has been utilised from the previous work performed by Memon (42); a completely new pressure head, meltpot and preheat system has been built for the present investigation.

3.2 Plasto-hydrodynamic pressure head

The apparatus consists of a pressure head in which the shaped orifice required by the process is formed. At the entrance to the pressure head is a polymer melt reservoir, through which the strip passes. Prior to the reservoir is a 5 roll straightener; this is to ensure that the material enters the pressure head with an acceptable degree of flatness. This assembly is then mounted on the draw bench. Plates 3.1 - 3.2 give different views of the assembled experimental apparatus.

3.1.1 Description of the Pressure Head

The pressure head consists of 6 pieces; a top and bottom plate, 2 shaped pressure inserts and 2 spacers, as shown in Figure 3.1. The loads imposed upon the pressure head are the hydrodynamic pressures and shear stresses generated by the process itself. In the x-direction, the internal forces are carried in double shear by the step in the top and bottom plates. In the y-direction, the top and bottom plates are held together with 6 retaining bolts. The shear loads, which would tend to pull the pressure inserts out of the pressure head in the z-direction, are countered by an exit plate secured to the top and bottom plates. A standard pressure vessel design factor of 3 has been used throughout the calculations for the pressure head.

Sealing of the pressure head is achieved by the steps into the top and bottom plates, the steps being precision ground to a transition fit, which together with the step acting as a mechanical labyrinth seal, provides sufficient sealing with such viscous fluids as polymer melts.

Heat is supplied by 3 electrical strip heaters totalling 2.625 kW of power. This is sufficient to bring the pressure head from ambient temperature to 250° centigrade in approximately 30 mins. The heaters are controlled by a Eurotherm Type 91 PID (proportional, integral, derivative) controller. This particular unit allows the terms of the controller algorithm to be tailored to a specific application.

Thermal insulation is provided by an enclosure utilising Kaowool ceramic fibre board. This material is rated at 0.07 W/m$^{\circ}$K.

3.1.2 Polymer melt reservoir

The polymer melt reservoir consists of a cylindrical body section and an upright feed hopper. Both the cylindrical body and hopper section are heated with electrical barrel heaters, which are controlled using Eurotherm Type 91 PID controllers. The capacity is sufficient for short experimental runs with the facility via the hopper for replenishment if required. This reduces the risk of polymer degradation due to insufficient throughput which could lead to oxidation of the polymer. The melt is further protected by the provision of an inert gas blanket; it is possible to pressurise the gas blanket to 6 bar to overcome any possible supply problems. Argon is the inert media used for the gas blanket. Meltpot details are given in Figure 3.2.

3.1.3 Five roll strip leveller

The material used for the experimental programme is procured in 100 kg coils. These coils are then rewound on to a small feed reel for use on the experimental apparatus. This leaves the feed stock with an initial curvature and in some sections a degree of twisting. The hydro-dynamic process requires great dimensional accuracy and, whilst the process will smooth or flatten some distortion in the material, by its very nature it will not remove gross distortion. To this end a 5 roll leveller is fitted prior to the melt pot.

The leveller consists of five staggered rolls mounted in a carrier block. The carrier blocks set the spacing of the rolls, being sandwiched together in a stack. The stack of carriers is then mounted in the roller box, and the roller box is then mounted on the apparatus base plate, prior to the meltpot. Engineering drawings of the assembly are given in Figures 3.3 and 3.4. Plate 3.3 shows the

assembled leveller with copper strip in place. Figure 3.5 gives an assembly drawing of the apparatus.

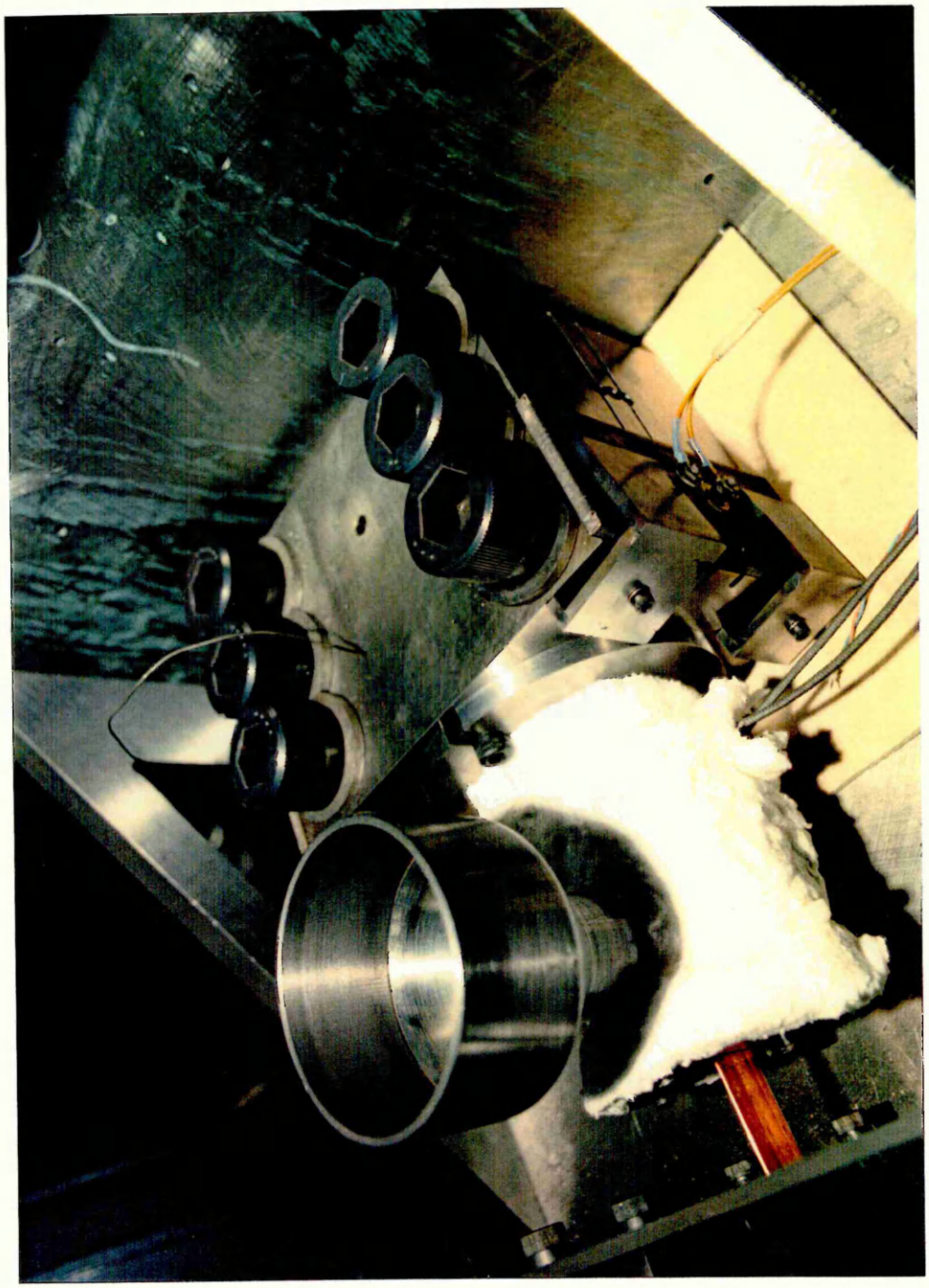

Plate 3.1 - Mounting details of the pressure head and meltpot.

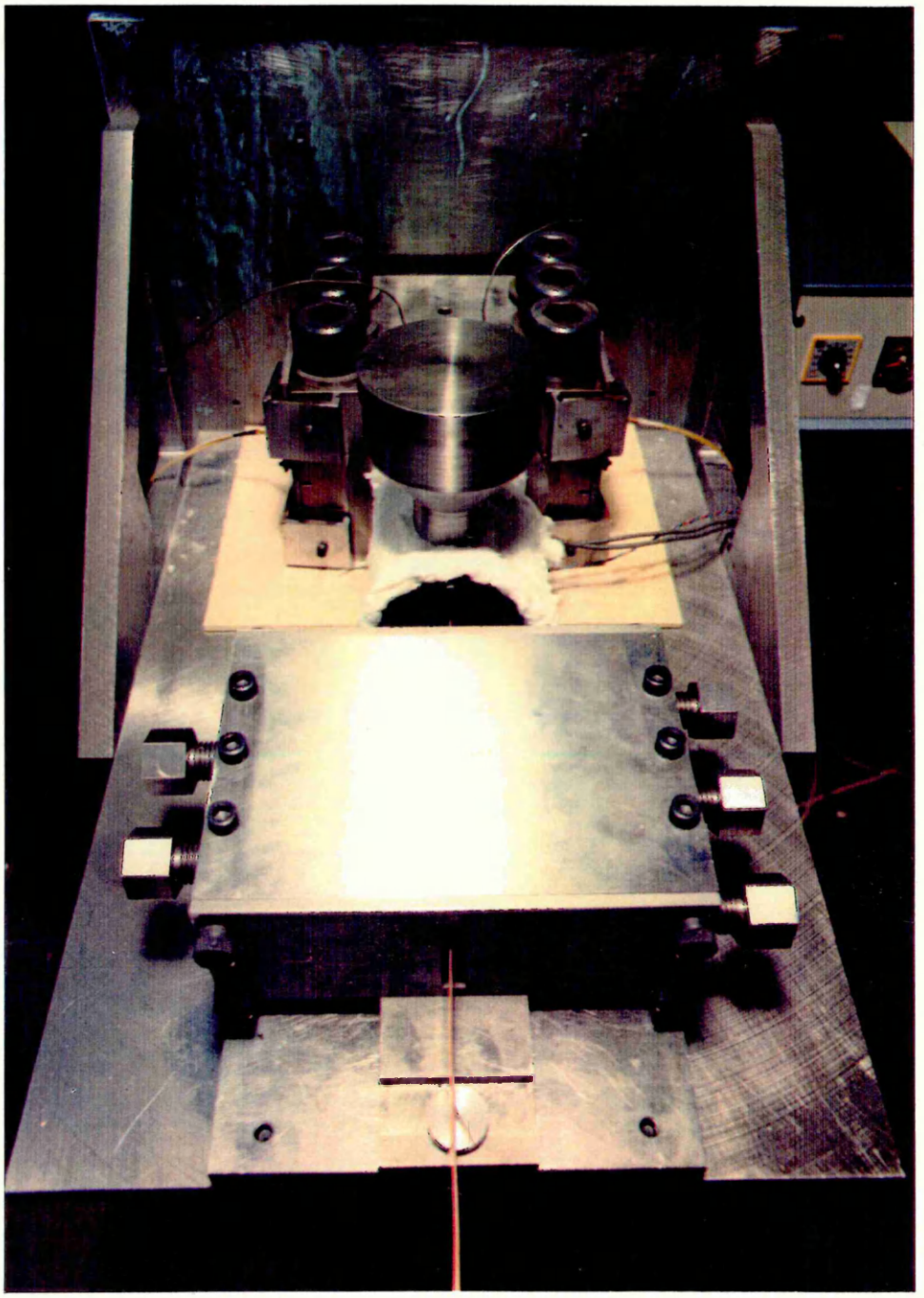

Plate 3.2 - A view of the process line for the Plasto-hydrodynamic drawing process.

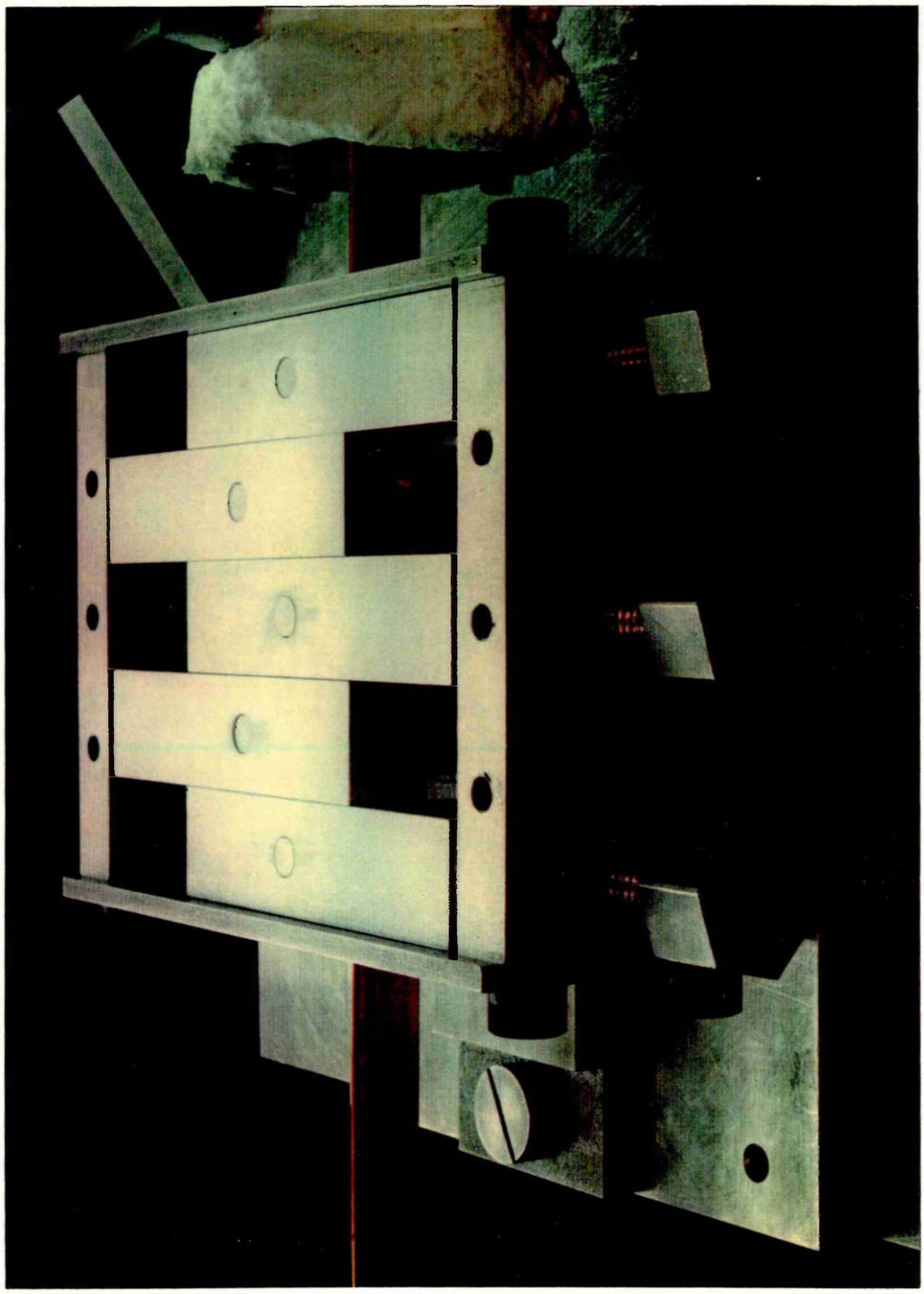

Plate 3.3 - Internal details of the roller leveller.

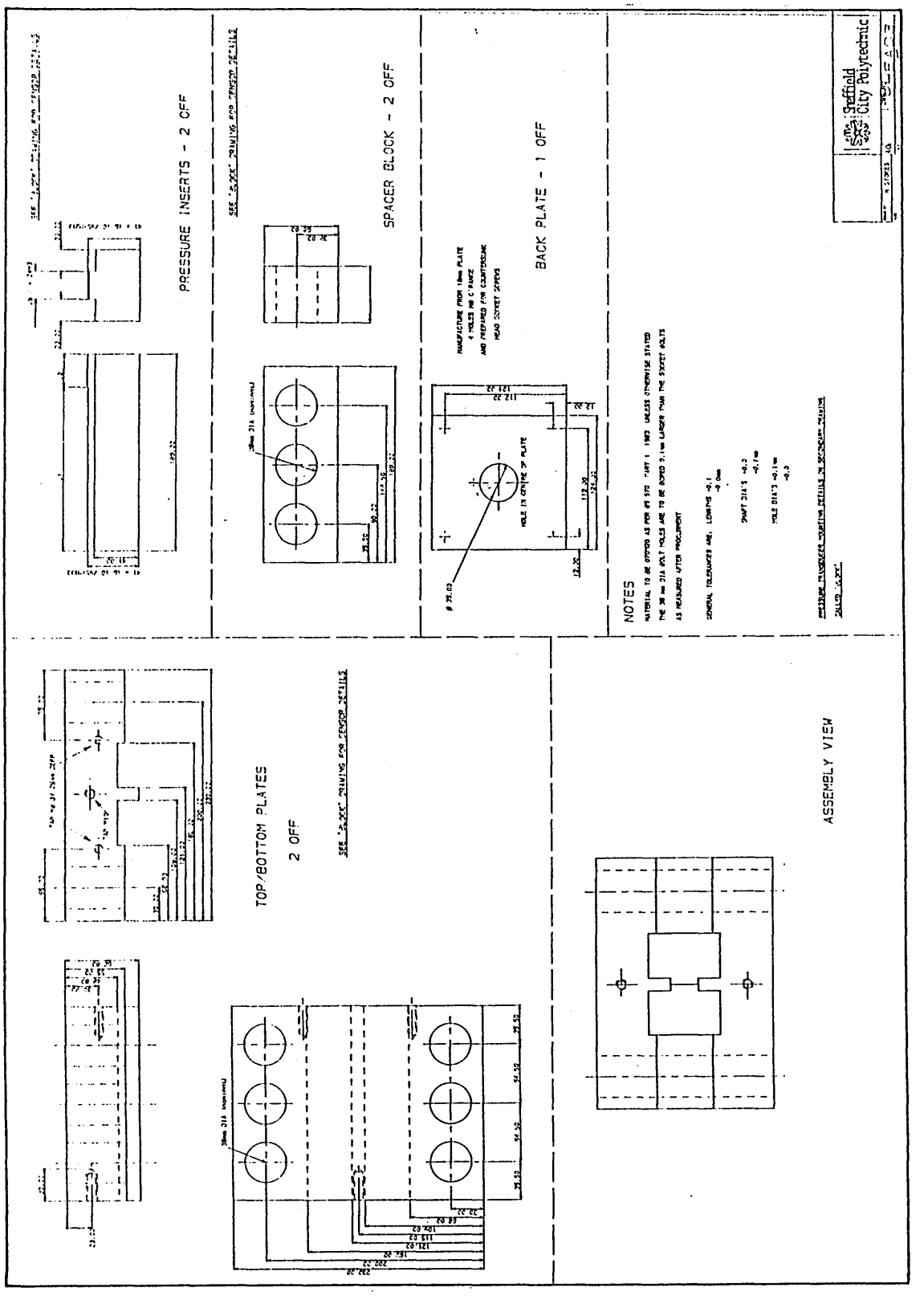

Figure 3.1 - Detailed drawings of the pressure head.

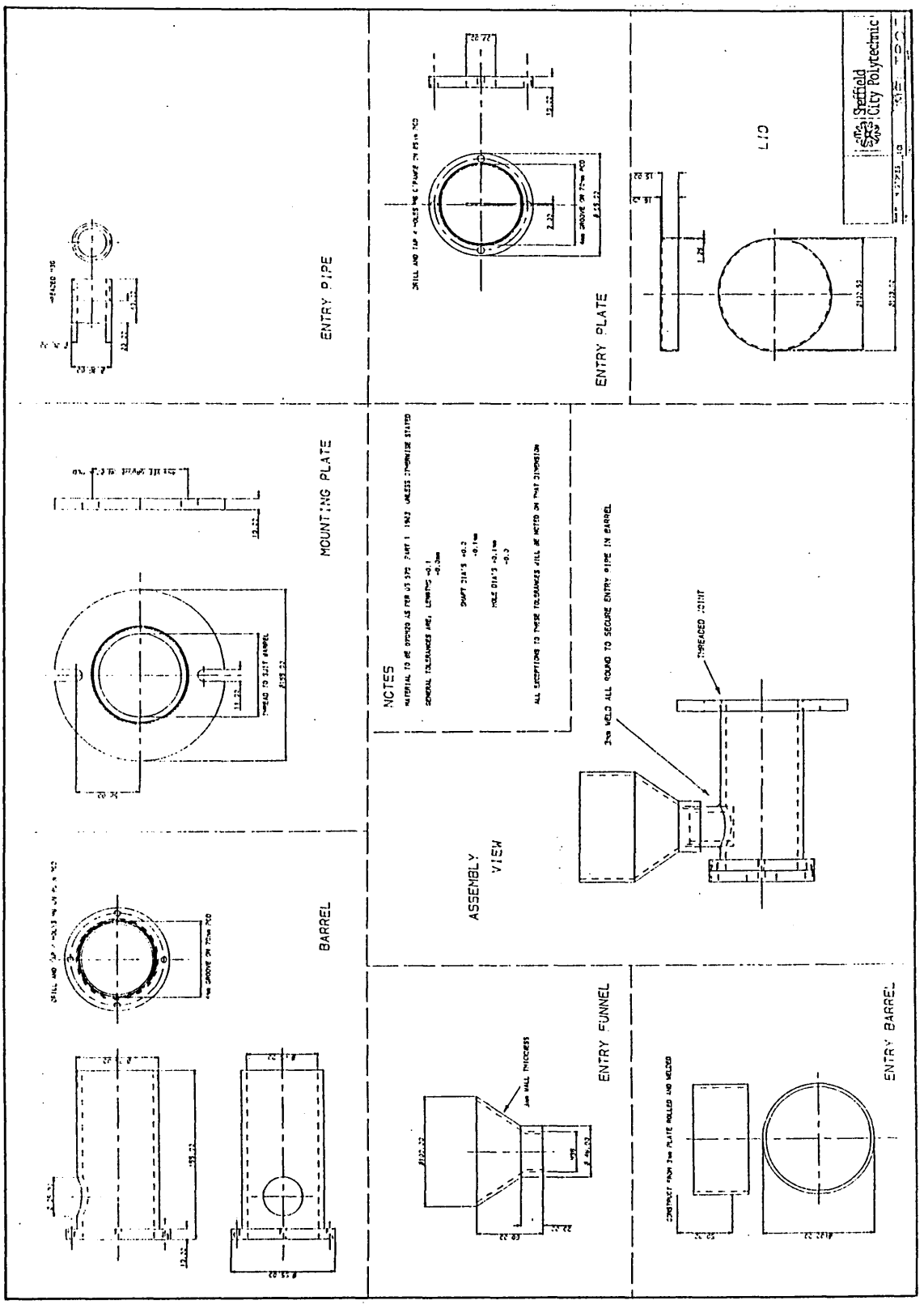

Figure 3.2 - Detailed drawings of the polymer meltpot.

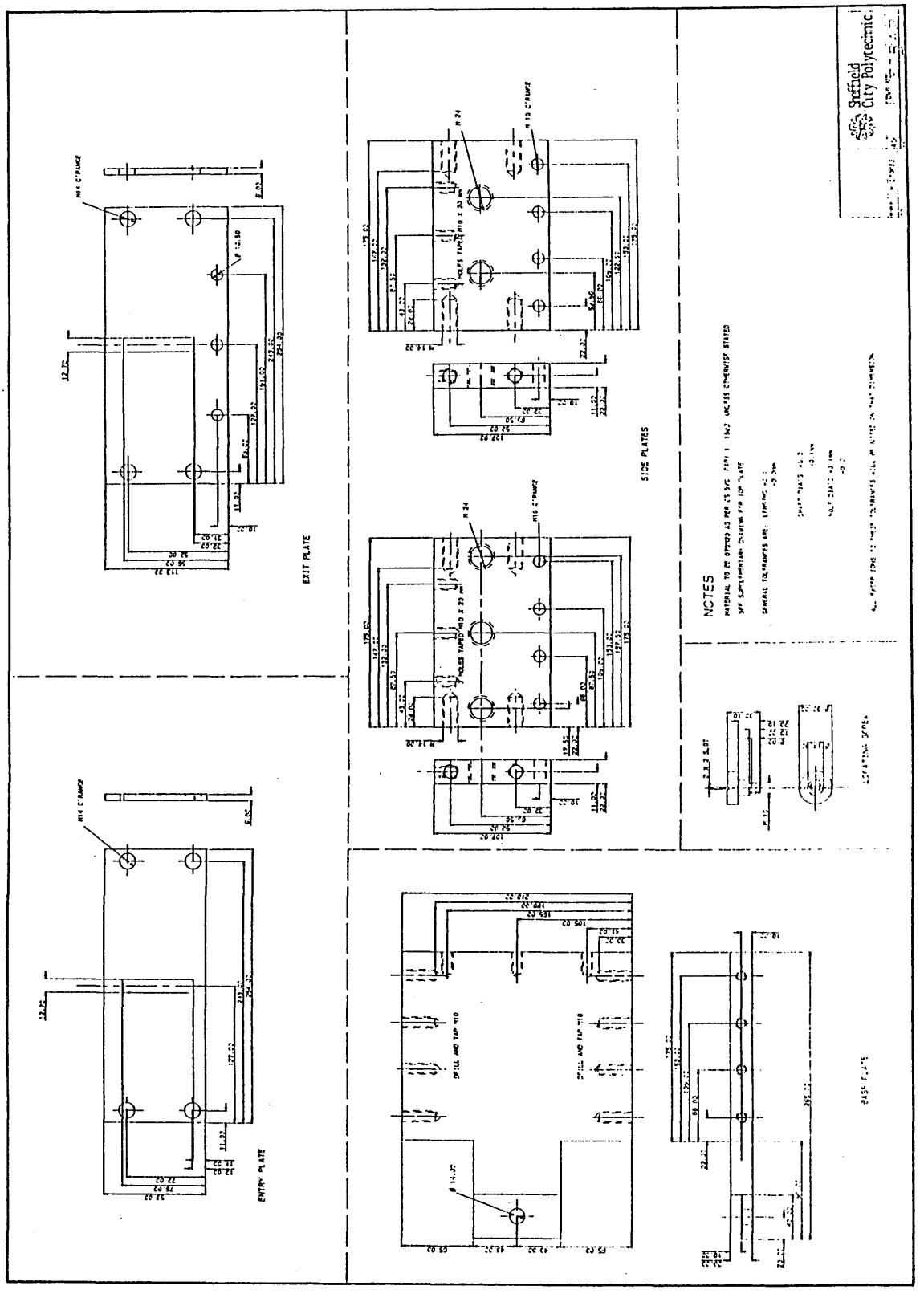

Figure 3.3 - Detailed drawings of the roller leveller frame.

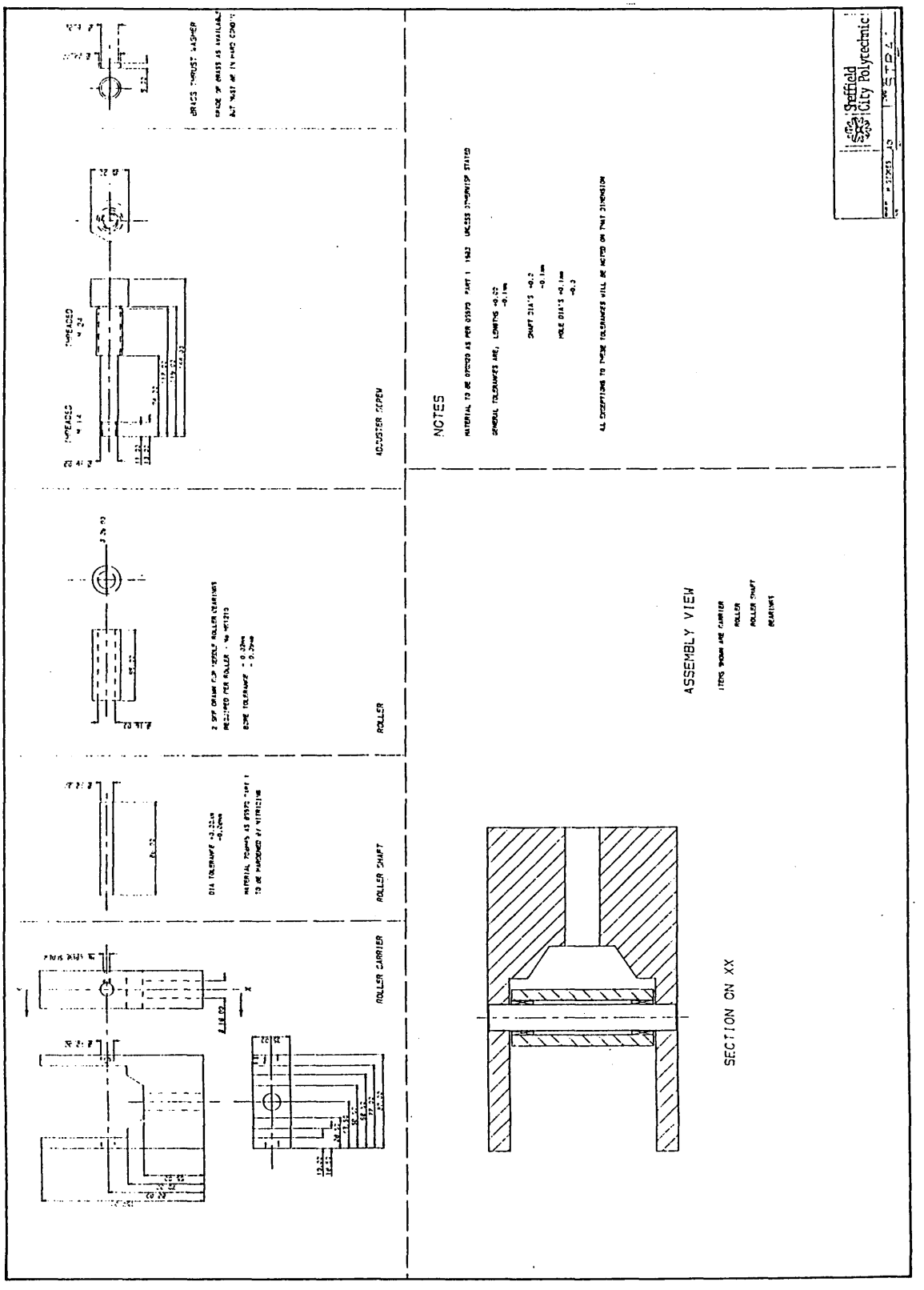

Figure 3.4 - Detailed drawings of the leveller roll carriers.

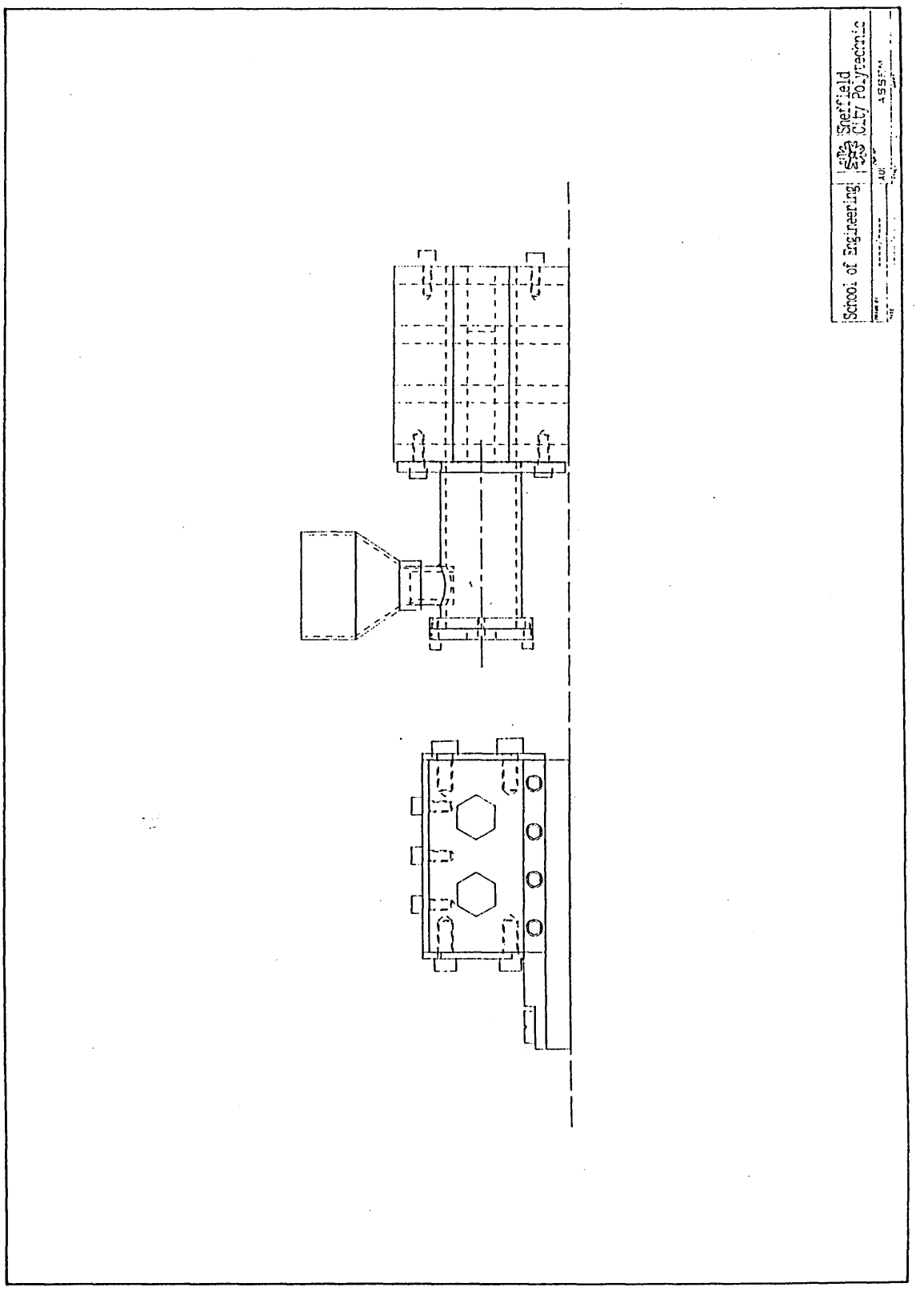

Figure 3.5 - Assembly drawing of the Plasto-hydrodynamic drawing apparatus.

CHAPTER 4

4.0 Experimental Results

4.1.1 General Description of Experimental Programme

The experimental programme is designed to investigate the distribution of thickness across the width face of the strip and the nominal reduction in area, thickness and width of section for material produced by the Plasto-Hydrodynamic Drawing (PHD) process. Theoretical work on the numerical optimisation of the process described later, indicated that the h_3/h_2 ratio (see Figure 5.2) affects the onset of slip and hence the achievable deformation. The experimental programme consisted of three distinct pressure head configurations. The L_1/L_2 and h_1/h_2 ratios were held constant; the h_3/h_2 ratio was then set to 5, 3.5 and 2. The melt temperature was also varied for each pressure head configuration, the temperatures being 235°C, 215°C and 195°C.

Material Details

Commercially available drawn copper tape (annealed or soft condition)

Nominal width 25.4 mm (1 inch)

Nominal thickness 1.58 mm (1/16 inch)

Aspect ratio 16:1

Pressure Head details

$L_1 = .159$ m $\qquad L_1/L_2 = 7.95$

$L_2 = .020$ m

$h_1 = .00025$ m $\qquad h_1/h_2 = 6.25$

$h_2 = .00004$ m

4.1.2 Thermal freezing and Preheat

Initial trials with the wide aspect ratio test rig were thought to be encouraging, as it was possible at the lowest draw velocity available to fracture the strip material; in fact, it was impossible not to fracture the strip material. Intensive investigation revealed that the polymer melt, initially at temperatures between 200°C and 280°C was freezing on the surface of the strip material which was at ambient temperature, causing the pressure head to become congested or clogged, thus fracturing the strip material.

The problem of thermal freezing was overcome by the installation of a preheat furnace prior to entry into the melt pot and pressure head. This consisted of a sheet steel box, lined with ceramic fibre. Heat was supplied by a three kilowatt heater and a fan unit.

4.2 Definition of Process Performance Indicators

Three performance indicators may be used with PHD, these are Percentage Reduction in Thickness (PRT), Percentage Reduction in Width (PRW) and Percentage Reduction in Area (PRA). Each of these may be defined as the change in an arbitrary variable, expressed as a percentage. The equations for the above terms are given below:-

$$PRT = \left(1 - \frac{t_i}{t_1}\right) * 100 \qquad (4.1)$$

$$PRW = \left(1 - \frac{W_i}{W_1}\right) * 100 \qquad (4.2)$$

$$PRA = \left(1 - \left(\frac{W_i t_i}{W_1 t_1}\right)\right) * 100 \qquad (4.3)$$

4.3 Experimental Procedures

4.3.1 Operation of the apparatus

The basic operational procedure is as follows:

i) set polymer melt, pressure head and preheat furnace temperatures,

ii) apply inert gas blanket to melt chamber,

iii) when the various components have achieved their set temperature a sequence of experimental draws are made for a predetermined velocity range,

iv) samples are then removed from the drawn section 1.5 metres from the initial point, the purpose of which is to ensure that any transient effects in the process have dissipated,

v) the samples are stripped of polymer and measured.

An inert gas blanket was used with the apparatus to prevent oxidisation of the polymer. All polymers are susceptible to this problem to a greater or lesser degree, particularly all grades of Nylon.

4.3.2 Removal of the polymer coating

Nylon was used throughout the experimental programme due to the generally good performance of this polymer group. Unfortunately Nylon produces an extremely well adhered coating on the strip material, which when mechanically removed resulted in damage to the surface of the strip material. In view of this a chemical solvent was used to remove the Nylon coating. The solvent used was

Meta-Cresol, which is toxic and as such its use must be in accordance with the C.O.S.H.H. (Care Of Substances Hazardous to Health) regulations. The procedure is given below:-

i) The sample is immersed in the m-cresol until sufficient time has elapsed to remove the coating.

ii) The sample is then washed in Sodium Hydroxide solution (1.0 M/L) to remove the m-cresol.

iii) The sample is then washed in distilled water.

iv) The sample is then washed in Acetone, and air dried.

4.3.3 Measurement procedures

Three geometrical properties of the experimental samples were measured. Firstly, the apparent width and the apparent thickness allowing the percentage reductions in width, thickness and area to be calculated. Secondly, the distribution of thickness across the width of the sample; this was assessed using a co-ordinate measuring machine and the corner radius of the section was assessed using enlarged photographs of encapsulated material samples. Thirdly, the corner radius of the section was assessed, as the commercially procured feed material had a small radius at the corners of the nominally square strip. The procedures used for these measurements are detailed below.

4.3.3.1 Measurement of Apparent Width and Thickness

The width of the sample was measured using a 0-25 mm flat anvil micrometer. The ratchet was utilised at all times. Three measurements were made, with the average being recorded.

The thickness of the sample was measured using a 0-25 flat and ball micrometer. The ratchet was utilised at all times. Measurements were made with the flat of the micrometer facing both sides of the sample, the smallest measurement being recorded, as any twisting or bowing of the samples caused during handling would tend to increase the measured value.

4.3.3.2 Measurement of the distribution of Thickness

The distribution of Thickness was measured using a Ferranti Metrology Systems - Merlin 750. The resolution of the measuring systems is rated at 0.0005 mm, with a repeatability of 2.5 microns.

The direct computer control facility of the system was utilised to assess the distribution of thickness. The section is mapped along its width by a sequence of pinch measurements. The flatness of the section has not been assessed as the material twists during handling and this is not considered an important parameter for this type of material. The processed material is of differing widths as the width is reduced in the process and samples at different velocities will have varying amounts of deformation. Because of this the cross-section analysis is made about the centre of the width face. This arrangement is given schematically in Figure 4.1. Pinch measurements are then made at a 2 mm spacing, 10 mm either side (above and below) of the centre line. The mapping was limited to this range as any further steps in the map would approach the corner section of the material with the possible introduction of error.

The pseudo code of the computer programme used to assess the distribution of cross-section is given overleaf.

```
Begin:
        place sample in prepared clamp (vertically on its edge)
        measure nominal thickness
        measure nominal width
        calculate nominal centre of section
        reset coordinate system to centre of strip
        for z = 10 to -10 step -2
                measure thickness at z
                output to printer z and thickness
        next z
End:
```

4.3.3.3 Measurement of Cross-section corner radius

To facilitate the examination of the sample corner radius, 5 mm long sections were removed from the drawn material. These were then encapsulated in Bakelite; a spring clip was used to hold the sections in vertical alignment. After encapsulation, the cross-section was revealed by removing the surface layer of Bakelite with rotating abrasive media, ranging from 320 to 1000 grit size, to produce a polished surface. Each sample was then photographed using a stereo-microscope with a 35mm camera attached. Enlargements of the images were made and the following procedure was used to assess the corner radius.

It was assumed that the shape of the section corner may be approximated by a curve of constant radius. A graphical construction was then made for each curve, as shown in Figure 4.2. A radius was then fitted to the corner graphically. Any errors incurred by the method will be minimised through the applied scaling factor - total magnification used was 70X approximately. Each corner of the sample was measured and a mean value for the section corner radius was then calculated.

4.4 Results

The magnitude of the reduction in thickness and width, achieved by the process can be seen to agree with the following general statements:

i) reduction is proportional to the draw velocity,

ii) reduction is inversely proportional to the process temperature.

4.4.1 Pressure head build 1 - h_3/h_2 ratio = 5

The maximum percentage reduction in area of 9.2% was achieved with the lowest temperature of 195° and at a maximum velocity of 0.447 m/s. The maximum percentage reduction in the width and the thickness was also recorded at this point, the reductions being 4.15% and 5.27% respectively. The achieved deformation is given in tabular form in Tables 4.1, 4.2 and 4.3, and in graphical form in Figures 4.3, 4.4 and 4.5.

4.4.2 Pressure head build 2 - h_3/h_2 ratio = 3.5

The maximum percentage reduction for all process indicators was achieved with the sequence of draws made at a temperature of 195°, however the wide fluctuations in the process performance are indicative of supply problems in the polymer melt making interpretation of this data problematic. The achieved deformation is given in tabular form in Tables 4.4, 4.5 and 4.6, and in graphical form in Figures 4.6, 4.7 and 4.8.

4.4.3 Pressure head build 3 - h_3/h_2 ratio = 2

A maximum percentage reduction in area of 11.59% was achieved at a process temperature of 215° and velocity of 0.131 m/s. This was accompanied by a

percentage reduction in thickness of 7.91%. Both of these values are outside the expected form of the results and will be discussed later. The achieved deformation is given in tabular form in Tables 4.7, 4.8 and 4.9, and in graphical form in Figures 4.9, 4.10 and 4.11.

Table 4.1 Temperature 235°, h_3/h_2 ratio = 5

Draw No	Velocity (m/s)	P.R.A. (%)	P.R.W. (%)	P.R.T. (%)
13.1	0.131	3.59	1.4636	2.1587
13.2	0.195	4.59	1.9778	2.6666
13.3	0.297	4.9898	2.1954	2.857
13.4	0.38	5.5109	2.4129	3.1746
13.5	0.447	5.4963	2.3338	3.238

Table 4.2 Temperature 215°, h_3/h_2 ratio = 5

Draw No	Velocity (m/s)	P.R.A. (%)	P.R.W. (%)	P.R.T. (%)
14.1	0.131	3.884	1.6218	2.22
14.2	0.195	5.394	2.215	3.174
14.3	0.297	5.933	2.452	3.492
14.4	0.38	6.048	2.5712	3.492
14.5	0.447	6.200	2.7294	3.492

Table 4.3 Temperature 195°, h_3/h_2 ratio = 5

Draw No	Velocity	P.R.A.	P.R.W.	P.R.T.
15.1	0.131	5.525	2.492	3.111
15.2	0.195	7.175	3.243	4.063
15.3	0.297	8.058	3.718	4.507
15.4	0.38	8.627	3.995	4.825
15.5	0.447	9.204	4.153	5.269

Table 4.4 Temperature 235°, h_3/h_2 ratio = 3.5

Draw No	Velocity	P.R.A.	P.R.W.	P.R.T.
20.1	0.131	6.65158	2.96677	3.79747
20.2	0.1616	7.22416	3.24368	4.11393
20.3	0.195	7.78049	3.44146	4.49368
20.4	0.252	8.07694	3.56013	4.68354
20.5	0.297	8.38729	3.75791	4.81013
20.6	0.349	8.37293	3.67880	4.87342
20.7	0.38	8.48582	3.79747	4.87342
20.8	0.411	8.64971	3.77769	5.06329
20.9	0.447	8.33530	3.63924	4.87342

Table 4.5 Temperature 215°, h_3/h_2 ratio = 3.5

Draw No	Velocity	P.R.A.	P.R.W.	P.R.T.
19.1	0.131	7.38451	3.28323	4.24051
19.2	0.1616	7.78049	3.44146	4.49368
19.3	0.195	8.64518	3.83703	5.000
19.4	0.252	8.43941	3.87659	4.74684
19.5	0.297	9.87422	4.43038	5.69620
19.6	0.349	9.48718	4.21282	5.50633
19.7	0.38	9.58062	4.31171	5.50633
19.8	0.411	9.42207	4.27215	5.37975
19.9	0.447	9.58062	4.31171	5.50633

Table 4.6 Temperature 195°, h_3/h_2 ratio = 3.5

Draw No	Velocity	P.R.A.	P.R.W.	P.R.T.
18.2	0.131	9.1135	4.07437	5.25317
18.3	0.1616	10.51675	4.98418	5.82278
18.4	0.195	10.98963	4.58861	6.70886
18.5	0.252	7.85266	2.80855	5.18987
18.6	0.297	14.03374	4.54906	9.93671
18.7	0.349	4.76787	2.29430	2.53165
18.8	0.38	10.95638	4.74684	6.51899
18.9	0.411	5.40774	2.57121	2.91139

Table 4.7 Temperature 235°, h_3/h_2 ratio = 2

Draw No	Velocity	P.R.A.	P.R.W.	P.R.T.
21.1	0.131	5.47586	2.45059	3.10127
21.2	0.1616	6.35078	2.84585	3.60760
21.3	0.195	6.74873	3.00395	3.86076
21.4	0.252	7.04668	3.12253	4.05063
21.5	0.297	7.12253	3.20158	4.05063
21.6	0.349	7.93781	3.47826	4.62026
21.7	0.38	7.76354	3.35968	4.55696
21.8	0.411	7.86241	3.39920	4.62026
21.9	0.447	7.86241	3.3992	4.62026

Table 4.8 Temperature 215°, h_3/h_2 ratio = 2

Draw No	Velocity	P.R.A.	P.R.W.	P.R.T.
22.1	0.131	11.58765	3.99209	7.91139
22.2	0.1616	8.262811	3.75494	5.06329
22.3	0.195	9.75910	4.30830	5.69620
22.4	0.252	10.13621	4.38735	6.01266
22.5	0.297	9.93141	4.42687	5.75950
22.6	0.349	9.95467	4.38735	5.82278
22.7	0.38	9.64258	4.24901	5.63291
22.8	0.411	9.44209	4.22925	5.44304
22.9	0.447	9.40472	4.18972	5.44304

Table 4.9 Temperature 195°, h_3/h_2 ratio = 2

Draw No	Velocity	P.R.A.	P.R.W.	P.R.T.
23.1	0.131	6.79873	2.15415	4.74684
23.2	0.1616	10.81515	4.4664	6.64557
23.3	0.195	11.44567	4.62451	7.1519
23.4	0.252	10.92585	4.58498	6.64557
23.5	0.297	11.29114	4.78261	6.83545
23.6	0.349	10.83712	4.68379	6.45570
23.7	0.38	10.64242	4.60474	6.32912
23.8	0.411	10.57258	4.72332	6.13924
23.9	0.447	10.32196	4.58498	6.01266

4.4.4 The Deformed Shape of the Processed Material

Referring to Figure 4.9, experiment 23 (195°C) was selected for analysis of cross-section and corner section radius. This was due to the generally good performance of this experiment, with no indication from the apparent width and thickness measurements of supply problems. Two further points were used during the analysis, these were one point from experiment 22 and one from experiment 21, at 0.2 m/s (approx), forming a vertical line on Figure 4.9.

The result of the distribution of cross-section analyses are shown graphically in Figures 4.12 and 4.13 respectively.

Plates 4.1 and 4.2 are of the encapsulated sample of the original section and plates 4.3 and 4.4 are of the trial draw 23-3. Figure 4.14 graphically presents the data for the entire corner radius analysis.

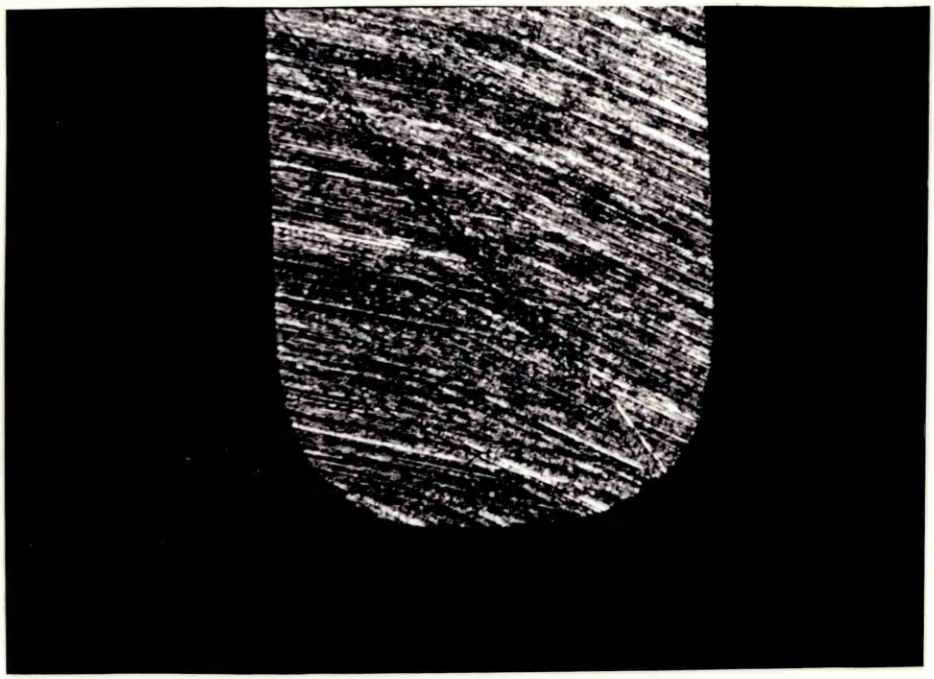

Plate 4.1 Original section 1st view

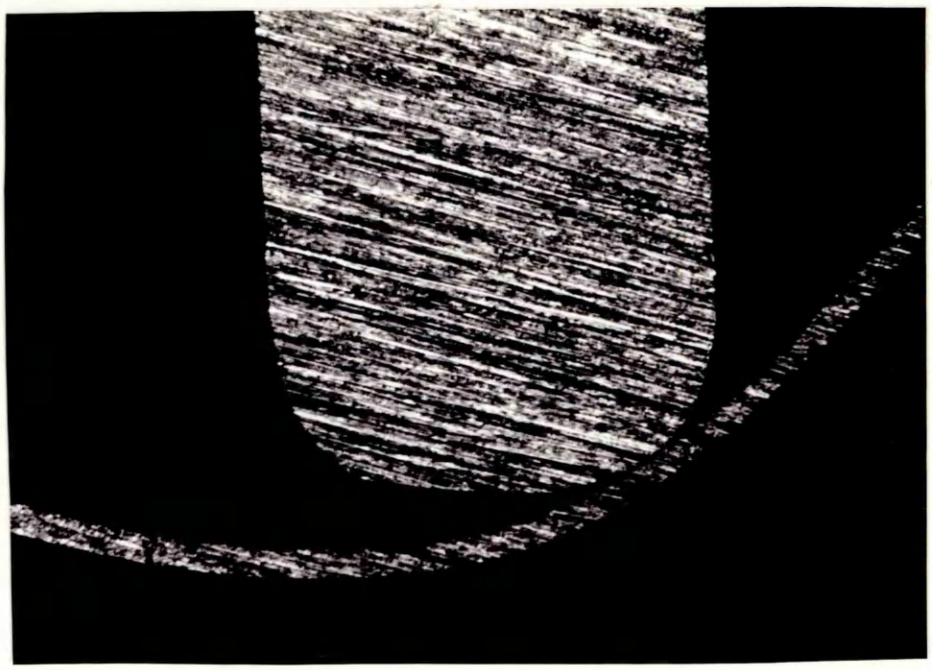

Plate 4.2 Original section 2nd view

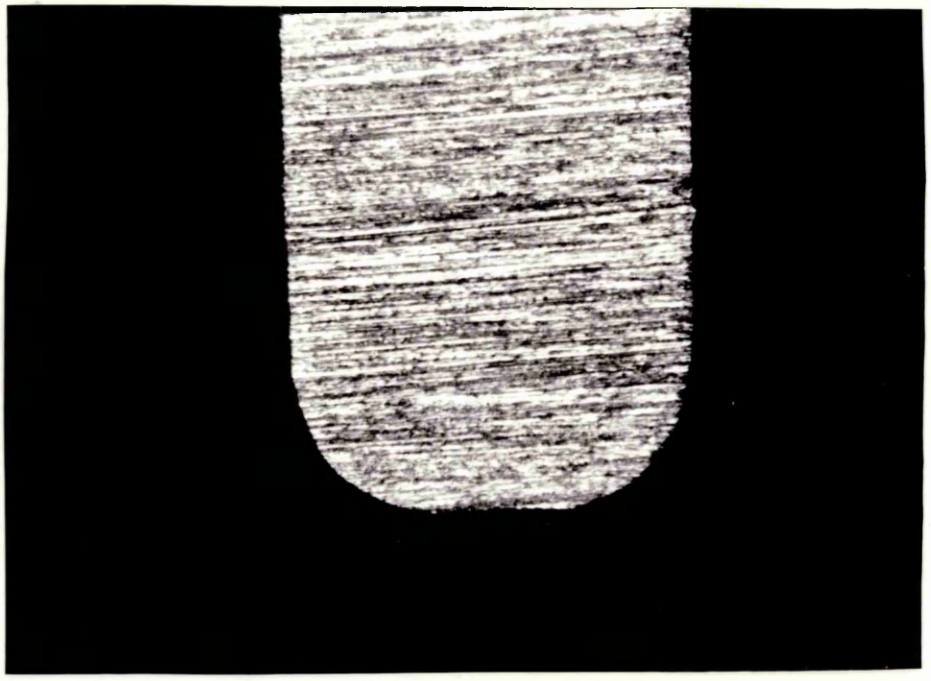

Plate 4.3 Trial draw No 23-3 1st view

Plate 4.4 Trial draw No 23-3 2nd view

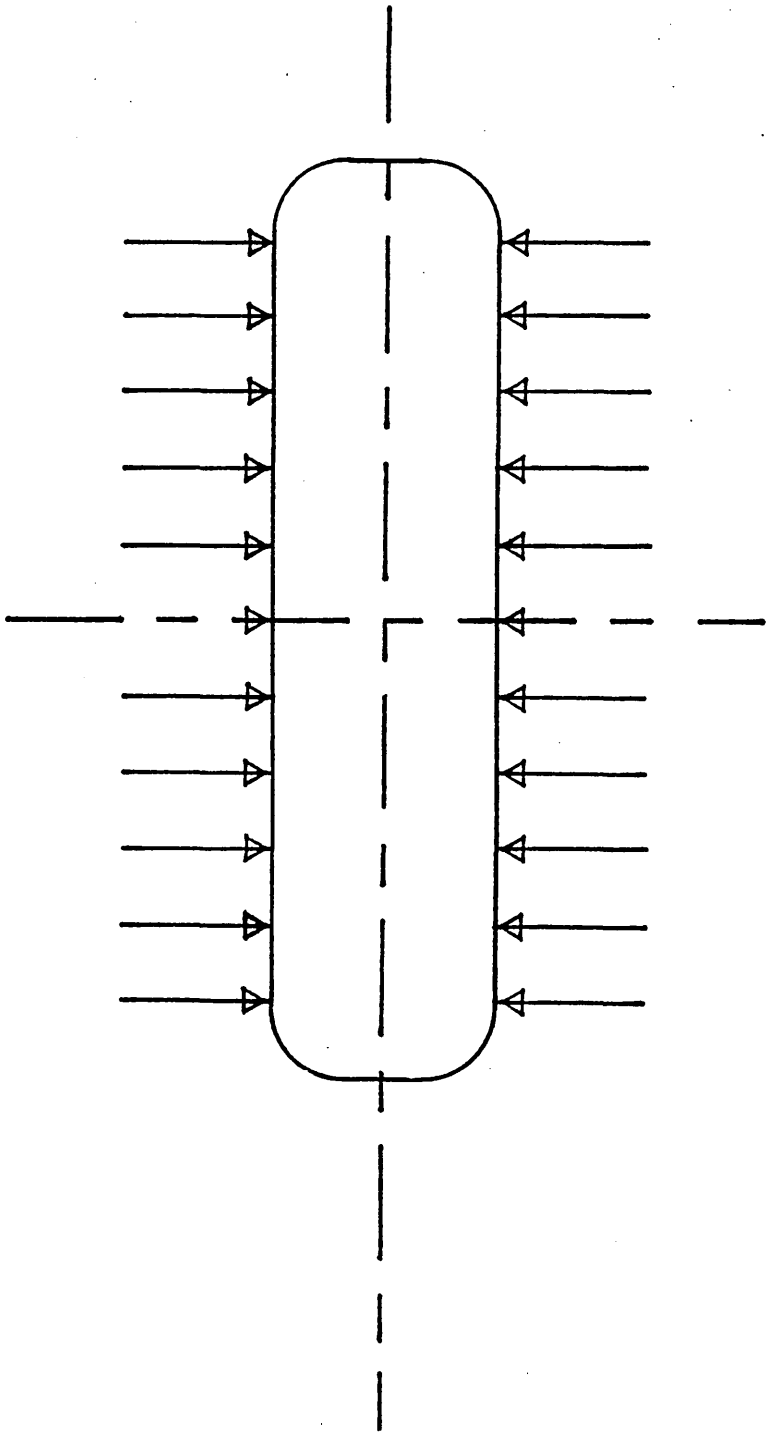

Figure 4.1 - Measuring points for the distribution of cross-section analysis.

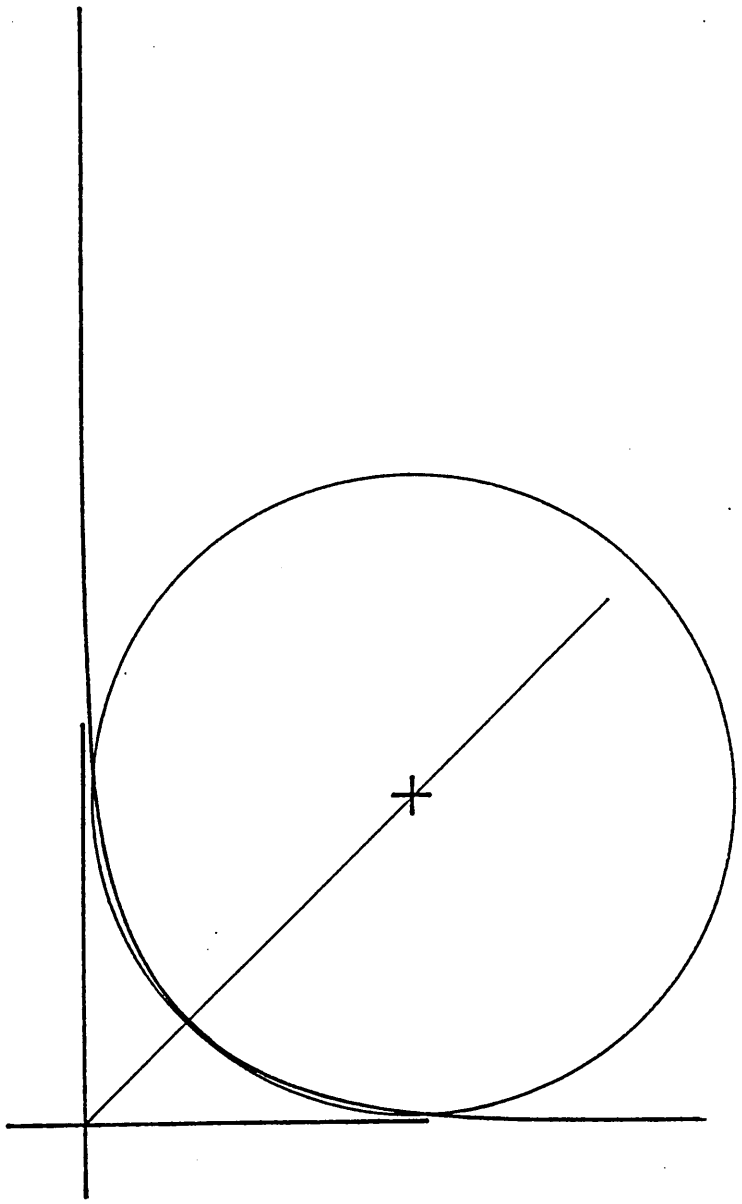

Figure 4.2 - Schematic of the method used to measure the section corner radius.

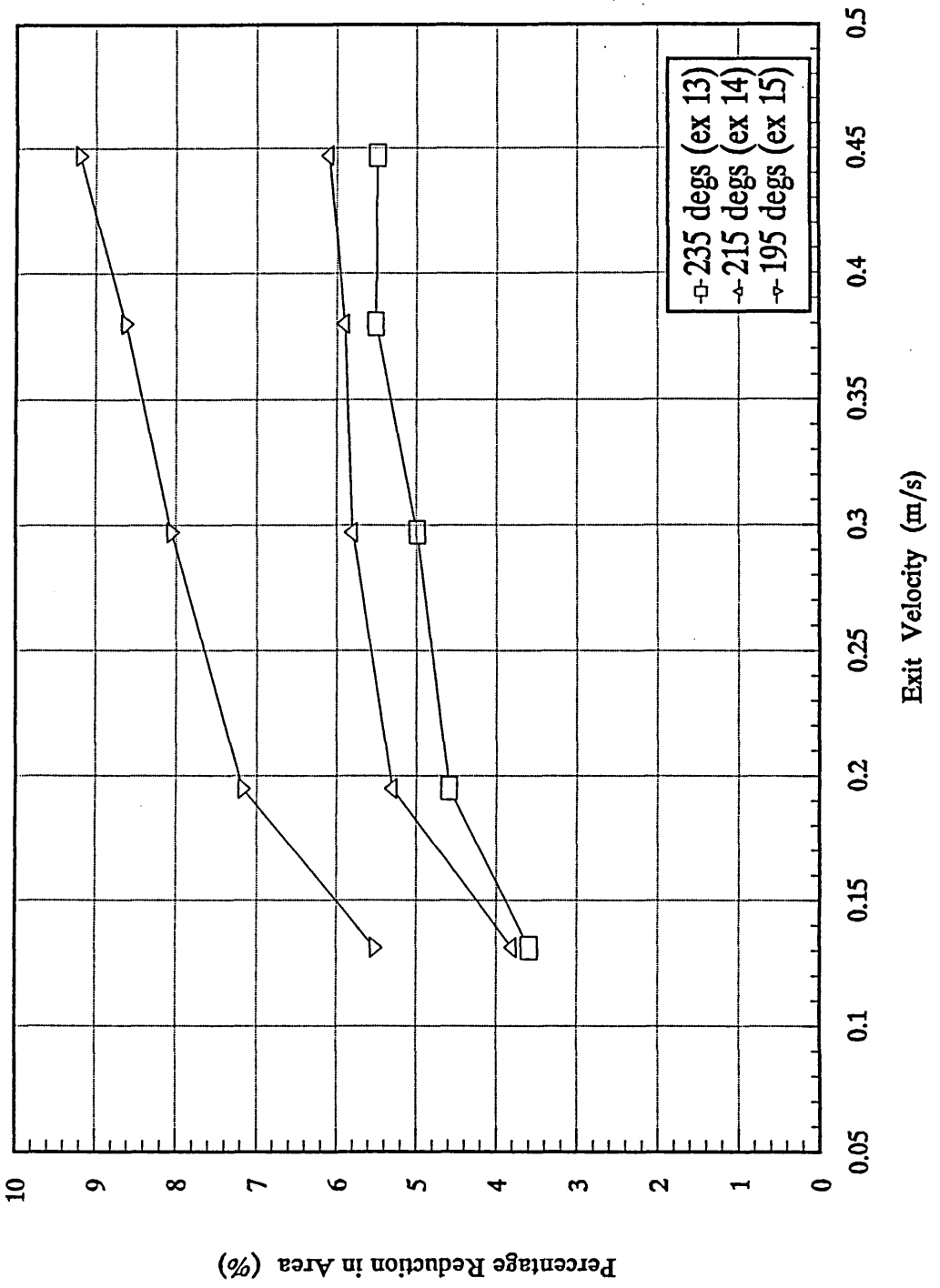

Figure 4.3 - Percentage Reduction in Area with a h_3/h_2 ratio of 5.

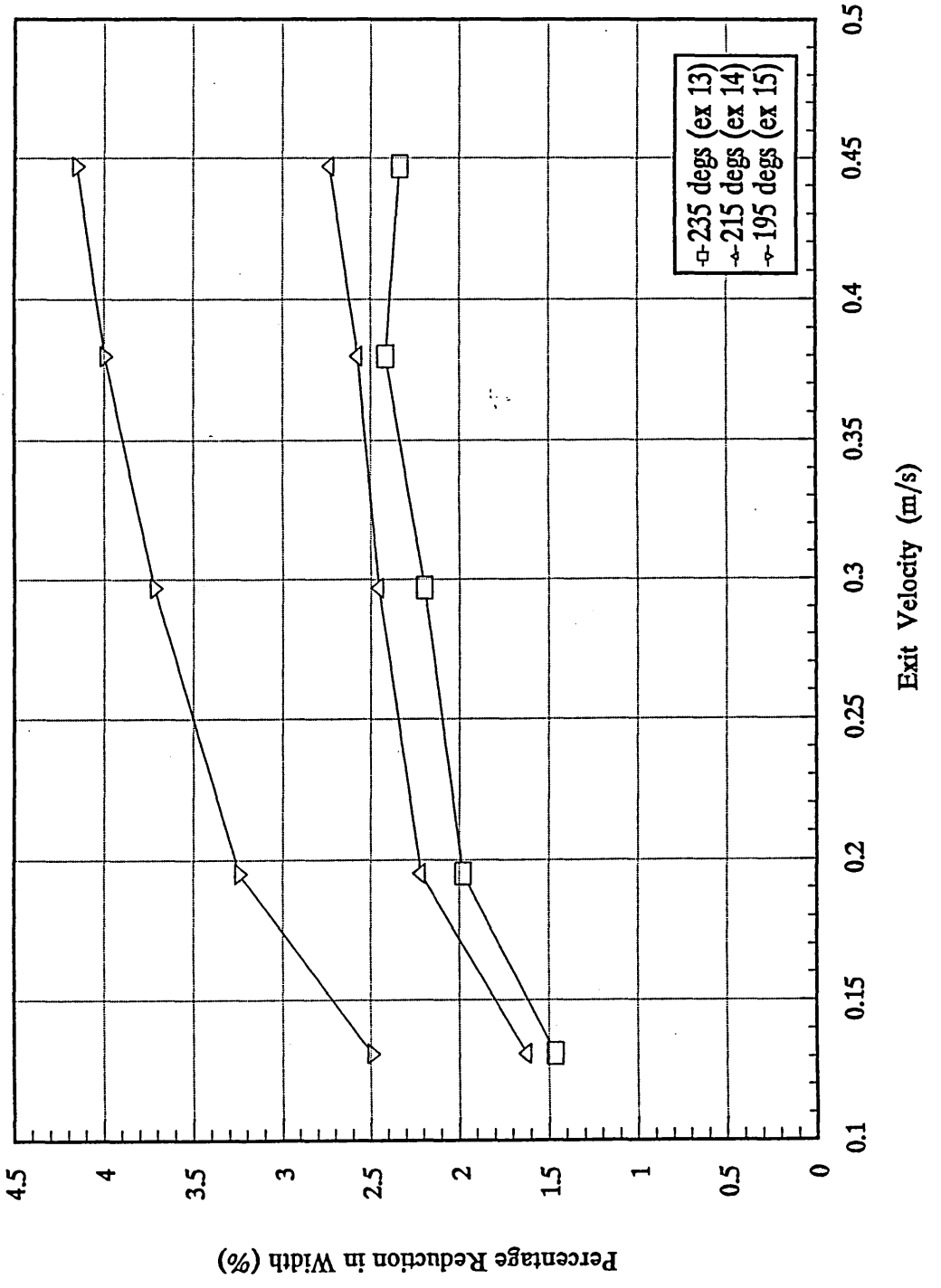

Figure 4.4 - Percentage Reduction in Width with a h_3/h_2 ratio of 5.

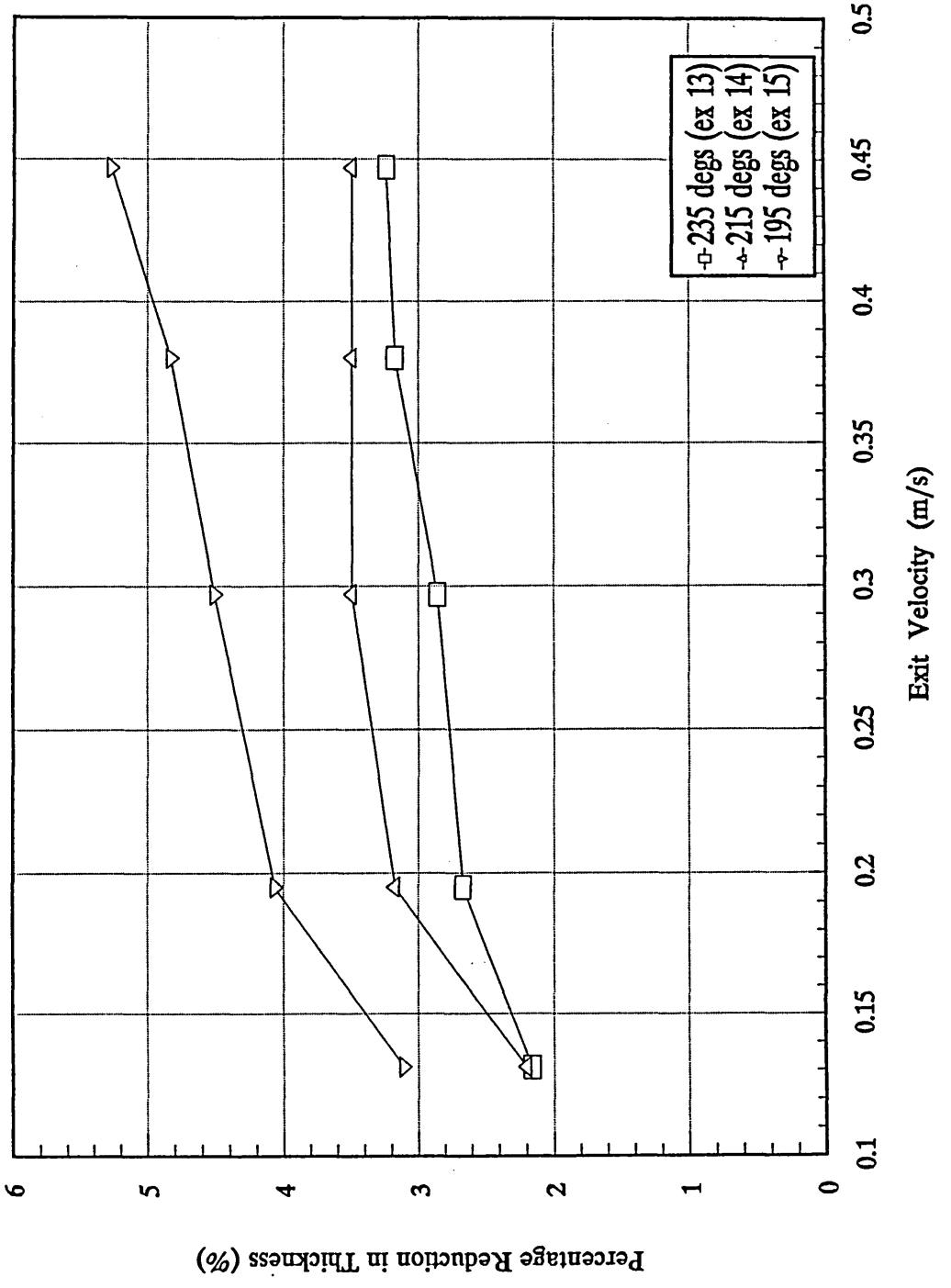

Figure 4.5 - Percentage Reduction in Thickness with a h_3/h_2 ratio of 5.

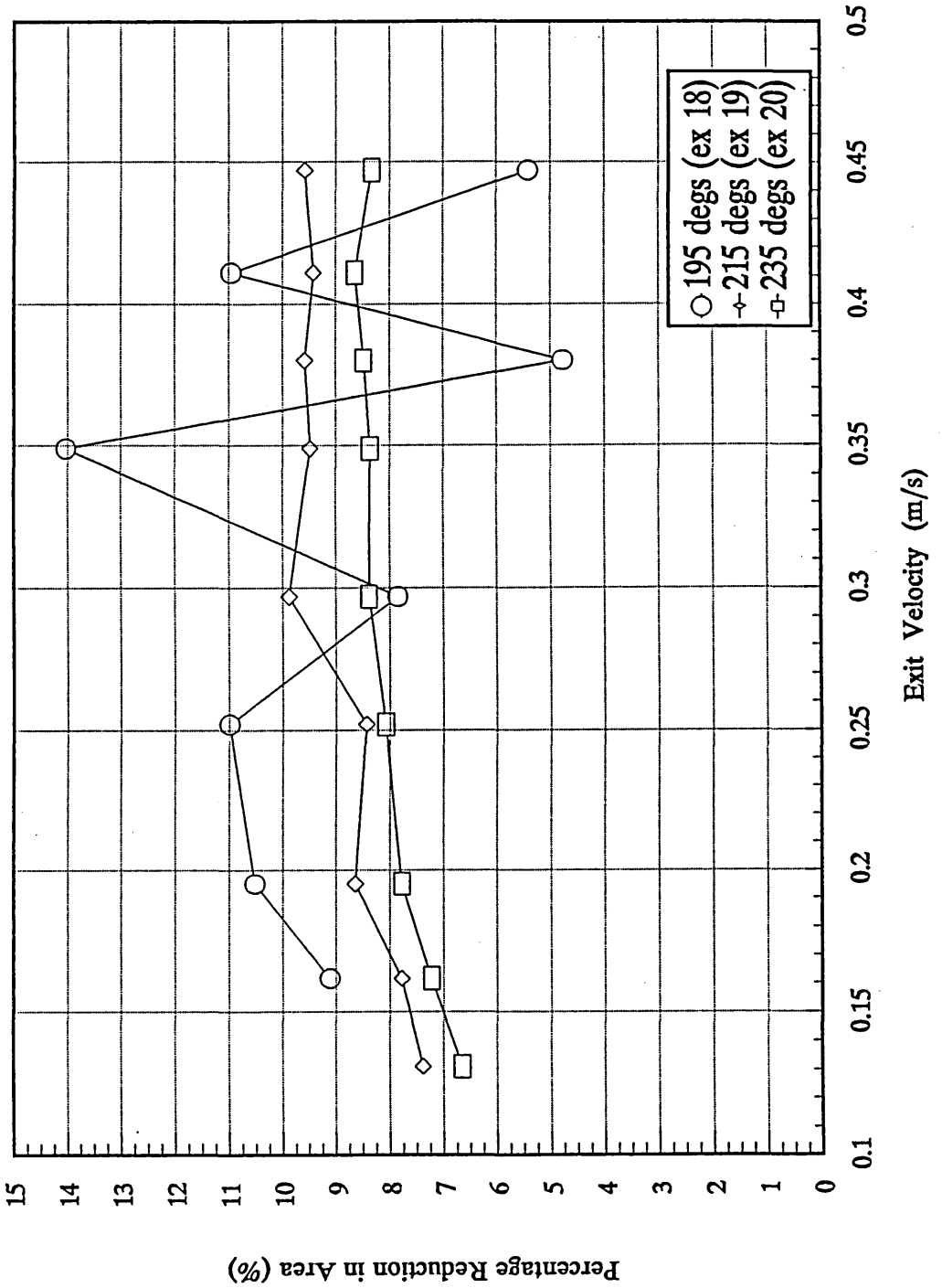

Figure 4.6 - Percentage Reduction in Area with a h_3/h_2 ratio of 3.5.

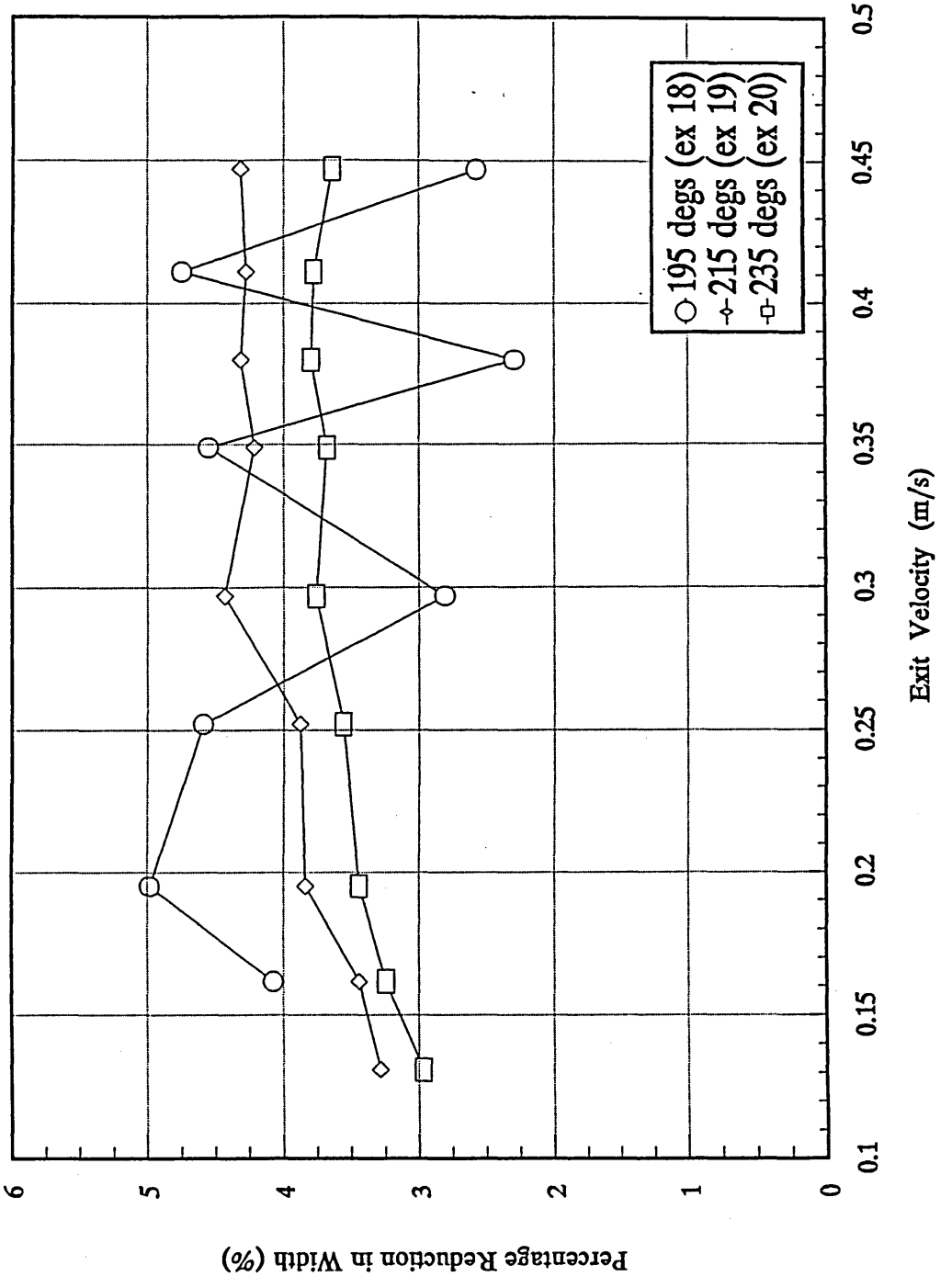

Figure 4.7 - Percentage Reduction in Width with a h_3/h_2 ratio of 3.5.

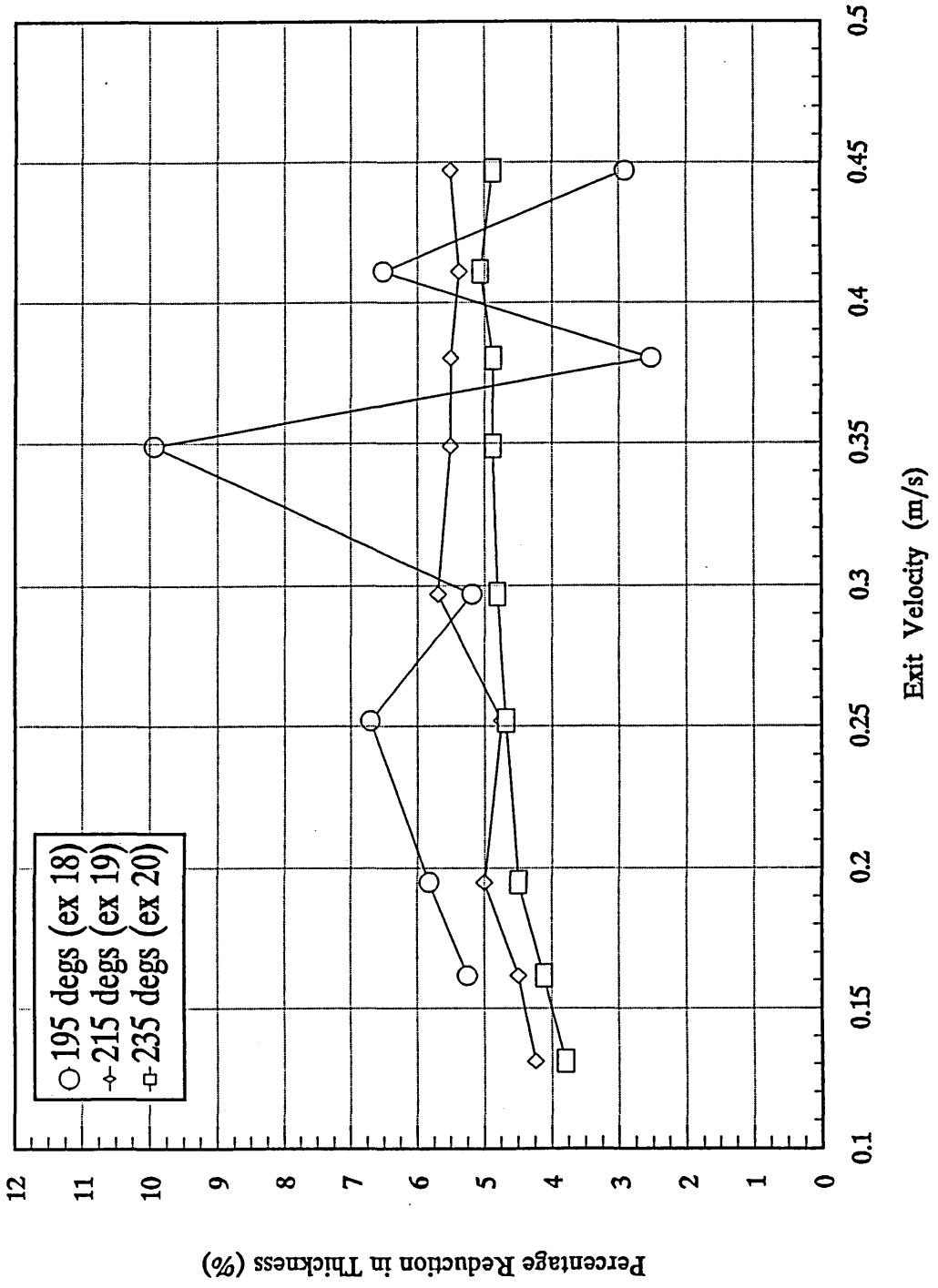

Figure 4.8 - Percentage Reduction in Thickness with a h_3/h_2 ratio of 3.5.

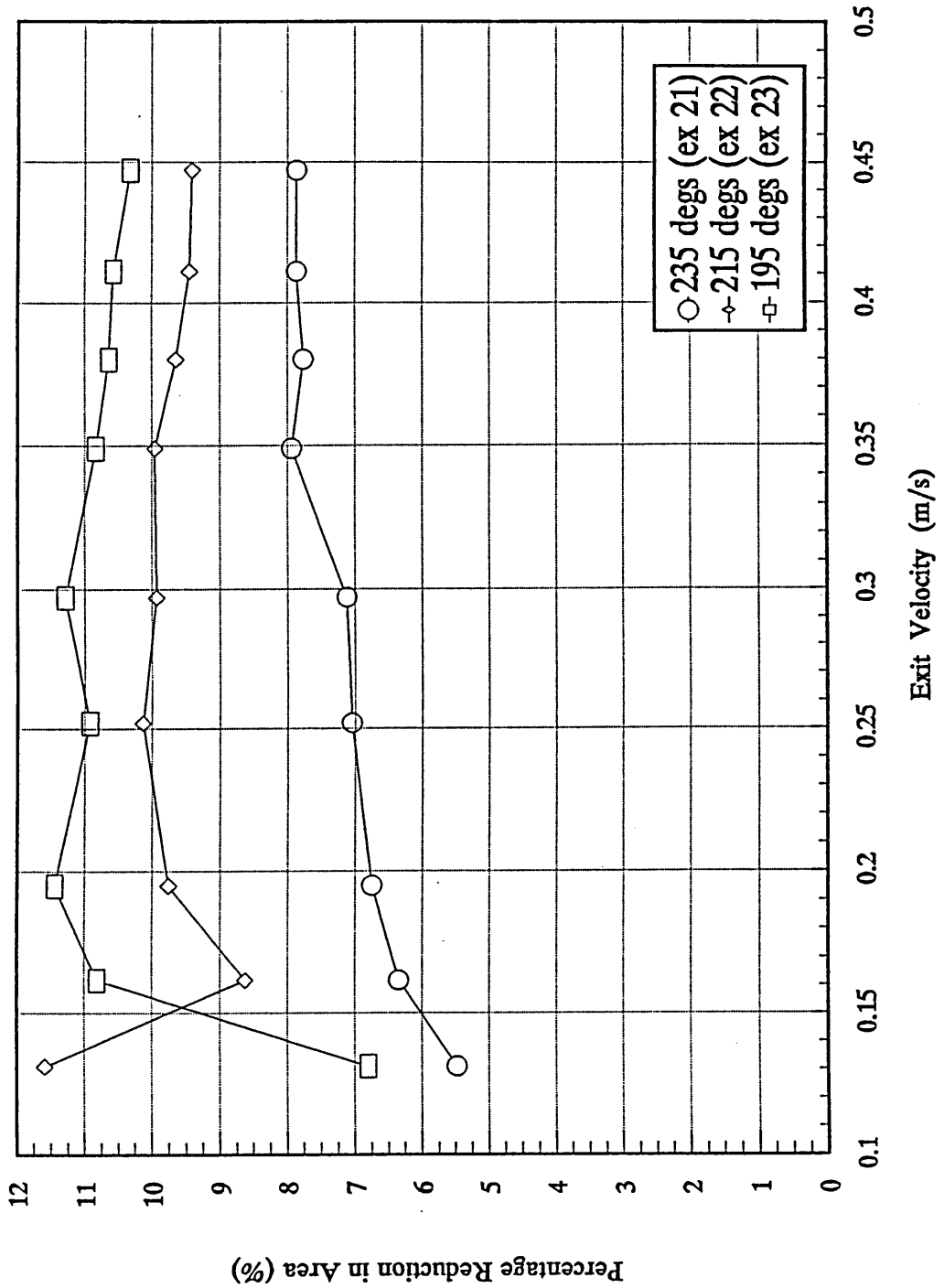

Figure 4.9 - Percentage Reduction in Area with a h_3/h_2 ratio of 2.

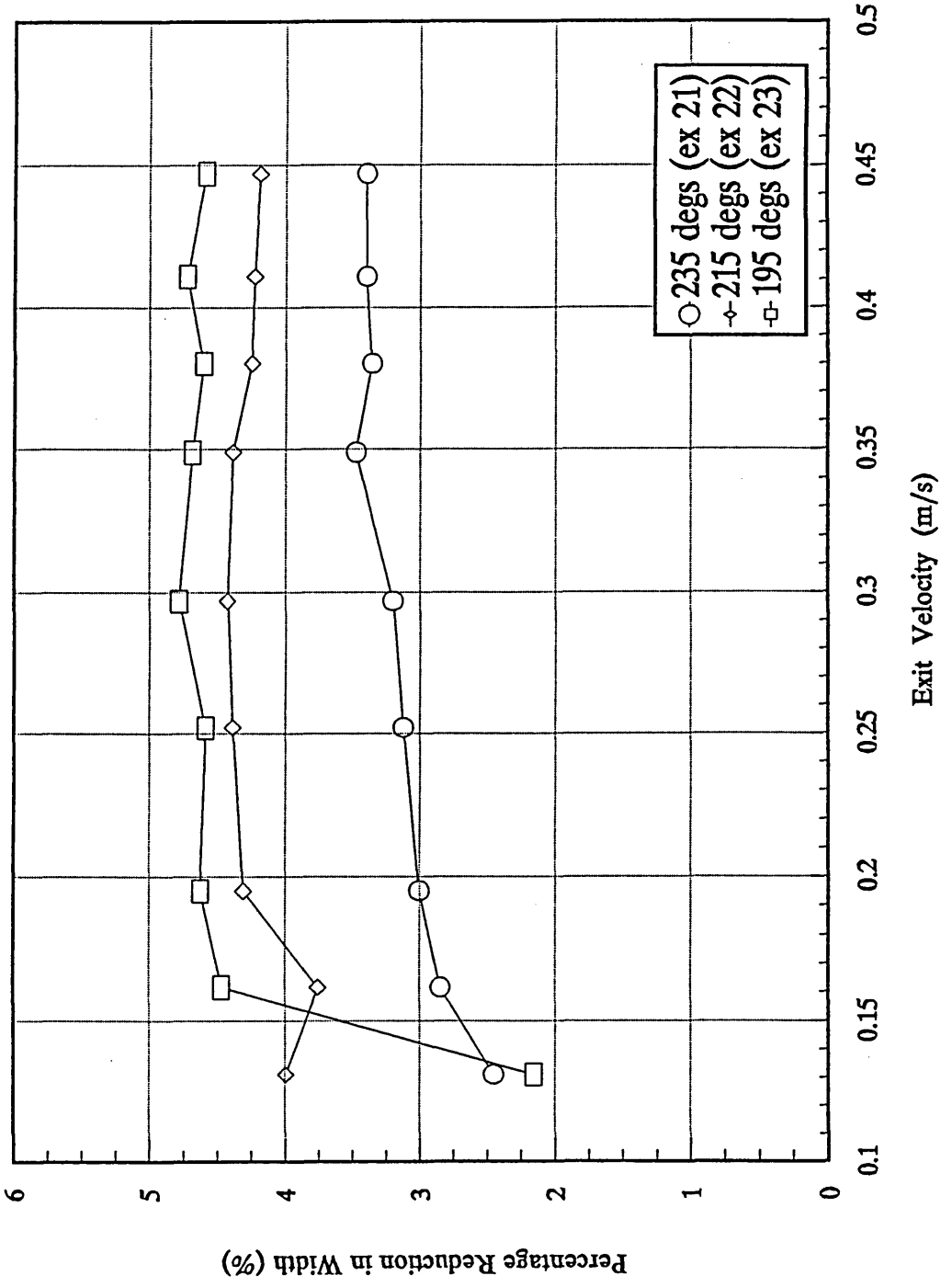

Figure 4.10 - Percentage Reduction in Width with a h_3/h_2 ratio of 2.

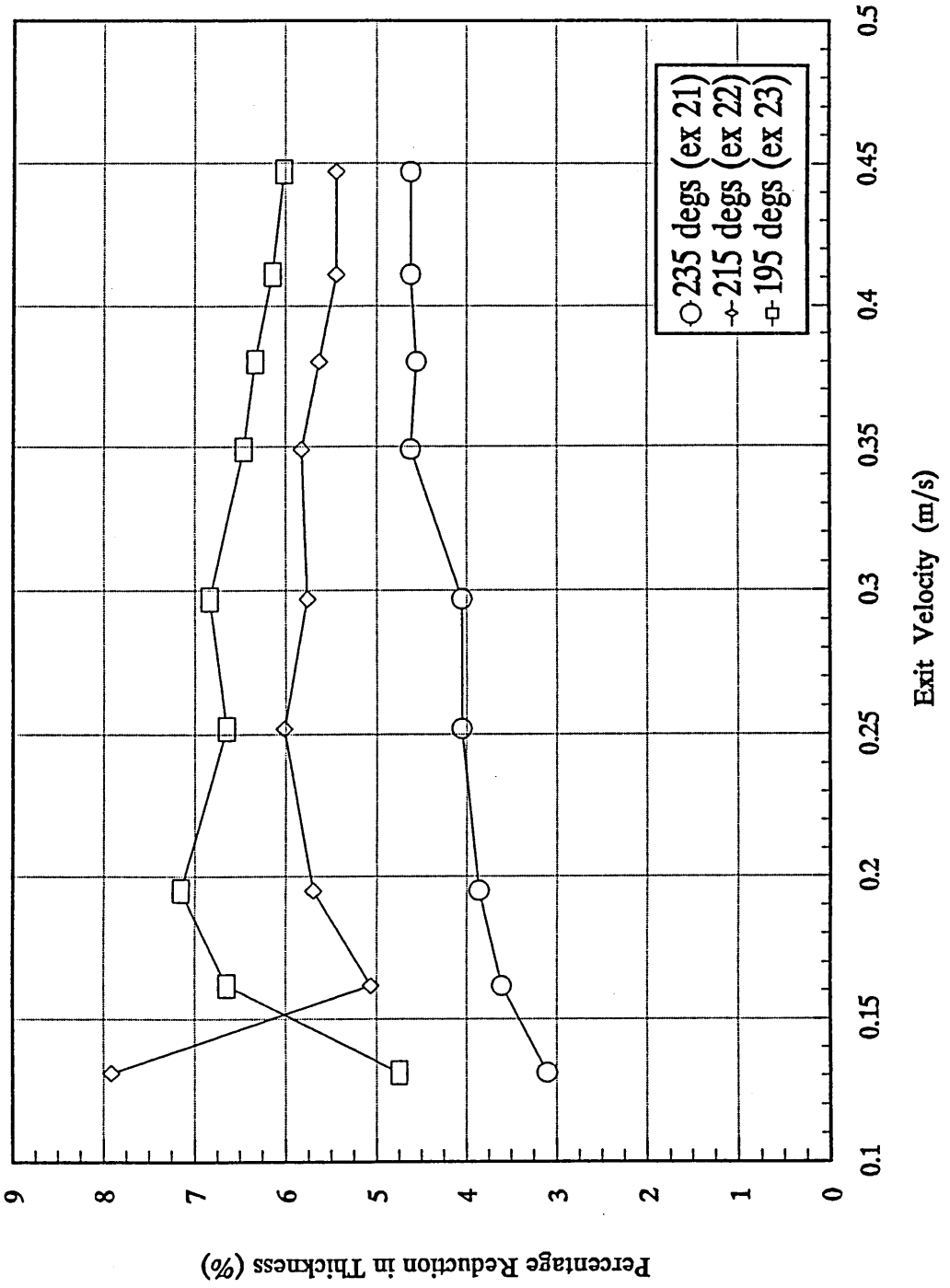

Figure 4.11 - Percentage Reduction in Thickness with a h_3/h_2 ratio of 2.

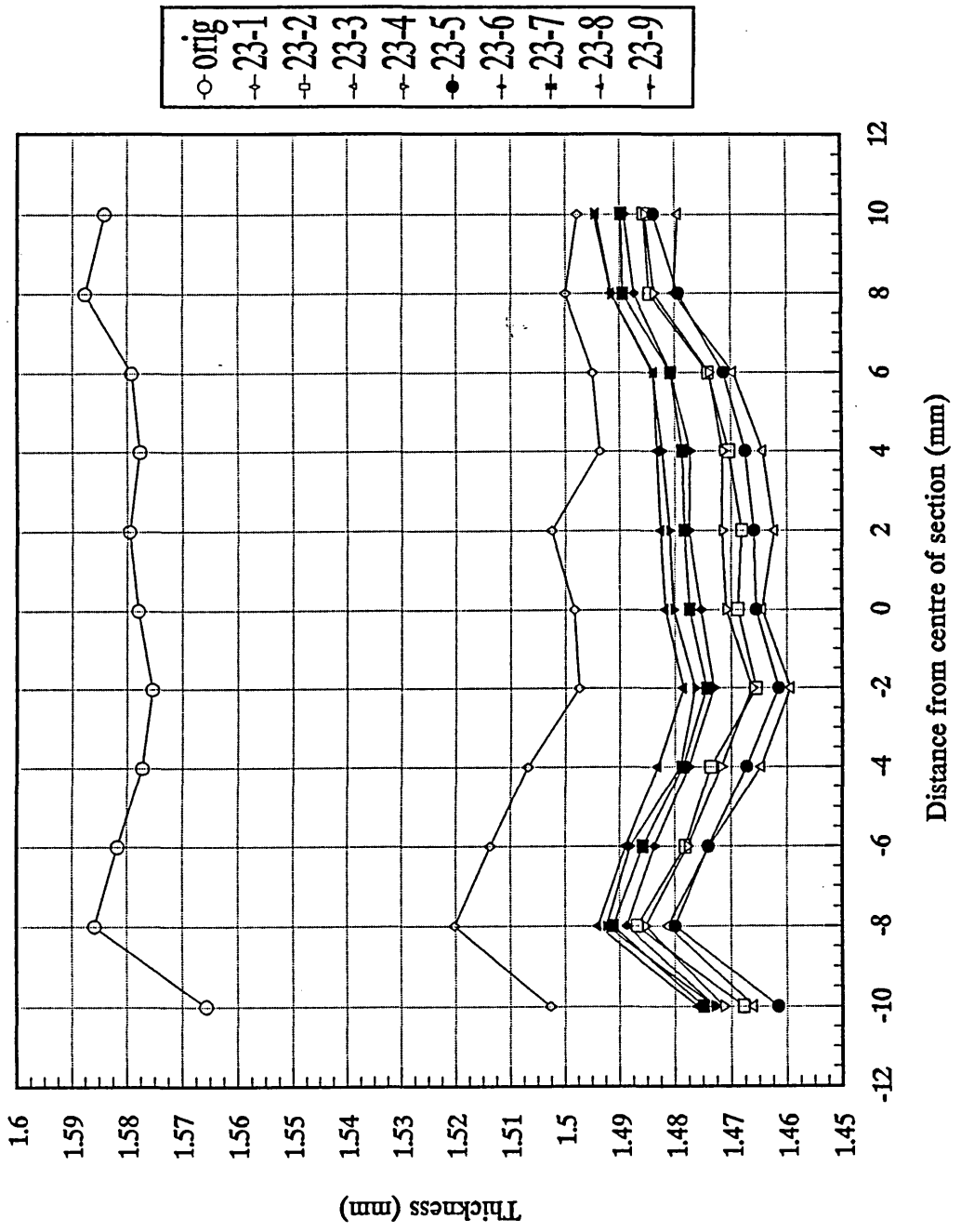

Figure 4.12 - Distribution of cross-section for experiment 23.

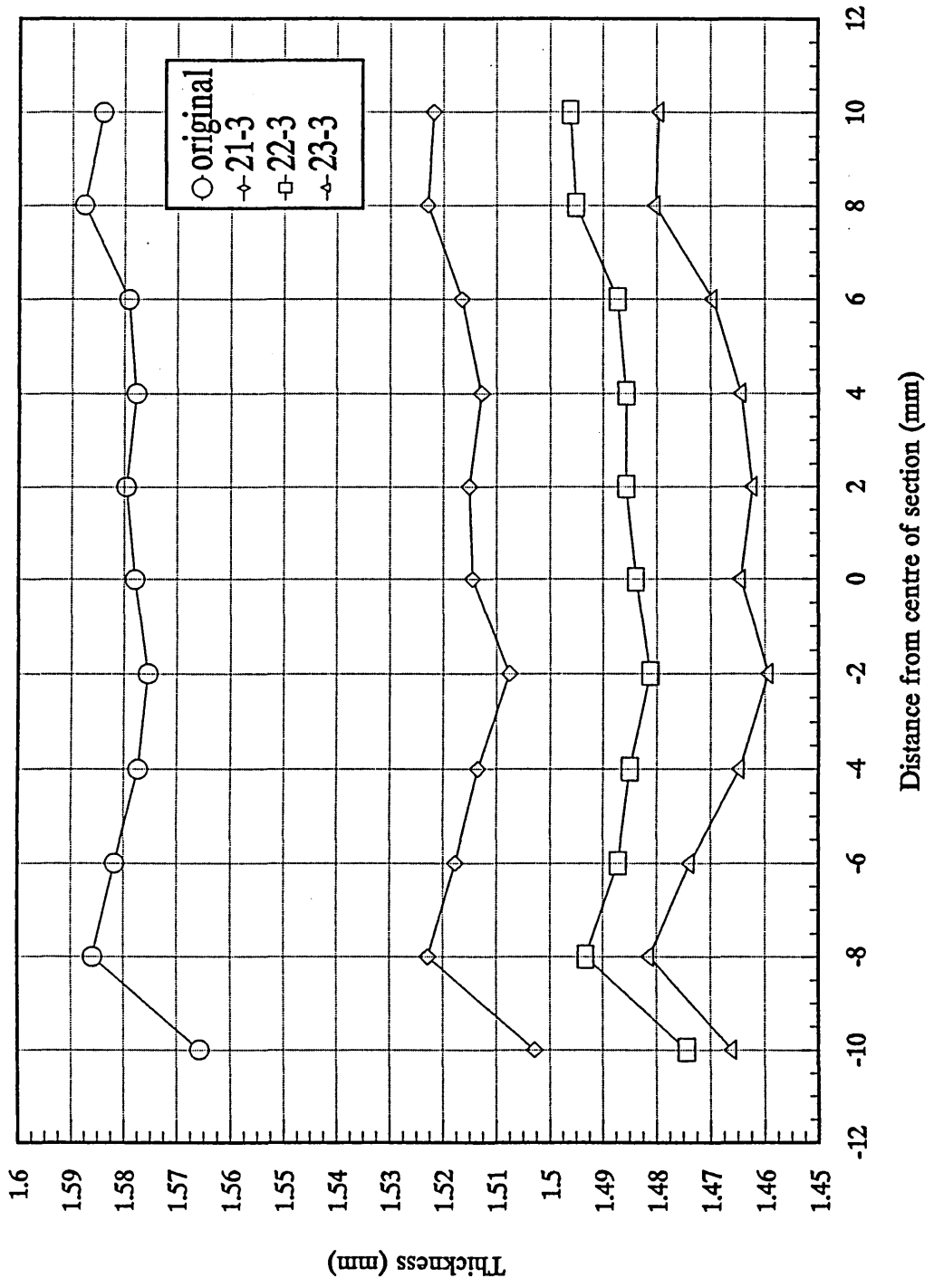

Figure 4.13 - Distribution of cross-section for a larger range of reduction.

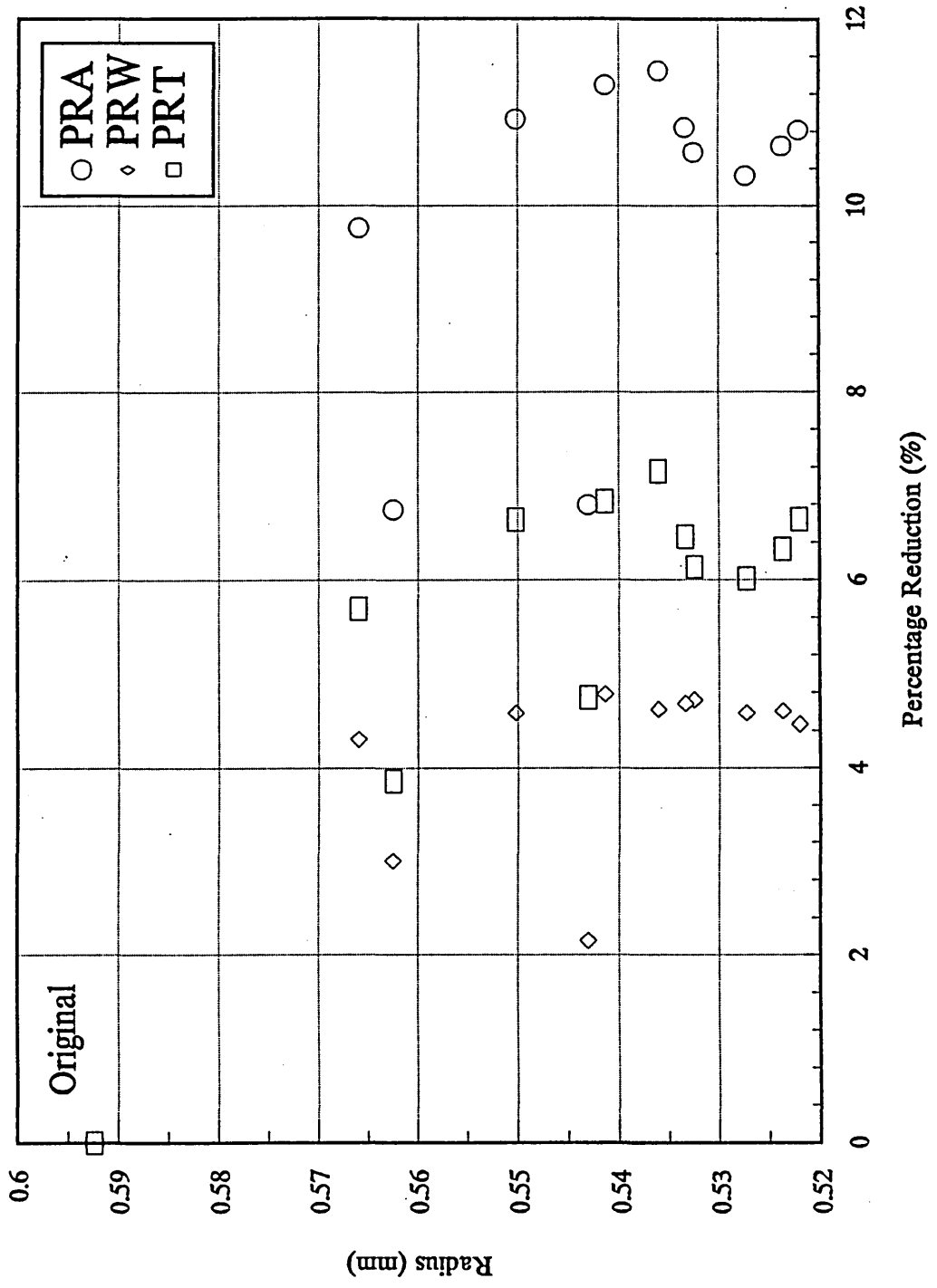

Figure 4.14 - Scatter plot of the cross-section corner radius against reduction.

CHAPTER 5

5.0 Numerical Analysis of the Plasto-hydrodynamic drawing of Rectangular strip

5.1 The Form and Solution of Die-less Drawing Models

5.1.1 The Form of Die-less Drawing Models

A review of previously published models for the Plasto-hydrodynamic drawing process, finds a common form for their development.

1) Statement of the fundamental fluid equations. For a Newtonian analysis the Navier-Stokes equations may be used, but they are invalid for non-Newtonian fluids and the linear momentum equation must be used. The continuity equation is valid for all fluids and may be used as appropriate. A constitutive equation relating the shear stress and shear rate must also be selected, based upon the knowledge of the behaviour of the fluid.

2) Simplifying assumptions are then applied to the flow equations to formulate a specific relationship between the pressure gradient and the strain rate. The nature of the assumptions are dictated by the geometry of the pressure head and the working fluid to be simulated. The shear rate terms will depend upon the constitutive equation selected for the model.

3) Mathematical manipulation of the resultant fluid equations coupled with consideration of the continuity and equilibrium conditions, will allow the determination of the following:

i) the maximum pressure in the inlet section of the pressure head if no deformation were to take place,

ii) the point of initial yield within the inlet section,

iii) the shear stress at the surface of the material to be deformed, both prior and post yielding,

iv) the hydrodynamic pressure within the deformation zone,

v) the axial stress in the deformation zone,

vi) the changes in the pressure head clearances and hence the percentage reduction in section within the deformation zone.

5.1.2 The Solution of Die-less Drawing Models

A numerical procedure is used to solve the system of equations to be derived by the procedure of development described in the previous section. A deformation zone is generated within the pressure head, with the correct combination of working fluid and pressure head geometry. The deformation zone is from the onset of yielding to the step in the pressure head geometry. The step limits the length of the deformation zone, as the pressure gradient will change sign at this point, vastly reducing the surface shear stress.

The algorithm facilitates solution for the deformation zone in steps using finite difference techniques in their explicit form. The slope of deformation $\partial h_1/\partial x$ will be seen to be an unknown quantity in the system of equations. The relationship which is used to determine the value of the slope of deformation is the Plastic Yield Equation (PYE), the derivation of which is given later.

$$P_i + \sigma_{xi} - \sigma_{yi} = 0 \qquad \text{Plastic Yield Equation}$$

The complexity of the expressions for the local pressure, stress in the x direction and yield stress terms in the plastic yield equation given previously, is such that no amount of manipulation will yield an explicit expression for $\partial h_i/\partial x$. Recourse is then made to iterative techniques. Memon (42) demonstrated that the slope of deformation is non-linear, thus an iterative calculation of $\partial h_i/\partial x$ is made at each step in the deformation zone. The overall logic of the solution procedure or algorithm is given below in pseudo code.

```
BEGIN: DETERMINE X1 the distance to the onset of yielding
       IF (X1 > L1) then QUIT
       DO WHILE .not. end of deformation zone
         ITERATE for ∂h1/∂x using 0=Pi+σi-σy
         DETERMINE nodal values of system variables
       ENDDO
       QUIT
END:
```

P 1.0 Pseudo code of the overall solution logic

5.2 The Newtonian Model; derivation and modifications to the modelling of slip

A Newtonian model of the Plasto-hydrodynamic drawing (PHD) process was developed based upon the model presented by Memon (42). The expressions used for the terms of the plastic yield equation are those developed by Memon (42) and are given below.

$$P_i = P_{i-1} + \frac{\partial p}{\partial x}\Delta x$$

$$\sigma_{xi} = \left(\frac{t_{i-1}}{t_i} + \frac{W_{i-1}}{W_i} - 2\right)\sigma_{yi} + \frac{2\tau_{1i}}{t_i}\Delta x + \frac{2\tau_{3i}}{W_i}\Delta x + \sigma_{x\,i-1}$$

$$\sigma_{yi} = S_i\left[\sigma_{yl} + K\left(\ln\left(\frac{W_1 t_1}{W_i t_i}\right)\right)^n\right]$$

The significant difference in the performance of the two models is accounted for in the modification in the way the flow instability of slip is modelled.

5.2.1 The Flow Instability of Slip

Under the action of high shear rates a flow instability termed 'slip' can be seen to occur in the processing of polymer melts. The shear stress at which this flow phenomena occurs is termed 'the critical shear stress'. The presence of slip in a process may be detected by the occurrence of various faults in the output product. Two of the most common faults are: shark skin which forms ridge like structures running transversely to the flow direction, and melt fracture which is denoted by helical or irregular patterns.

Various studies (55-61) have been published which have attempted to identify the parameters governing the onset of melt instability. Whilst no definite conclusions have been drawn, the following points have generally been agreed:

i) the onset of slip occurs at some critical shear stress,

ii) the critical shear stress is not greatly affected by changes in temperature,

iii) the critical shear stress varies in the range of 0.1 to 1.0 MN/m^2 for most polymers,

iv) slip may be demonstrated by a discontinuity in the slope of the shear stress - shear strain curve,

v) the occurrence of slip may be effected by the die entrance shape

and the die surface finish,

vi) the flow instability occurs when non-Newtonian fluids are involved.

5.2.2 The Modelling of Slip

A clearer understanding of the phenomena of slip may be achieved by consideration of figure 5.1, which demonstrates the form of the discontinuity in the flow curve. Given below are the pressure gradient and shear stress equations derived by Memon (42).

$$\left(\frac{\partial p}{\partial x}\right)_i = \frac{1}{h_i^3}\left[\frac{Pm h_1^3}{L_1} + 6\mu(V_i h_i - V h_1)\right]$$

$$\tau_i = -\frac{h_i}{2}\left(\frac{\partial p}{\partial x}\right)_i - \frac{\mu V_i}{h_i}$$

Defining μ as the instantaneous viscosity, which is the local gradient of the shear stress - shear strain rate curve, it can be seen from figure 5.1 that μ falls to zero during the period of the instability. Inspection of the above equation for the pressure gradient reveals that the velocity component is eliminated, leaving only the pressure component. A comparison of the relative magnitudes of the remaining terms, demonstrates a 3 orders of magnitude reduction in the pressure gradient. As a consequence of this, the pressure gradient yields an extremely small increase in pressure from this point forward and thus, to all intents and purposes, the pressure gradient may be regarded as zero. Another justification for this assumption, is by reference to Memon's (42) expression for Pm, the

theoretical maximum pressure that could be generated by this geometry at the stated velocity.

$$Pm = \frac{6\mu V (h_1 - h_2)}{\left(\frac{h_1^3}{L_1} + \frac{h_2^3}{L_2}\right)}$$

Substitution of the zero viscosity condition would render Pm equal to zero, hence eliminating the remaining term in the pressure gradient equation.

Application of the zero pressure gradient and viscosity assumptions to the expression for shear stress would result in a zero shear stress condition, which is inconsistent with the data presented by Tordella (61) and idealised in figure 5.1a.

If the shear strain rate is seen to increase and the shear stress remains constant then the no-slip condition at the flow boundary used by Newton must have been violated. The flow can then be said to be behaving somewhat analogous to a pencil rubber when drawn across a table. The material is under an imposed constant shear stress, but it is slipping at the interface with the table. As such, an assumption of constant shear stress is made after the occurrence of the slip phenomena.

The assumptions previously outlined for the modelling of slip, are consistent with those put forward by Memon (42), even if their justification is not. What then is the modification to the modelling of the slip phenomena? The modification to the modelling of slip is not in the flow assumptions made in the respective models, but to their implementation in the solution algorithm.

5.2.3 Modifications to the solution algorithm

Modifications to the algorithm for the solution of the PYE consist of two distinct parts. Firstly, the position where the algorithm makes the test for the slip condition has been repositioned. Secondly, the form of the test for the condition of slip has been altered. The effect of these changes is examined below.

The test for the condition of slip has been moved from prior to the solution of the deformation zone, to within the solution of the deformation zone. As such, the condition of slip is tested for at every nodal point as the model moves forward through the solution region. This will increase the dynamic response of the algorithm to the onset of slip, in that it will no longer wait until the next velocity in a sequence before using the slip assumptions, but will immediately change the assumptions governing the system of equations. A second outcome of this change, is that it is no longer possible or desirable to keep the pressure distribution constant for all further velocities, a new pressure distribution being calculated for each individual execution of the model.

```
BEGIN: DO FOR specified velocity range
       | DETERMINE X_I the distance to the onset of yielding
       | IF (X_I > L_I) THEN QUIT
       | IF τ_width face > τ_critical THEN slip=.TRUE.
       | DO WHILE .not. end of deformation zone
       | | IF .NOT.SLIP THEN
       | | | USE no-slip flow assumptions
       | | | ITERATE for ∂h_I/∂x using  0 = P_i + σ_i - σ_y
       | | | DETERMINE nodal values of system variables
       | | ELSE
       | | | ASSUME previous non-slip pressure profile is valid
       | | | USE slip flow assumptions
       | | | ITERATE for ∂h_I/∂x using  0 = P_Prev + σ_i - σ_y
       | | | DETERMINE nodal values of system variables
       | | ENDIF
       | ENDDO
       ENDDO
       QUIT
END:
```

P 5.1 Memon's algorithm for the solution of the Plastic Yield Equation

The form of the test for slip was extended, rather than modified, to include the edge of the strip material. The shear stress on the edge of the material is interesting, in that the effective pressure gradient is that of the width face which has been propagated round the cross section in accordance with the hydrostatic assumption. A detailed analysis of the behaviour of the edge shear stress will be given during the following comparison of the various models proposed for the process.

```
BEGIN: GET the entry velocity for the simulation
       DETERMINE X_l the distance to the onset of yielding
       IF (X_l > L_l) THEN QUIT
       DO WHILE .not. end of deformation zone
       | IF τ_width face > τ_critical .OR. τ_edge face > τ_critical THEN slip=.TRUE.
       |  IF .NOT.SLIP THEN
       |  |  USE no-slip flow assumptions
       |  |  ITERATE for ∂h_l/∂x using  P_i + σ_i - σ_y = 0
       |  |  DETERMINE nodal values of system variables
       |  ELSE
       |  |  USE slip flow assumptions
       |  |  P_i = CONSTANT
       |  |  ITERATE for ∂h_l/∂x using  CONSTANT + σ_i - σ_y = 0
       |  |  DETERMINE nodal values of system variables
       |  ENDIF
       ENDDO
       QUIT
END:
```

P 5.2 Modified algorithm for the solution of the Plastic Yield Equation

5.3 The non-Newtonian Model; derivation and assumptions

The non-Newtonian model of the plasto-hydrodynamic process will be developed in two stages;

i) the hydrodynamic modelling,

ii) the plastic deformation of the material.

5.3.1 The Hydrodynamic Model

5.3.1.1 General fluid equations

The Navier-Stokes equations may not be used for the derivation of a non-Newtonian model as Stokes' (62) viscosity law, which is the general form of Newton's viscosity law, is used with the Linear Momentum equations for their derivation. Thus, we may use only those equations which are valid for all fluids. Three equations will be used as the basis for the model and are stated below in their incompressible form:

i) Mass conservation or Continuity

$$\frac{\partial u}{\partial x} + \frac{\partial v}{\partial y} + \frac{\partial w}{\partial z} = 0 \qquad \textbf{(5.1)}$$

ii) Conservation of Linear Momentum

$$\rho g_x - \frac{\partial p}{\partial x} + \frac{\partial \tau_{xx}}{\partial x} + \frac{\partial \tau_{xy}}{\partial y} + \frac{\partial \tau_{xz}}{\partial z} = \rho\left(\frac{\partial u}{\partial t} + u\frac{\partial u}{\partial x} + v\frac{\partial u}{\partial y} + w\frac{\partial u}{\partial z}\right)$$

$$\rho g_y - \frac{\partial p}{\partial y} + \frac{\partial \tau_{yx}}{\partial x} + \frac{\partial \tau_{yy}}{\partial y} + \frac{\partial \tau_{yz}}{\partial z} = \rho\left(\frac{\partial v}{\partial t} + u\frac{\partial v}{\partial x} + v\frac{\partial v}{\partial y} + w\frac{\partial v}{\partial z}\right) \qquad \textbf{(5.2)}$$

$$\rho g_z - \frac{\partial p}{\partial z} + \frac{\partial \tau_{zx}}{\partial x} + \frac{\partial \tau_{zy}}{\partial y} + \frac{\partial \tau_{zz}}{\partial z} = \rho\left(\frac{\partial w}{\partial t} + u\frac{\partial w}{\partial x} + v\frac{\partial w}{\partial y} + w\frac{\partial w}{\partial z}\right)$$

iii) the Power Law constitutive equation

$$\tau_{ij} = K\,(\dot{\gamma}_{ij})^n \tag{5.3}$$

where K = consistency index

n = flow behaviour index

and the fluid is assumed to be isotropic in nature. In double subscript notation; the first is defined as the direction of the normal to the plane associated with the stress, while the second denotes the coordinate direction of the stress itself. Normal stresses have a repeated index, since the stress direction and the normal to the plane on which the stress acts are collinear.

The stress terms in equation 5.2 may be replaced by the appropriate form of the constitutive equation 5.3:

$$\rho g_x - \frac{\partial p}{\partial x} + \frac{\partial\left(K\dot{\varepsilon}_{xx}^{\,n}\right)}{\partial x} + \frac{\partial\left(K\dot{\gamma}_{xy}^{\,n}\right)}{\partial y} + \frac{\partial\left(K\dot{\gamma}_{xz}^{\,n}\right)}{\partial z} = \rho\left(\frac{\partial u}{\partial t} + u\frac{\partial u}{\partial x} + v\frac{\partial u}{\partial y} + w\frac{\partial u}{\partial z}\right) \tag{5.4}$$

$$\rho g_y - \frac{\partial p}{\partial y} + \frac{\partial\left(K\dot{\gamma}_{zx}^{\,n}\right)}{\partial x} + \frac{\partial\left(K\dot{\varepsilon}_{yy}^{\,n}\right)}{\partial y} + \frac{\partial\left(K\dot{\gamma}_{yz}^{\,n}\right)}{\partial z} = \rho\left(\frac{\partial v}{\partial t} + u\frac{\partial v}{\partial x} + v\frac{\partial v}{\partial y} + w\frac{\partial v}{\partial z}\right) \tag{5.5}$$

$$\rho g_z - \frac{\partial p}{\partial z} + \frac{\partial\left(K\dot{\gamma}_{zx}^{\,n}\right)}{\partial x} + \frac{\partial\left(K\dot{\gamma}_{zy}^{\,n}\right)}{\partial y} + \frac{\partial\left(K\dot{\varepsilon}_{zz}^{\,n}\right)}{\partial z} = \rho\left(\frac{\partial w}{\partial t} + u\frac{\partial w}{\partial x} + v\frac{\partial w}{\partial y} + w\frac{\partial w}{\partial z}\right) \tag{5.6}$$

From standard texts on fluid mechanics; $u=V_x$, $v=V_y$, $w=V_z$. Then

$$\dot{\varepsilon}_{xx} = \frac{\partial V_x}{\partial x} = \frac{\partial u}{\partial x} \tag{5.7}$$

$$\dot{\varepsilon}_{yy} = \frac{\partial V_y}{\partial y} = \frac{\partial v}{\partial y} \tag{5.8}$$

$$\dot{\varepsilon}_{zz} = \frac{\partial V_z}{\partial z} = \frac{\partial w}{\partial z} \tag{5.9}$$

$$\dot{\gamma}_{xy} = \dot{\gamma}_{yx} = \left(\frac{\partial V_y}{\partial x} + \frac{\partial V_x}{\partial y}\right) = \left(\frac{\partial v}{\partial x} + \frac{\partial u}{\partial y}\right) \tag{5.10}$$

$$\dot{\gamma}_{xz} = \dot{\gamma}_{zx} = \left(\frac{\partial V_x}{\partial z} + \frac{\partial V_z}{\partial x}\right) = \left(\frac{\partial u}{\partial z} + \frac{\partial w}{\partial x}\right) \tag{5.11}$$

$$\dot{\gamma}_{yz} = \dot{\gamma}_{zy} = \left(\frac{\partial V_y}{\partial z} + \frac{\partial V_z}{\partial y}\right) = \left(\frac{\partial v}{\partial z} + \frac{\partial w}{\partial y}\right) \tag{5.12}$$

Assumptions

i) The flow is steady, laminar and incompressible, and the gap h_1 does not change during the length of L_1 (see figure 5.2). Then, restating equation 5.1

$$\frac{\partial u}{\partial x} + \frac{\partial v}{\partial y} + \frac{\partial w}{\partial z} = 0 \tag{5.1}$$

but v = w = 0 for steady laminar constrained flow, then

$$\frac{\partial u}{\partial x} = 0$$

Thus the velocity V, which equals u cannot change in the direction of the flow (x), resulting in a constant velocity during L_1, assuming no slip.

ii) The width of the material is very large compared to the side gap h_3, with all derivatives of z being equal to zero, thus

$$\frac{\partial}{\partial z} = 0$$

iii) The xz plane is tangential to the earth's surface, then gravity forces in the x and z directions are zero.

Making use of these assumptions and substitution of equations 5.7 - 5.12 into 5.4 - 5.6, yields:

$$-\frac{\partial p}{\partial x} + \frac{\partial\left(K\left(\frac{\partial u}{\partial y}\right)^n\right)}{\partial y} = 0 \qquad \textbf{(5.13)}$$

$$-\frac{\partial p}{\partial y} - \rho g = 0 \qquad \textbf{(5.14)}$$

$$-\frac{\partial p}{\partial z} = 0 \qquad \textbf{(5.15)}$$

Taking equations 5.14 and 5.15 in reverse order.

For equation 5.15

$$\frac{\partial p}{\partial z} = 0$$

If the pressure gradient is zero in the z direction, we therefore have constant pressure in the z direction. This condition has been referred to by some workers as the hydrostatic assumption.

For equation 5.14

$$-\frac{\partial p}{\partial y} - \rho g = 0 \qquad (5.14)$$

$$\frac{\partial p}{\partial y} = -\rho g_y$$

separating variables

$$\int \partial p = \int -\rho g_y . \partial y$$

integrating

$$p = -\rho . g . y + C \qquad (5.16)$$

Equation 5.16 is the hydrostatic pressure equation. It can be shown that C is equal to zero or to atmospheric pressure depending upon whether gauge or

absolute pressure is required.

This demonstrates that the pressure will vary through the film thickness. The maximum value of $y = h_1$ is typically $1x10^{-4}$ in magnitude and, therefore any pressure generated by hydrostatic effects will be very small in comparison to those by hydrodynamic action, and are disregarded.

5.3.1.2 The Model

Equation 5.13 will now be used as the basis of the hydrodynamic model. The analysis will initially be for the general case and then be made specific for a particular land of the pressure head. Restating equation 5.13

$$-\frac{\partial p}{\partial x} + \frac{\partial\left(K\left(\frac{\partial u}{\partial y}\right)^n\right)}{\partial y} = 0 \qquad (5.13)$$

$$\frac{\partial\left(K\left(\frac{\partial u}{\partial y}\right)^n\right)}{\partial y} = \frac{\partial p}{\partial x}$$

integrating w.r.t. y

$$K\left(\frac{\partial u}{\partial y}\right)^n = \frac{\partial p}{\partial x} y + A \qquad (5.17)$$

$$\left(\frac{\partial u}{\partial y}\right) = \left(\frac{\partial p}{\partial x}\frac{y}{K} + \frac{A}{K}\right)^{1/n}$$

int w.r.t. y (function of a linear function rule)

$$u = \frac{1}{\left(\frac{\partial p}{\partial x}\frac{1}{K}\right)^{\left(\frac{1}{n}+1\right)}}\left[\frac{\partial p}{\partial x}\frac{y}{K} + \frac{A}{K}\right]^{\frac{1}{n}+1} + B \qquad (5.18)$$

Boundary Conditions

i) u=V @ y=0 (Strip surface)

ii) u=0 @ y=h (Pressure Head surface)

sub i) in equation 5.18

$$V = \frac{1}{\left(\frac{\partial p}{\partial x}\frac{1}{K}\right)^{\left(\frac{1}{n}+1\right)}}\left[0 + \frac{A}{K}\right]^{\frac{1}{n}+1} + B$$

$$\therefore B = V - \frac{1}{\left(\frac{\partial p}{\partial x}\frac{1}{K}\right)^{\left(\frac{1}{n}+1\right)}}\left(\frac{A}{K}\right)^{\frac{1}{n}+1} \qquad (5.19)$$

sub ii) in equation 5.18

$$0 = \frac{1}{\left(\frac{\partial p}{\partial x}\right)^{\left(\frac{1}{n}+1\right)}}\left[\frac{\partial p}{\partial x}\frac{h}{K} + \frac{A}{K}\right]^{\frac{1}{n}+1} + B \qquad (5.20)$$

sub equation 5.19 into equation 5.20

$$0 = \frac{1}{\left(\frac{\partial p}{\partial x}\frac{1}{K}\right)^{\left(\frac{1}{n}+1\right)}}\left[\left(\frac{\partial p}{\partial x}\frac{h}{K} + \frac{A}{K}\right)^{\frac{1}{n}+1} - \left(\frac{A}{K}\right)^{\frac{1}{n}+1}\right] + V \qquad (5.21)$$

Analysis of equation 5.21 has failed to yield an explicit expression for the constant of integration A.

The volumetric flow rate is defined as:

$$Q = \int_0^h u \, . \, dy$$

$$Q = \int_0^h \left[\frac{1}{\left(\frac{\partial p}{\partial x}\frac{1}{K}\right)^{\left(\frac{1}{n}+1\right)}} \left(\frac{\partial p}{\partial x}\frac{y}{K} + \frac{A}{K} \right)^{\frac{1}{n}+1} + B \right] . \, dy$$

$$Q = \left[\frac{1}{\left(\frac{\partial p}{\partial x}\frac{1}{K}\right)^{2}\left(\frac{1}{n}+1\right)\left(\frac{1}{n}+2\right)} \left(\frac{\partial p}{\partial x}\frac{y}{K} + \frac{A}{K} \right)^{\frac{1}{n}+2} + By \right]_0^h$$

$$Q = \left[\frac{1}{\left(\frac{\partial p}{\partial x}\frac{1}{K}\right)^{2}\left(\frac{1}{n}+1\right)\left(\frac{1}{n}+2\right)} \left(\frac{\partial p}{\partial x}\frac{h}{K} + \frac{A}{K} \right)^{\frac{1}{n}+2} + Bh \right] - \left[\frac{1}{\left(\frac{\partial p}{\partial x}\frac{1}{K}\right)^{2}\left(\frac{1}{n}+1\right)\left(\frac{1}{n}+2\right)} \left(\frac{A}{K} \right)^{\frac{1}{n}+2} \right] \qquad (5.22)$$

We define a function λ such that

$$\lambda(1) = \frac{1}{n} + 1$$

$$\lambda(2) = \frac{1}{n} + 2$$

$$\lambda(m) = \frac{1}{n} + m$$

giving upon substitution of equation 5.19 in equation 5.22

$$Q = \frac{1}{\left(\frac{\partial p}{\partial x}\frac{1}{K}\right)^2 \lambda(1)\lambda(2)}\left[\left(\frac{\partial p}{\partial x}\frac{h}{K} + \frac{A}{K}\right)^{\lambda(2)} - \left(\frac{A}{K}\right)^{\lambda(2)}\right] + \left[V - \frac{1}{\left(\frac{\partial p}{\partial x}\frac{1}{K}\right)\lambda(1)}\left(\frac{A}{K}\right)^{\lambda(1)}\right]h \quad (5.23)$$

For steady state flow;

$$\frac{\partial(Q_1)}{\partial x} = \frac{\partial(Q_2)}{\partial x} = 0$$

hence Q is a constant.

Inspection of equation 5.23 reveals that severe algebraic difficulties prevent an explicit expression for the pressure gradient being derived. However, we may say that prior to the onset of deformation and after the step, all variables in equation 5.23 are constant, x is not included in the expression and that the value of the pressure gradient in these areas must also remain constant. In view of this we may now use the following:

$$\left(\frac{\partial p}{\partial x}\right)_1 = \frac{Pm}{L_1} \quad (5.24)$$

$$\left(\frac{\partial p}{\partial x}\right)_2 = -\frac{Pm}{L_2} \quad (5.25)$$

From our assumption of steady state flow, we may also state

$$Q_1 = Q_2$$
$$Q_1 - Q_2 = 0 \quad (5.26)$$

The term Q_2 in equation 5.26 requires the constants of integration of the velocity equation to be evaluated as applied to the second land. Therefore a

system of three non-linear algebraic equations in three unknowns is formed: equation 5.21 being applied to both the first and second lands, with equation 5.26 utilising equation 5.24 and 5.25 to allow an expression for Pm to be developed.

Solution was attempted by the following iterative method. Equation 5.21 was rewritten to equal R_1, equation 5.26 was rewritten to equal R_2 and 5.21 was applied to the second land and made to equal R_3; appropriate values for the relevant geometric variables being used. When the equations are satisfied then R_1, R_2 and R_3, the residuals, will equal zero:

$$R_1 + R_2 + R_3 = 0$$

It is possible for an error to occur when a permutation of positive and negative residual values cancel each other to produce a false solution to the equations. This may be avoided in the following manner; the residuals are individually squared and then summed to form equation 5.27 below.

$$(R_1)^2 + (R_2)^2 + (R_3)^2 = 0 \qquad (5.27)$$

When the sum of the squared residuals equals zero or is less than a predetermined value of allowable error, then the system of equations is said to be satisfied.

The significance of the constant of integration A should be noted at this time. It is seen with reference to equation 5.17 that the constant A is the shear stress on the width face of the strip.

5.3.1.2.1 Algebraic problems encountered in Power Law equation solution

Algebraic problems encountered in the solution of the system of equations produced by the integration of the velocity equations are of two types:

i) domain errors in evaluation of negative numbers risen to fractional powers,

ii) multi-modality of the solution region.

Each of these problems will be discussed in turn.

Both equations 5.21 and 5.23 require the evaluation of the following term:

$$\left(\frac{A}{K}\right)^{\lambda(n)} \text{ or } \left(\frac{\tau}{K}\right)^{\lambda(n)}$$

Evaluation of such terms is by the use of logarithms, but the shear term in the first land opposes motion and is negative. The logarithm of a negative quantity is unknown, consequently the evaluation of 5.21 and 5.23 is not possible for fractional values of $\lambda(n)$, but only for those values of n which result in an integer value of $\lambda(n)$, such as 0.5 and 0.3333.

The form of the system of equations prohibits the use of gradient methods for their solution. A direct search method was used in an attempt to solve the system of equations. However, the system of equations was found to exhibit multiple solutions in three dimensional space. Analysis of equation 5.26 failed to identify a method of determining the physically realistic solution automatically. A method was then sought to reduce or simplify the system of equations.

5.3.1.2.2 The Reduction of the System of Equations

The dimension of the system of equations may be reduced from three to one if an independent expression for either the hydrodynamic pressure gradient or the shear stress could be derived. Intensive review of the tribological publications relating to the use of power law fluids in all types of bearing revealed a solution for the hydrodynamic pressure gradient. The analysis of Jianming and Gaobing(63) utilised a perturbation solution in the optimisation of a Rayleigh step bearing using a power law fluid. The following expression may be derived from this analysis assuming constant density:

$$Q = \frac{Uh}{2} - \frac{h^3}{12\eta_0 n}\left(\frac{\partial p}{\partial x}\right) \qquad (5.28)$$

where

$$\eta_0 = K\left(\frac{U}{h}\right)^{n-1}$$

Application of continuity of flow allows the pressure distribution both prior to, and after, the onset of deformation to be determined.

5.3.1.2.3 Prediction of Maximum Pressure

Application of continuity with respect to the first and second lands yields:

$$Q_1 = Q_2$$

Substitution of equation 5.28 for the land flow rates, and utilisation of equation 5.24 and 5.25 yields:

$$\frac{Uh_1}{2} - \frac{h_1^3}{12nK}\left(\frac{Pm}{L_1}\right)\left(\frac{h_1}{U}\right)^{n-1} = \frac{Uh_2}{2} + \frac{h_2}{12nK}\left(\frac{Pm}{L_2}\right)\left(\frac{h_2}{U}\right)^{n-1}$$

An explicit expression for Pm may be formed by collecting terms and rearranging, to give equation 5.29:

$$\frac{Pm}{12nKU^{n-1}}\left(\frac{h_2^{n+2}}{L_2} + \frac{h_1^{n+2}}{L_1}\right) = \frac{U}{2}(h_1 - h_2)$$

$$Pm = \frac{6nKU^n(h_1 - h_2)}{\left(\frac{h_2^{n+2}}{L_2} + \frac{h_1^{n+2}}{L_1}\right)} \qquad (5.29)$$

It may be seen by inspection, that equation 5.29 will reduce to Memon's (42) Newtonian equation for the maximum pressure on substitution of n=1 and K=μ.

5.3.1.2.4 Determination of Surface Shear Stress

With Pm known from equation 5.29, equation 5.21 may be solved in isolation to yield A, the surface shear stress. The system of equations has been reduced to one non-linear equation from three and, therefore, any convenient root finding method may now be used for the evaluation of the shear stress. A direct search algorithm has been used successfully.

5.3.1.2.5 Prediction of the point of initial Yielding

The principal stresses acting on the strip prior to deformation are

$$\sigma_1 = \sigma_x \qquad \sigma_2 = -P_1 \qquad \sigma_3 = -P_3$$

but $P_3 = P_1$

$$\sigma_2 = \sigma_3 = -P_1$$

Substitution of these values into the von-Mises yield criterion, yields,

$$\frac{1}{2}\left[(\sigma_1 + P_1)^2 + (-P_1 + P_1)^2 + (-P_1 - \sigma 1)^2\right] = \sigma_y^2$$

simplification yields,

$$\sigma_x + P = \sigma_y \tag{5.30}$$

Assuming that yielding begins at an arbitrary distance X_1 from the entry of the pressure unit, then equilibrium of forces in the x direction will give

$$\sigma_x W t = 2\tau_1 W X_1 + 2\tau_3 t X_1$$

$$\sigma_x = \frac{2\tau_1 X_1}{t} + \frac{2\tau_3 X_1}{W} \tag{5.31}$$

where W and t are the section width and thickness, respectively. Then given a linear pressure profile, from equation 5.23

$$\frac{P_1}{X_1} = \frac{Pm}{L_1}$$

$$P_1 = \frac{Pm}{L_1} X_1 \qquad (5.32)$$

Substitution of equations 5.33 and 5.32 into 5.31 gives

$$\frac{2\tau_1 X_1}{t} + \frac{2\tau_3 X_1}{W} + \frac{PmX_1}{L_1} = \sigma_y$$

$$\therefore \; X_1 = \frac{\sigma_y}{\left(\frac{2\tau_1}{t} + \frac{2\tau_3}{W} + \frac{Pm}{L_1}\right)} \qquad (5.33)$$

5.3.1.2.6 Geometric Variables within the deformation zone

After Memon (42), the numerical solution of the model is now achieved using finite differences. Assuming a linear deformation profile between nodes, then the film thickness h_{1i} and h_{3i} at any point may be evaluated by marching forward from the point of the onset of deformation, using a difference scheme. The implicit and explicit forms are given below:

$$\left(\frac{\partial h}{\partial x}\right) = \frac{h_{i+1} - h_i}{\Delta x} \qquad \textbf{Implicit form}$$

and

$$h_{i+1} = h_i + \left(\frac{\partial h}{\partial x}\right) \Delta x \qquad \textbf{Explicit form}$$

For h_1 and h_3, the film thicknesses:

$$h_{1i+1} = h_{1i} + \left(\frac{\partial h_1}{\partial x}\right)\Delta x \tag{5.34}$$

$$h_{3i+1} = h_{3i} + \left(\frac{\partial h_3}{\partial x}\right)\Delta x \tag{5.35}$$

The deformation may be described by

$$t_{i+1} = t_i - 2\frac{\partial h_1}{\partial x}\Delta x \tag{5.36}$$

$$w_{i+1} = w_i - 2\frac{\partial h_3}{\partial x}\Delta x \tag{5.37}$$

where t and w are the thickness and width dimensions, respectively.

5.3.1.2.7 Prediction of Pressure and Pressure Gradient within the deformation zone

Equation 5.32 enables the pressure at the boundary of the deformation zone to be evaluated. Given a value for the pressure at the boundary of the deformation zone, an explicit finite difference relationship may be used to evaluate the pressure within as the solution moves forward, as with equations 5.34 to 5.37. The difference equation for the pressure in the deformation zone is given overleaf:

$$P_{i+1} = P_i + \frac{\partial p}{\partial x}\Delta x \qquad (5.38)$$

An expression is now required for the pressure gradient, not only for the evaluation of equation 5.38 but as a precursor for the evaluation of the surface shear stresses. Application of continuity with respect to the first land and the flow within the deformation zones yields:

$$Q_1 = Q_i$$

Substitution of:

i) equation 5.28 for the flow rates,

ii) equation 5.24 for the first land pressure gradient and the correct geometric variables yields:

$$\frac{U_1 h_1}{2} - \frac{h_1^3}{12nK}\left(\frac{Pm}{L_1}\right)\left(\frac{h_1}{U_1}\right)^{n-1} = \frac{U_i h_i}{2} - \frac{h_i}{12nK}\left(\frac{\partial p}{\partial x}\right)_i \left(\frac{h_i}{U_i}\right)^{n-1}$$

An explicit expression for the pressure gradient may be formed by collecting terms and rearranging, to yield:

$$\left(\frac{\partial p}{\partial x}\right)_i = \frac{6nK}{h_i^3}\left(\frac{U_i}{h_i}\right)^{n-1}\left[(U_i h_i - U_1 h_1) + \frac{h_1^{n+2}}{6nKU_1^{n-1}}\left(\frac{Pm}{L_1}\right)\right] \qquad (5.39)$$

It may be seen by inspection, that equation 5.39 will reduce to Memon's (42) Newtonian equation for the maximum pressure on substitution of n=1 and K=μ.

5.3.1.2.8 Determination of Surface Shear Stress within the deformation zone

With the local pressure gradient known from equation 5.39, equation 5.21 may be reformed in terms of the local geometry to yield:

$$0 = \frac{1}{\left[\left(\left(\frac{\partial p}{\partial x}\right)_i \frac{1}{K}\right)\left(\frac{1}{n}+1\right)\right]}\left[\left(\left(\frac{\partial p}{\partial x}\right)_i \frac{h_{1i}}{K} + \frac{A}{K}\right)^{\frac{1}{n}+1} - \left(\frac{A}{K}\right)^{\frac{1}{n}+1}\right] + V_i \qquad (5.40)$$

Subsequent solution will yield the local surface shear stress. The edge shear stress τ_3 is found by reforming equation 5.40 in terms of the edge clearance h_{3i} to yield:

$$0 = \frac{1}{\left[\left(\left(\frac{\partial p}{\partial x}\right)_i \frac{1}{K}\right)\left(\frac{1}{n}+1\right)\right]}\left[\left(\left(\frac{\partial p}{\partial x}\right)_i \frac{h_{3i}}{K} + \frac{A}{K}\right)^{\frac{1}{n}+1} - \left(\frac{A}{K}\right)^{\frac{1}{n}+1}\right] + V_i \qquad (5.41)$$

Solution of equation 5.41 will yield the local edge shear stress τ_{3i} (constant of integration A). Equation 5.41 contains the same pressure gradient term as equation 5.40, due to the use of the hydrostatic assumption which imposes a constant pressure around the cross-section of the material and, implicitly, a constant pressure gradient around the cross-section.

5.3.2 Axial Stress in the Deformation Zone

5.3.2.1 Axial Stress due to Homogeneous Deformation

Referring to figure 5.3, from equilibrium of forces in the x direction

$$\sigma_{x_{i+1}} A_{i+1} - \sigma_{x_i} A_i - 2P_{i+\frac{1}{2}} W_{i+\frac{1}{2}} \Delta x \, Sin\alpha - 2P_{i+\frac{1}{2}} t_{i+\frac{1}{2}} \Delta x \, Sin\beta - 2\tau_{1i+\frac{1}{2}} W_{i+\frac{1}{2}} \Delta x \, Cos\alpha$$

$$- 2\,\tau_{3i+\frac{1}{2}}\, t_{i+\frac{1}{2}} \Delta x \, Cos\beta = 0$$

for small values of an arbitrary angle ϕ, Sin $\phi = \phi$ and Cos $\phi = 1.0$. The axial stress at the i+1 node may then be found from,

$$\sigma_{x_{i+1}} = \frac{1}{A_{i+1}}\left[\sigma_{x_i} A_i + 2P_{i+\frac{1}{2}} W_{i+\frac{1}{2}} \Delta x\alpha + 2P_{i+\frac{1}{2}} t_{i+\frac{1}{2}} \Delta x\beta + 2\tau_{1i+\frac{1}{2}} W_{i+\frac{1}{2}} \Delta x + 2\tau_{3i+\frac{1}{2}} t_{i+\frac{1}{2}} \Delta x\right] \qquad (5.42)$$

Equation 5.42 is then the governing equation to evaluate the axial stress in the deformation zone due to homogeneous deformation between two adjacent nodes.

5.3.2.2 Axial Stress in the Deformation zone due to Redundant Work

During the PHD process the working material is reduced in cross-sectional area. It is assumed that for small steps Δx, this reduction may be approximated by a linear profile. The process of deformation will produce internal shear distortion of the workpiece in addition to that required to produce the homogeneous reduction in area over a step. Energy is required to produce this shear deformation and is termed Redundant work, as it makes no useful contribution in effecting the desired change of shape. The following analysis for redundant work follows that presented by Körber and Eichinger (63) in their refined version of Sachs (64) slab analysis of wire drawing. During the PHD process

the material is sheared on 2 planes, because of this the analysis will be applied to both.

Inspection of figure 5.4 reveals that an element distance y from the axis of symmetry, Δx long and dy thick, is sheared through an angle ϕ. The angle ϕ varies from zero at the axis to a maximum of dh1/dx or dh3/dx.

Then, applying the analysis across the thickness of the working material

$$\phi = \left(\frac{2y}{t_{i+\frac{1}{2}}}\right)\frac{\partial h_1}{\partial x}$$

Work done to shear element

$$WD = Force \;.\; Distance$$

$$= \left(\sigma_{sy}\;\Delta x\; W_{i+\frac{1}{2}}\right)\left(dy\left(\frac{2y}{t_{i+\frac{1}{2}}}\right)\frac{\partial h_1}{\partial x}\right)$$

given σ_{sy} is the shear yield stress. The total energy required to shear the section may be found from

$$E = \left(\frac{2.\sigma_{sy}\Delta x W_{i+\frac{1}{2}}}{t_{i+\frac{1}{2}}}\frac{\partial h_1}{\partial x}\right).\int_0^{\frac{1}{2}\left(t_{i+\frac{1}{2}}\right)} y.dy$$

$$= \frac{1}{4}.\sigma_{sy}.\Delta x.W_{i+\frac{1}{2}}\;.\;t_{i+\frac{1}{2}}\;.\frac{\partial h_1}{\partial x}$$

Energy required to shear section / unit volume is then

$$\textit{Energy / Unit Volume} = \frac{1}{4}\sigma_{sy}\frac{\partial h_1}{\partial x}$$

Assuming a constant velocity across the section then

$$\textit{Volumetric flow rate of material} = t_{i+\frac{1}{2}} W_{i+\frac{1}{2}} V_{i+\frac{1}{2}}$$

then, for the power required for redundant work

$$= \frac{1}{4}\sigma_{sy}\frac{\partial h_1}{\partial x}\, t_{i+\frac{1}{2}} W_{i+\frac{1}{2}} V_{i+\frac{1}{2}}$$

Remembering that,

$$\textit{Power} = \textit{Force} \;.\; \textit{Velocity}$$

then, across the thickness

$$\sigma_{redundant} = \frac{1}{4}\frac{\partial h_1}{\partial x}\sigma_{sy} \qquad (5.43)$$

A similar analysis may now be made across the width of the material:

$$\phi_2 = \left(\frac{2y}{W_{i+\frac{1}{2}}}\right)\frac{\partial h_3}{\partial x}$$

Work done to shear element

$$\textit{WD} = \textit{Force} \;.\; \textit{Distance}$$

$$= \left(\sigma_{sy}\ \Delta x\ t_{i+\frac{1}{2}}\right)\left(dy\left(\frac{2y}{W_{i+\frac{1}{2}}}\right)\frac{\partial h_3}{\partial x}\right)$$

given σ_{sy} is the shear yield stress. The total energy required to shear the section may be found from

$$E = \left(\frac{2.\sigma_{sy}\Delta x\ t_{i+\frac{1}{2}}\frac{\partial h_3}{\partial x}}{W_{i+\frac{1}{2}}}\right) \cdot \int_0^{\frac{1}{2}\left(W_{i+\frac{1}{2}}\right)} y.dy$$

$$= \frac{1}{4}.\sigma_{sy}.\Delta x.W_{i+\frac{1}{2}} \cdot t_{i+\frac{1}{2}} \cdot \frac{\partial h_3}{\partial x}$$

Energy required to shear section / unit volume is then

$$\textit{Energy / Unit Volume} = \frac{1}{4}\sigma_{sy}\frac{\partial h_3}{\partial x}$$

Assuming a constant velocity across the section then

$$\textit{Volumetric flow rate of material} = t_{i+\frac{1}{2}}W_{i+\frac{1}{2}}V_{i+\frac{1}{2}}$$

then, for the power required for redundant work

$$= \frac{1}{4}\sigma_{sy}\frac{\partial h_3}{\partial x}\ t_{i+\frac{1}{2}}W_{i+\frac{1}{2}}V_{i+\frac{1}{2}}$$

Remembering that,

$$\textit{Power} = \textit{Force} \cdot \textit{Velocity}$$

then

$$\sigma_{redundant} = \frac{1}{4}\frac{\partial h_3}{\partial x}\sigma_{sy} \qquad (5.44)$$

Both equation 5.43 and 5.44 were integrated over half the section and should be multiplied by a factor of 2. Then, combining equation 5.43 and 5.44 for the total redundant work yields:

$$\sigma_{total\ R.W.} = \frac{1}{2}\sigma_{sy}\left(\frac{\partial h_1}{\partial x} + \frac{\partial h_3}{\partial x}\right)$$

In PHD the value of the shear strain terms (in brackets) change from node to node within the deformation zone. If the current values of the shear strain terms are used then an error will result in the computation. The reason for this is shown in figure 5.5. After the onset of yielding, the stress due to redundant work is evaluated using the angle B_1 over the first step. The use of B_2 for the next step is in error as a part of B_2 equal to B_1 has already been accounted for. To alleviate this problem δB should be used, giving $\delta B_1 = B_1$ for the first node, and $\delta B_2 = B_2 - B_1$ and so forth throughout the deformation zone. Amending equation 5.45 yields:

$$\sigma_{total\ R.W.} = \frac{1}{2}\sigma_{sy}\left[\delta\left(\frac{\partial h_1}{\partial x}\right) + \delta\left(\frac{\partial h_3}{\partial x}\right)\right]$$

and in nodal form within the deformation zone:

$$\sigma_{total\ R.W.} = \frac{1}{2}\sigma_{sy}\left[\delta\left(\frac{\partial h_{1i}}{\partial x}\right) + \delta\left(\frac{\partial h_{3i}}{\partial x}\right)\right] \qquad (5.46)$$

5.3.2.3 Total axial stress in the deformation zone

The total axial stress in the deformation zone may now be found by the summation of equations 5.42 and 5.46 below:

$$\sigma_{x_{i+1}} = \frac{1}{A_{i+1}}\left[\sigma_{x_i}A_i + 2P_{i+\frac{1}{2}}W_{i+\frac{1}{2}}\Delta x\alpha + 2P_{i+\frac{1}{2}}t_{i+\frac{1}{2}}\Delta x\beta + 2\tau_{1i+\frac{1}{2}}W_{i+\frac{1}{2}}\Delta x + 2\tau_{3i+\frac{1}{2}}t_{i+\frac{1}{2}}\Delta x\right]$$

$$+ \frac{1}{2}\sigma_{sy}\left[\delta\left(\frac{\partial h_{1i}}{\partial x}\right) + \delta\left(\frac{\partial h_{3i}}{\partial x}\right)\right] \qquad (5.47)$$

5.4 Strain Hardening within the Deformation Zone

The working material is assumed to behave as a rigid plastic material, with non-linearly strain hardening characteristics. The strain hardening behaviour is assumed to follow a power law form, given below:

$$\sigma_y = \sigma_{oy} + K\varepsilon^n \qquad (5.48)$$

where

σ_y = current yield stress

σ_{oy} = original yield stress

K = strain hardening constant

n = strain hardening index

The longitudinal strain may be evaluated using the theory of volume constancy:

$$\varepsilon_1 + \varepsilon_2 + \varepsilon_3 = 0$$

which for PHD becomes:

$$\varepsilon_x + \varepsilon_W + \varepsilon_t = 0$$

$$\ln\left(\frac{x_i}{x_o}\right) + \ln\left(\frac{W_i}{W_o}\right) + \ln\left(\frac{t_i}{t_o}\right) = 0$$

$$\varepsilon = \ln\left(\frac{x_i}{x_o}\right) = -\ln\left(\frac{W_i t_i}{W_o t_o}\right)$$

This expression may then be substituted into equation 5.48.

5.5 Relationship between $\partial h_1/\partial x$ and $\partial h_3/\partial x$

A relationship between the ratios of the components of strain increment and that of the induced stresses that is applicable to rigid plastic materials, is the Lévy-Mises equations or flow rule, which states:

$$\frac{d\epsilon_x}{\acute{\sigma}_x} = \frac{d\epsilon_y}{\acute{\sigma}_y} = \frac{d\epsilon_z}{\acute{\sigma}_z} = d\lambda \qquad (5.49)$$

or

$$d\epsilon_{ij} = \acute{\sigma}_{ij}\, d\lambda$$

where

$$\acute{\sigma}_i = \sigma_i - \sigma_m$$

given

$$\sigma_m = \frac{\sigma_1 + \sigma_2 + \sigma_3}{3} \qquad \textbf{\{mean normal strain\}}$$

It was previously assumed that $\sigma_1=\sigma_x$, σ_2=-P and σ_3=-P. Consequently $d\varepsilon_1=d\varepsilon_l$, $d\varepsilon_2=d\varepsilon_t$ and $d\varepsilon_3=d\varepsilon_w$

Then from equation 5.49:

$$\frac{d\epsilon_t}{(-P - \sigma_m)} = \frac{d\epsilon_w}{(-P - \sigma_m)}$$

$$\therefore \quad d\epsilon_t = d\epsilon_w$$

$$\therefore \frac{dt_i}{t_i} = \frac{dW_i}{W_i} \qquad \textbf{(5.50)}$$

From equations 5.36 and 5.37 at the onset of yielding or any two contiguous steps:

$$t_i = t_1 - 2\frac{\partial h_1}{\partial x}.\Delta x \qquad \textbf{(5.36)}$$

$$W_i = W_1 - 2\frac{\partial h_3}{\partial x}.\Delta x \qquad \textbf{(5.37)}$$

then

$$dt_i = t_i - t_1 = -2\frac{\partial h_1}{\partial x}.\Delta x$$

$$\Delta x = -\frac{dt_i}{2\frac{\partial h_1}{\partial x}} \qquad (5.51)$$

Again

$$dW_i = W_i - W_1 = -2\frac{\partial h_3}{\partial x}\Delta x$$

thus

$$\Delta x = -\frac{dW_i}{2\frac{\partial h_3}{\partial x}} \qquad (5.52)$$

Equating 5.51 and 5.52

$$\frac{dt_i}{\left(\frac{\partial h_1}{\partial x}\right)} = \frac{dW_i}{\left(\frac{\partial h_3}{\partial x}\right)}$$

$$\frac{\partial h_3}{\partial x} = \frac{dW_i}{dt_i}\frac{\partial h_1}{\partial x}$$

From 5.50

$$\frac{\partial h_3}{\partial x} = \frac{W_i}{t_i}\frac{\partial h_1}{\partial x}$$

$$\frac{\partial h_3}{\partial x} = \frac{\left(W_1 - 2\frac{\partial h_3}{\partial x}\Delta x\right)}{\left(t_1 - 2\frac{\partial h_1}{\partial x}\Delta x\right)}\cdot\frac{\partial h_1}{\partial x}$$

which may be reduced to

$$\frac{\partial h_3}{\partial x} = \frac{W_1}{t_1}\frac{\partial h_1}{\partial x}$$

$$\frac{\partial h_3}{\partial x} = m.\frac{\partial h_1}{\partial x}$$

where m is the aspect ratio of the strip.

5.6 Numerical Solution

All the required relationships have been derived that are required for the modified algorithm to be implemented and the deformatiom to be simulated. The FORTRAN code for the model produced from these equations is given appendix 1.

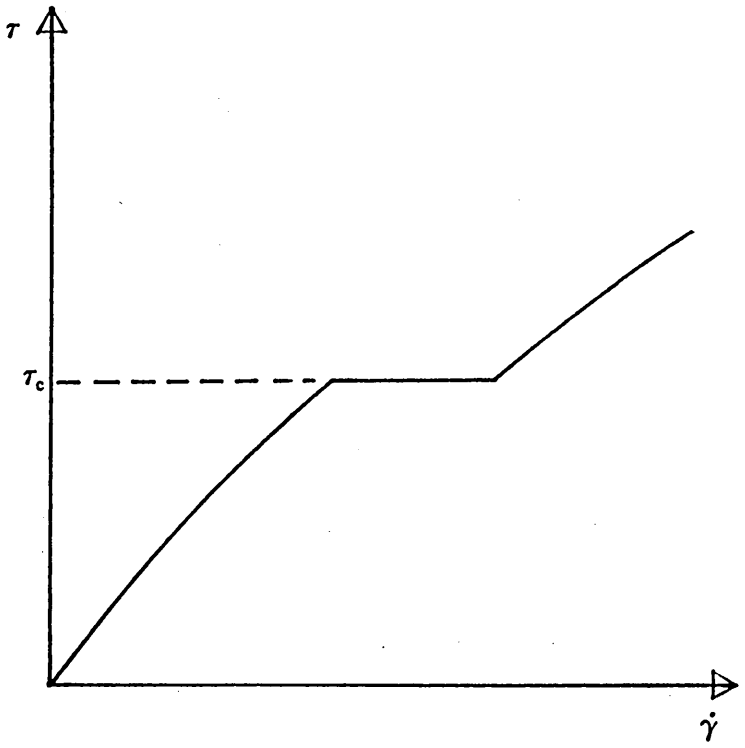

(a)

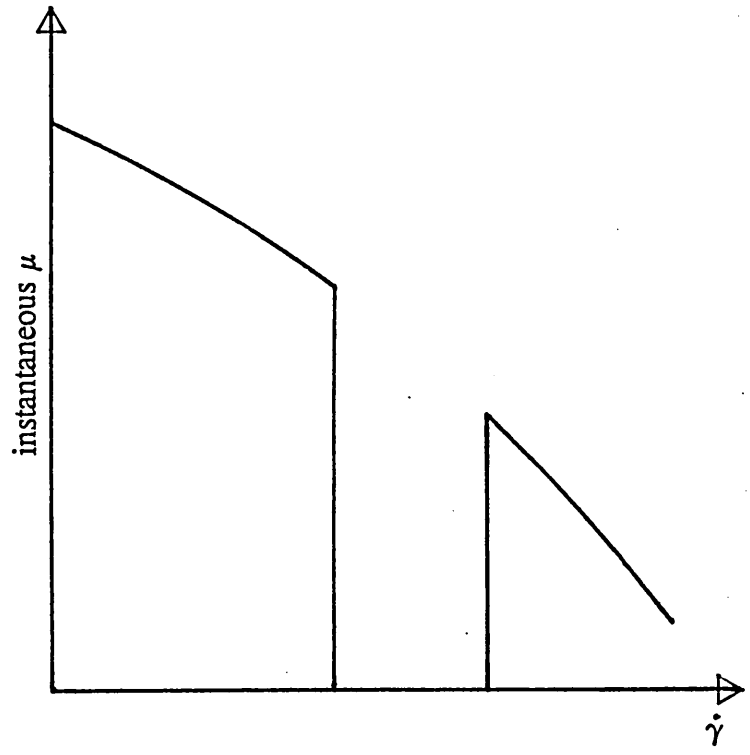

(b)

Figure 5.1 - Schematic diagrams demonstrating the instability of slip.

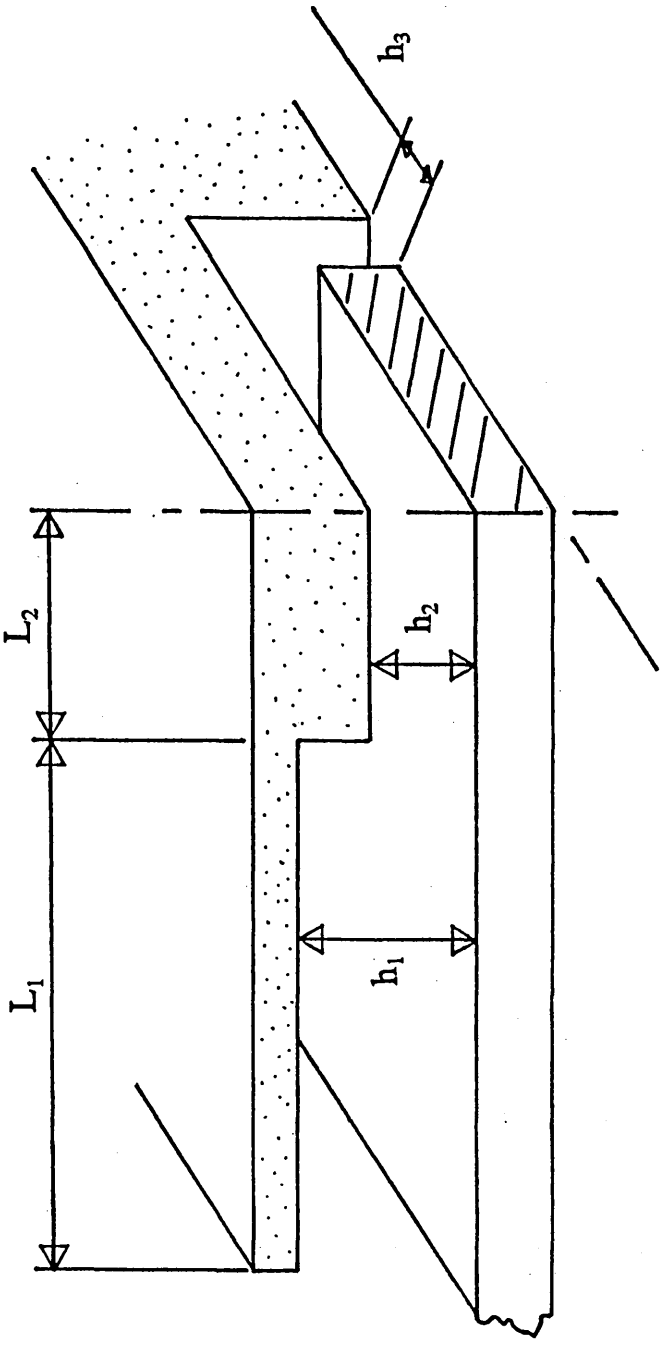

Figure 5.2 - Geometrical parameter definitions for the Plasto-hydrodynamic pressure head.

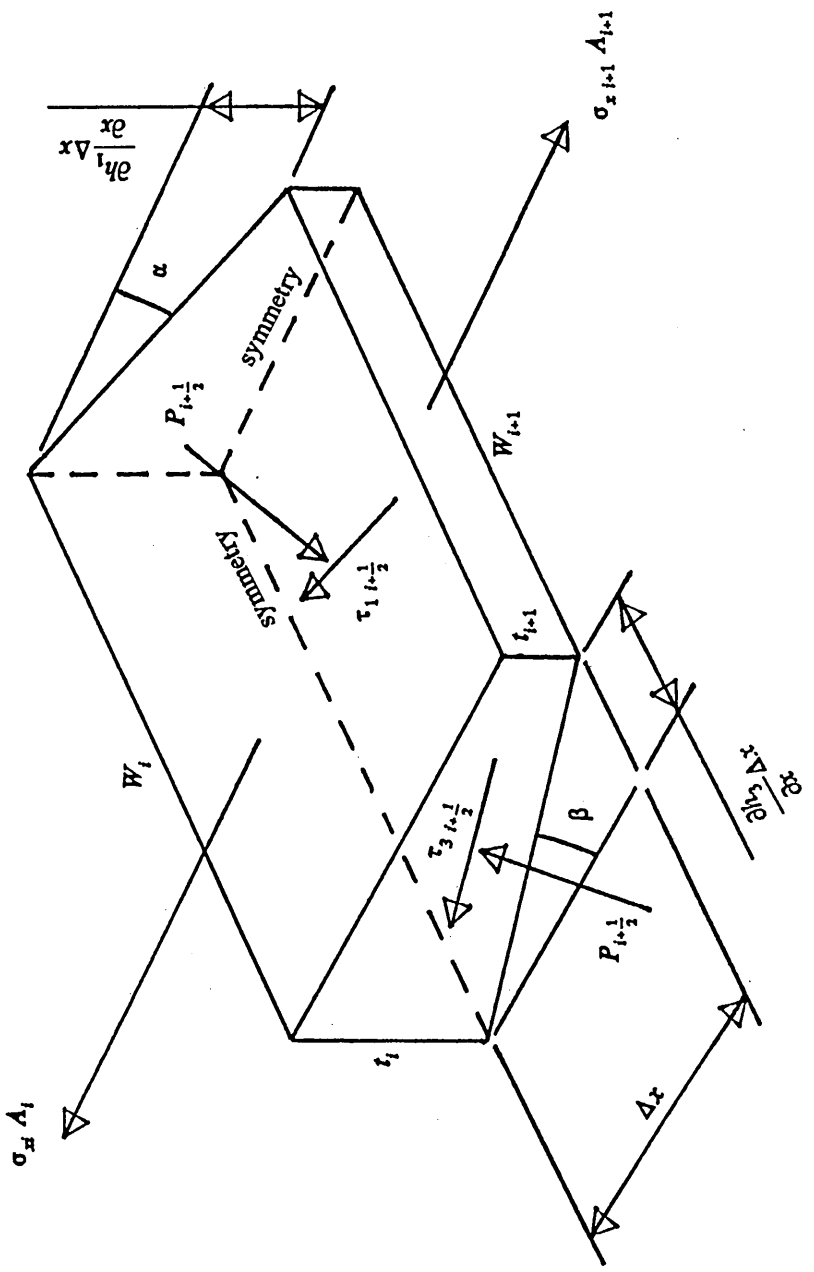

Figure 5.3 - Forces acting on an element of length Δx within the deformation zone.

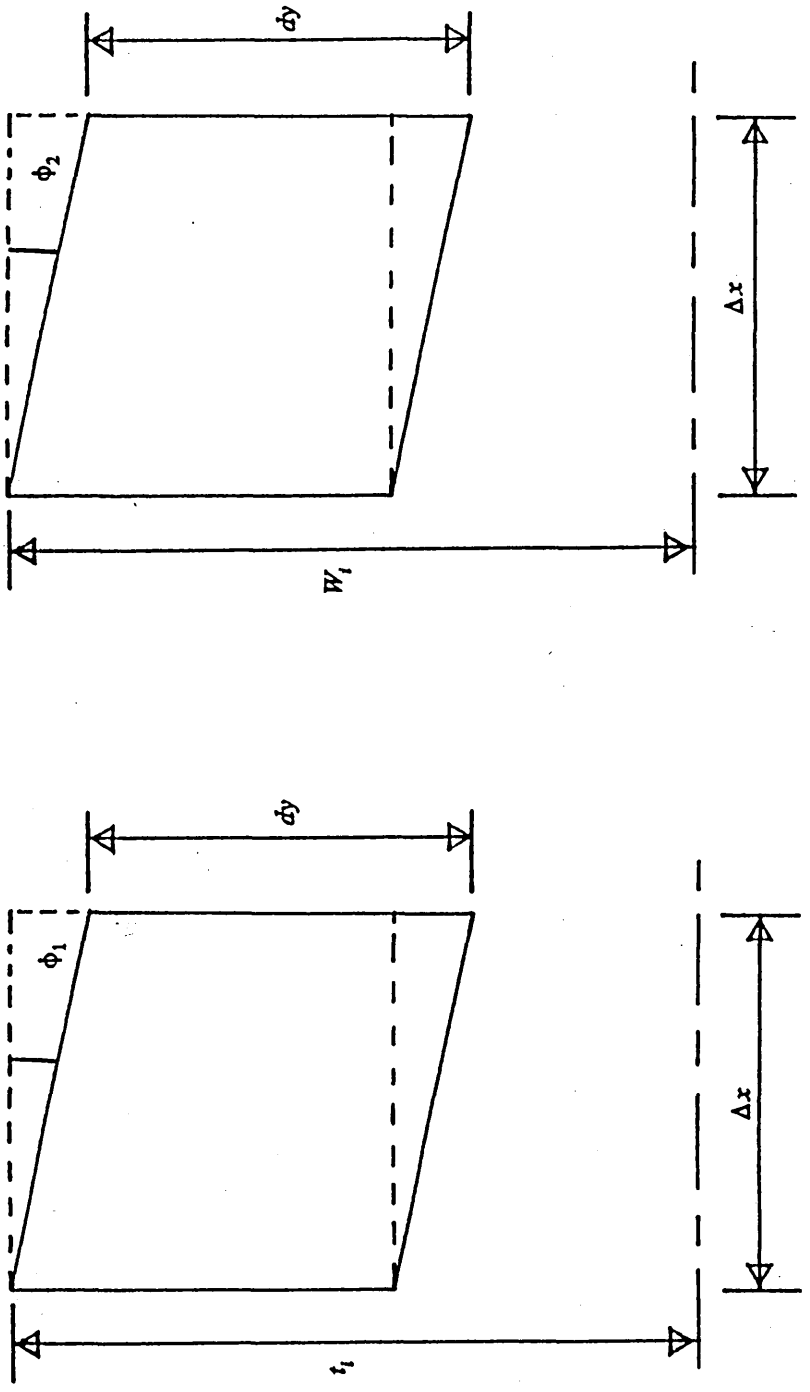

Figure 5.4 - Shear distortion diagrams for the planes used in the Redundant work analysis.

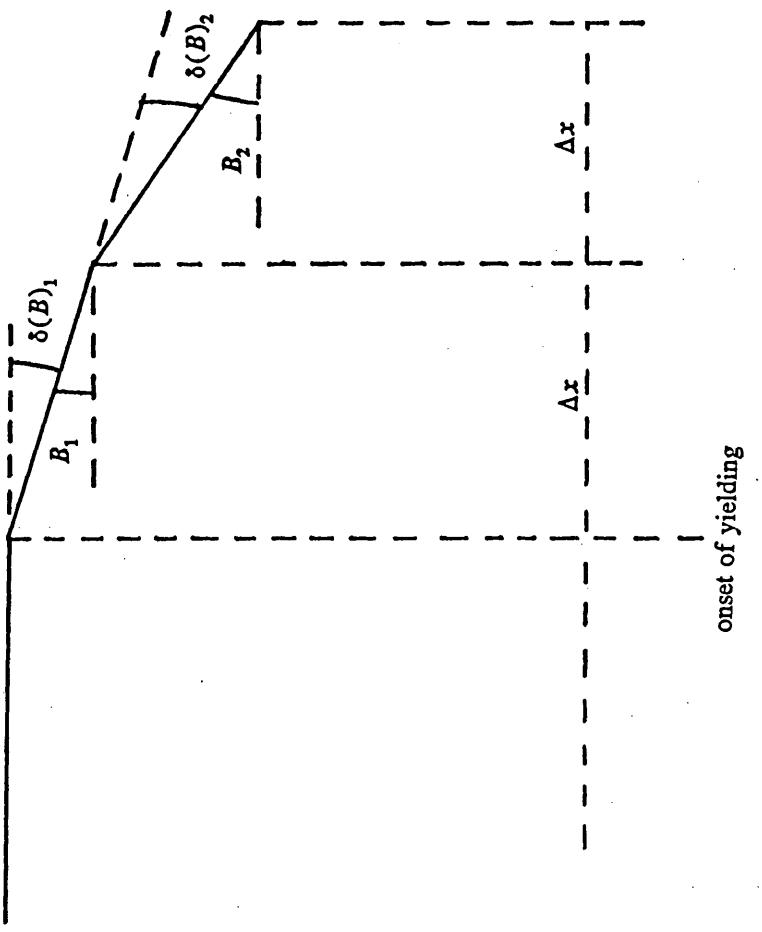

Figure 5.5 - Fundemental definition of δ(B).

CHAPTER 6

6.0 Numerical Optimisation of the Plasto-hydrodynamic deformation process

A Plasto-hydrodynamic pressure head is characterised by five geometrical parameters, L_1, L_2, h_1, h_2 and h_3, the dimensions of the cavity. A consequence of the hydrodynamic nature of the process is an extreme sensitivity to the land and side clearances, and to a lesser extent the land lengths.

The first analysis of a stepped configuration was by Rayleigh (66), who proposed that a linear bearing of this form would yield the maximum load bearing capacity assuming an infinite width. More recent work has been concentrated within two main areas:

a) the finite width Rayleigh bearing,

b) analyses for non-Newtonian lubricants.

Rohde (67) used a finite element model with an applied numerical optimisation algorithm, to modify the standard orthogonal step into a pocket configuration, which predicted an increase in bearing capacity. Kettleborough (68, 69) carried out both experimental and numerical work on pocketed step bearings, but no attempt was made to optimise the profile. Non-Newtonian analyses have recently been presented for Rayleigh step bearings by Elkouh and Yang (70), Wang and Jin (71) and Bourgin and Gay (72), a variety of techniques being utilised for the various analyses.

Prior to the work published by Stokes (73) no application of a formal optimisation method to plasto-hydrodynamic drawing had been presented. The objective of this section is to apply a formal optimisation method to ascertain the pressure head geometry, which would produce maximum deformation for a

specified process velocity.

The following is a brief review of basic optimisation theory as presented by Bunday (74).

6.1 Optimisation of a function of one variable

A function f(x) is said to have a local minimum at some point x_o if, for all values of x in the surrounding region of x_o, f(x) is at least as large as $f(x_o)$. This can further be defined as a global minima, if the surrounding region encompasses all possible values of x. Figure 6.1 details a function f(x). It has both a local and global minima at x_o and x^* respectively.

The classical method for the evaluation of x_o and x^* is to equations which must be satisfied by x_o and x^*. The function given graphically in figure 6.1 is assumed to be continuous. Inspection of the curve for f(x) shows that the derivative f'(x) (gradient) is zero at x_o and x^*. Then x_o and x^* will be solutions of the equation

$$f'(x)=0 \qquad (6.1)$$

The values x_m and x_c, at which there is a local maximum and a point of horizontal inflexion respectively, also satisfy equation 6.1. Thus satisfaction of equation 6.1 is not sufficient to prove a minimum, it is only a necessary condition.

Further inspection of figure 6.1 reveals that at x_o and x^*, f'(x) changes sign, negative to positive. At x_m the sign change is reversed, positive to negative, whilst at the point of inflexion x_c, f'(x) does not change sign. It can be concluded from these observations that, at any minima f'(x) is increasing in value, with the rate of increase being the second derivative f''(x), then

$$f''(x_o)>0 \quad , \quad f''(x^*)>0, \qquad while \quad f''(x_m)<0$$

Proof of these conclusions is by Taylor series expansion of f(x) about the point of interest x_o (x^* or x_m), by an arbitrary increment h.

$$f(x_o+h)-f(x_o)=hf'(x_o)+\frac{h^2}{2!}f''(x_o)+... \qquad (6.2)$$

Inspection of each term in equation 6.2 reveals the following:

i) for x_o to be a minimum the left hand side is non-negative for all values of h within the neighbourhood of x_o,

ii) the first term on the right hand side of equation 6.2 contains $f'(x_o)$ which will be zero at x_o from equation 6.1, thus removing this term,

ii) the next term contains h^2 and $f''(x_o)$, h^2 will be positive for all values of h and as such the derivative term must be positive definite.

Then for a minimum

$$f''(x_o)>0 \qquad (6.3)$$

Using the same method of analysis, point x_m can be shown to be a maximum. To establish which point is the global minimum a comparison must be made of $f(x_o)$ and $f(x^*)$.

6.2 Optimisation of a function of n variables

Given a function of n real variables,

$f(x_1,x_2,x_3,.....,x_n)=f(x)$

where the co-ordinates $(x_1,x_2,x_3,.....,x_n)$ in Euclidean space are denoted by an n dimensional column vector **x**, the gradient of the function $(\partial f/\partial x_1,\partial f/\partial x_2,...,\partial f/\partial x_n)$ is denoted by $\nabla\mathbf{f(x)}$ or in some texts $\mathbf{g(x)}$. The Hessian matrix of $\mathbf{f(x)}$ is denoted by $\mathbf{G(x)}$ and is a symmetric n x n matrix with elements

$$G_{ij}=\frac{\partial^2 f}{\partial x_i \partial x_j}$$

Again the function f(x) is said to have a local minimum at x_o, and as such f(x) must be at least as large as $f(x_o)$ for all points in the neighbourhood of x_o. For the point x_o to be a global minimum x^* then, $f(x) \geq f(x^*)$ for all x.

Equation 6.2 can be generalized using the above definitions to give

$$f(x_o+h)-f(x_o)=\sum_{i=1}^{n} h_i\frac{\partial f}{\partial x_i}(x_1..,x_n)+\frac{1}{2!}\sum_{i=1}^{n}\sum_{j=1}^{n} h_i h_j\frac{\partial^2 f}{\partial x_i \partial x_j}(x_1..,x_n)....$$

$$=h^T\nabla f(x_o)+\frac{1}{2}h^T G(x_o)h+.... \qquad (6.4)$$

Given a minimum of f(x) at x_o, all of the first partial derivatives $\partial f/\partial x_i (i=1...,n)$ must vanish or an appropriate selection of h_i could result in $f(x_o+h)-f(x_o)$ becoming negative. Thus a requisite condition for a minimum at x_o is

$$\nabla f(x_o)=0 \qquad (6.5)$$

$$i.e. \quad \frac{\partial f(x_o)}{\partial x_i} = 0 \quad (i=1,.....,n) \tag{6.6}$$

Then as before, the sign of $f(x_o+h)-f(x_o)$ is determined by that of the second term

$$\frac{1}{2}h^T G(x_o)h \tag{6.7}$$

If $G(x_o)$ is positive definite then equation 6.7 is positive for all h. Thus the required conditions to specify a minimum are

$$\nabla f(x_o)=0, \quad G(x_o) \textit{ positive definite} \tag{6.8}$$

and for a maximum

$$\nabla f(x_m)=0, \quad G(x_m) \textit{ negative definite} \tag{6.9}$$

6.3 Methods of solution

Optimisation theory may be initially separated into linear and nonlinear programming. Linear programming problems are specified by a linear, multi-variable function which is to be maximised or minimised subject to a number of linear constraints. Dantzig (75) developed an algorithm to solve this type of problem termed the simplex method, which in modified form is the basis of modern linear programming theory. Problems that are amenable to solution by linear programming include resource allocation problems in government planning, production planning and the management of transportation distribution systems.

In problems where the assumption of linearity cannot be made, nonlinear programming techniques must be utilised. Specialised techniques have been developed for some problems, but there is no general procedure for nonlinear programming. There are two approaches to nonlinear problems; classical and numerical, with various subdivisions in the latter.

6.3.1 Classical methods

The Classical method is to form equation 6.6, and then solve for n unknowns in n equations, after which equations 6.8 and 6.9 are used to determine whether a maximum or minimum has been found. This requires that the function to be optimised must be differentiable. The present models of the plasto-hydrodynamic drawing process are not closed form, requiring the solution of the Plasto-Hydrodynamic Equation (PHE) at each nodal point within the region of deformation. For this reason classical methods were deemed unsuitable and a numerical approach was pursued.

6.3.2 Numerical methods

Numerical methods have two major subdivisions, unconstrained and constrained optimisation; either class of problem may be solved by direct search or gradient algorithms.

A function is said to be unconstrained if there are no bounds placed upon the possible values which any of the function variables may take. The inverse defines a constrained function; a possible example would be the optimisation of the stresses in a hollow drive shaft with the outside and internal diameters as variables. It would be nonsense for the internal diameter of the shaft to be larger

than the outside diameter.

A direct search method uses repeated evaluations of the function to directly search for the minimum. Various methods have been developed to solve multi-dimensional problems, examples of which are the Simplex method by Nelder and Mead (76) and the pattern based method of Hooke and Jeeves (77).

A gradient method uses the gradient of the function as well as the function value to search for the minimum. Various methods have been developed for multi-dimensional problems, examples of which are the convergent descent method by Fletcher and Powell (78), also the method of conjugate gradients by Fletcher and Reeves (79).

Note that both categories do search for the minimum and as such are search methods. Hooke and Jeeves (77) stated that the advantages of direct search methods over classical are:

> (a) They can produce solutions to problems which have been unsuccessfully attempted by classical methods.
>
> (b) They provide faster solutions for some problems that are solvable by classical methods.
>
> (c) They are well adapted to use on electronic computers, since they tend to use repeated identical arithmetic operations with a simple logic. Classical methods, developed for human use, often stress minimisation of arithmetic by increased sophistication of logic.
>
> (d) They provide an approximate solution, improving all the while, at all stages of the calculation. This feature can be important when a tentative solution is needed before the calculations are completed.
>
> (e) They require (or permit) different kinds of assumptions about the

functions involved in various problems, and thus suggest new classifications of functions which may repay study.

Two points should be noted when using numerical methods. Firstly, all algorithms have a termination criteria or accuracy attached to their use. Secondly, an assumption of uni-modality is made by the methods. A function is uni-modal if it has only one and thus a global minimum. A function with multiple local minima is said to be multi-modal.

6.4 The Merit function

The merit function is an equation, expression or model of a process that is to be subjected to optimisation. The function gives a quantitative result to a particular choice of values for an n dimensional argument vector. The general form of such a function is

$$M = M(x_1, x_2, x_3, \ldots x_n)$$

The merit function in this case is the plasto-hydrodynamic model in whatever form.

6.5 Choice of solution algorithm

The choice of solution algorithm was influenced by the merit function. The plasto-hydrodynamic model is not differentiable in its present form, consequently a direct search method was selected. The method chosen for the optimisation was the pattern search method of Hooke and Jeeves (77). Selection was also influenced by the following:

i) published data for the method demonstrates the method's effectiveness

for multi-dimensional problems,

ii) the logic of the algorithm is relatively uncomplicated, thus aiding the accurate production of the required FORTRAN code for the study.

6.5.1 The Pattern search method of Hooke and Jeeves (77)

The Pattern search method moves through n dimensional Euclidean space towards the function minimum, by separating the movement and the evaluation of direction into two separate processes. These are: i) Local Explorations, ii) Pattern Moves.

Local Explorations are made about the current position vector. This is achieved by incrementing the first term in the position vector by the amount held in the search step length vector, and evaluating the function value. If the returned value is an improvement upon the current function value, then the direction of this change is saved in the pattern vector. If an improvement is not gained, the term is then decremented and tested again. Should this also fail to yield an improvement, then no change is made to the pattern vector. This process is continued until all terms in the position vector have been tested. The result is a vector holding the 'pattern' which has yielded an improved function value.

The logic of the method then states that, since this direction or pattern has yielded an improved function value, it would be reasonable to keep moving in this direction through space. This is achieved by a Pattern Move.

A Pattern Move relocates the current position vector twice the length of the search step length vector, and a Local Exploration is made. If an improvement is found, then the new position is adopted and the process begins again. If the move failed to find an improvement, then the search step length

vector used in the Local Exploration is reduced and a new exploration is made about the current position. This reduction continues until the size of the Euclidean vector formed by the search step length vector falls below a present minimum, thus stopping the process. The overall logic of the method is given below.

The overall logic of the Pattern search method

```
Begin:
    Choose an initial base point b_i {where b is a positional vector, i=1,2... n}
    Choose a search step length h_i for each variable x_i
    1: Explore region about b_1
    IF {Exploration yields an improvement} THEN
        2: Set new base point b_i=b_i+1
        Make a pattern move forming P_i
        Explore region about P_i
        IF {Exploration yields an improvement} THEN
            goto 2
        ELSE
            Decrease step length
            goto 1
        ENDIF
    ELSE
        IF {Search Step less than minimum} THEN
            STOP
        ELSE
            Decrease step length
            goto 1
        ENDIF
    ENDIF
End:
```

The logic for an exploration about an arbitrary point is detailed overleaf followed by equation of the Pattern Move, these procedures being the fundamental units of the method.

Logic for a Local Exploration about a point in n-dimensional space

```
Begin:
    DO for all dimensions
    Increase coordinate by step length h_i
    IF (function reduced) THEN
        Retain new coordinate in b_i+1
        Retain new function value
    ELSE
        Decrease coordinate by step length h_i
        IF (function reduced) THEN
            Retain new coordinate in b_i+1
            Retain new function value
        ELSE
            Keep original coordinate value in b_i+1
            Keep original coordinate value
        ENDIF
    ENDIF
    ENDDO
End:
```

The equation of a Pattern Move

$$P_i = b_i + 2(b_{i+1} - b_i)$$

6.5.2 Optimisation code testing

The logic given above was coded into a FORTRAN subroutine. Before application of the code to the plasto-hydrodynamic model the correctness of the code was tested by the use of Rosenbrock's (80) parabolic valley function, below

$$f(x_1,x_2) = 100(x_2 - x_1^2)^2 + (1 - x_1)^2 \qquad \textit{Rosenbrock's function}$$

which has a global minimum at x=(1,1). The form of the function is given graphically in figure 6.2. The optimisation code successfully found the minimum in 30 iterations, which is comparable to that taken by the conjugate gradient

method of Fletcher and Reeves.

6.6 The Optimisation procedure

The optimisation program allows the specification of an array of start points and the entry velocity for the optimisation process. Multiple applications of the optimisation process are made on the merit function to establish confidence in the result, as it is possible for the shape of the n-dimensional surface to have local minimums, and/or the optimisation algorithm to detect false minimums, because of badly chosen search step lengths/initial positions. The procedure was then to start the process away from any expected optimum point, in an attempt to force the algorithm to find its own optimum. The start point, end point and the percentage reduction in area achieved at the end point, were saved to a data file for later evaluation.

6.7 The merit functions and optimisation programme

As stated previously, five dimensions are required to define the geometry of plasto-hydrodynamic pressure head, L_1, L_2, h_1, h_2 and h_3, which form a 5 dimension problem. The order of the problem was reduced from 5 to 3 by the use of ratios. Defined thus,

$$x_1 = L_1/L_2$$

$$x_2 = h_1/h_2$$

$$x_3 = h_3/h_2$$

given that the overall length of the pressure head and the clearance h_2 were held constant.

The material and fluid properties are declared as constants in the code and are for pure copper strip and a generic form of polyethylene. The material property values used for the non-Newtonian merit function are essentially the same as that for the Newtonian, except for the following differences:

i) the Newtonian viscosity constant is not used, instead the power law constant and power law index are utilised by the function,

ii) strain rate sensitivity is not included in the power law model and as such the strain rate sensitivity data is not applicable.

The data used by both merit functions is given in table 6.1.

6.7.1 The Plasto-hydrodynamic Newtonian merit function

The model used for the Newtonian merit function is that described in section 5.2, using the equations developed by Memon (42) and the modifications to the solution algorithm presented in chapter 5. A full listing of the FORTRAN code for the Newtonian optimisation program is given in appendix 2.1.

6.7.2 The Plasto-hydrodynamic non-Newtonian (Power Law) merit function

The non-Newtonian merit function uses the non-Newtonian (power law) model developed in chapter 5. A full listing of the FORTRAN code for the non-Newtonian optimisation program is given in appendix 2.2.

6.7.3 The Optimisation Programme

The optimisation programme consisted of three sections:-

Multi point optimisation sequences using the Newtonian merit function were made to determine the effect of the velocity on the optimum pressure head geometry. The sequences explored the velocity range of 0.1 - 0.4 m/s in steps of 0.05 m/s.

The velocity range specified above was repeated using the non-Newtonian merit function. This was in order to establish a correlation between the non-Newtonian merit function, simulating a Newtonian fluid (n=1), and the Newtonian merit function.

Finally, the effect of non-Newtonian fluid behaviour on the optimum pressure head geometry was assessed, by repeating the multi point optimisation sequence over the same velocity range as the Newtonian and correlation sequences.

Figure 6.3 shows in 3 dimensional space a sample array of start points and end points of a typical analysis as a scatter diagram. The space shown may be considered to be a scalar field, in that each point in space has an associated magnitude but no direction. This is analogous to the temperature distribution in a three dimensional body. Although this representation is accurate, a clearer understanding is gained from orthogonal views of such space and these are used later.

6.8 Optimisation Results

6.8.1 Newtonian model optimisation results

Figures 6.4 - 6.10 give 3 orthogonal views of a 3D scatter plot of start/end points for each entry velocity. The mean value for each variable at each velocity step is given in table 6.2 and is presented graphically in figure 6.11. Table 6.3 gives the standard deviation of each variable at each velocity step and is shown graphically in figure 6.12.

6.8.2 Non-Newtonian optimisation Results

6.8.2.1 Correlation between the Power Law and Newtonian merit functions

The results of the power law Newtonian (n=1) sequence are presented in tabular form in tables 6.4 (mean value) and 6.5 (standard deviation). Graphical interpretations of the data are given in figures 6.13 - 6.19. Graphical summaries are given in figures 6.20 (mean values) and 6.21 (standard deviations).

6.8.2.2 Effect of Non-Newtonian fluid behaviour

The results of the power law non-Newtonian sequence are presented in tabular form in tables 6.6 (mean value) and 6.7 (standard deviation). Graphical interpretations of the data are given in figures 6.22 - 6.28. Graphical summaries are given in figures 6.29 (mean values) and 6.30 (standard deviations).

Table 6.1 Merit function material properties

Merit Function Material Properties	Newtonian f(x)	Non-Newtonian f(x)
Viscosity N/s	120	n/a
Power Law consistency constant	n/a	120 or 25000
Power Law index	n/a	1 or 0.33333
Critical Shear Stress MN/m^2	0.32	0.32
Yield Stress MN/m^2	70	70
Strain Hardening index	0.6	0.6
Strain Hardening constant	600	600
Strain Rate Sensitivity constant	3.8	n/a
Strain Rate Sensitivity index	55000	n/a
Width mm	25.4	25.4
Thickness mm	1.59	1.59
Overall length mm	180	180
h_2 step land clearance mm	0.02	0.02

Table 6.2 Mean function values for Newtonian optimisation sequences

	Mean values of merit function variables			
Velocity	L_1/L_2	h_1/h_2	h_3/h_2	P.R.A.
0.1	25.0865	5.1245	1.001	9.83449
0.15	21.4429	7.24625	1.559	9.34354
0.2	17.6084	8.8453	2.160	8.90071
0.25	28.3665	10.4587	2.778	8.7391
0.3	28.8697	12.0142	3.428	8.32282
0.35	38.338	13.4056	4.130	7.96573
0.4	65.4311	14.9782	4.80	7.70613

Table 6.3 Standard deviations for the Newtonian optimisation sequences

	Standard deviations of merit function variables			
Velocity	L_1/L_2	h_1/h_2	h_3/h_2	P.R.A.
0.1	10.8445	0.257952	0.00351355	0.104956
0.15	6.2183	0.153191	0.00790158	0.2000089
0.2	7.81611	0.105956	0.0100012	0.236915
0.25	7.87859	0.125471	0.0151068	0.089066
0.3	11.4469	0.0866103	0.0152876	0.116584
0.35	15.7719	0.134531	0.0314687	0.141113
0.4	8.51273	0.0847327	0.0212222	0.0282338

Table 6.4 Mean function values for the Non-Newtonian correlation data

	Mean values of merit function variables			
Velocity	L_1/L_2	h_1/h_2	h_3/h_2	P.R.A.
0.1	34.4889	5.00129	1.26549	10.0933
0.15	29.3642	7.13631	1.60948	9.9352
0.2	30.9082	8.90088	2.18583	9.56429
0.25	28.0797	10.7461	2.78307	9.20269
0.3	24.0943	12.1949	3.4213	8.87311
0.35	37.8673	13.7368	4.07202	8.5223
0.4	51.0822	15.2387	4.77531	8.14635

Table 6.5 Standard deviations for the Non-Newtonian correlation data

	Standard deviations of merit function variables			
Velocity	L_1/L_2	h_1/h_2	h_3/h_2	P.R.A.
0.1	11.9737	0.293287	0.663519	0.37274
0.15	8.71265	0.259069	0.0222441	0.0689366
0.2	4.00317	0.268701	0.0234229	0.0425776
0.25	10.3344	0.25081	0.0450921	0.149206
0.3	7.61495	0.210057	0.0345471	0.0523116
0.35	13.5388	0.172893	0.0393446	0.0820465
0.4	19.8696	0.0804685	0.0266115	0.090566

Table 6.6 Mean function values for the Non-Newtonian optimisation sequences

	Mean values of merit function variables			
Velocity	L_1/L_2	h_1/h_2	h_3/h_2	P.R.A.
0:1	22.0193	6.72982	1.57173	10.2524
0.15	24.0063	8.89162	2.75772	9.55771
0.2	23.1096	11.1	4.79335	8.30515
0.25	27.922	13.4764	7.07218	6.68342
0.3	40.0581	16.1862	8.40996	5.22493
0.35	47.2365	19.1433	9.98123	4.1191
0.4	55.2568	22.0437	12.8215	3.36849

Table 6.7 Standard deviations for the Non-Newtonian optimisation sequences

	Standard deviations of merit function variables			
Velocity	L_1/L_2	h_1/h_2	h_3/h_2	P.R.A.
0.1	4.32386	0.428734	0.0367016	0.0777017
0.15	6.81155	0.29614	0.078876	0.102866
0.2	3.17104	0.137886	0.521752	0.172934
0.25	3.85538	0.256771	0.934669	0.253306
0.3	8.51912	0.423074	0.992194	0.264345
0.35	7.16997	0.525901	1.54599	0.243374
0.4	8.65922	0.546227	4.08478	0.185862

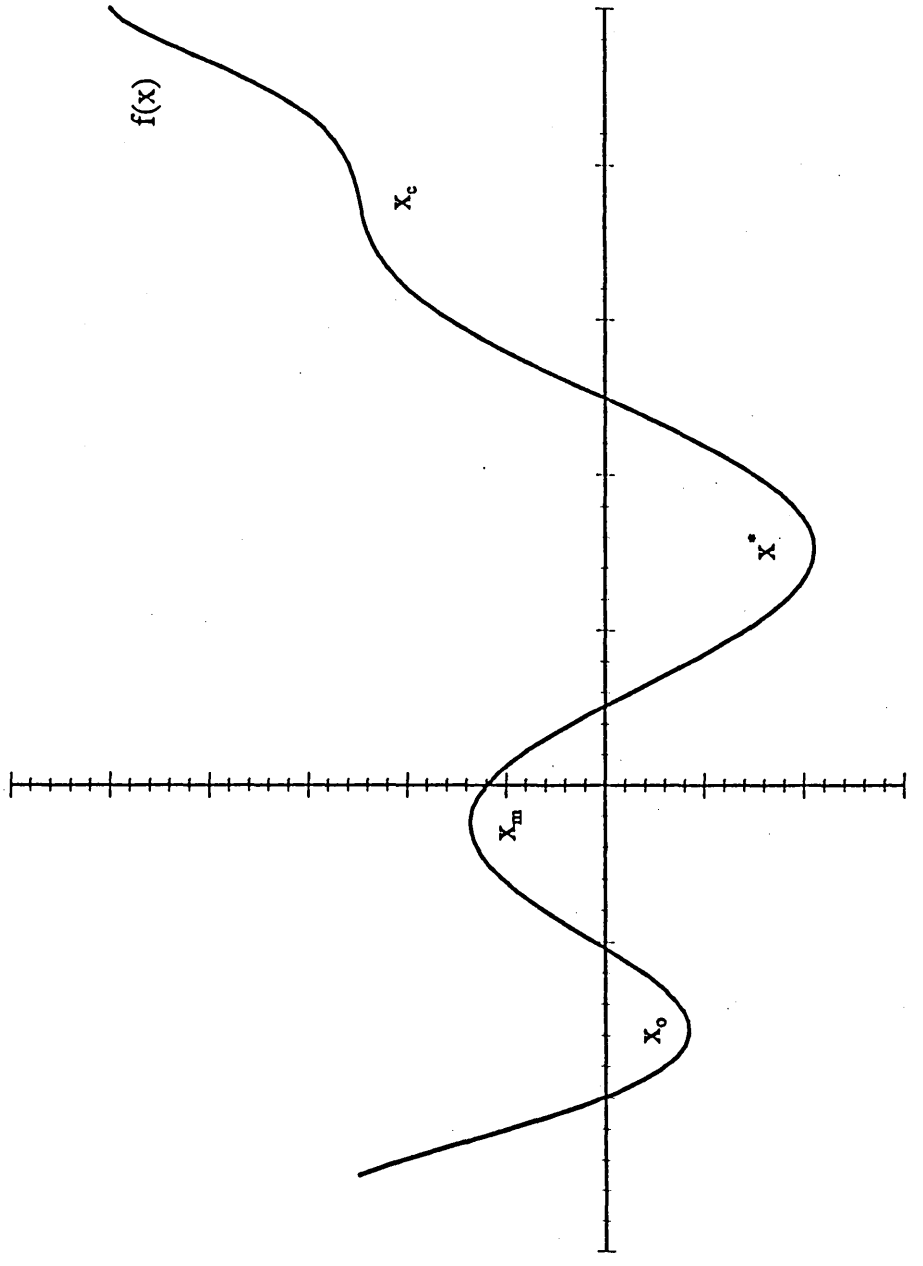

Figure 6.1 - Local and global minima for an arbitary function f(x).

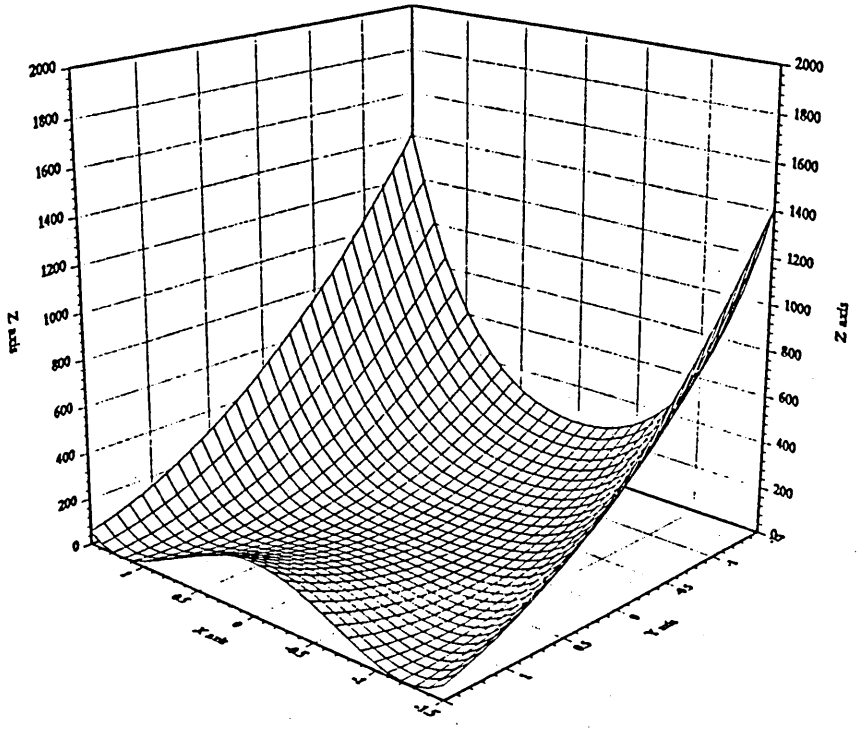

(a)

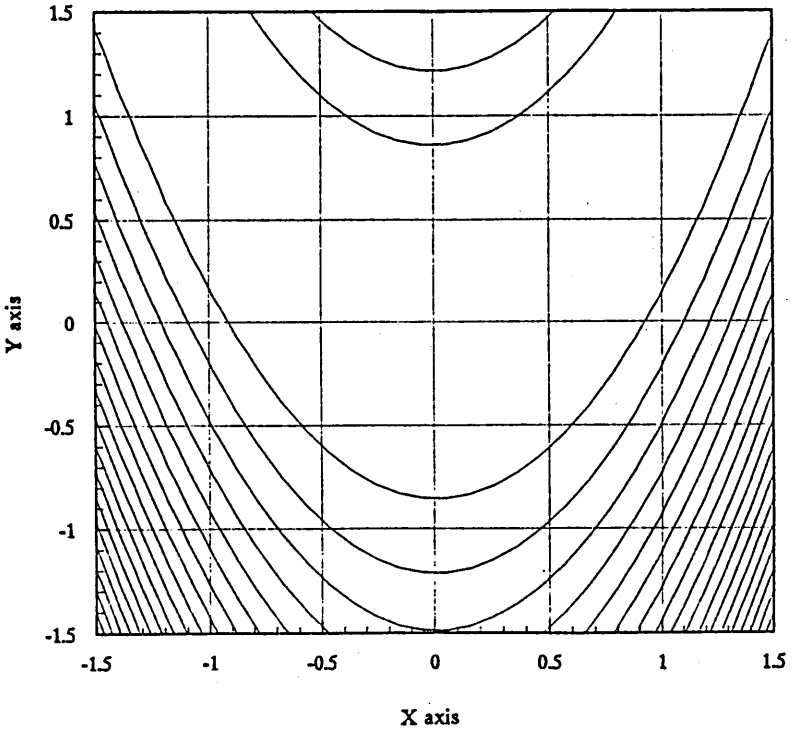

(b)

Figure 6.2 - Rosenbrock's parabolic valley function: a) surface plot, b) topological plot.

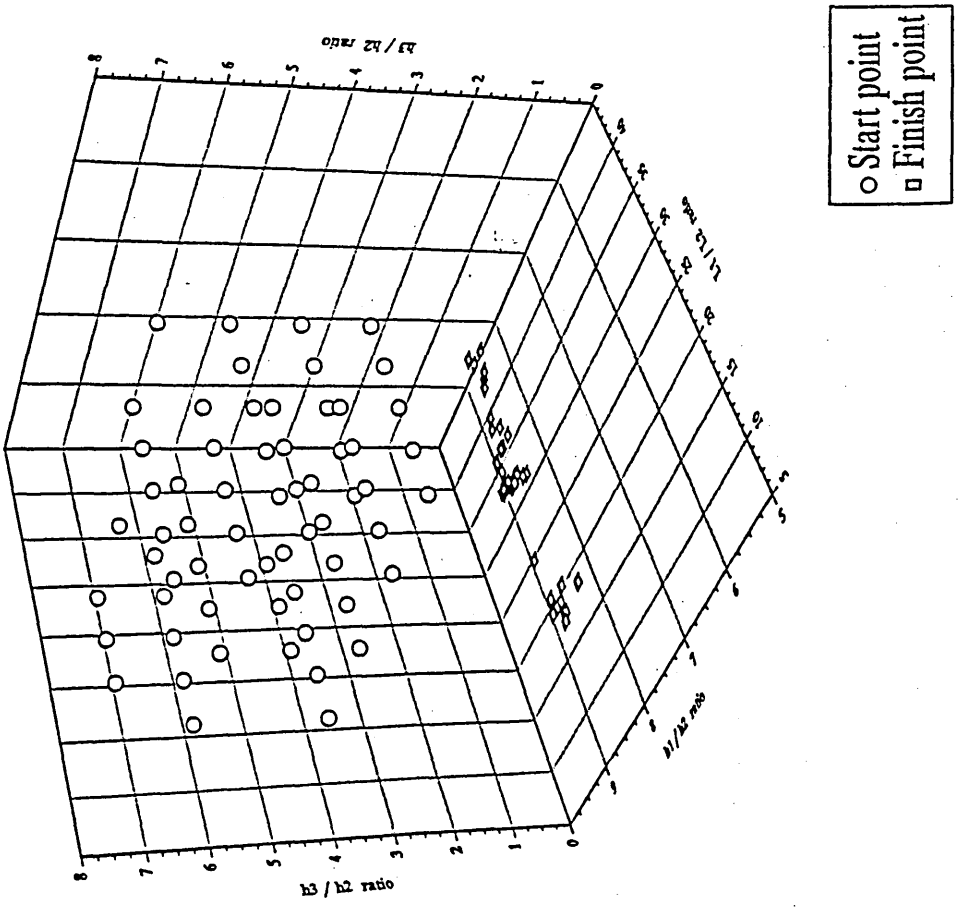

Figure 6.3 - Three dimensional scatter plot showing arrays of start and finish points of an optimisation sequence.

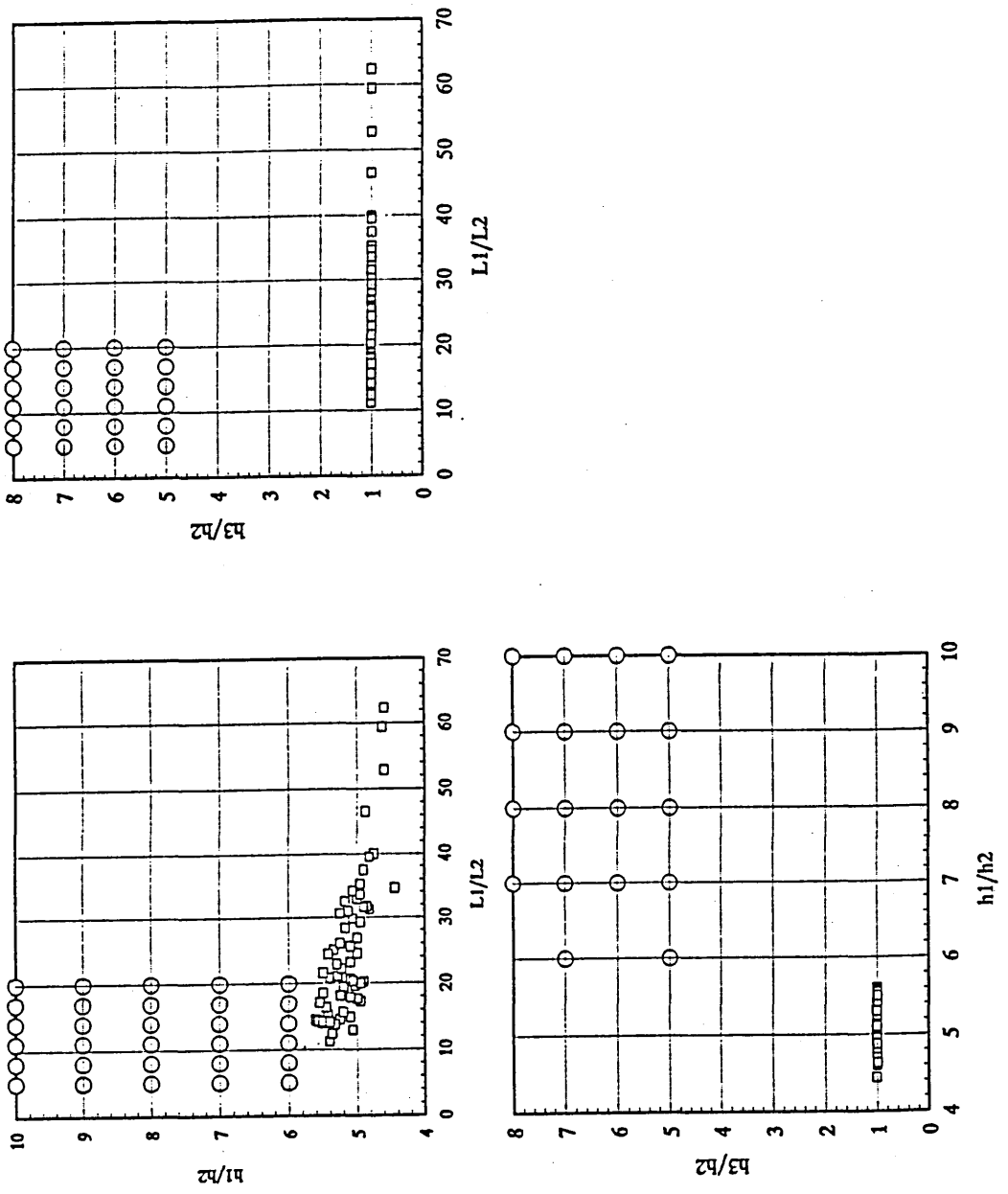

Figure 6.4 - Orthogonal views of the 3 dimensional scatter plot produced by the optimisation sequence for an entry velocity of 0.1 m/s.

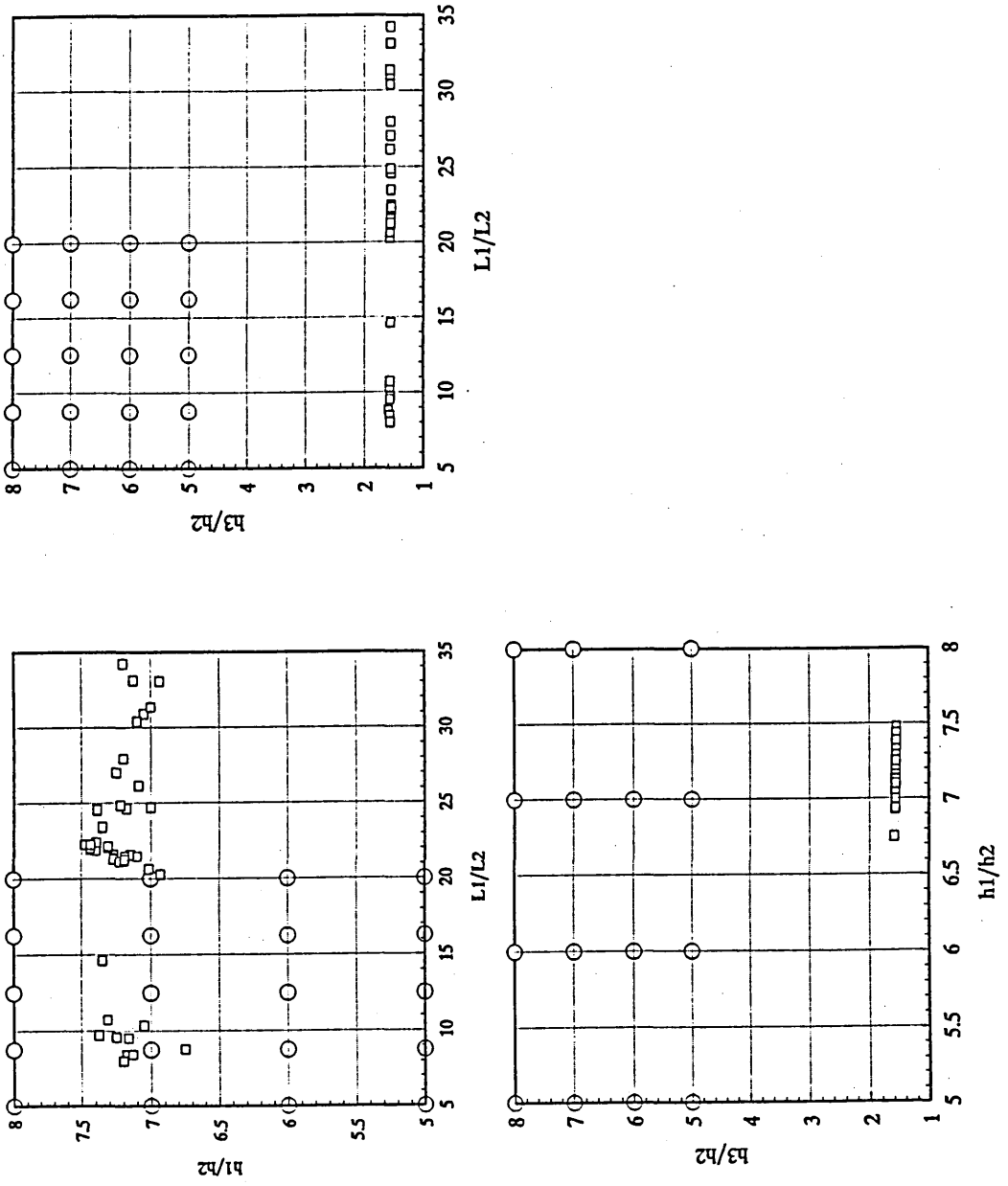

Figure 6.5 - Orthogonal views of the 3 dimensional scatter plot produced by the optimisation sequence for an entry velocity of 0.15 m/s.

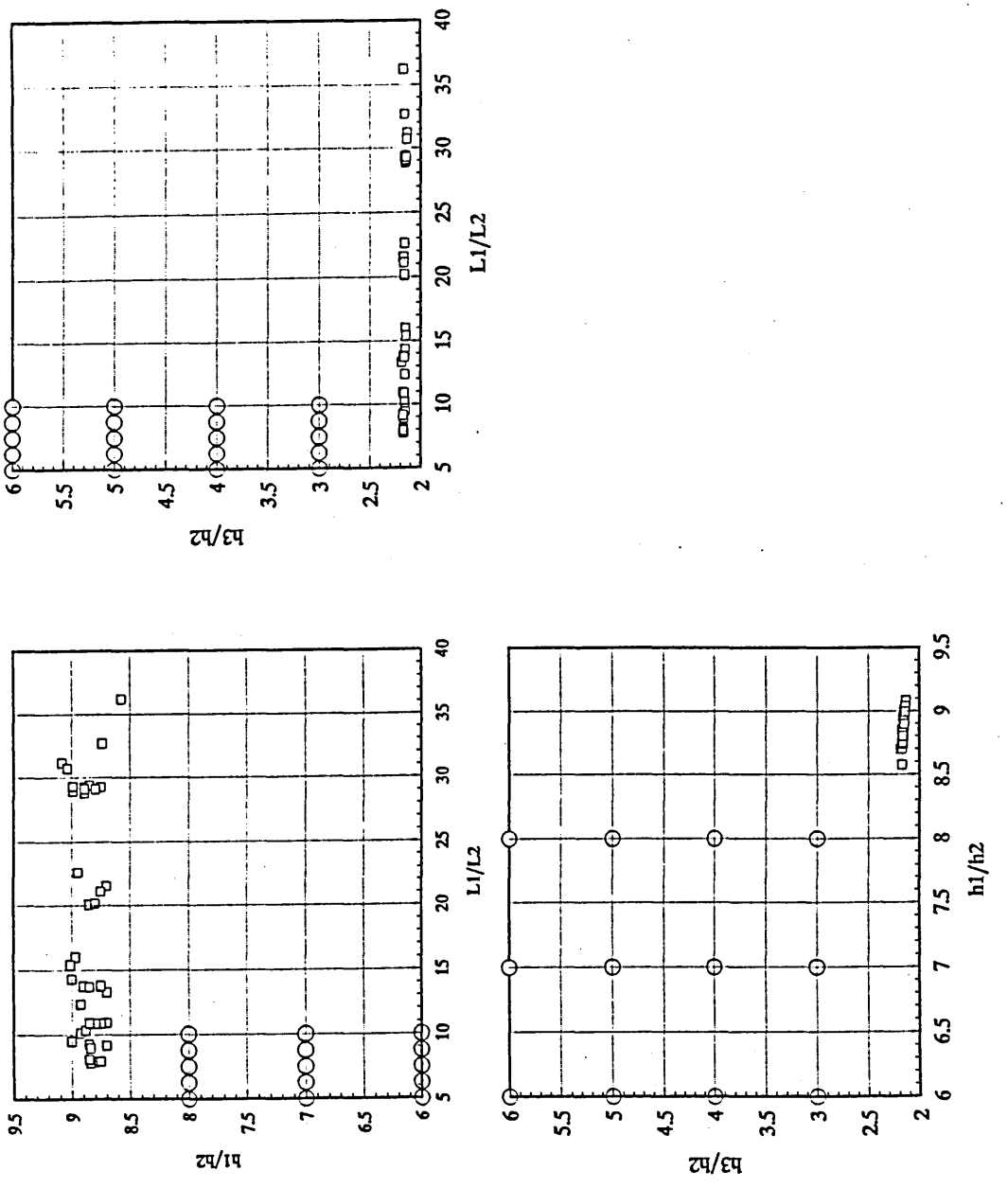

Figure 6.6 - Orthogonal views of the 3 dimensional scatter plot produced by the optimisation sequence for an entry velocity of 0.2 m/s.

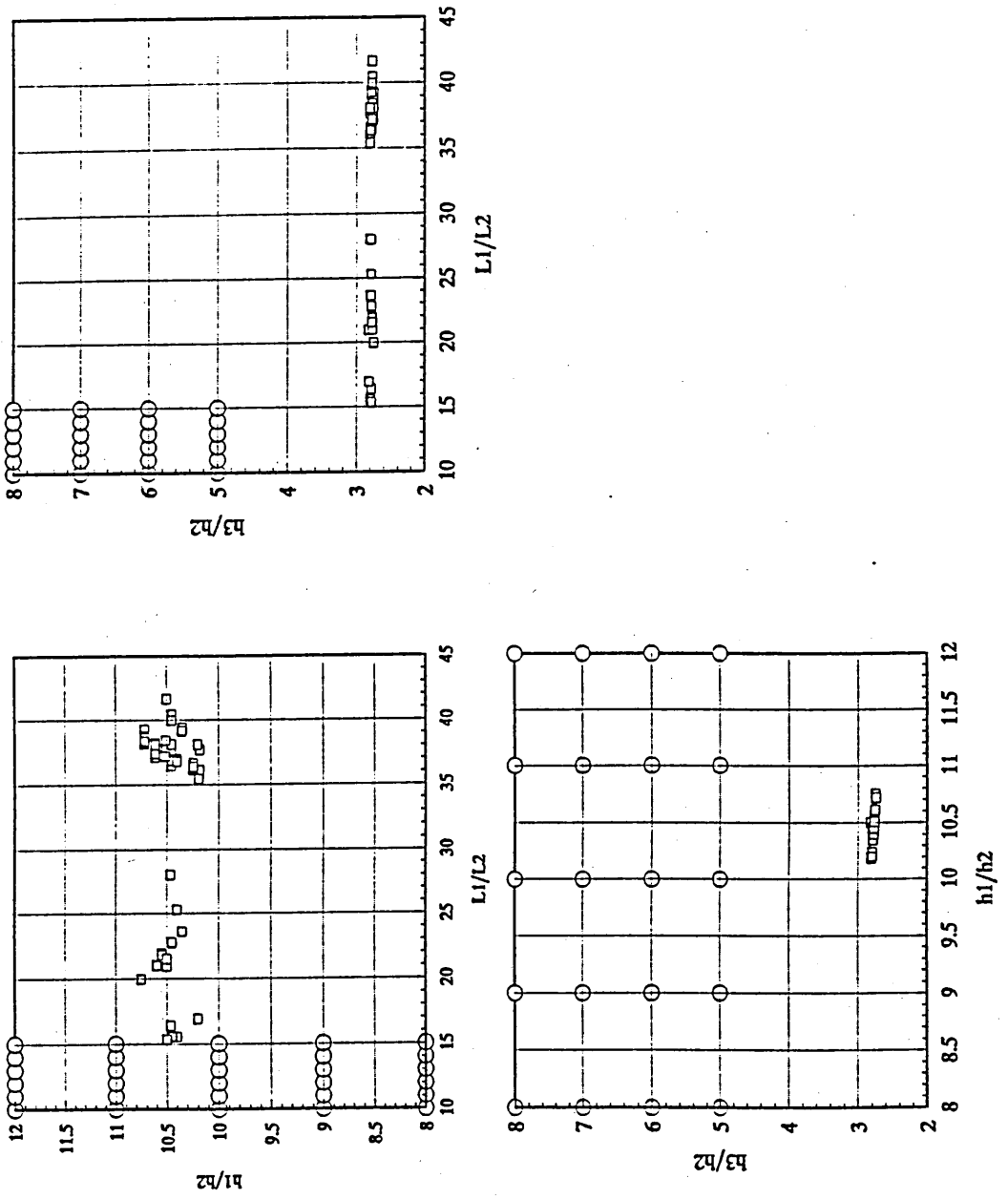

Figure 6.7 - Orthogonal views of the 3 dimensional scatter plot produced by the optimisation sequence for an entry velocity of 0.25 m/s.

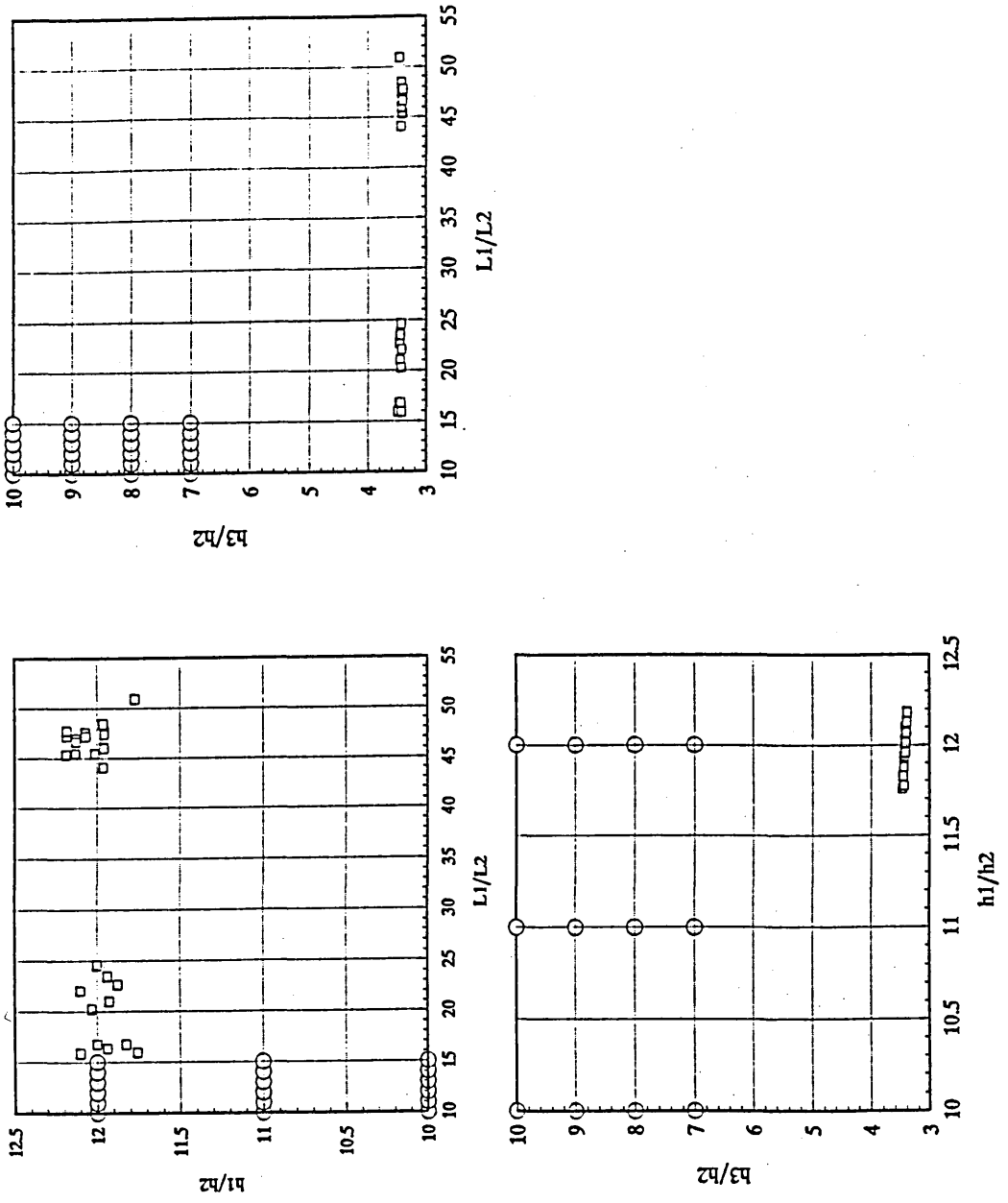

Figure 6.8 - Orthogonal views of the 3 dimensional scatter plot produced by the optimisation sequence for an entry velocity of 0.3 m/s.

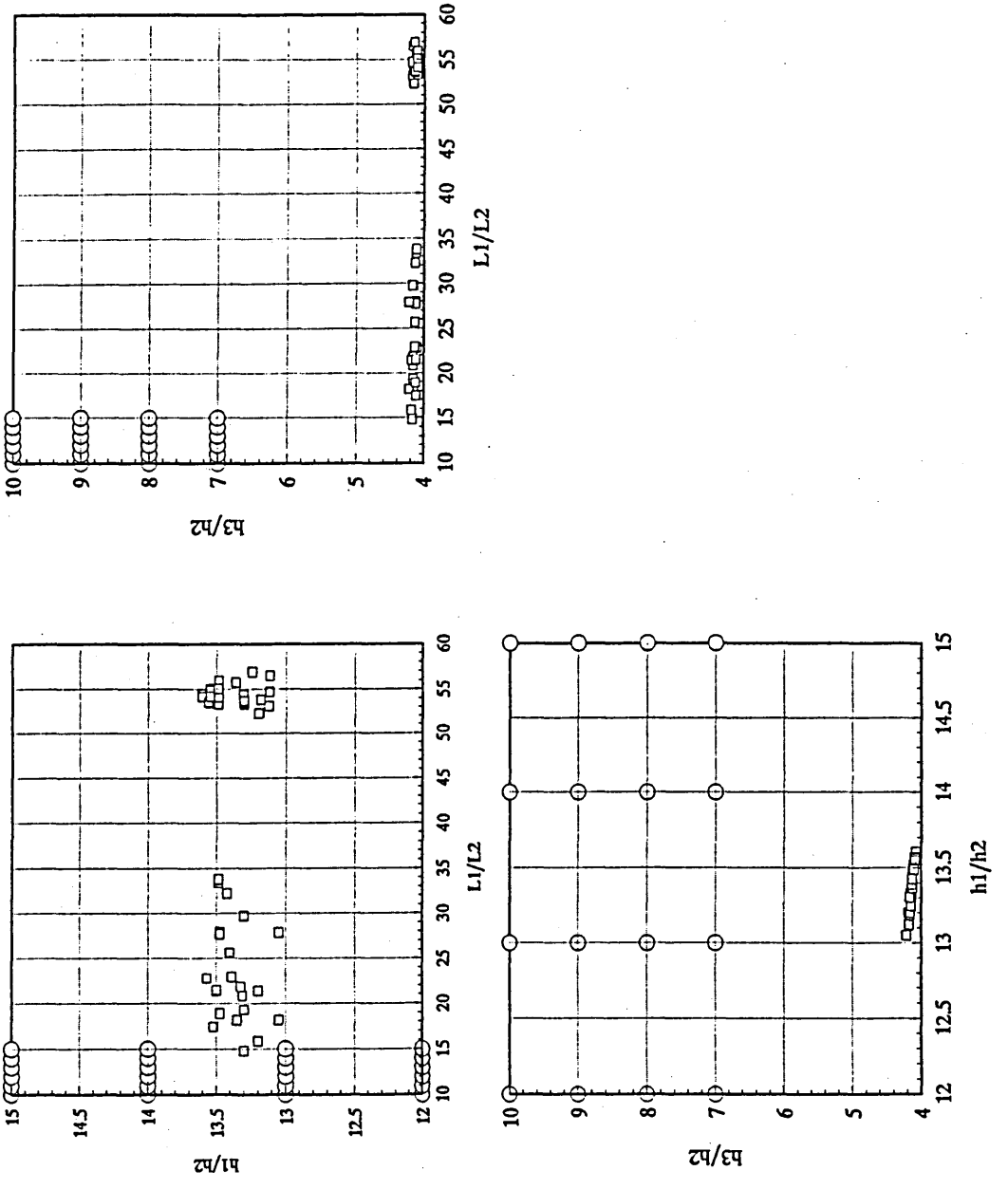

Figure 6.9 - Orthogonal views of the 3 dimensional scatter plot produced by the optimisation sequence for an entry velocity of 0.35 m/s.

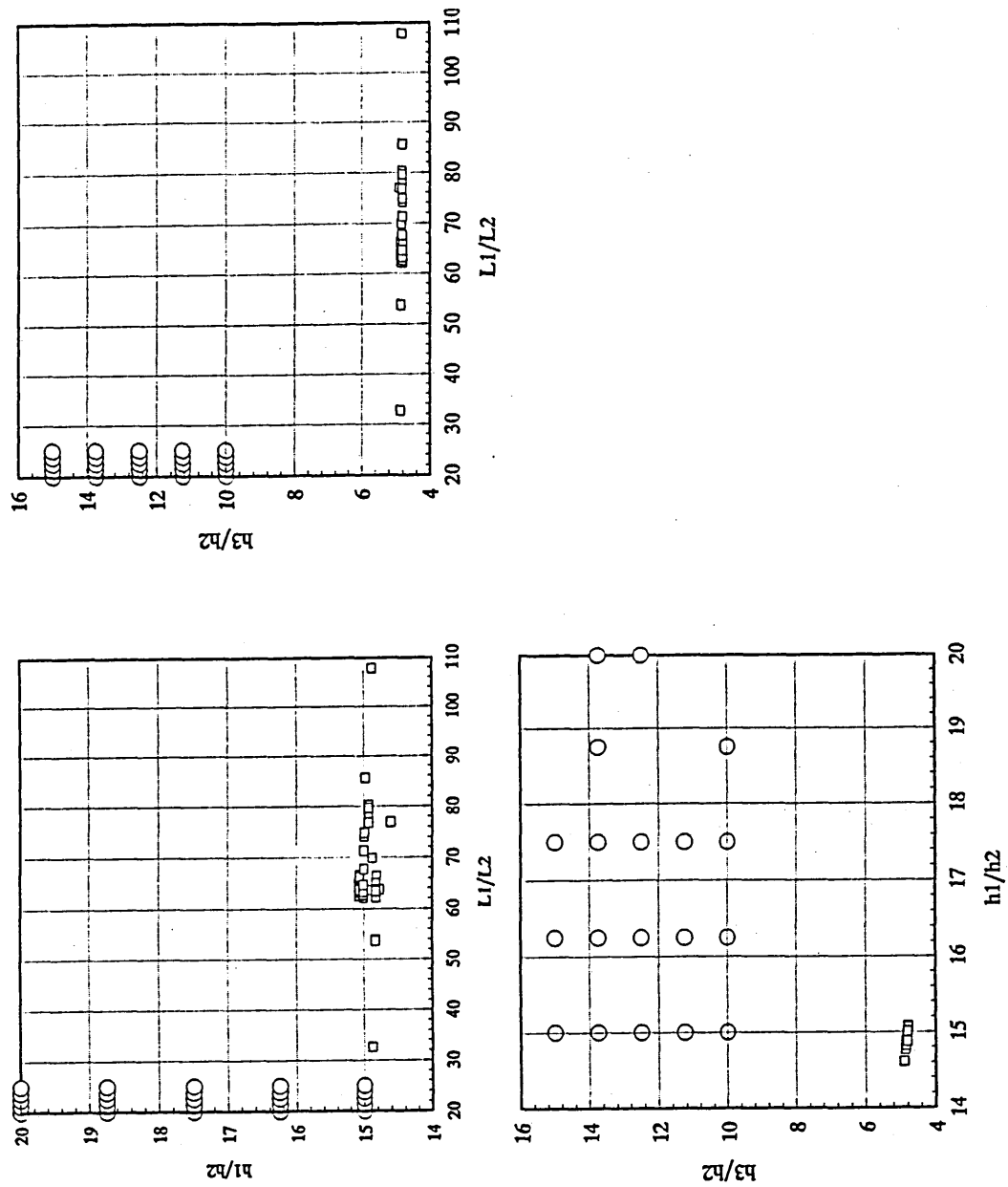

Figure 6.10 - Orthogonal views of the 3 dimensional scatter plot produced by the optimisation sequence for an entry velocity of 0.4 m/s.

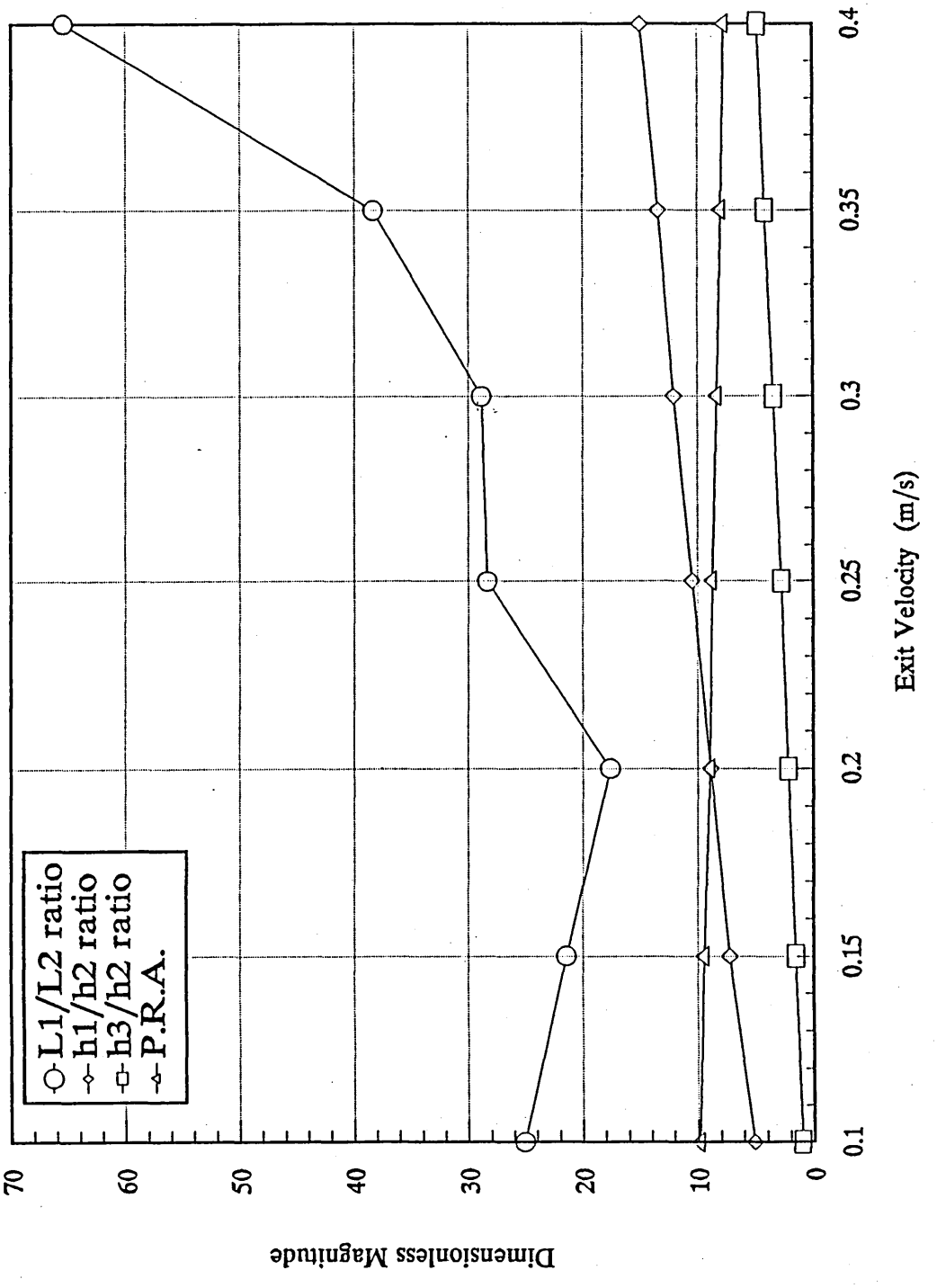

Figure 6.11 - Optimum pressure head geometry ratios for various process entry velocities.

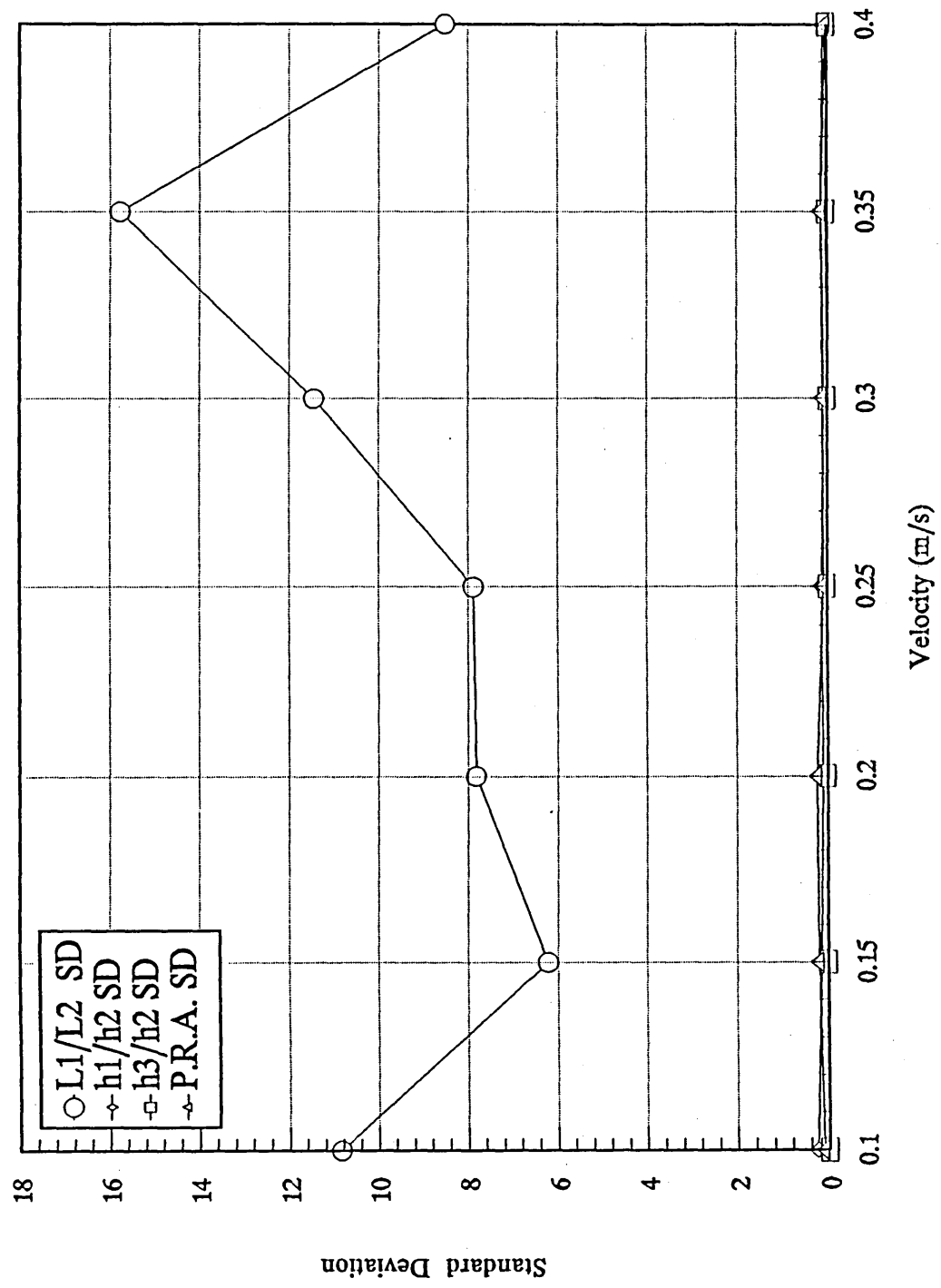

Figure 6.12 - Standard deviations of the optimum pressure head geometry ratios for various process entry velocities.

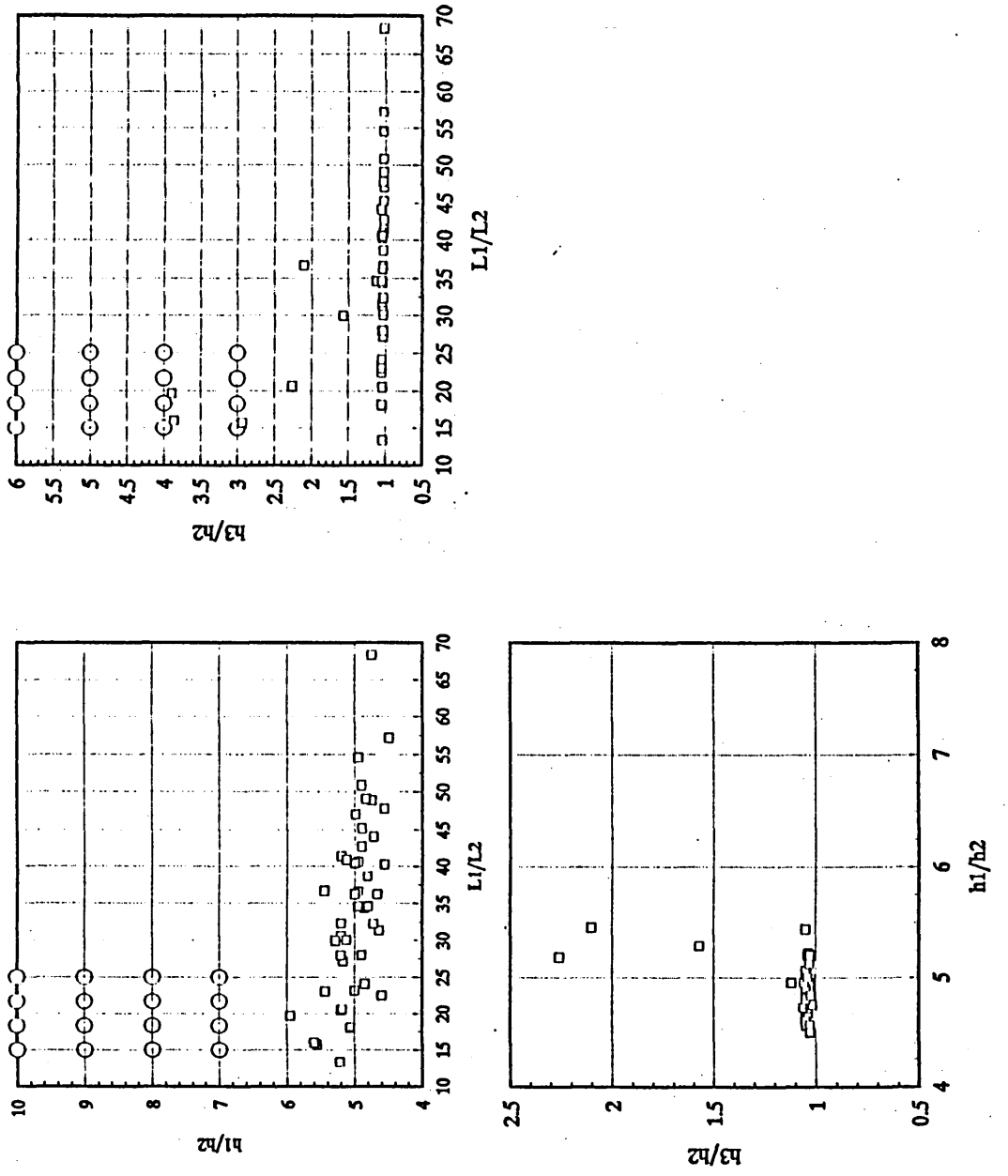

Figure 6.13 - Orthogonal views of the 3 dimensional scatter plot produced by the optimisation sequence for an entry velocity of 0.1 m/s.

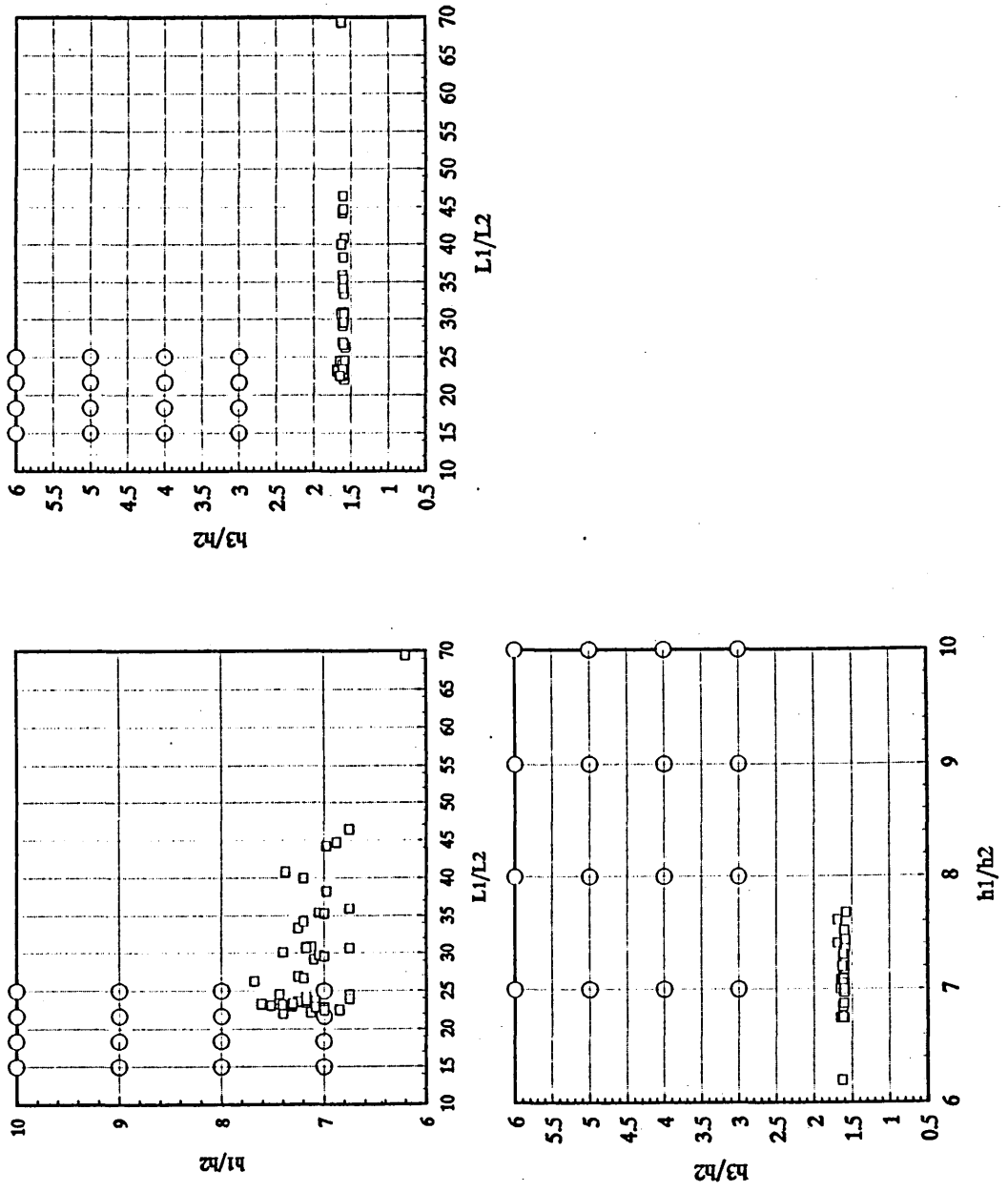

Figure 6.14 - Orthogonal views of the 3 dimensional scatter plot produced by the optimisation sequence for an entry velocity of 0.15 m/s.

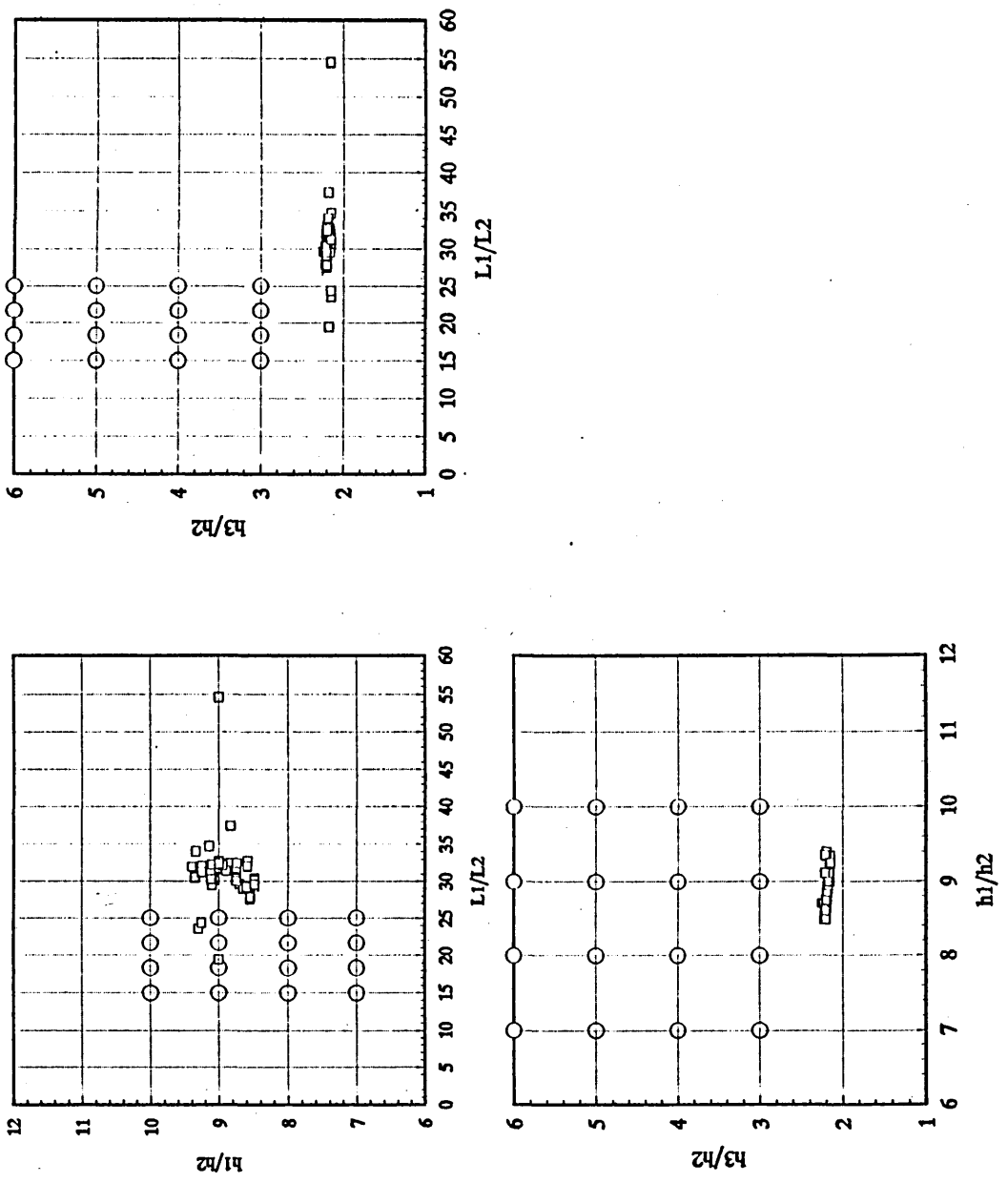

Figure 6.15 - Orthogonal views of the 3 dimensional scatter plot produced by the optimisation sequence for an entry velocity of 0.2 m/s.

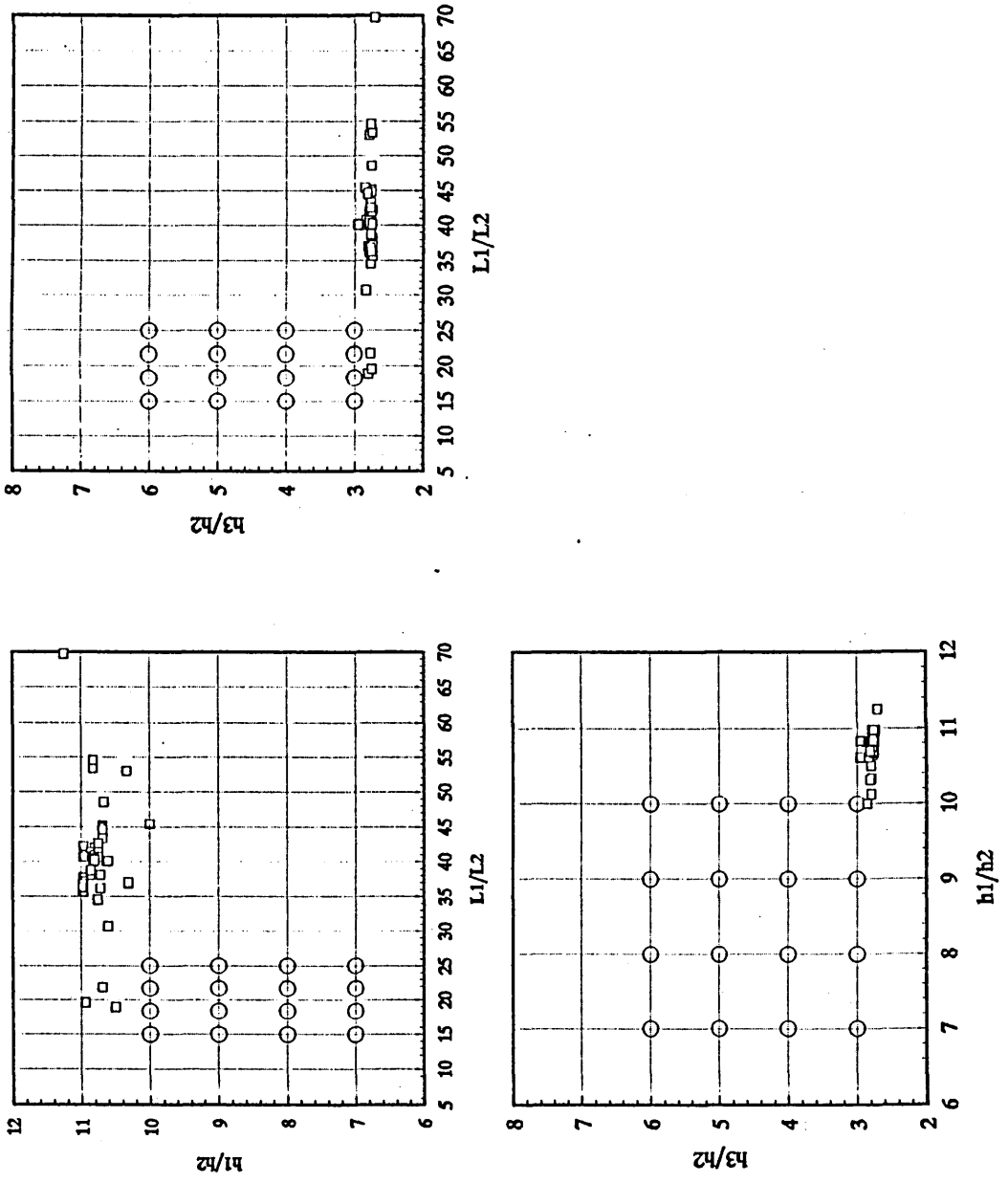

Figure 6.16 - Orthogonal views of the 3 dimensional scatter plot produced by the optimisation sequence for an entry velocity of 0.25 m/s.

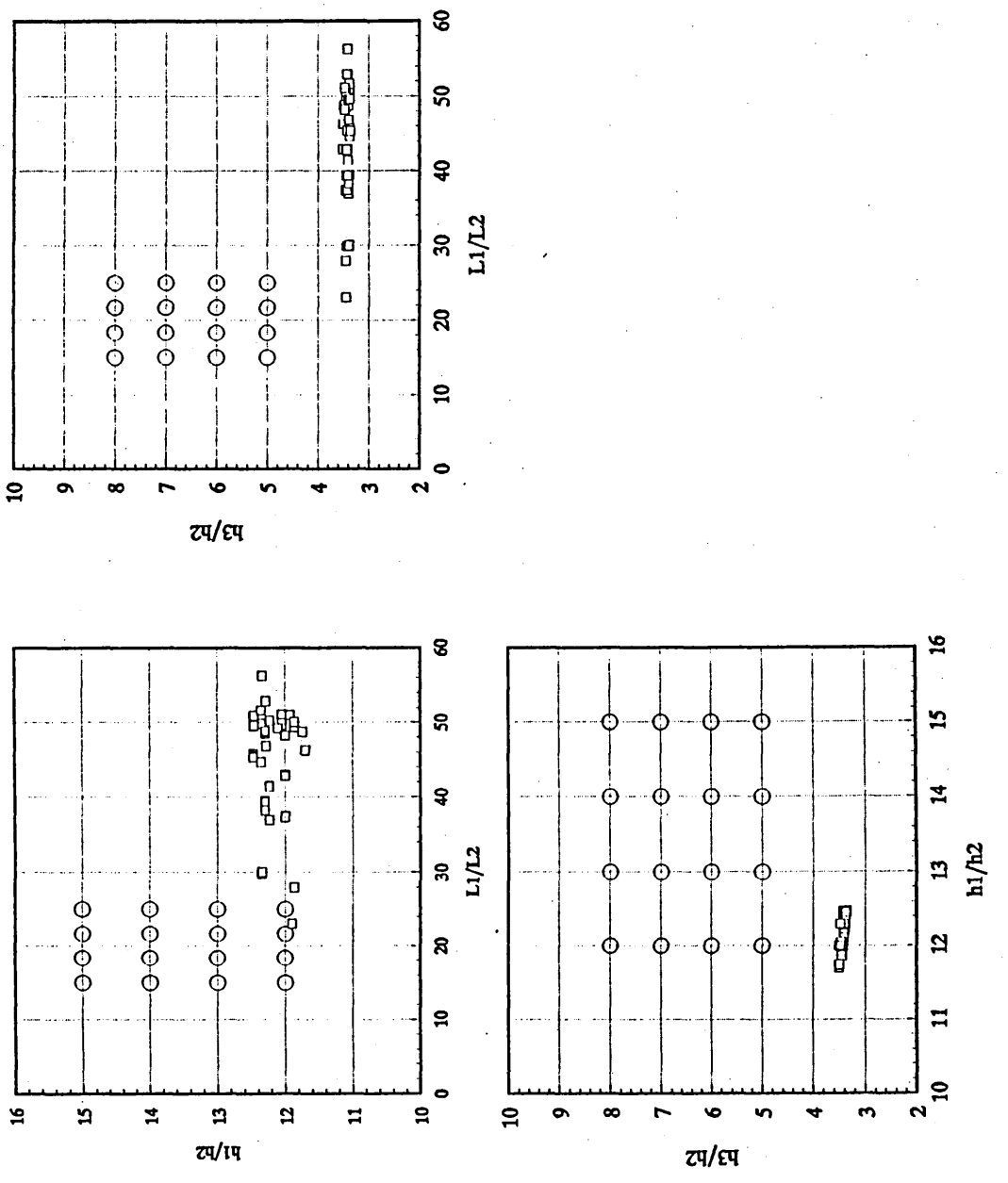

Figure 6.17 - Orthogonal views of the 3 dimensional scatter plot produced by the optimisation sequence for an entry velocity of 0.3 m/s.

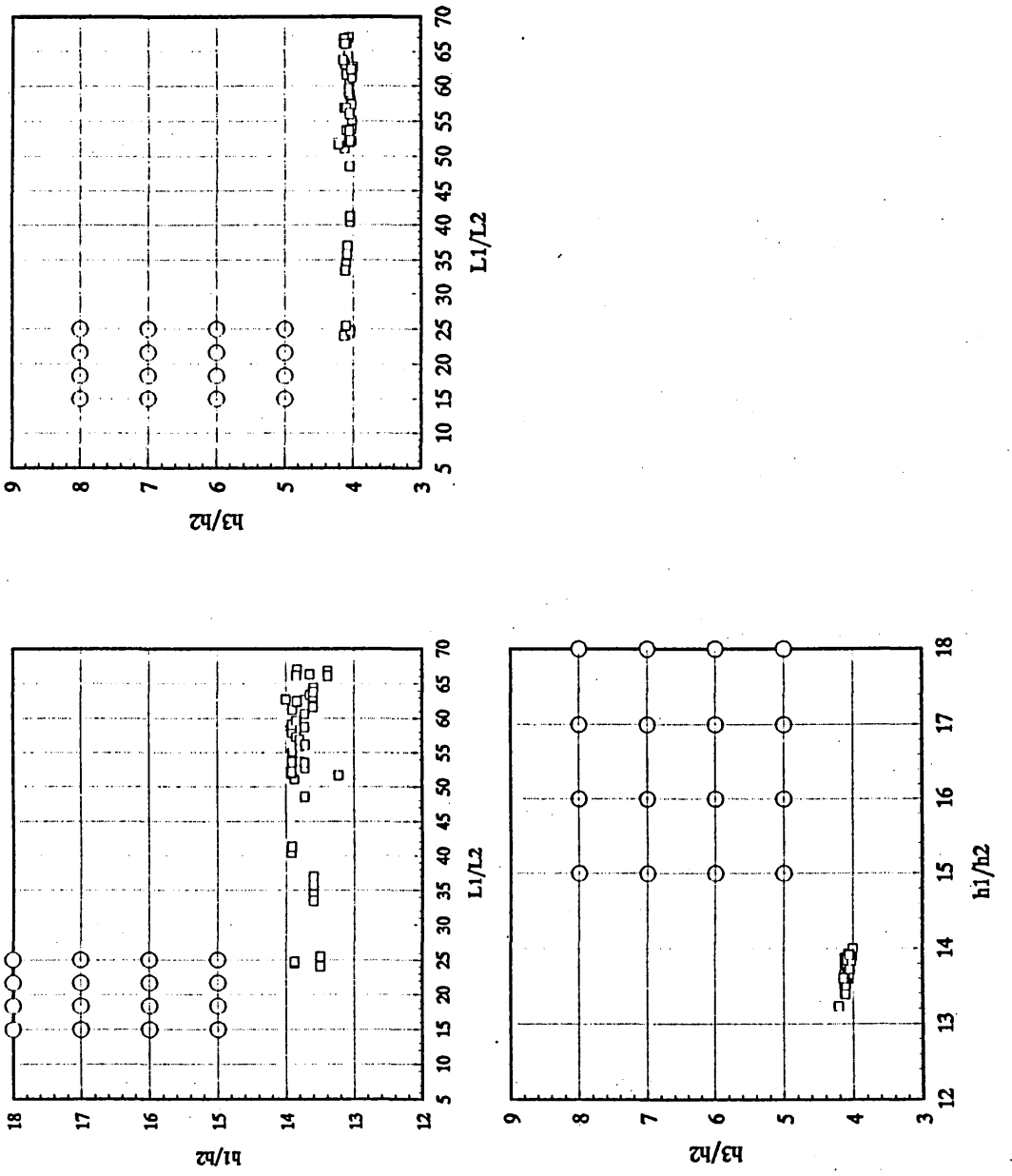

Figure 6.18 - Orthogonal views of the 3 dimensional scatter plot produced by the optimisation sequence for an entry velocity of 0.35 m/s.

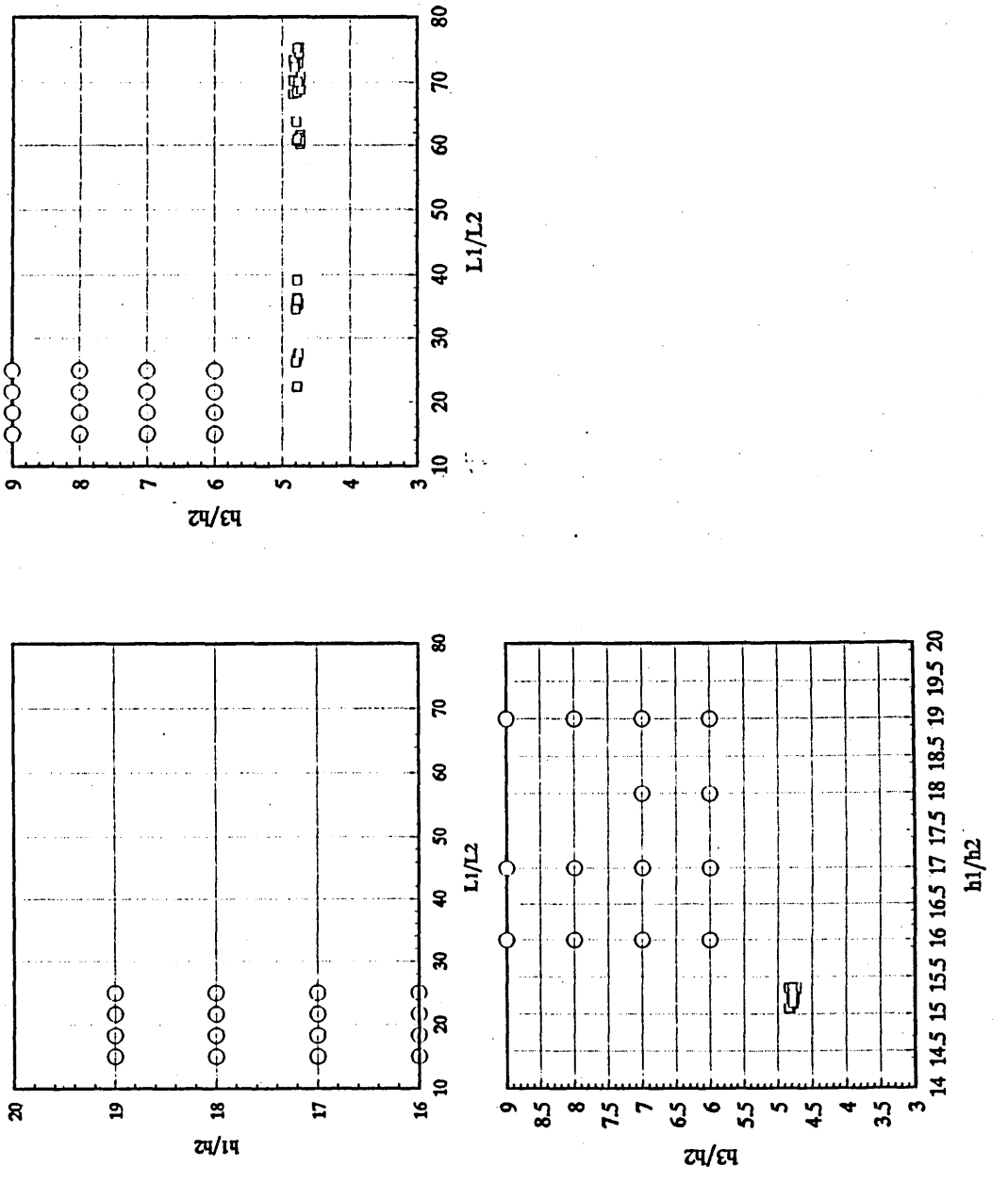

Figure 6.19 - Orthogonal views of the 3 dimensional scatter plot produced by the optimisation sequence for an entry velocity of 0.4 m/s.

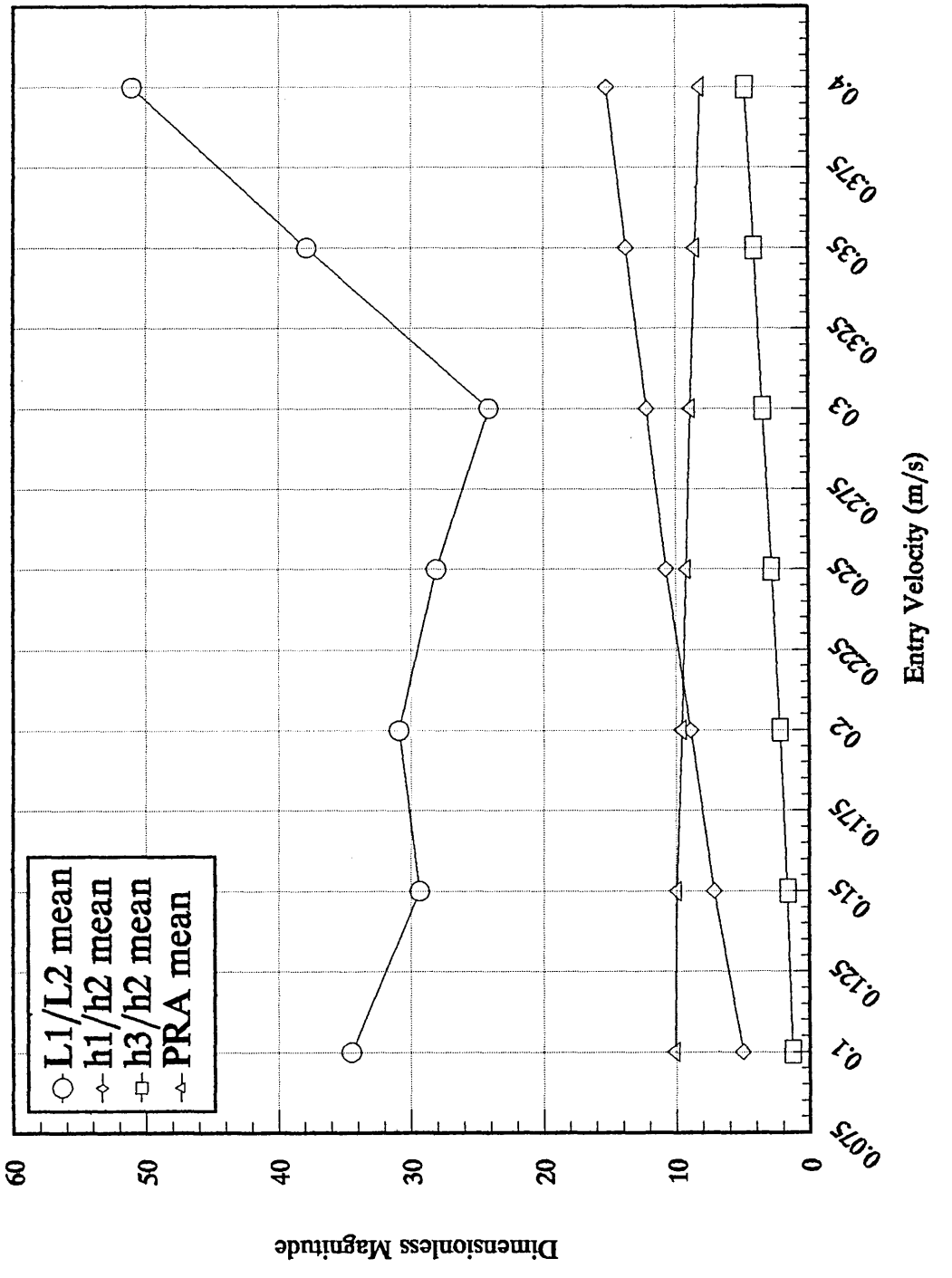

Figure 6.20 - Optimum pressure head geometry ratios for various process entry velocities.

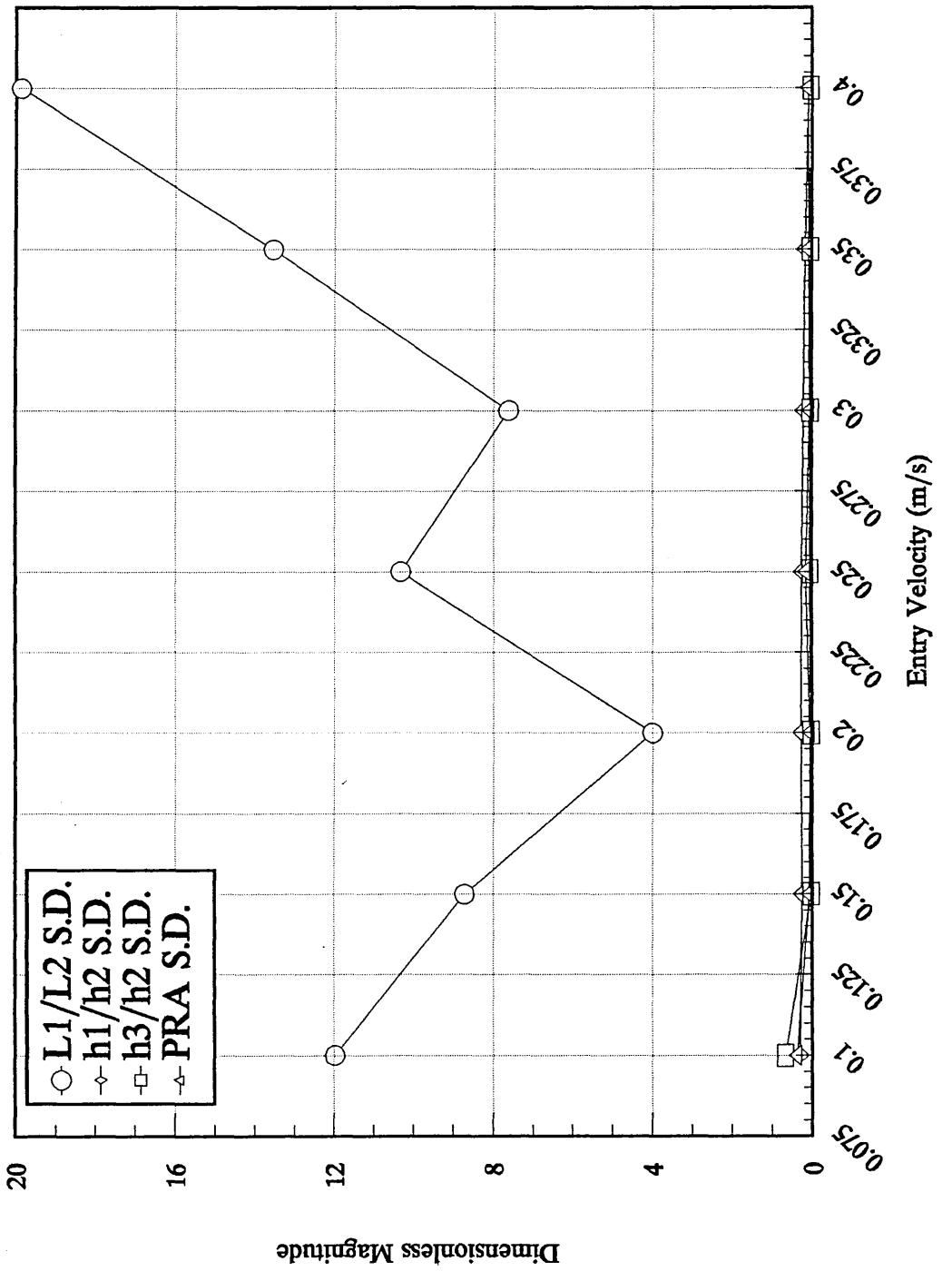

Figure 6.21 - Standard deviations of the optimum pressure head geometry ratios for various process entry velocities.

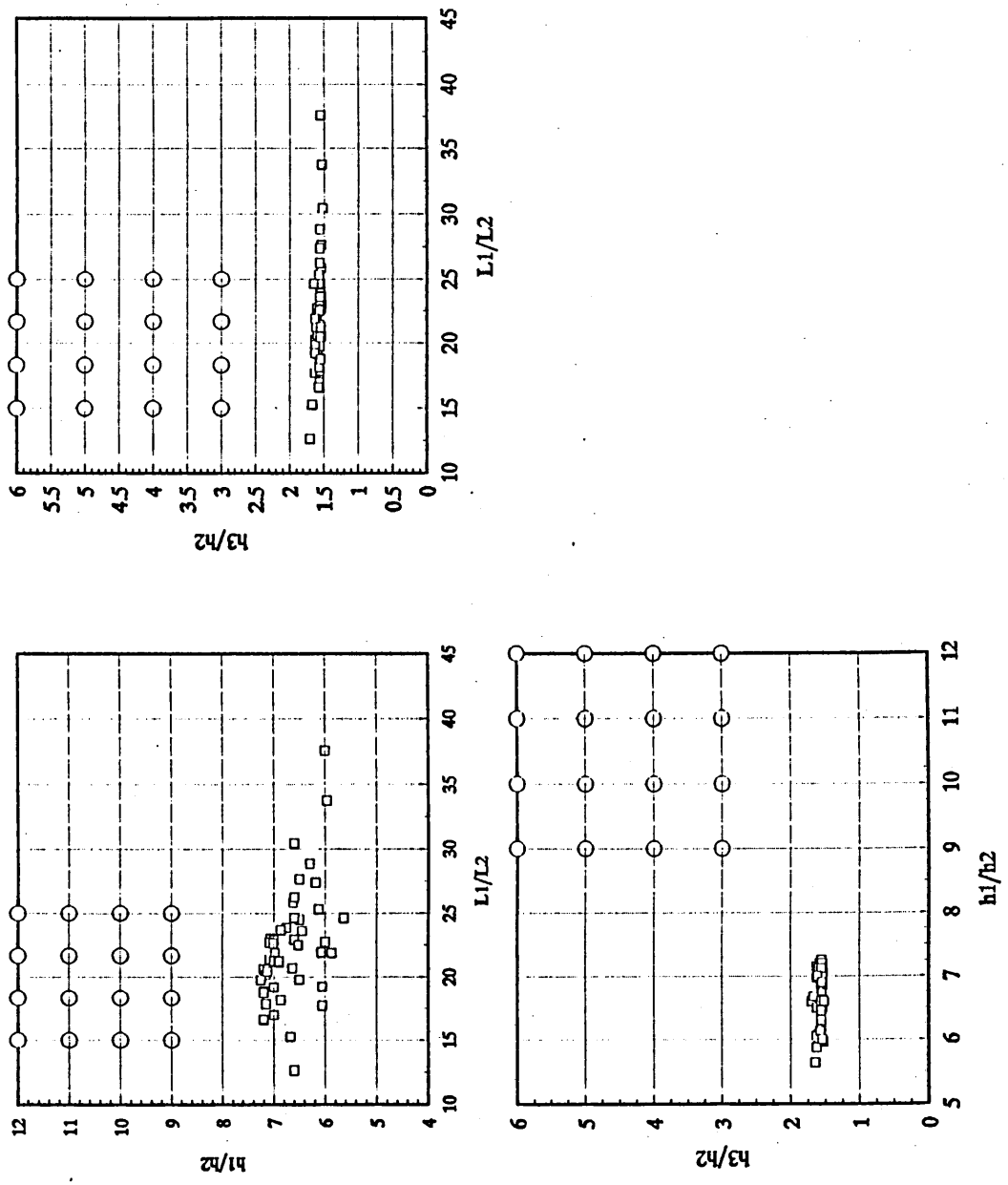

Figure 6.22 - Orthogonal views of the 3 dimensional scatter plot produced by the optimisation sequence for an entry velocity of 0.1 m/s.

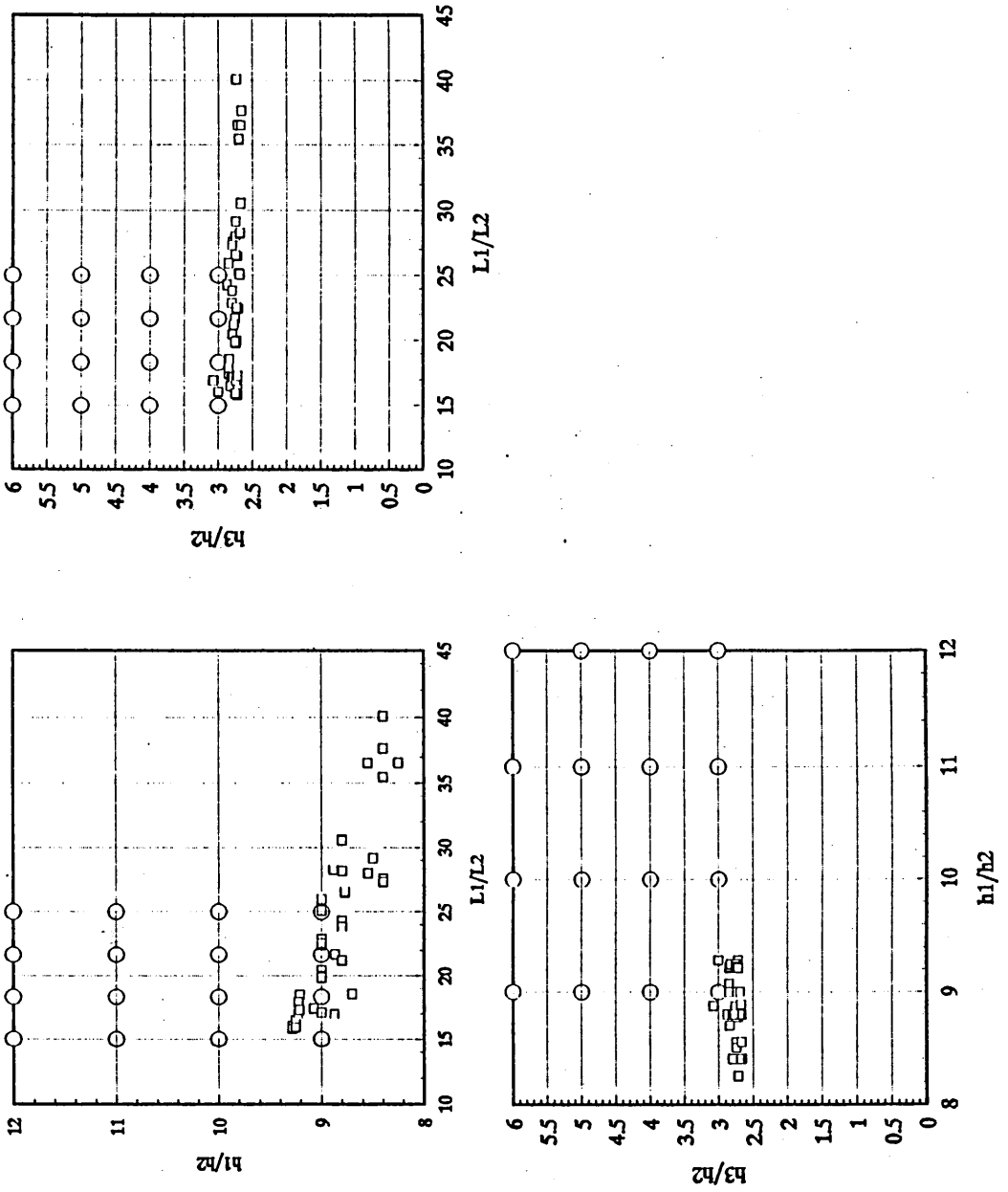

Figure 6.23 - Orthogonal views of the 3 dimensional scatter plot produced by the optimisation sequence for an entry velocity of 0.15 m/s.

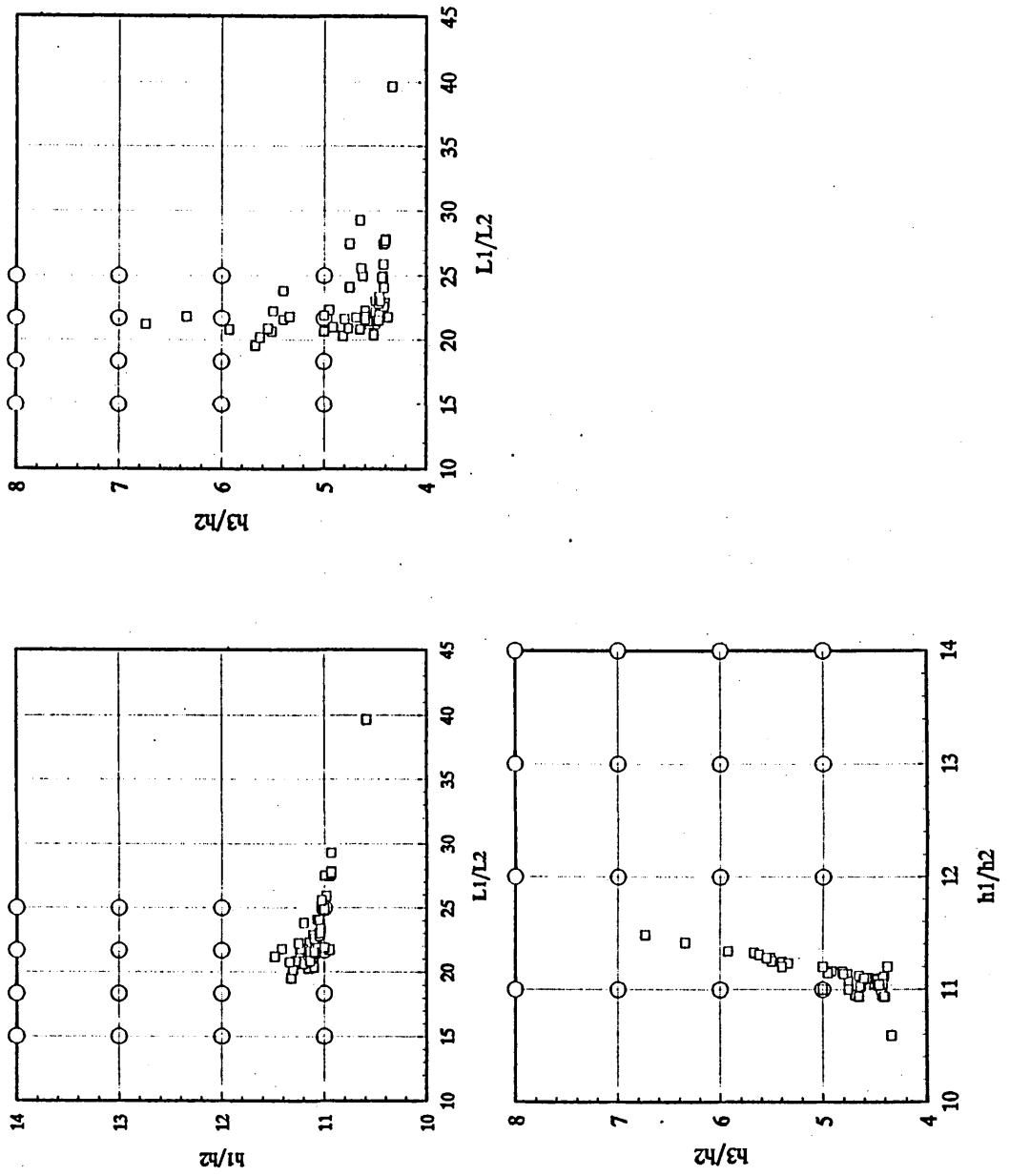

Figure 6.24 - Orthogonal views of the 3 dimensional scatter plot produced by the optimisation sequence for an entry velocity of 0.2 m/s.

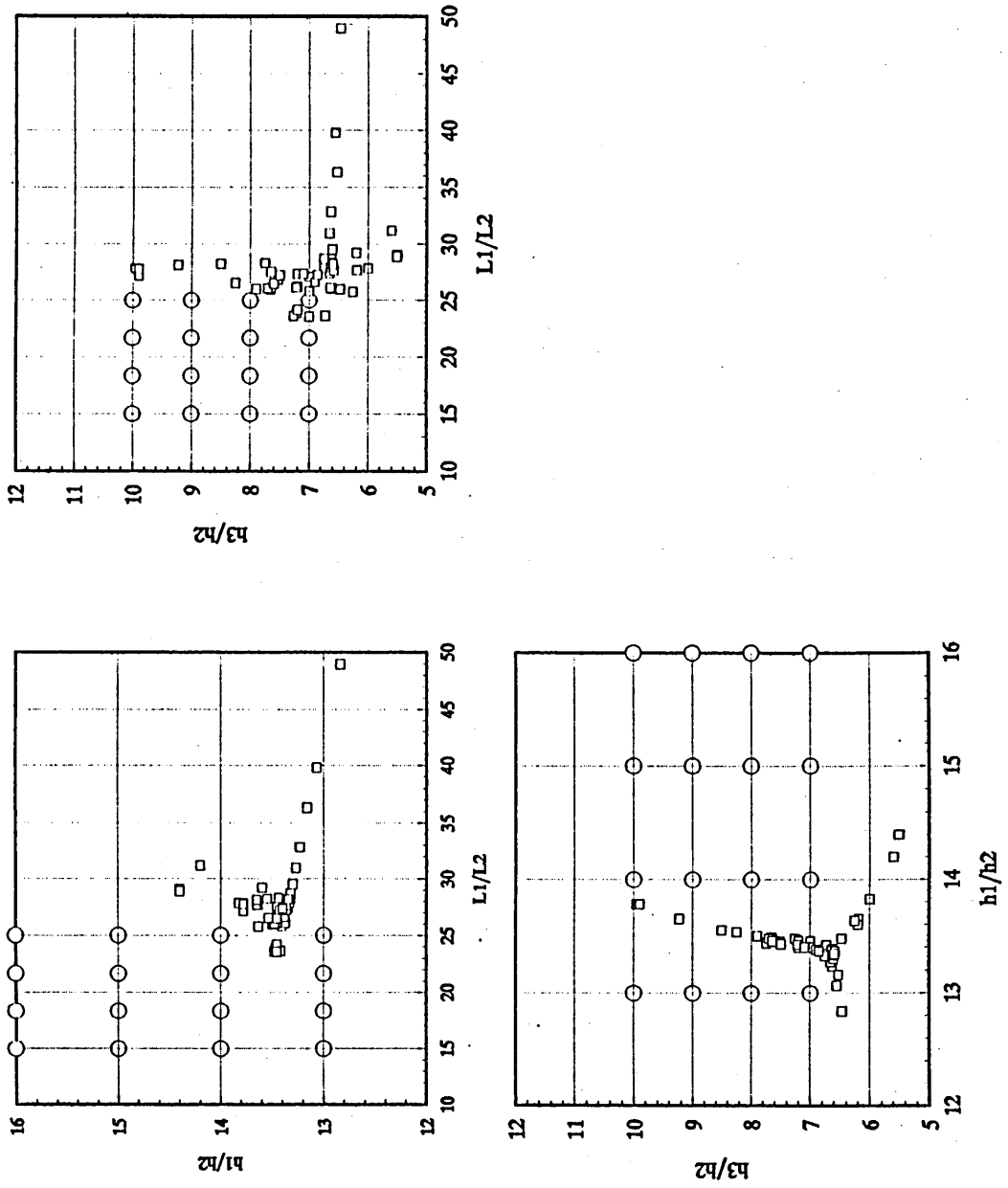

Figure 6.25 - Orthogonal views of the 3 dimensional scatter plot produced by the optimisation sequence for an entry velocity of 0.25 m/s.

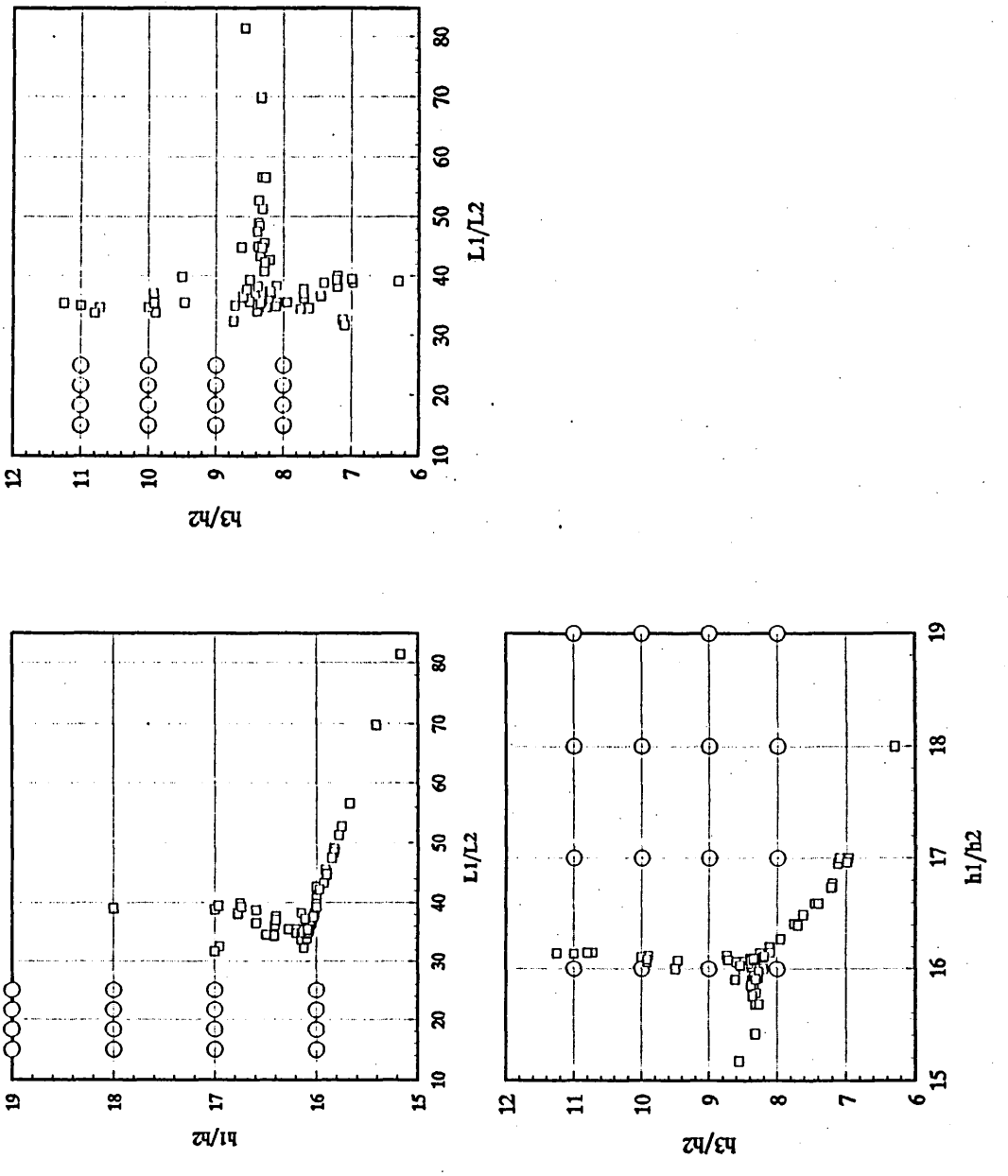

Figure 6.26 - Orthogonal views of the 3 dimensional scatter plot produced by the optimisation sequence for an entry velocity of 0.3 m/s.

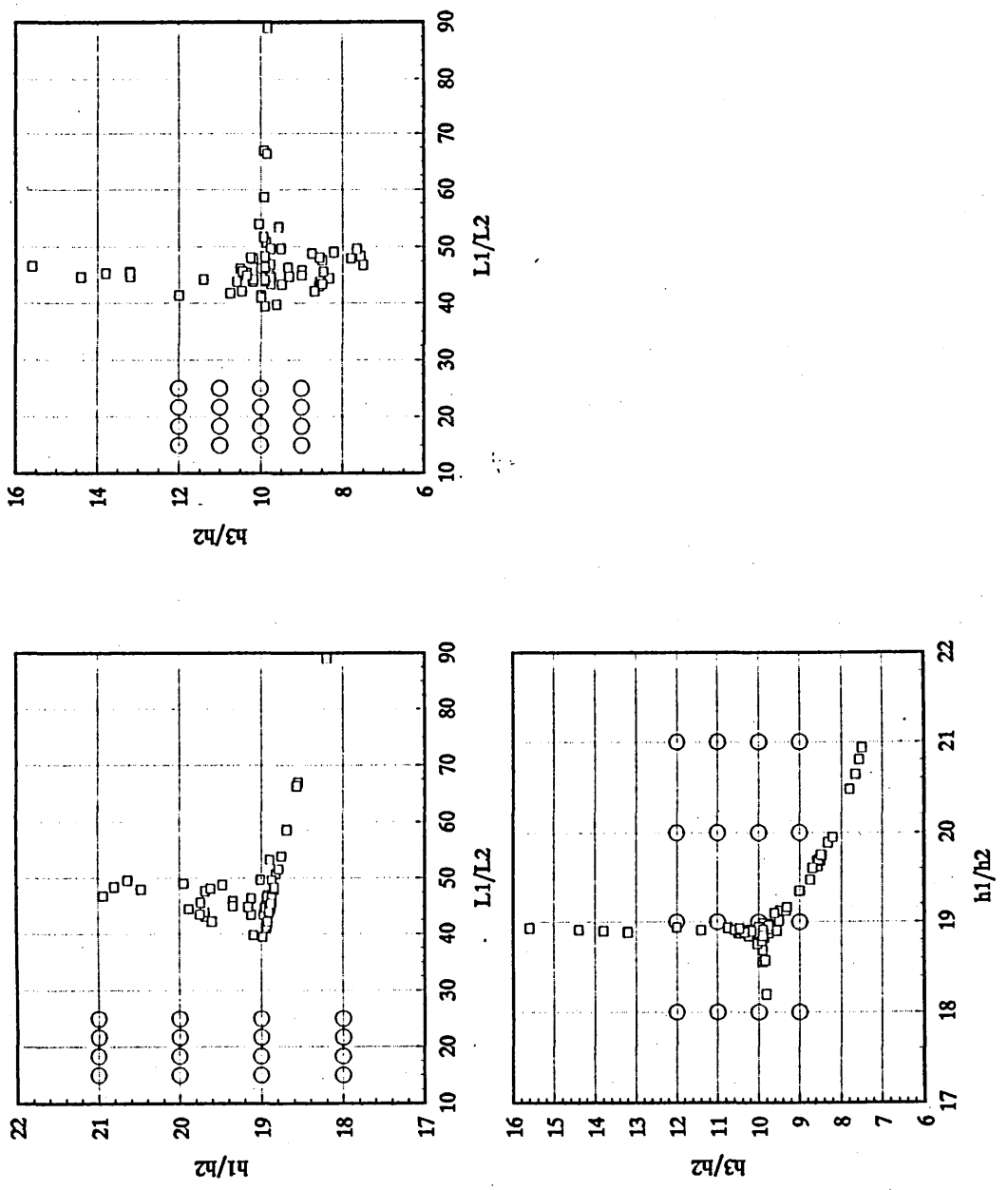

Figure 6.27 - Orthogonal views of the 3 dimensional scatter plot produced by the optimisation sequence for an entry velocity of 0.35 m/s.

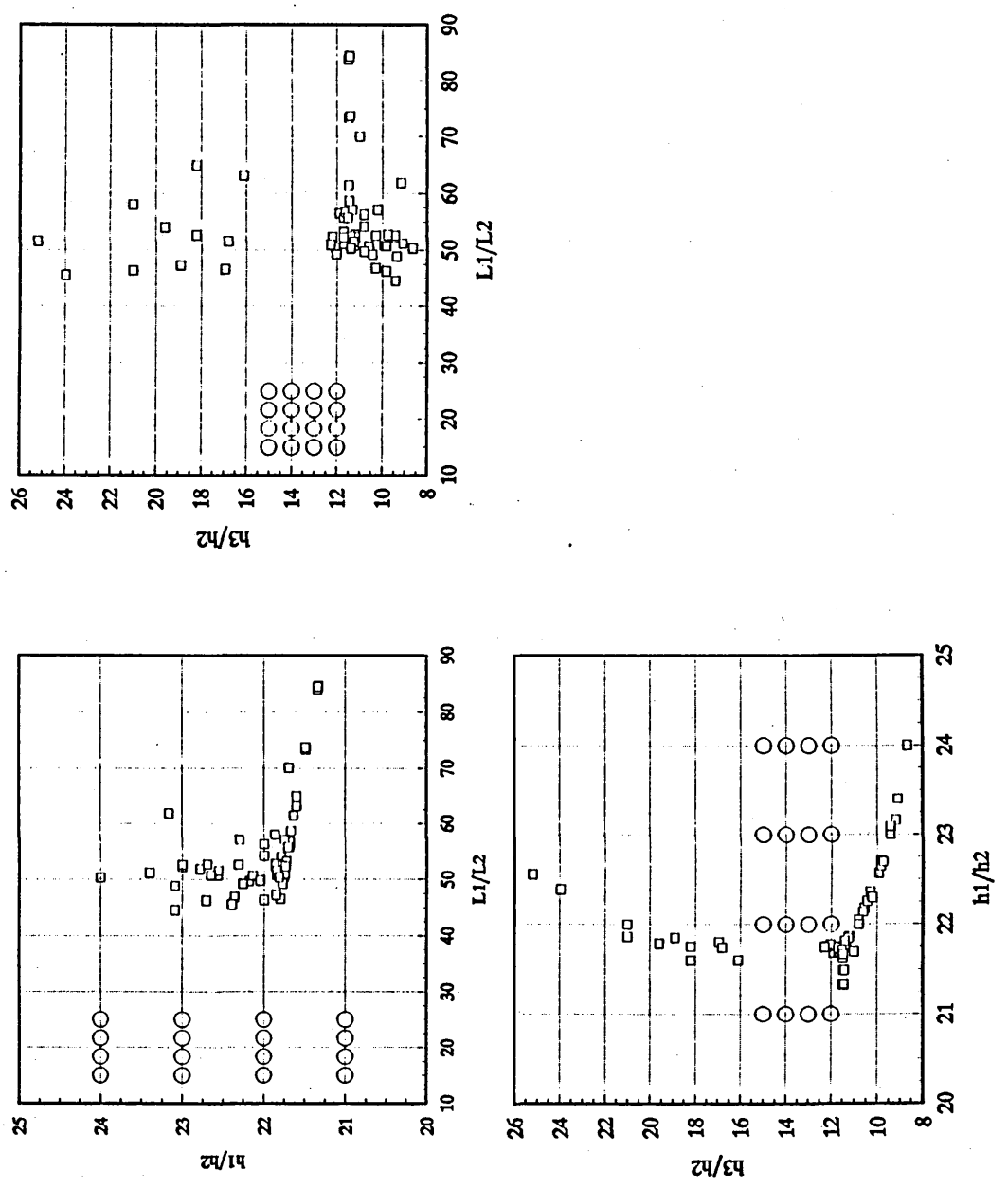

Figure 6.28 - Orthogonal views of the 3 dimensional scatter plot produced by the optimisation sequence for an entry velocity of 0.4 m/s.

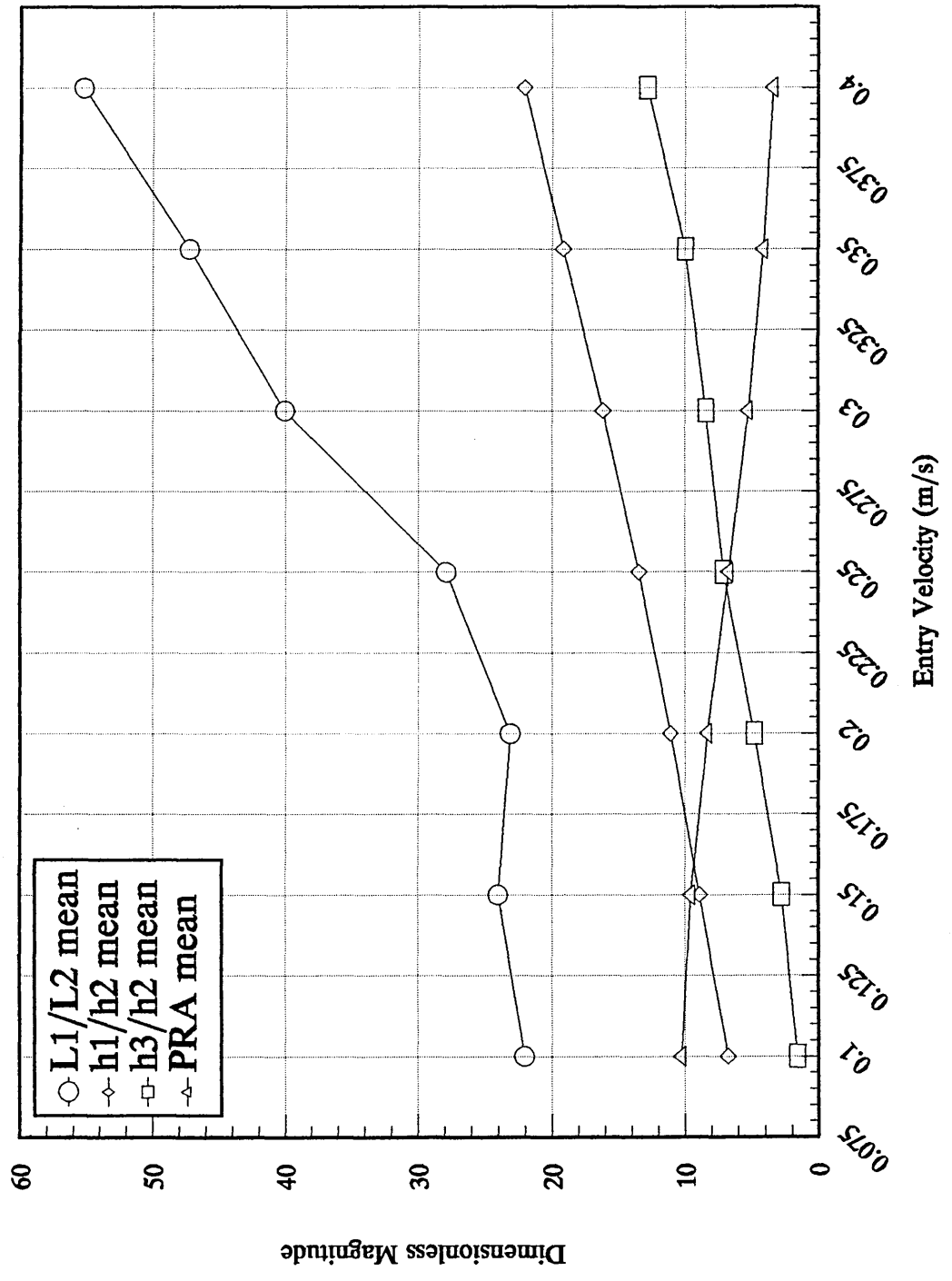

Figure 6.29 - Optimum pressure head geometry ratios for various process entry velocities.

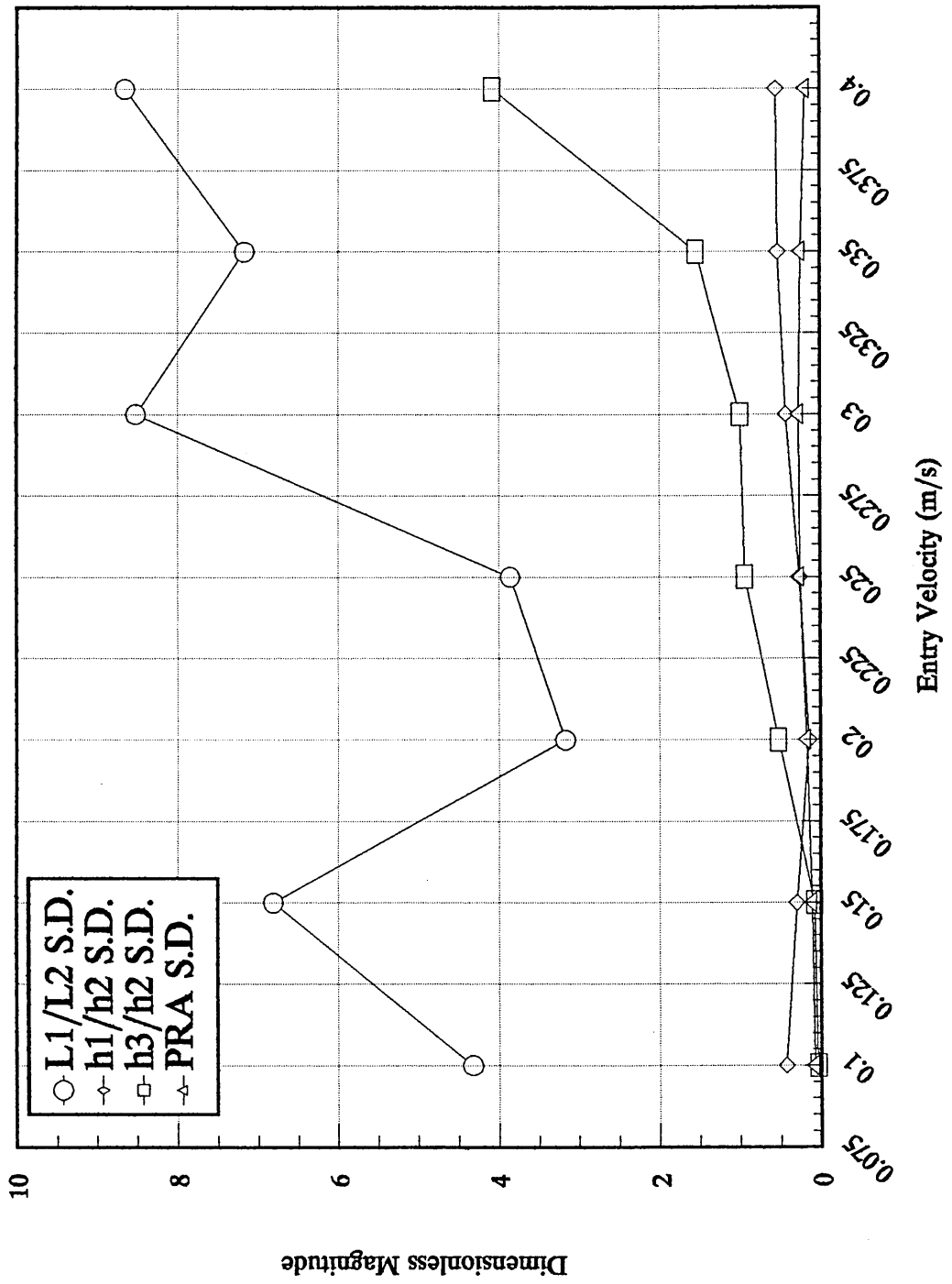

Figure 6.30 - Standard deviations of the optimum pressure head geometry ratios for various process entry velocities.

CHAPTER 7

7.0 The Validity of the Hydrostatic Assumption

The Hydrostatic assumption was stated in chapter 5 as;

> *the width of the material is very large compared to the side clearance h_3, with all derivatives of z being equal to zero, thus*

$$\frac{\partial}{\partial z} = 0$$

This is a very succinct way of stating arguably the most important assumption made in the modelling of Plasto-hydrodynamic drawing of rectangular sections. This may now be expanded. For a wide rectangular section placed within a convergent flow, hydrodynamic pressures and flows will be generated; a simple case widely described in tribological texts is that of a linear Rayleigh pad bearing. Two major phenomena are usually demonstrated by various means. Firstly, the maximum pressure generated in the bearing is at the step change in section. Secondly, the pressure reduces towards the edge of the bearing due to leakage, as shown in figure 7.1. The hydrostatic assumption then states that if the section is enclosed, and the clearance between the enclosure and section is very small in comparison with the width of the section, then the leakage flow will be negligible compared to the convergent flow, and hydrodynamic pressure loss across the face of the strip will be negligible and is assumed to be zero. With this assumption the pressure field around any arbitrary cross section becomes constant, as the pressure derivative in the z direction is zero. The significance of this result is that the fluid modelling within the overall plasto-hydrodynamic model is reduced by one dimension, ie 3D

to 2D.

The dimension of the fluid model is then further reduced during the integration of the fluid equations; this is achieved by specifying that the point of interest is at y=0 (surface of material). The dimension of the fluid modelling is thus reduced from 2D to 1D.

7.1 The Computational Fluid Dynamic Analysis

The validity of the hydrostatic assumption was examined by means of a series of 3-dimensional fluid models. The models were developed and solved using a commercially available software package called FLUENT. This package allows the analysis of complex 3D problems using a wide variety of boundary conditions and solution algorithms.

For this analysis it was required to solve the incompressible form of the Navier-Stokes equations, given below in vector form,

$$\rho\frac{D\bar{V}}{Dt} = \rho\bar{B} + \left(-\nabla\bar{p} + \mu\nabla^2\bar{V} \right) \qquad \textbf{Navier-Stokes Eqns}$$

The FLUENT system will not solve any form of the governing equation for plastic deformation. It was then decided to ignore plastic deformation of the material. This was justified by using a geometrical configuration for the pressure head and material velocity that, according to the present model, would only just meet the criteria for plastic deformation. This point must be passed through during acceleration to higher process velocities at the start up of the process, and may be considered a valid point for analysis. The validity of the assumption after substantial deformation has taken place is more uncertain and will not be addressed

at this time.

Two questions may then be posed:-

i) What effect does the aspect ratio of the working material have on the pressure field?

ii) If the assumption is valid, at what proportion of the velocity required for deformation will the pressure field meet the hydrostatic assumption?

7.1.1 The Model Geometry

Five models were used to address these questions - their functional relations are shown in figure 7.2. The geometry used for the models is given below:

L1	= 50 mm	L1/L2 ratio	= 5:1
L2	= 10 mm		
h_1	= 0.4 mm	h_1/h_2 ratio	= 2:1
h_2	= 0.2 mm		
h_3	= 0.2 mm	h_3/h_2 ratio	= 1:1

A plasto-hydrodynamic pressure head is symmetrical about two perpendicular planes, and as such a quarter section mesh was used to limit the number of computational cells below an upper bound of 50000. The planes of symmetry are shown in figure 7.3, with figures 7.4 and 7.5 showing details of the finished mesh used for the analysis.

This geometry was given to the numerical model of the plasto-hydrodynamic drawing process, and the velocity required to initiate deformation calculated. This was then used in the CFD models to ascertain the effect of the aspect ratio. The 16:1 aspect ratio model was then used at two lower velocities

to establish the velocity limits of the hydrostatic assumption, these being 2/3 V and 1/3 V. The initial velocity and viscosity used for the study were V=0.5 m/s and μ=180 Pa.s.

7.1.2 Boundary Conditions

Inspection of the inlet and outlet regions of the model reveals that the velocity profiles were unknown, but that ambient pressure is felt in these regions. A technique referred to as 'link cutting' is available within the FLUENT system. 'Link cutting' enables the solver to isolate contiguous cells during the iteration process, such that the velocity of the inlet and outlet cells was not used during the solution of the internal region of the model. A pressure boundary was applied to the inlet and outlet regions, thereby sufficiently specifying the bounds of the problem for computation.

7.1.3 Model Convergence

The models used were found to have an extremely slow convergence. Typically, in excess of 120,000 iterations were required for solution, even though the equations are well posed; the models are incompressible, laminar and steady-state. This may be attributable to two factors:

i) the large number of computational cells,

ii) the hydrodynamic nature of the problem.

For two reasons each model uses 14,625 computational cells. Firstly, the high shear rates in the pressure head clearances require a minimum of five cells perpendicular to the nominal direction of fluid flow. Early models with 3 cells

(recommended initial number) would not converge to the required accuracy. Secondly, as the aspect ratio of the pressure head clearances is very high (wide, long and extremely thin), to maintain an aspect ratio of less than five for the computational cells required a large number of cells in the width and length dimensions of the model.

Inspection of the Navier-Stokes equations given in section 7.1 reveals that the pressure is not explicitly included, but only the pressure gradient. This fact causes many complications in the solution of fluid problems; the description of which is beyond the scope of this text. It was noted that during the iteration of the equations a narrow band of high pressure is formed in the front, and at the centre, of the step. This was then slowly propagated outwards towards the edges of the model. The rate of propagation was extremely slow and is thought to be a consequence of the lack of an explicit pressure term.

7.2 Results

7.2.1 The effect of the aspect ratio on the hydrostatic assumption

The overall form of the pressure field at the surface of the strip, may be shown as a surface. This requires that the data be processed in the following manner: The x coordinate represents the distance into the pressure head from the entry. The y coordinate is the distance around the periphery of the strip material, with the origin located at the centre of the width face. This processing effectively flattens or maps the surface of the material onto a plane as shown in figure 7.6. The pressure magnitude is now indicated by the height of the surface at any x,y location. The pressure fields for the 8:1, 16:1 and 32:1 aspect ratio models are given in figures 7.7, 7.8 and 7.9 respectively. Figures 7.10 - 7.12 show various

comparisons of the CFD computed pressure fields and pressure field given by Rayleigh (66), which is denoted as the 'theoretical' curve on the figures in question. Figure 7.10 gives pressure profiles for the length of the pressure head, located at the plane of symmetry (centre of width face) for all three models. Figure 7.11 gives the pressure distribution in front of the step for all three models. Figure 7.12 gives the pressure distribution in front of the step for the 16:1 aspect ratio model at the velocities specified in section 7.1.1.

The relevance of this data to the modelling of the PHD process will be examined in detail in the following chapter.

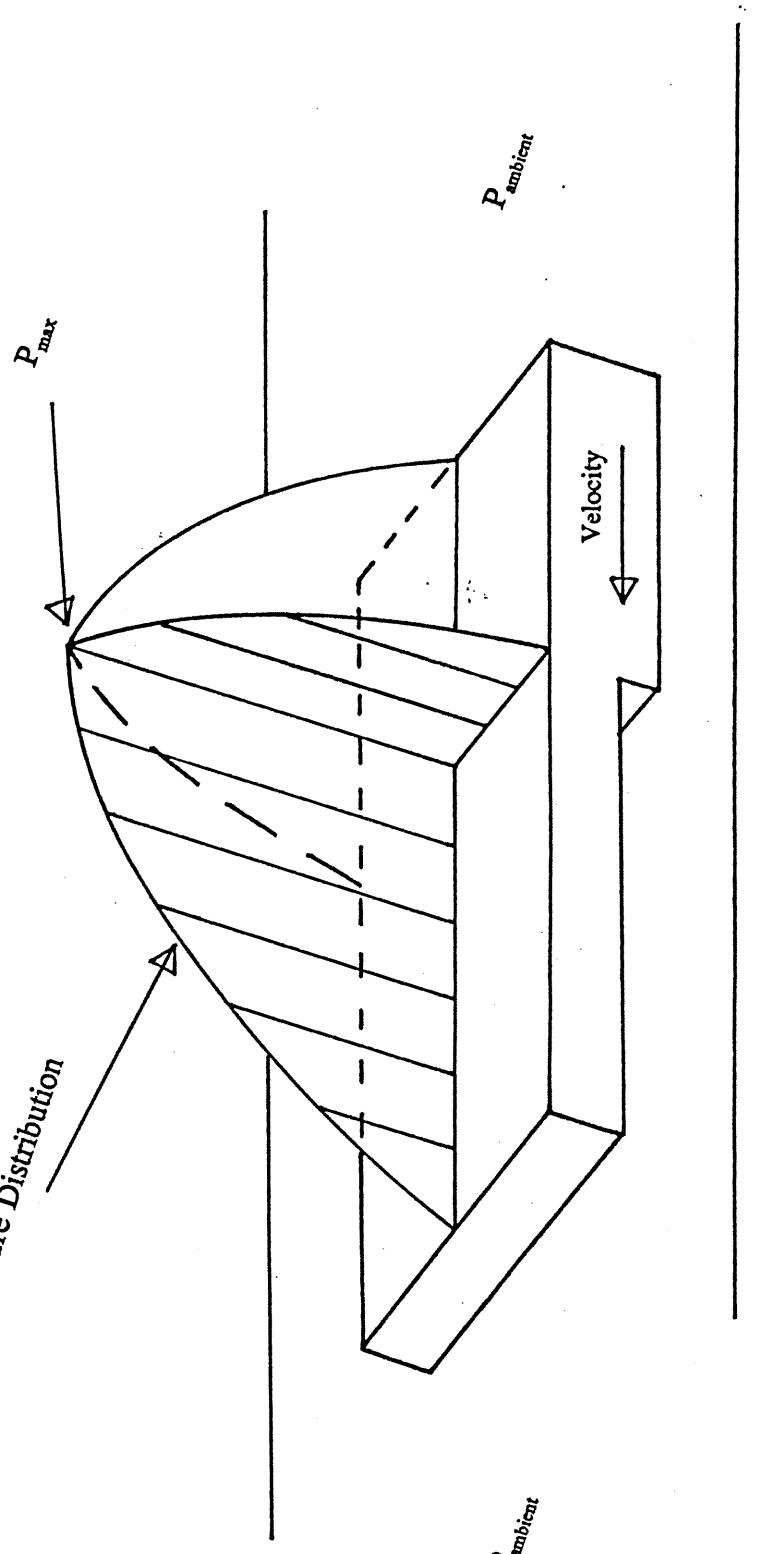

Figure 7.1 - Schematic of a linear Rayleigh pad bearing.

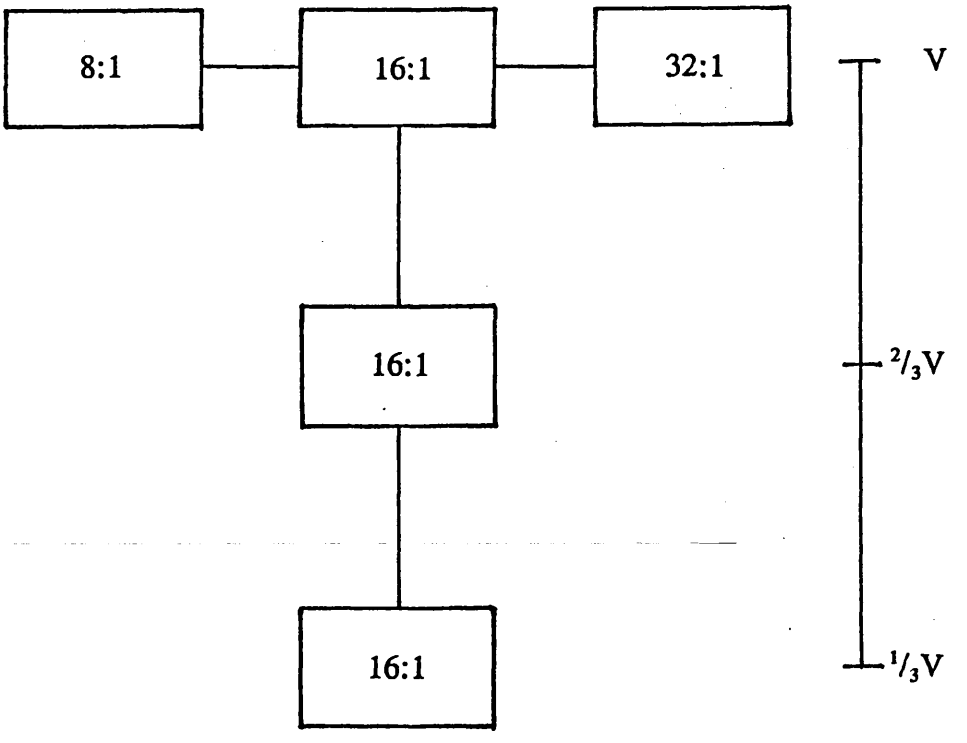

Figure 7.2 - Schematic giving the functional relations of the CFD models.

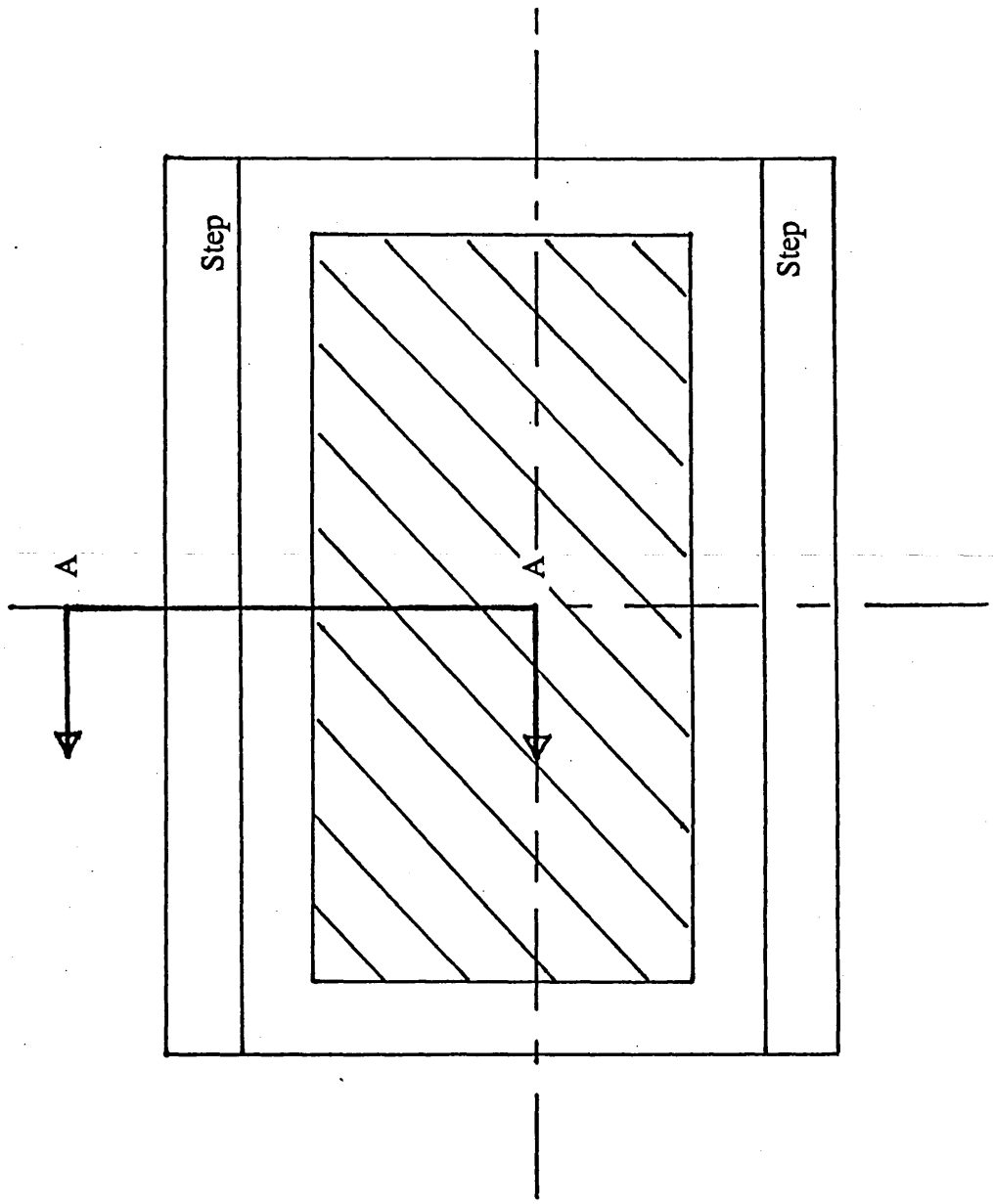

Figure 7.3 - End view of a pressure head demonstrating available planes of symmetry.

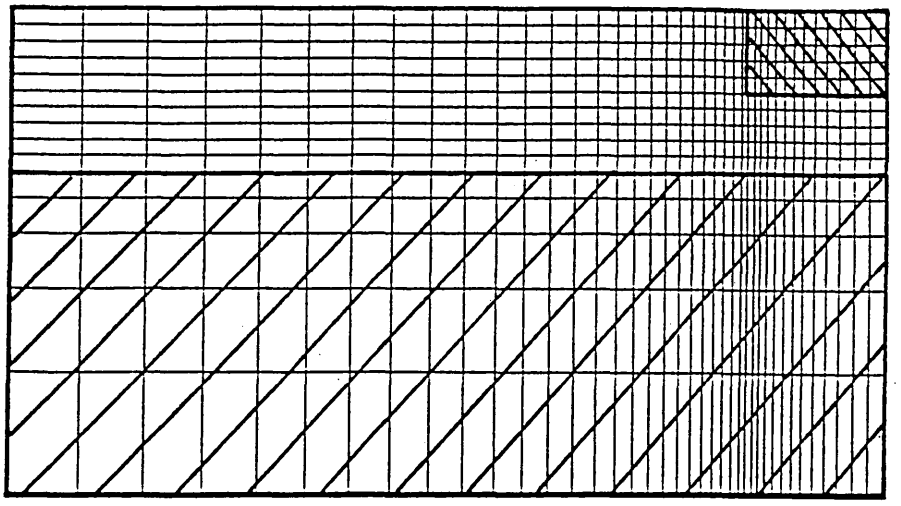

(a)

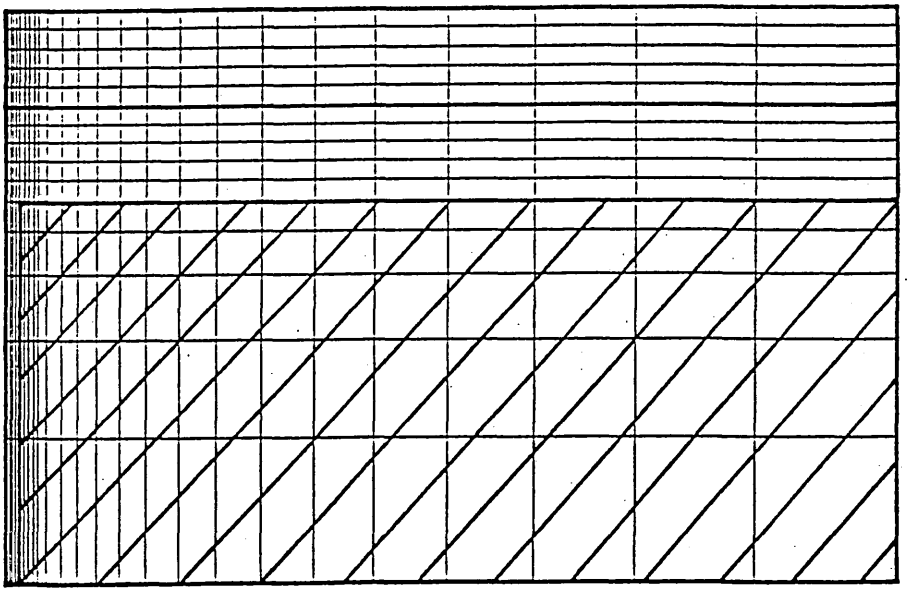

(b)

Figure 7.4 - Representative views of meshes used in CFD analyses: a) section on A-A, b) upper left quadrant of figure 7.3.

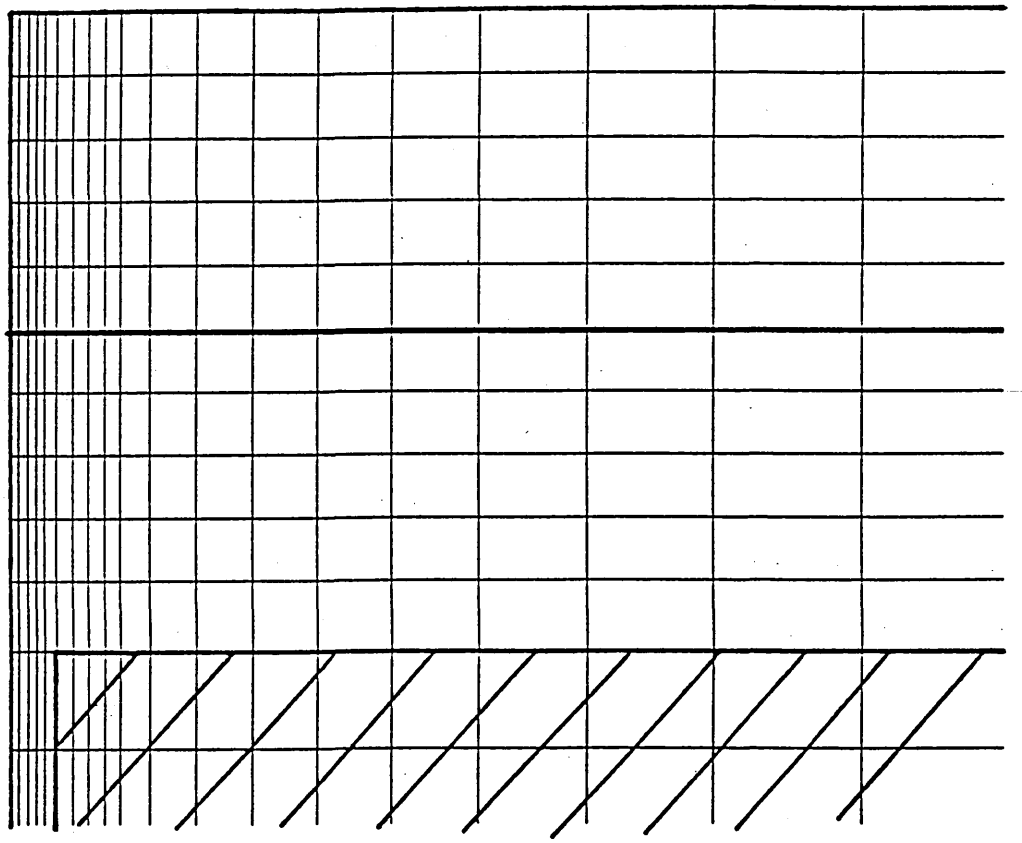

Figure 7.5 - Magnified view of corner section of mesh, revealing details of non-uniform mesh.

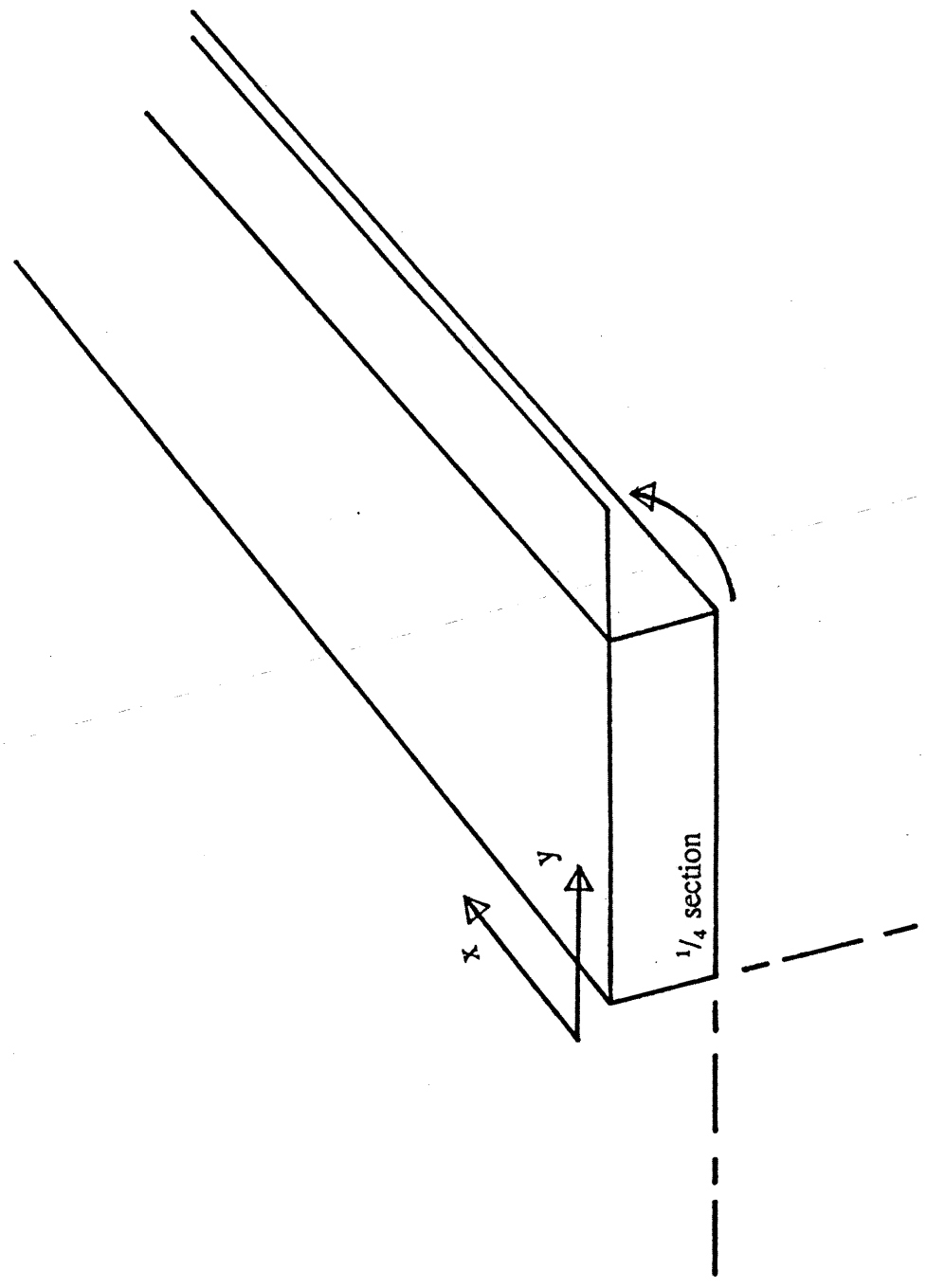

Figure 7.6 - Mapping of material 1/4 section onto a plane.

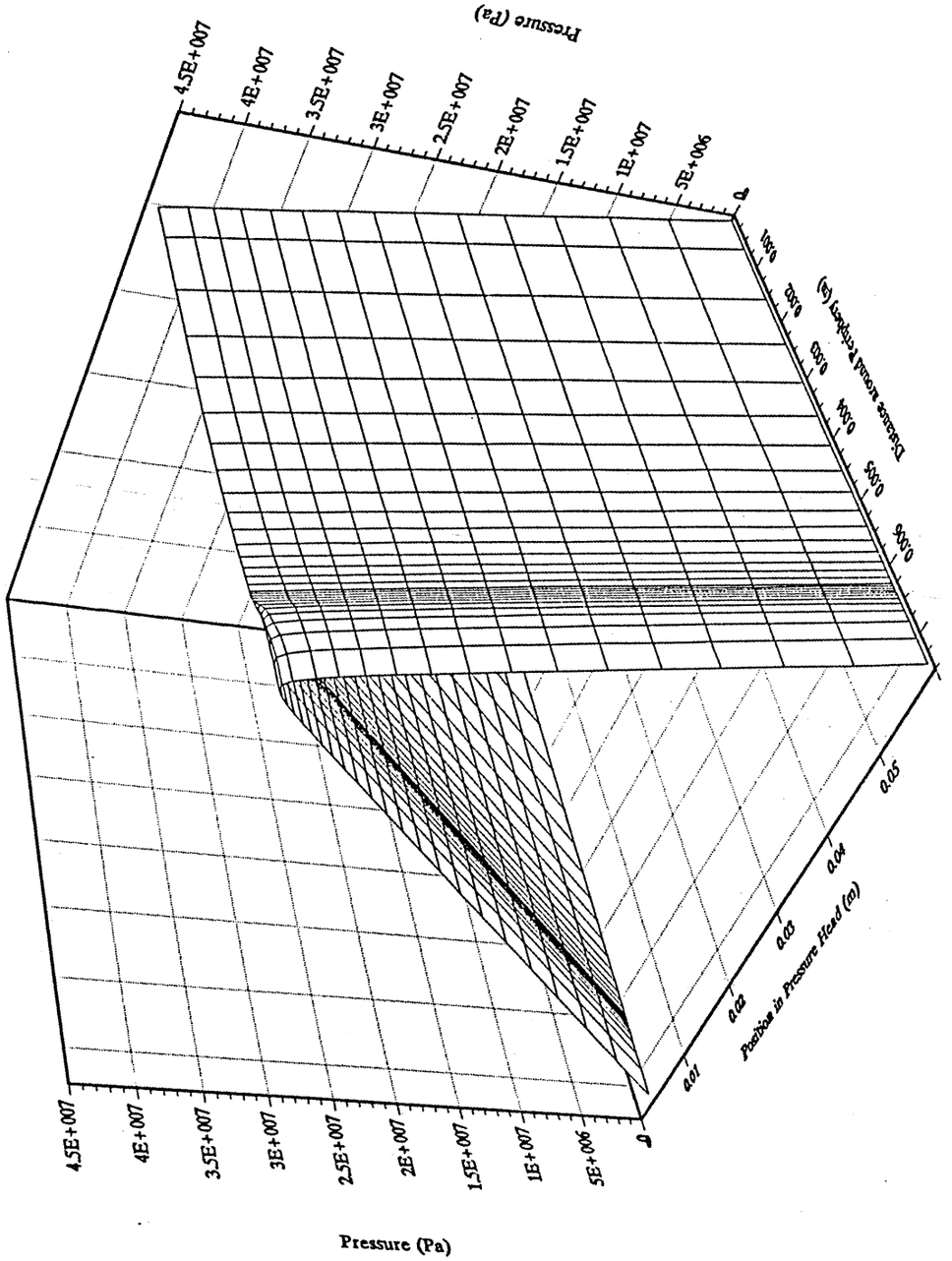

Figure 7.7 - Surface plot of the pressure field for the 8:1 aspect ratio model.

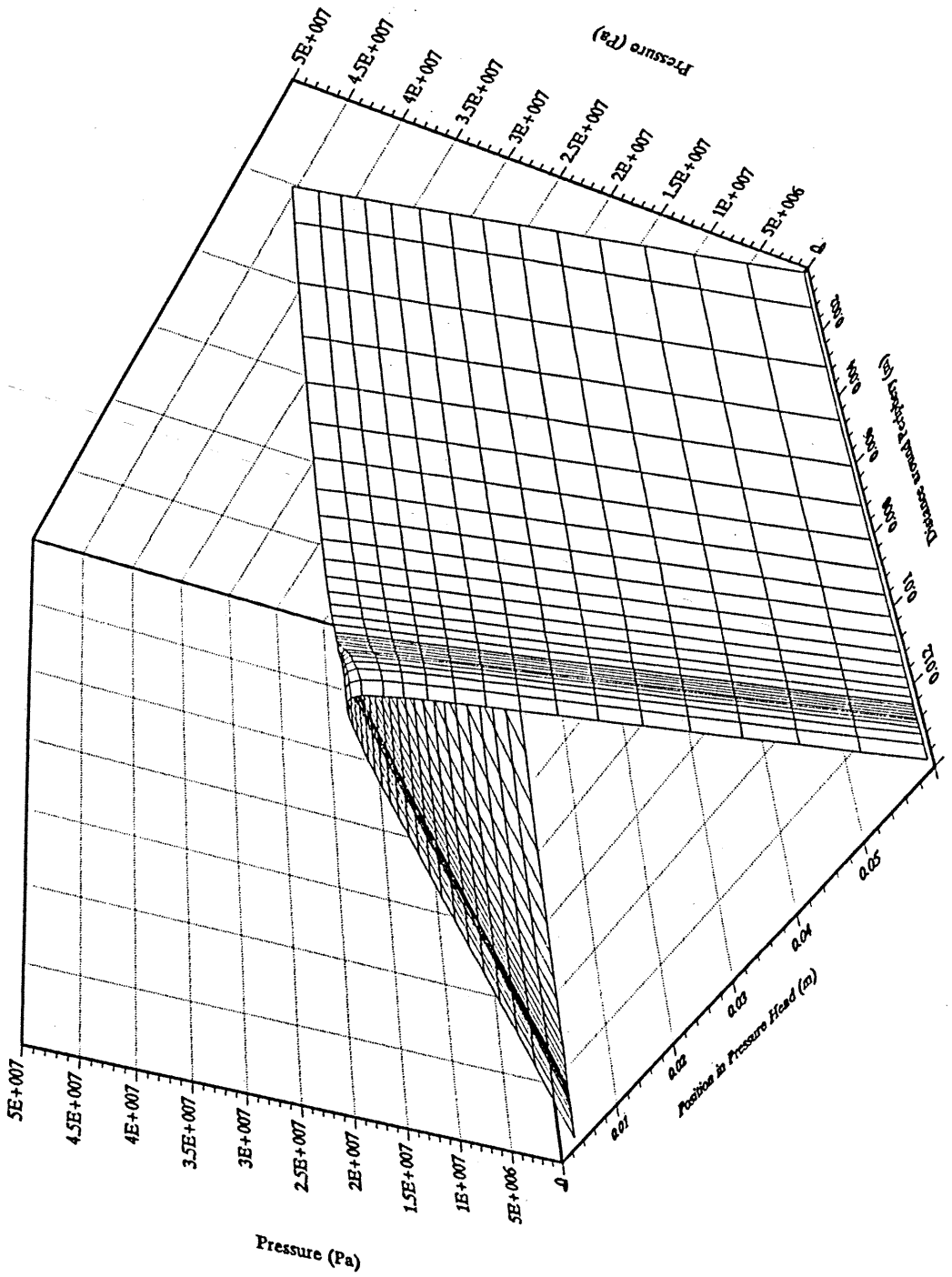

Figure 7.8 - Surface plot for the pressure field of the 16:1 aspect ratio model.

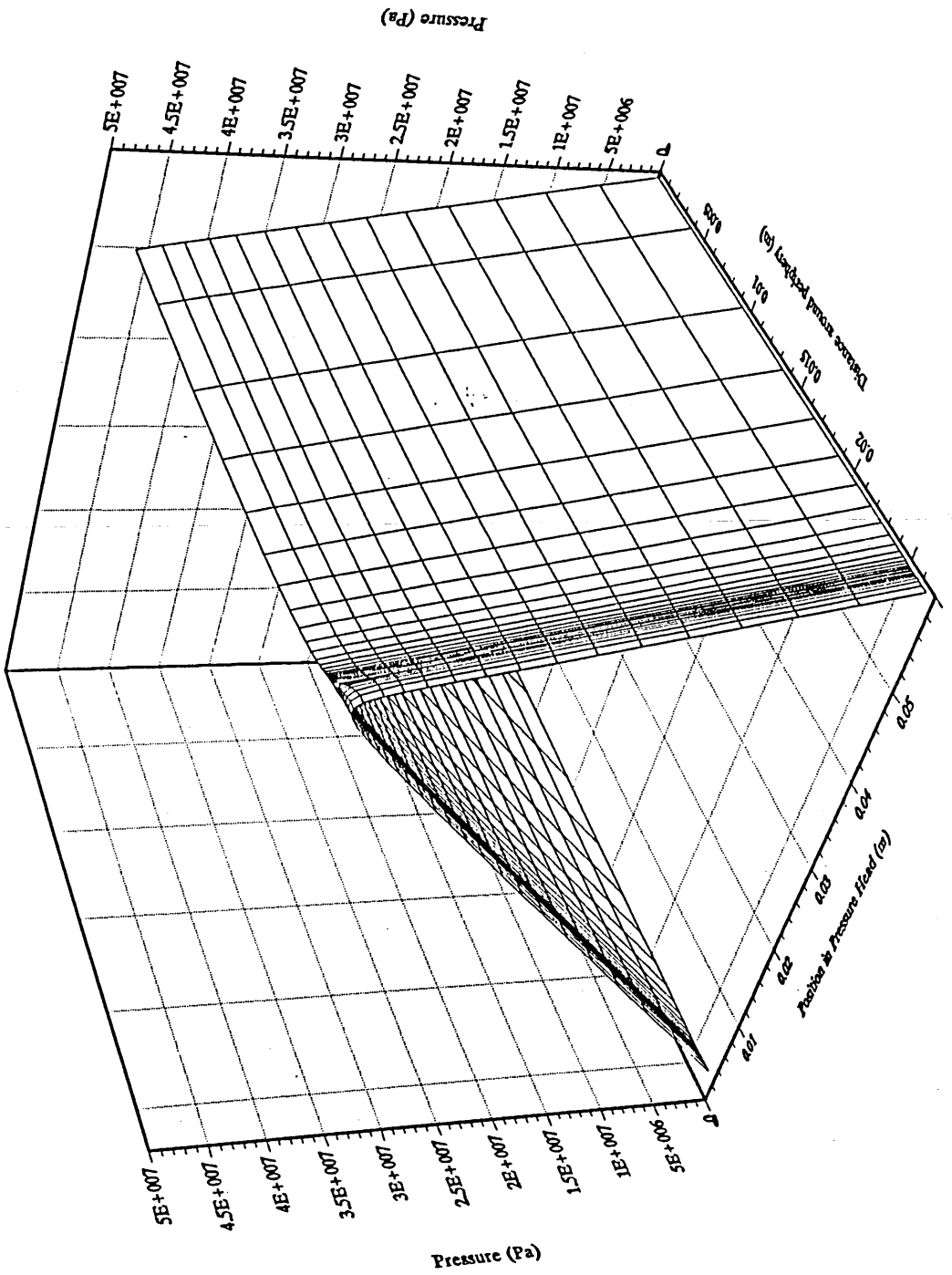

Figure 7.9 - Surface plot for the pressure field of the 32:1 aspect ratio model.

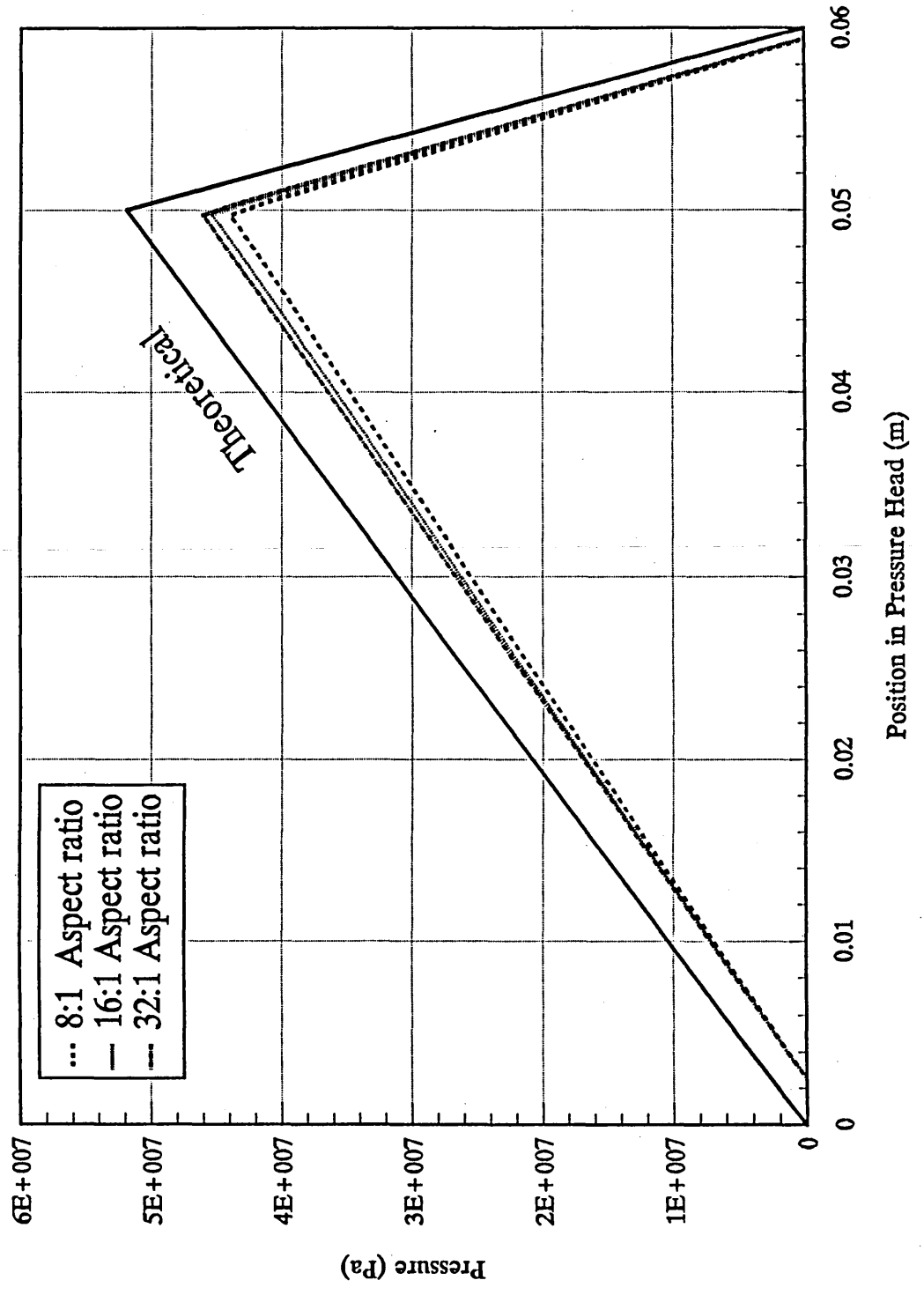

Figure 7.10 - Pressure profiles over the length of the 8:1, 16:1 and 32:1 models.

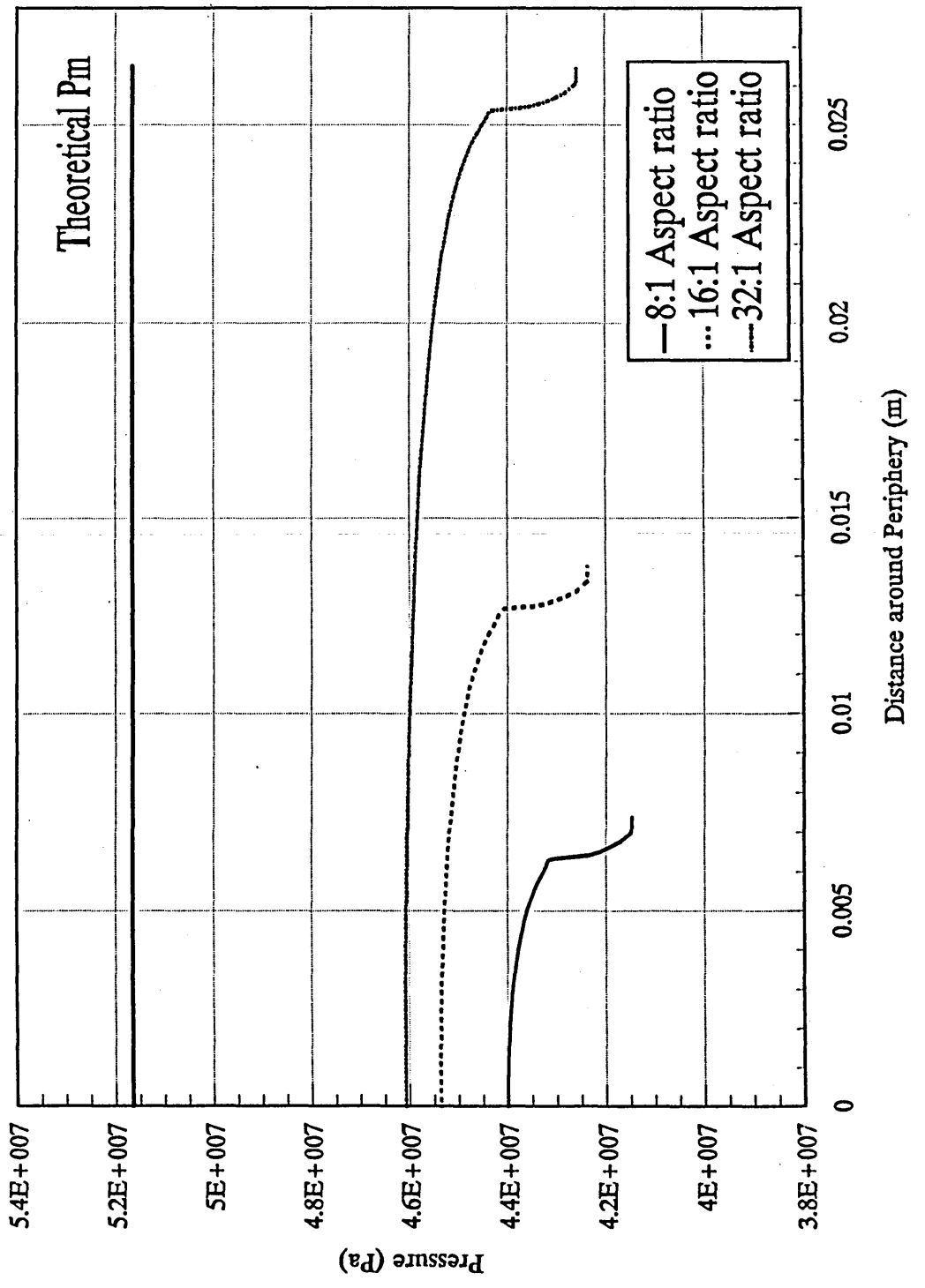

Figure 7.11 - Pressure profiles across the face of the step for the 8:1, 16:1 and 32:1 aspect ratio models.

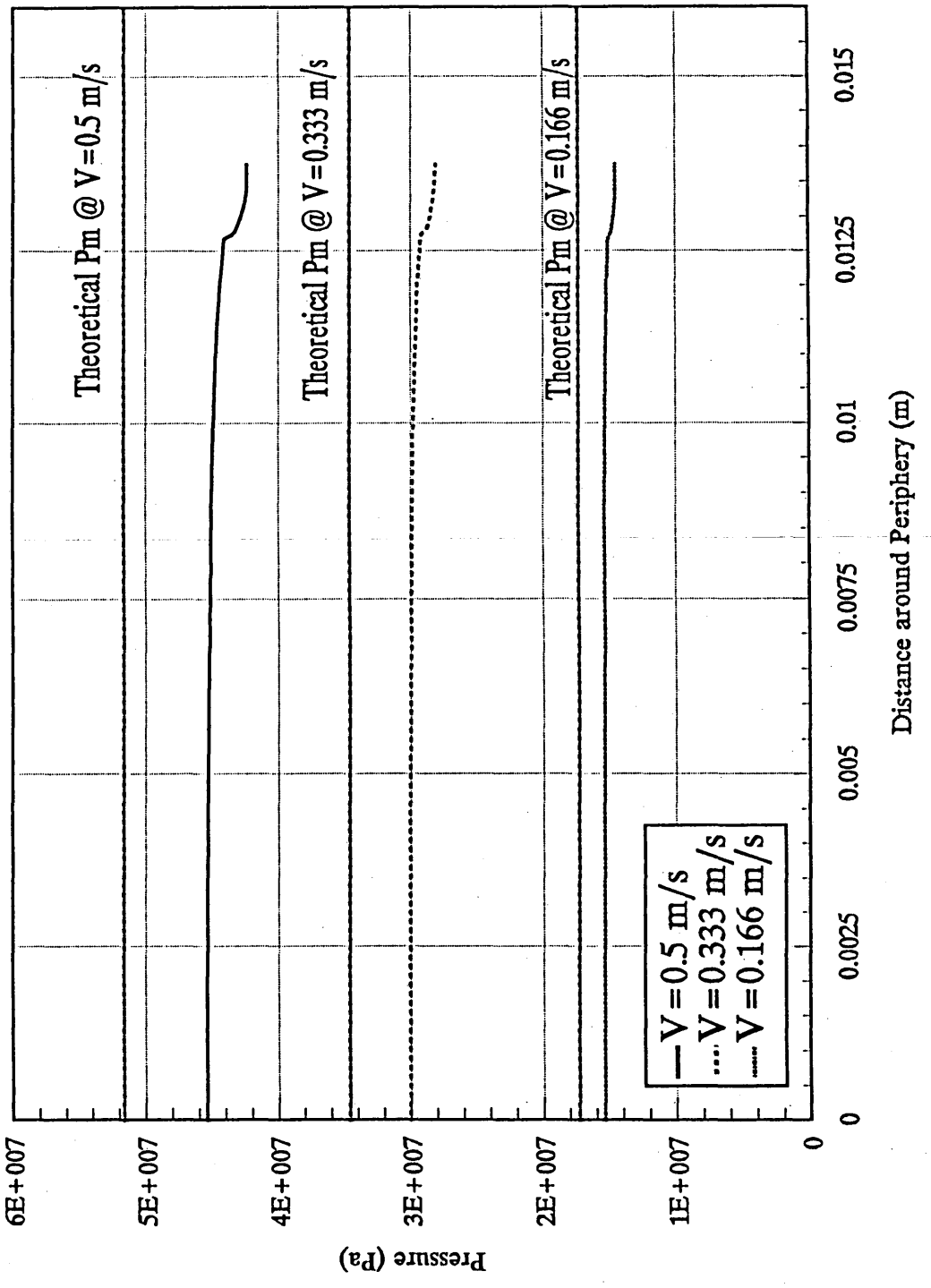

Figure 7.12 - Pressure profiles in front of the step for the 16:1 model at strip velocities of 0.5, 0.333 and 0.1666 m/s.

CHAPTER 8

8.0 Discussion

The present work investigates the deformed shape of wide strip produced by the plasto-hydrodynamic drawing process. The work consists of two main themes: Firstly, an in-depth theoretical analysis of the process parameters and the computational methods used therein; this is required for predictive control of the process. Secondly, an experimental programme was undertaken to ascertain the performance of the process with wide strip. The results of the theoretical and experimental analyses will be discussed and their outcomes compared.

8.1 Theoretical Modelling

Deformation induced by a plasto-hydrodynamic process on any arbitrary section is controlled by the working fluids temperature, exit velocity and the geometry of the pressure head assembly. Control of the process may then take one of two forms:

Firstly, each material size may undergo extensive testing to determine deformation performance; all thermal parameters and process velocities must be accurately controlled and be repeatable. The disadvantage with this form of control is that any variation in supplied materials or process parameters requires further experimental work before control is regained.

Secondly, predictive control may be achieved by the use of a mathematical model which would take into account any changes in the process parameters, and thus allow control of the process to be regained immediately. The disadvantage of this method is that it presumes that all significant physical phenomena may be accurately incorporated in any mathematical model.

In this work four areas of theoretical analysis have been addressed with regard to the mathematical modelling of the plasto-hydrodynamic drawing of wide strip. These are:

i) computational methods,

ii) a non-Newtonian model,

iii) a Computational Fluid Dynamic analysis of the hydrostatic assumption,

iv) numerical optimisation of the plasto-hydrodynamic drawing process.

8.1.1 Computational Methods

In section 5.2, a new computational algorithm was developed and applied to existing equations to form a new Newtonian model of the plasto-hydrodynamic drawing process. The ramifications of the assumptions made will now be further examined.

8.1.1.1 The Onset of Slip

Figure 8.1 shows 6 shear stress curves, three τ_1 and their corresponding τ_3 curves. It is seen that the value of τ_1 gradually reduces within the deformation zone until slip is detected on the edge face, and all shear stresses are then assumed equal to the critical shear stress τ_{crit}. The value of the edge shear stress τ_3 is seen to rise from an initial value until violation of the slip condition. This behaviour has been consistently observed with both the Newtonian and Power Law models; for this reason the violation of the limiting critical shear stress by τ_3 has been identified as the cause of the onset of slip. At this point it should be noted that, due to the iterative nature of the power law solution,

it is not possible to compute the component parts of the shear stress term, and as such the rest of this section will utilise the Newtonian model for the purpose of explanation. To understand the impact of any parameter on the process the effect of that parameter on τ_3 must be understood. The behaviour of τ_3 is seen to be of a complex nature. Figures 8.2, 8.3, and 8.4 show the effect on τ_3 of increasing velocity, at h_3/h_2 ratios of 5, 3, and 1 respectively. It is seen that for a large h_3/h_2 ratio of (5), τ_3 consistently increases from an initial value during the deformation zone. Examination of figure 8.3 reveals that τ_3 falls slightly before rising towards τ_{crit}. Figure 8.4 demonstrates that at small h_3/h_2 ratios, τ_3 falls rapidly from a high initial value by approximately 50% of this value before rising towards τ_{crit}. The cause of this variation is examined below.

The hydrostatic assumption forces the pressure gradient developed on the width face to be propagated around the section to its edge. This means that the pressure gradient felt on the edge face has no direct mathematical relationship to the side clearance h_3. This is evident in Memon's (42) equation for the edge shear stress given below as equation 8.1.

$$\tau_{3i} = -\left(\frac{\partial p}{\partial x_{1i}}\right)\frac{h_{3i}}{2} - \frac{\mu V_i}{h_{3i}} \qquad (8.1)$$

Equation 8.1 can be seen to consist of two terms: Firstly, a pressure driven term containing the pressure gradient, which is effectively scaled by the side clearance. This term will increase in direct proportion to h_3. Secondly, a velocity driven term scaled by μ but whose initial magnitude will depend upon the quotient of V (local velocity) and h_3. After this point the magnitude will depend upon the relative rates of change of V and h_3. An expression for the

relative change of V and h_3 is not clearly discernible. However, a review of the performance of both terms may be made by separating τ_3 into its component parts and plotting them against pressure head position. This is shown for a velocity of 0.1 m/s, at aspect ratios of 5, 3, and 1 in figures 8.5, 8.6, and 8.7. It is seen that the initial value of the velocity term is inversely proportional to h_3. The rate of increase of h_3 is seen to be greater than that of V, denoted by a fall in magnitude after the initial point. The pressure term is generally dominant in the creation of τ_3.

8.1.1.2 The Solution of Equations within the Slip Regime

It was previously stated that at some predetermined value of shear stress τ_{crit}, slip will occur at the boundary of the working fluid. As a consequence of this, a constant shear stress will be felt for any increase in the shear rate. This directly affects the calculated pressure field, as it was shown in section 5.2.2 that beyond this point the pressure gradient must effectively be zero. This causes the Plastic-yield equation (PYE) to effectively be modified, from

$$P + \sigma_x - \sigma_y = 0 \qquad \textbf{PYE before slip}$$

to

$$C + \sigma_x - \sigma_y = 0 \qquad \textbf{PYE after slip}$$

where C is a constant and is equal to the pressure at the onset of slip. During the iterative solution of the equation after the onset of slip, it is seen that any change in σ_x can only be balanced by a change in σ_y alone and not σ_y and

pressure as before the onset of slip. This will change the dynamic response of the equations to further deformation. This change in response is found in the thickness curve for the deformation zone. Figure 8.8 demonstrates the change in the slope at the onset of slip for different velocities.

Figure 8.9 shows the percentage reduction in area for each curve in figure 8.8, plotted against entry velocity. A distinctive bell shape is seen in the performance of the process. The mechanism for the formation of this performance curve may now be discerned. Process performance is seen to initially increase with velocity. The critical shear stress is exceeded at higher velocities causing a degradation in draw performance. As the process velocity rises, the loss in performance increases due to the earlier introduction of slip; thus forming the bell shaped performance curve. This form of performance curve is only produced by models employing this treatment of slip; previous models show a flat response after the onset of slip.

8.1.2 The non-Newtonian Model

A new non-Newtonian model of the plasto-hydrodynamic process was developed in chapter 5. The impact of various assumptions and model parameters will now be examined further.

8.1.2.1 Laminar flow

For the assumption of laminar flow to be valid, the Reynold's number (Re) for the internal flow in the pressure head must be below the critical Reynold's number, which is normally assumed to be 2300. For internal flows, Reynold's number is calculated from the following expression:

$$Re = \frac{\rho V D}{\mu}$$

where

ρ = Density

V = Velocity

D = Characteristic dimension

μ = Viscosity

The Re will now be calculated for the pressure head geometry used during this study, using generic worst case material properties.

Polymer properties

μ = 100 Pa.s

ρ = 1200 Kg/m^3

Characteristic dimensions

h_1 = 0.2 mm

h_2 = 0.04 mm

h_3 = 0.04 - 0.2 mm

W = 25.4 mm

The maximum velocity of the current test apparatus is 0.5 m/s. Substitution of these values into the expression for Re number yields a Re number range of 2.4 x 10^{-4} to 0.147. The extremely low values are a consequence of the thin film like dimensions of the pressure head and the high viscosity of the fluid.

Therefore, the assumption of laminar flow is seen to be valid.

8.1.2.2 Isothermal Conditions

It was assumed during the derivation of the non-Newtonian model, that isothermal conditions exist. However, the process generates heat internally, due to viscous dissipation in the fluid and the plastic deformation of the strip. This omission will introduce some error into the solution of the equations. However, the pressures generated are extremely high, which will cause an increase in viscosity. The effect of these unaccounted for phenomena are contrary in nature, and some degree of cancelling will occur.

8.1.2.3 The General Form of the Power Law constitutive equation

The non-Newtonian model developed in chapter 5, utilised the Power Law (PL) model of shear rate dependent behaviour. The form of PL used was given in equation 5.3, and is repeated below:

$$\tau_{ij} = K(\dot{\gamma}_{ij})^n \qquad (5.3)$$

The type of behaviour the PL describes is dependent upon the value of n, the consistency index. Three regimes may be identified:

i) $n<1$, represents pseudoplastic or shear thinning behaviour;

ii) $n=1$, at this point the PL reduces to the Newtonian case;

iii) $n>1$, this case represents dilatant or shear thickening behaviour.

Whilst the PL may be applied to a wide range of fluids, there are various limitations associated with its use which are examined below.

The PL has no physical theory for its derivation. In essence it is a

curve fit to the shear stress - shear strain rate curve. As such its accuracy is dependent upon the data of the fluid's behaviour; ideally such data should encompass the operating range of the model.

The PL equation is not dimensionally stable, as any change in n the consistency index, will change the units of K, the consistency constant.

Problems may be encountered in computations that reach zero shear rate. Zero risen to a power is zero, but a computer would normally use logarithms to make the calculation, causing an error at zero shear rate.

8.1.2.4 The effects and limitations of the Power Law equation on model performance

The power law model utilises two parameters to describe fluid behaviour. These are n, the consistency index and K, the consistency constant, as described previously. The effect and limits of these parameters on model performance will now be examined.

8.1.2.4.1 The limitations of the consistency index n

In section 5.3.1.2.1 algebraic problems encountered in the solution of the power law flow equation were discussed. A restriction was placed upon the λ function, such that an integer must be returned for a specific value of n. A further more subtle restriction will now be discussed. Restating equation 5.21 below:

$$0 = \frac{1}{\left(\frac{\partial p}{\partial x}\right)^{\lambda(1)}}\left[\left(\frac{\partial p}{\partial x}\frac{h}{K} + \frac{\tau}{K}\right)^{\lambda(n)} - \left(\frac{\tau}{K}\right)^{\lambda(1)}\right] + V \qquad (5.21)$$

This equation may be rewritten in the following form

$$0 = C_1\left[\left(\left(\frac{\tau}{K}\right) + C_2\right)^{\lambda(1)} - \left(\frac{\tau}{K}\right)^{\lambda(1)}\right] + V$$

where

$$C_1 = \frac{1}{\left(\frac{\partial p}{\partial x}\right)\lambda(1)}$$

$$C_2 = \frac{\partial p}{\partial x}\frac{h}{K}$$

The terms within the square brackets will now be examined assuming an integer value of the λ function. The first term would expand to form a 1/n + 1 order polynomial equation. By inspection, it may be seen that the polynomial equation would contain as its first term a term equal to the second term in the square brackets, but opposite in sign. This would reduce the order of the polynomial formed by 1 to 1/n. As an example, assume n=0.5 then equation 5.21 may be expanded to yield;

$$0 = \tau^2 + C_2 K\tau + K^2\left[\frac{C_2^2}{3} + \frac{V}{C_1 C_2}\right]$$

Then forming the components of the discriminant of a quadratic equation a, b and c:

$$a = 1$$

$$b = C_2 K$$

$$c = K^2 \left[\frac{C_2^2}{3} + \frac{V}{C_1 C_2} \right]$$

Substitution of representative values for terms in the above equations, yields the following comparison of magnitudes:

$$a = 1 \times 10^0$$

$$b = 1 \times 10^5$$

$$c = 1 \times 10^{14}$$

It can be seen from the values above, that the roots of equation 5.21 for n=0.5 will be a complex conjugate pair, and that the power law model in its present form is unstable with this value of n, as the shear stress is indeterminable.

The theory of equations states that only odd integer polynomial equations are guaranteed to have at least one real root. With this in mind, a 1/n range of 1 to 7 was explored with the model to determine the limits of its stability. The pressure head geometry is that given in table 6.1 with the following exceptions:

i) $\tau_{crit} = 0.5$ MN/m^2,

ii) the velocity was held constant at 0.15 m/s,

iii) the power law index and constant were modified, as denoted in the tabulated results.

Table 8.1 below, gives the results for the range of 1/n values studied, and the PRA predicted, with the power law constant and index utilised.

Table 8.1 Results of stability survey for the power law model

1/n	n	K	P.R.A.
1	1.0	120	14.186
2	0.5	UNSTABLE	******
3	0.3333	25000	13.493
4	0.25	UNSTABLE	******
5	0.2	UNSTABLE	******
6	0.1666667	107500	11.637
7	0.1428571	160000	13.523

No attempt was made to achieve maximum predicted PRA during the survey, only an attempt to predict reasonable deformation performance. The points of instability found during the survey are seen to be scattered among odd and even 1/n values. The following points should be noted that, in the case of 1/n = 5:

i) the program will only seek to establish roots in a physically realistic range,

ii) although the range was extended for the survey this does not preclude a real root at some physically unrealistic point beyond the range of the algorithm.

To clarify the behaviour of the polynomials formed at various 1/n values, the error associated with the solution of the equation 5.21 for τ_1 prior to deformation is given graphically in figure 8.10. It is seen that the 1/n values which are stable show a linear or nominally cubic form to their residual

curves, whilst the unstable 1/n values show a nominally quadratic form to their residual curves. The residuals curves should then enable other 1/n values than those studied to be assessed for stability.

The limitation on the value of n, the consistency index, is seen to be not only those values n which produce an integer value of the λ function but, also those values which produce stable integer values of the λ function.

8.1.2.4.2 The effect of the consistency constant K

An arbitrary value of n=0.3333, with a fixed velocity of 0.15 m/s, was used to determine the effect of the consistency constant, K. The consistency constant K was then varied through the range 12000 - 34000. The predicted deformation is shown graphically in figure 8.11. It is seen that the consistency constant K has a direct scaling effect on the predicted deformation performance until the onset of slip, where the performance is seen to reach a plateau. This form of response to the value of K is reasonable on inspection equation 5.3.

8.1.2.5 Redundant Work within the Plasto-hydrodynamic model

In any reduction process that produces a convergent flow of material, a degree of internal shear distortion will be induced. The energy to effect this distortion is termed Redundant Work. In section 5.3.2.2, an attempt was made to quantify the increase in axial stress that the inclusion of this phenomena would produce. The analysis proved to be unstable in practice, with the central region of the performance either crashing the program or entering into an endless loop. Figure 8.12 shows a comparison of the PL model with, and without, redundant

work activated. It is seen that, prior to the unstable region both curves are in close agreement and after, the analysis with redundant work decays rapidly from a higher initial predicted performance. The instability in the analysis could not be eliminated, even after extensive review and numerical investigation.

It is the view of the author, that the instability is due to a combination of two factors. Firstly, the analysis over-predicts the deformation during the early part of the deformation zone, and thus moves the solution into an unstable region where no sensible solution to the plastic-yield equation (PYE) may be found. Possible indications of this are given in figure 8.12. Intuitively one would conclude that the inclusion of redundant work would produce a higher stress for a specified value of b, the slope of deformation. This would then produce lower levels of deformation, as the PYE would be satisfied with this lower slope. This is seen not to be so from figure 8.12. Secondly, during the derivation of the expression for the axial stress it is assumed that $\sigma_1 = \sigma_x$ and $\sigma_2 = \sigma_3 =$ Pressure. From fundamental definitions, there is zero shear stress on a plane of principal stress. However, the plasto-hydrodynamic process depends upon there being a large shear stress at the surface of the material, where this said principal stress is acting. To compound this, the presence of shear distortion or shear strain, which varies across the section, has previously been admitted to. This implies not only a varying state of stress and strain but of yield stress across the section. A possible solution to these dilemmas would be a three dimensional plasticity model of the section, with the PL model being used to calculate the boundary conditions.

It was decided that such an undertaking was beyond the remit of the

current work.

8.1.2.6 The effect of h_1/h_2 ratio on τ_1

Until now this discussion has concentrated on the dominant role of τ_3 in the onset of slip and its influence on the process performance. However, due to the aspect ratio of the material, and hence the greater area upon which τ_1 acts, this term will be dominant in the creation of σ_x.

Figure 8.13 shows τ_1 over the length of the deformation zone for a h_1/h_2 range of 6-10. It is seen that the level of stress is inversely proportional to the h_1/h_2 ratio.

8.1.3 A Computational Fluid Dynamic Analysis of the Hydrostatic Assumption

In section 7.1 the following two questions were put forward for solution by Computational Fluid Dynamic (CFD) analysis:

i) what effect does the aspect ratio of the working material have on the pressure field?

ii) if the hydrostatic assumption (HA) is valid, at what proportion of the velocity required for deformation will the pressure field meet the HA?

The results of these analyses will now be discussed.

8.1.3.1 The effect of aspect ratio on the pressure field prior to deformation

The pressure fields given in figures 7.7, 7.8 and 7.9 are for aspect ratios of 8:1, 16:1 and 32:1, and demonstrate the following points:

Firstly, the general form of the pressure fields are consistent with the

analysis of Rayleigh (66), in that the pressure gradients of the two lands are linear in form. This is emphasised again in figure 7.10 where the pressure profile for the longitudinal plane of symmetry is given. It may also be seen that all the pressure gradients are lower than those predicted by the analytical model. The degree of error is reduced with increasing aspect ratio. A possible reason for the observed loss in predicted pressure but not of form, is that the side clearance allows fluid to be bled away from the step thus reducing the overall pressure, but the volume of fluid lost is insufficient to cause gross disruption of the normal hydrodynamic flow pattern. Figure 8.14 shows the velocity vectors for the 32:1 model in cross section. This demonstrates the fluid flow towards the edge of the strip material, and the localisation of the disruption within the general flow pattern.

Secondly, there is a small zone of low pressure at the edge of the strip adjacent to the step. Figure 7.11 gives the pressure profiles of the different aspect ratio models immediately before the step. The reduction in pressure at the longitudinal plane of symmetry is again seen. A gradual reduction in pressure is seen across the face of the strip, with the pressure loss increasing rapidly as the edge of the strip is approached. It is seen that for the majority of the strip face the HA is reasonable.

The overall reduction in pressure is seen as the most important of the two phenomena described. The losses at the longitudinal plane of symmetry are 14.79%, 12.16% and 10.77% for the 8:1, 16:1 and 32:1 models respectively. The hydrodynamic pressure is one of the three terms in the Plastic-yield Equation (PYE) and as such, errors of this magnitude will have a significant effect on the predicted performance.

8.1.3.2 The effect of velocity on the accuracy of the Hydrostatic Assumption

Figure 7.12 shows pressure profiles immediately in front of the step for the 16:1 ratio model at three different velocities, 0.5 m/s, 0.333 m/s and 0.166 m/s. The reduction in the overall predicted pressure discussed above is seen to be present at reduced velocities. It is seen that the variation in pressure at the edge of the strip adjacent to the step is reduced at lower velocities. The reduction in the pressure variation across the face of the strip indicates that the HA is reasonable for all velocities, and not just the extreme conditions at the point of yielding.

8.1.3.3 Comparison of CFD analysis with previously published results

Prior to the current work, details of initial CFD based studies into the HA were published (Stokes (81), appendix 3). Differences in model performance are seen between the two sets of models. A distinct drop in the predicted pressure field is seen to occur near the edge of the strip in the initial studies, which is contrary to the predictions of the current study. Comparison of figure 7.4b with its equivalent shown in appendix 3, reveals a greatly improved graduation in the grid spacing across the width of the strip for the current analyses. The change in model performance is attributed to this smoothing of the grid structure and its inherent increase in accuracy.

8.1.4 Numerical Optimisation of the Plasto-hydrodynamic Drawing Process

The numerical optimisation of the Plasto-hydrodynamic drawing process consists of two distinct parts.

Firstly, the Newtonian optimisation, coupled with an equivalent optimisation sequence with the power law model simulating Newtonian flow characteristics (n=1).

Secondly, an optimisation sequence with a power law index (n) of 0.33333 and power law constant (K) of 25000. Fluids with these power law parameters equate to a generic Nylon 12 at shear strain rates of 1×10^3, above which is the estimated operating range of the PHD process.

8.1.4.1 Newtonian Optimisation

The results of the numerical optimisation of the Newtonian plasto-hydrodynamic model demonstrate the following:

i) the optimum h_1/h_2 ratio is a linear function of velocity,

ii) the optimum h_3/h_2 ratio is a linear function of velocity,

iii) the optimum L_1/L_2 ratio fluctuates with velocity - the standard deviations of the samples are very large compared to those of the other ratios thus preventing a correlation being made,

iv) the overall peak performance of the process is seen to reduce with velocity.

8.1.4.2 The equivalent Non-Newtonian Optimisation

The results of the numerical optimisation of the non-Newtonian plasto-hydrodynamic model emulating a Newtonian fluid (figures 6.20 and 6.21)

demonstrate the same general features as described for the Newtonian model above.

8.1.4.3 Comparison of Newtonian and equivalent optimisation sequences

A comparison of the predicted pressure head geometrical ratios for the Newtonian and the non-Newtonian equivalent optimisation sequences is made graphically in figures 8.15 and 8.16. A plot of the land length ratio is not included, due to the excessive amount of scatter. It is seen from figure 8.15 that the models agree to within 0.5 (dimensionless units) approximately for the optimum h_1/h_2 ratio. The agreement of the two models is even greater for h_3/h_2 ratio, within 0.25 approximately. Figure 8.17 shows a comparison of the mean Percentage Reduction in Area (PRA) for the two models - a constant difference of 1.0% PRA, approximately, is seen. The differences between the two models may be explained by consideration of two groups of factors.

Firstly, the power law model omits strain rate sensitivity from its formulation. Published data by Hashmi (82) demonstrated that the effect of this phenomena was small in this type of problem and, as previously described, the phenomena of redundant work was incorporated in an attempt to improve the plasticity modelling. With the problems encountered during the modelling of redundant work, the power law merit function contains neither redundant work nor strain rate sensitivity in its formulation.

Secondly, the power law merit function uses linearly interpolated mid-point values when calculating the axial stress σ_x during the solution of the equation system. In contrast to this, the Newtonian merit function derived from Memon's (42) discretisation scheme with the new algorithm, uses the value of

the current node over the entire step.

The differences in the performance of the two merit functions can then be attributed to these variations in formulation.

8.1.4.4 The Effect of non-Newtonian fluid behaviour

The results of the numerical optimisation sequence of the power law model using the fluid parameters of a generic Nylon 12 are given graphically in figure 6.29, and demonstrate the following:

i) the optimum h_1/h_2 ratio is a linear function of velocity,

ii) the optimum h_3/h_2 ratio is a linear function of velocity,

iii) the optimum L_1/L_2 ratio fluctuates with velocity; the standard deviations of the samples are very large compared to those of the other ratios thus preventing a correlation being made,

iv) the overall peak performance of the process is seen to reduce with velocity, and at a greater rate than that of the Newtonian/equivalent optimisation sequences.

The increased rate of reduction in drawing performance is thought to be a consequence of the shear thinning behaviour of the fluid. A detailed analysis of the shear stresses and, in particular the exact effect of the velocity component, is not possible due to the use of the iterative solution method required for their computation.

8.1.4.5 The use of Surfaces in the visualisation of System performance

During the derivation of the merit functions, ratios were used to reduce the problem to 3 dimensions. A series of performance surfaces may be generated by holding the h_3/h_2 ratio constant, giving x, y equal to L_1/L_2, h_1/h_2 respectively and z equal to PRA. Then, by varying the h_3/h_2 ratio by small increments about the optimum value for a specified process velocity, a sequence of performance surfaces may be built up demonstrating the development of the merit function's performance in three dimensional space. Figures 8.18 to 8.21 give the performance surface development of the modified Newtonian model at a velocity of 0.2 m/s for h_3/h_2 ratios of 1.5, 2.0, 2.16 (the optimum) and 2.5 respectively.

The major topological feature of the performance surfaces is a ridge form lying parallel to the L_1/L_2 axis with a step in the region of the origin. The position of this ridge explains the apparent insensitivity of both merit functions to L_1/L_2 ratio, in that above a value of approximately 8 the ridge appears essentially flat. The formation of the ridge may be explained as the sum of two competing phenomena. Firstly, it was shown in section 8.1.2.6 that τ_1 is inversely proportional to h_1/h_2 ratio, producing increasing PRA. Secondly, at some point the critical shear stress τ_{crit} will be exceeded, thus causing the onset of slip and its associated loss of performance. Reducing h_1/h_2 ratio further will introduce slip into the calculation at an earlier point. This will increase the effect of slip and reduce the performance to a greater and greater extent.

The step close to the origin at small values of L_1/L_2 and h_1/h_2 ratio was found to be formed as a consequence of slip being present throughout the deformation zone.

Detailed inspection of figure 8.20 for example, reveals small scale ridging of the surface between the origin and a h_1/h_2 ratio of 8 (approximately); figure 8.22 gives an alternate view of the surface shown in figure 8.20. From table 6.4 we see that the optimum value of h_1/h_2 ratio is within the region affected by slip - an explanation for the large scatter of the L_1/L_2 predictions is now possible. Figure 8.23 shows a cross-section at h_1/h_2 equal to 9 of the surface given in figure 8.20, giving more detail of the ridging. It is shown that in the region of the optimum (PRA) the surface is multi-modal, in that it contains many local optima of which only one may be the global optimum. This violates a fundamental assumption made during the derivation of all numerical optimisation procedures, that of uni-modality. The program can then be assumed to have fallen into a ridge leading to a local optimum and have been unable to escape. This would be possible towards the end of the search when the search step would be small (less than the ridge width). The distribution of the L_1/L_2 ratio would then be a function of the distribution of the local maxima of the surface.

The exact causal mechanism for the production of the small scale surface ridging is as yet unknown, but it can be postulated that it is a consequence of the dynamical interaction of the plasto-hydrodynamic deformation process and the non-linear phenomena of slip.

A review of figures 8.18 to 8.21 gives the development of the performance surface with increasing h_3/h_2 ratio. It is observed that the height of the ridge increases up to its optimum as predicted by the optimisation sequences, and that the width of the ridge also increases with increasing h_3/h_2 ratio.

It can be seen that the technique of using sequences of performance surfaces yields a much improved picture of pressure head performance.

8.2 Experimental Results

8.2.1 The Overall Reduction in Cross Section

In section 8.1.1.1 the theoretical reasoning behind the controlling effect of h_3/h_2 ratio on the deformation process was discussed; a prior indication of the importance of this was given in the work on numerical optimisation in chapter 6. The experimental programme was then designed to test the validity of this analysis. Three differing pressure head configurations were used, combined with three polymer melt temperatures to produce sufficient data for reasonable study.

Figures 4.3 - 4.11 show the experimental results in a form that clearly shows the effect of temperature. It is seen that the process performance is inversely proportional to temperature in all experimental conditions used for this study.

Figures 8.24 - 8.32 show the experimental data recast to show the effect of h_3/h_2 ratio on process performance. The plots are at constant temperature and varying h_3/h_2 ratio.

Figures 8.24 - 8.26 are for a temperature of 195°C; they show PRA, PRW and PRT respectively. The plots of the data for the h_3/h_2 equal to 3.5 show great fluctuations in magnitude. No evidence can be found to explain the variations in performance. Two possible explanations are;

i) the polymer suffered from thermal degradation; this is unlikely as after each rebuilding of the pressure head for a new configuration, fresh polymer was used and then protected by an inert gas blanket at

all times,

ii) the strip material varied in quality over the length of the batch.

Unfortunately the fluctuations in the experimental data were not discovered until after the configuration of the pressure head had been changed by precision grinding of the pressure head inserts.

However, reviewing figures 8.24 - 8.26 shows that the trace for a h_3/h_2 ratio of 2 consistently produces the greater reductions, and that the trace for a h_3/h_2 ratio of 5 consistently produces the lowest performance. This correlation is only possible if one ignores some of the greater fluctuations in the h_3/h_2 ratio of 3.5 data.

Figures 8.27 - 8.29 are for a temperature of 215°C; they show PRA, PRW and PRT respectively. A much better correlation with the theoretical prediction of the controlling effect of h_3/h_2 ratio is seen.

Figures 8.30 - 8.32 are for a temperature of 235°C; they show PRA, PRW and PRT respectively. The traces for all the performance indicators show the greatest performance with a h_3/h_2 ratio of 3.5 not of 2, and the lowest performance with a h_3/h_2 of 5. The experimental data for the different ratios were achieved using different batches of material. These were:

$h_3/h_2 = 5$	batch 1, σ_{yo}=74.58 MPa,
$h_3/h_2 = 3.5$	batch 2, σ_{yo}=88.49 MPa,
$h_3/h_2 = 2$	batch 3, σ_{yo}=72.17 MPa.

This would not explain the form of these results. No fluctuations are seen and the data is reasonably smooth.

8.2.2 Results for the Distribution of Cross Section

The results for the analysis of Cross Section were shown graphically in figure 4.12. The performance of the sample plotted against velocity is given in figure 4.11 and is denoted as experiment 23. A vertical section through figure 4.11 was made at a velocity of 0.2 m/s (approximately) and analysed, the results of which are given graphically in figure 4.13. It is seen from figure 4.12 and figure 4.13, that the original section has an hourglass form (approximately). This form is seen to be preserved with all the levels of deformation achieved. It is seen from the results that the quality of form of the feed stock determines that of the output, and no smoothing is incurred during deformation by the plasto-hydrodynamic drawing process.

8.2.3 Results for the Reduction of section corner radius

Plates 4.1 - 4.4 show representative samples of the section corner radius. A graphical method was used to assess the reduction in corner radius with overall deformation. The results of this analysis are shown in figure 4.14. Inspection of figure 4.14 shows a large variation in the achieved corner radius for a specified reduction. The precise form of any relationship between corner radius and reduction may not be identified, other than to state that the corner radius of the output product is reduced during plasto-hydrodynamic drawing.

8.3 Comparison of Experimental Results and Model Predictions

8.3.1 Selection of experimental data

From the results given in chapter 4 the experimental data at 235°C has been selected for direct comparison with the power law model. This is due to the low level of scatter exhibited by the data at this temperature.

8.3.2 Selection of material properties utilised in the power law model

The material properties of the strip material are those found in chapter 2. The usage of each batch of material was as follows:

i) batch 1 was used at a h_3/h_2 of 5

ii) batch 2 was used at a h_3/h_2 of 3.5

iii) batch 3 was used at a h_3/h_2 of 2

The property values of the relevant batch were utilised in the comparison.

The fluid parameters for the power law were fitted to the data supplied by the manufactures, which resulted in the following values:

i) consistency constant, K = 32000

ii) consistency index, n = 0.33333

A graphical representation of the resultant fluid properties and the manufactures' data is given in figure 8.33.

8.3.3 The value of the Critical Shear Stress τ_{crit}

The viscosity data provided by EMS-Grilon for the Grilamid L25 was insufficient to identify the critical shear stress of the polymer. The value of τ_{crit} is highly subjective for most polymers, with published values only available for those that are unsuitable for the plasto-hydrodynamic process. To avoid the use of a single

subjective value for τ_{crit}, the selected experimental data is compared with the power law model with three different values of τ_{crit} these being 0.4 MN/m², 0.5 MN/m² and 0.6 MN/m².

8.3.4 Analysis of Experimental and Simulated drawing performance

The experimental results at 235°C and the predictions of the power law model are given graphically in figures 8.34 - 8.36 for h_3/h_2 ratios of 5, 3.5 and 2, respectively.

The distinctive bell shaped curve shown previously is seen to be absent from the experimental results, with a nominally linear increase in drawing performance with increasing velocity. This form of drawing performance is comparable to that shown by the power law model when the pressure head is slipping over its entire length.

The predictions of the power law model at each τ_{crit} value will now be examined:

i) τ_{crit} = 0.4 MN/m²; the curves of predicted performance at all h_3/h_2 ratios are in the slip condition over the entire length of the deformation zone. They show a good correlation in form with the experimental data, but the error in predicted performance varies from 5% to 50%.

ii) τ_{crit} = 0.5 MN/m²; the curves of predicted performance show a good correlation in form where the model is entirely in the slip condition. The ranges where the model is not in the slip condition produce a poor correlation in both form and the level of predicted performance.

iii) τ_{crit} = 0.6 MN/m², at this elevated level of critical shear stress the power law model is only in slip over the entire length of the deformation at two places in the simulated range. The shape of the performance curve over the remainder of the simulated range shows the righthand portion of a bell shaped curve. The model greatly over-predicts the drawing performance in the bell shaped or non-slip range of the simulation.

8.3.5 Summary of the comparison between experimental and theoretical data

The model predictions with τ_{crit} equal to 0.4 MN/m² show the closest correlation to the experimental data. The predicted PRA is seen to increase in a nominally linear form with velocity. The level of performance is consistently under-predicted by the power law model and a lack of sensitivity to changes in h_3/h_2 ratio is also demonstrated by the power law model.

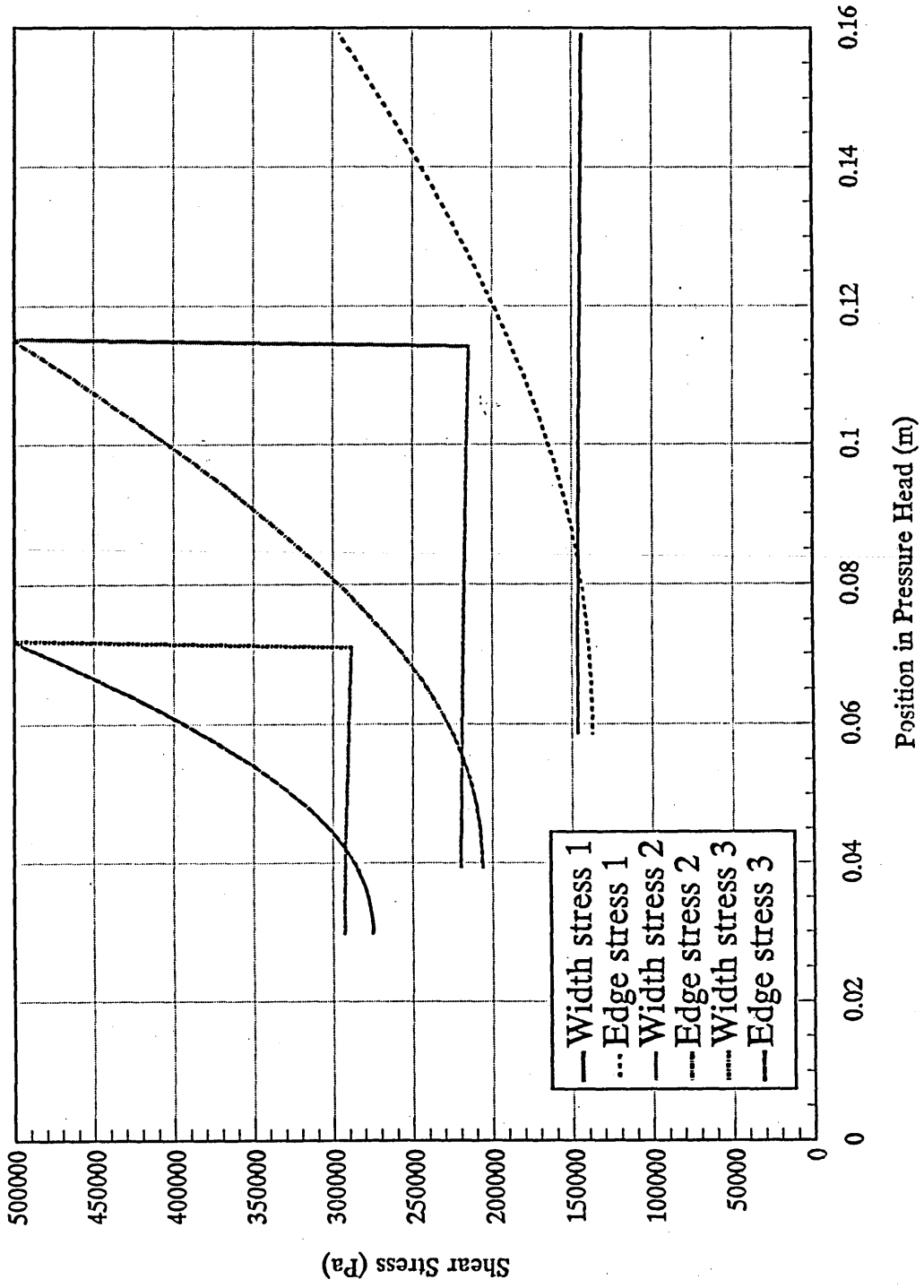

Figure 8.1 - Sample shear stress plots, giving τ_1 and τ_3.

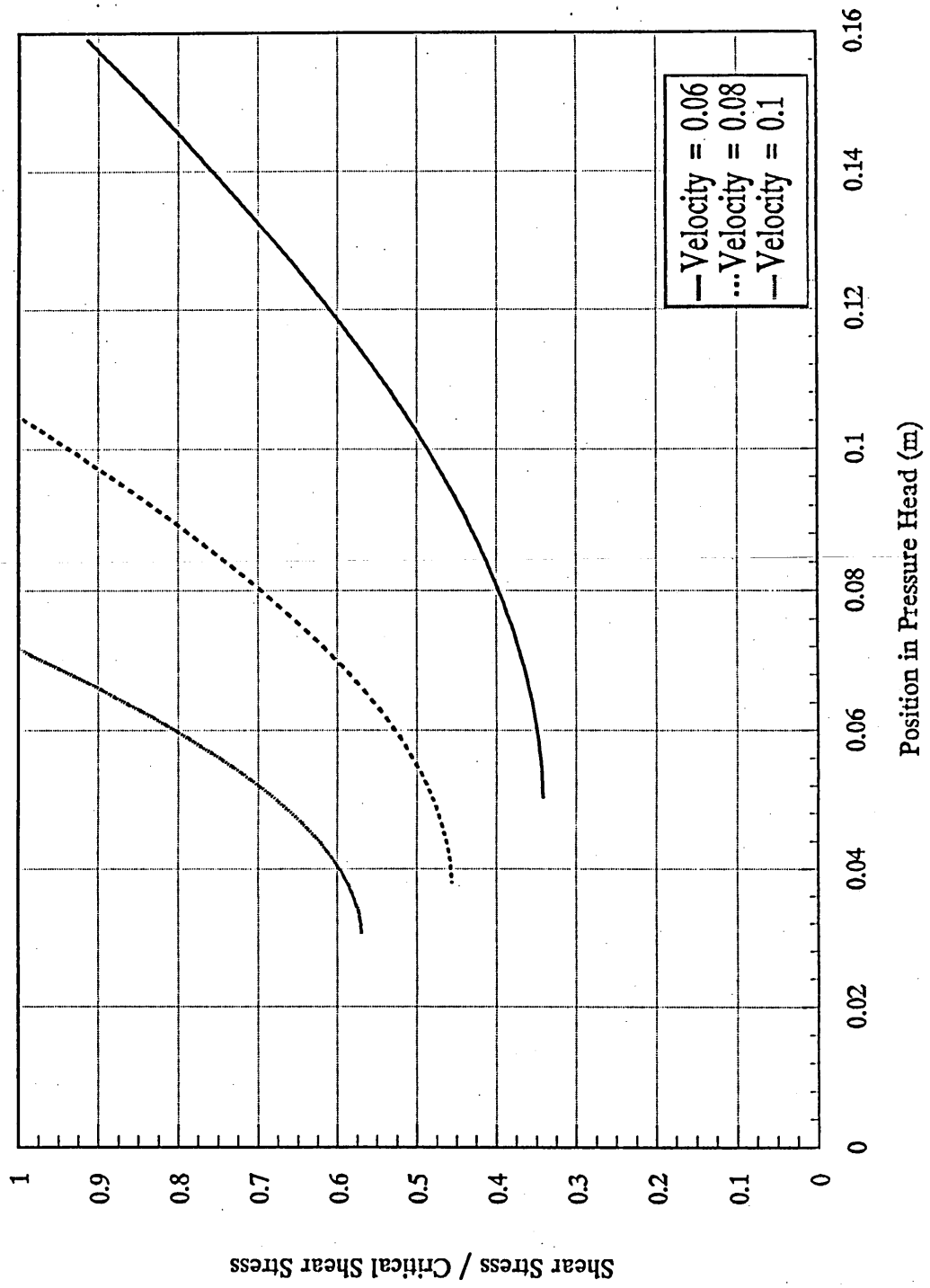

Figure 8.2 - Effect of h_3/h_2 ratio on τ_3, h_3/h_2 ratio = 5.

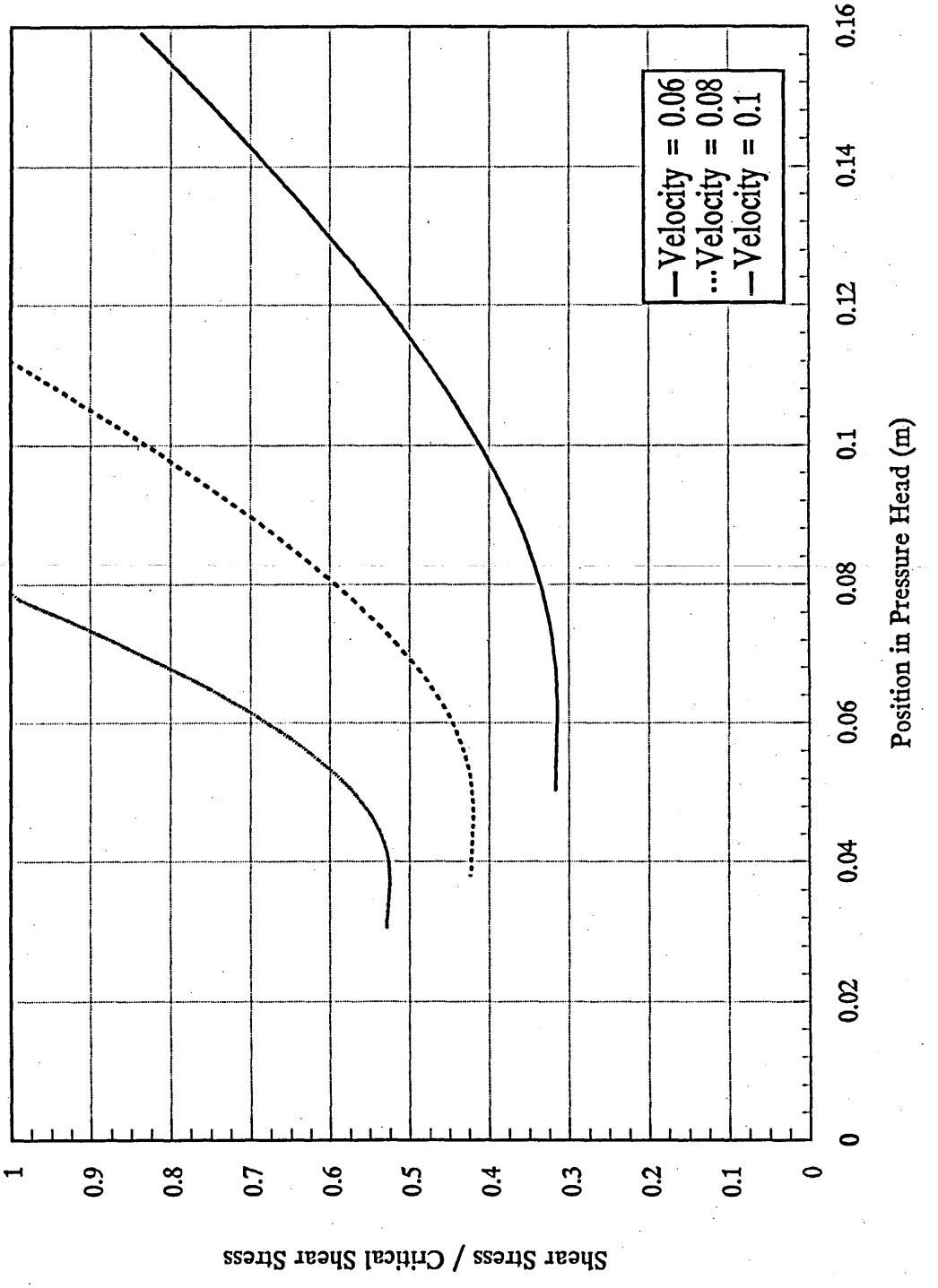

Figure 8.3 - Effect of h_3/h_2 ratio on τ_3, h_3/h_2 ratio = 3.

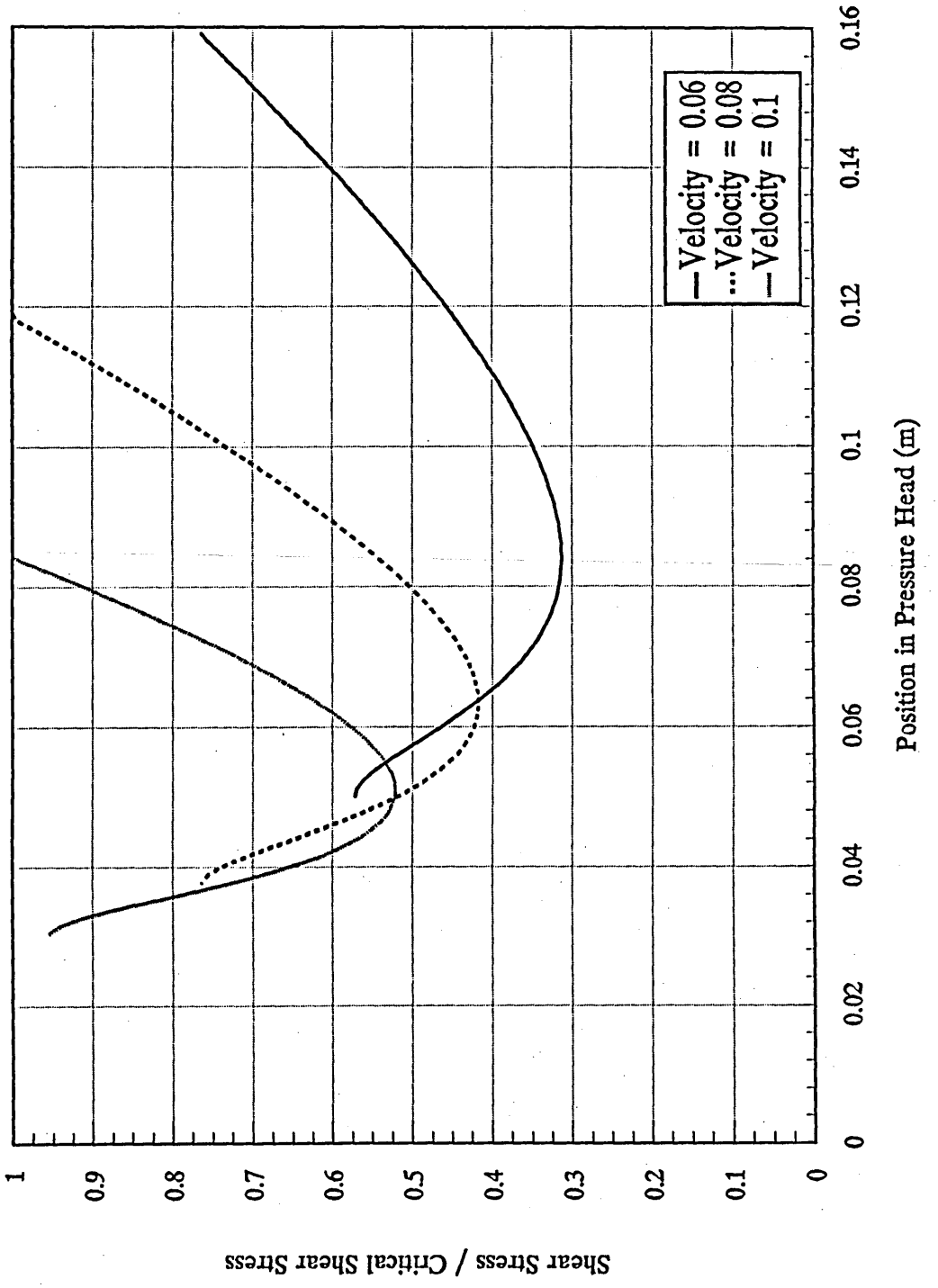

Figure 8.4 - Effect of h_3/h_2 ratio on τ_3, h_3/h_2 ratio = 1.

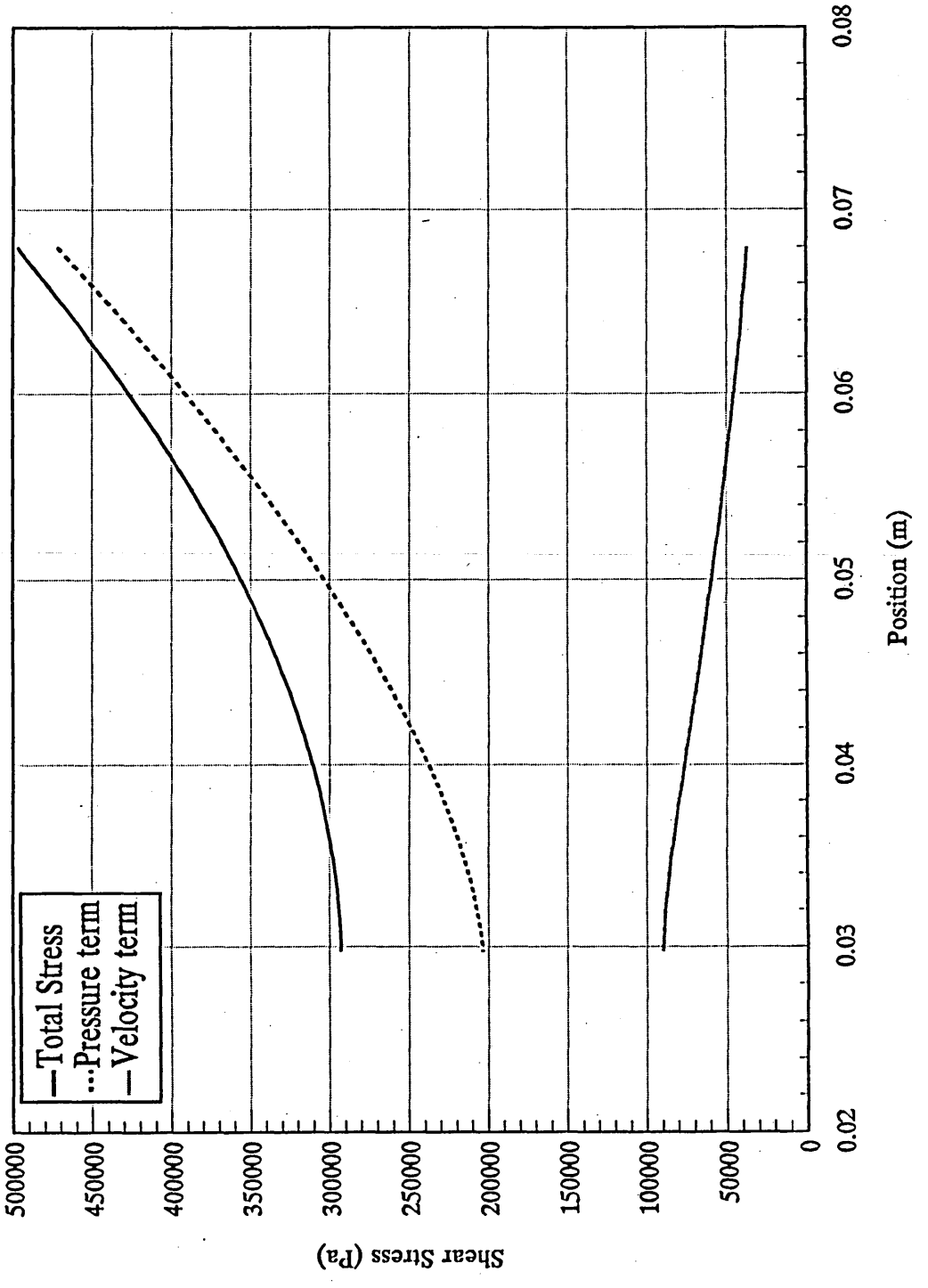

Figure 8.5 - Shear stress (τ_3) components for a h_3/h_2 ratio of 5 at a velocity of 0.1 m/s.

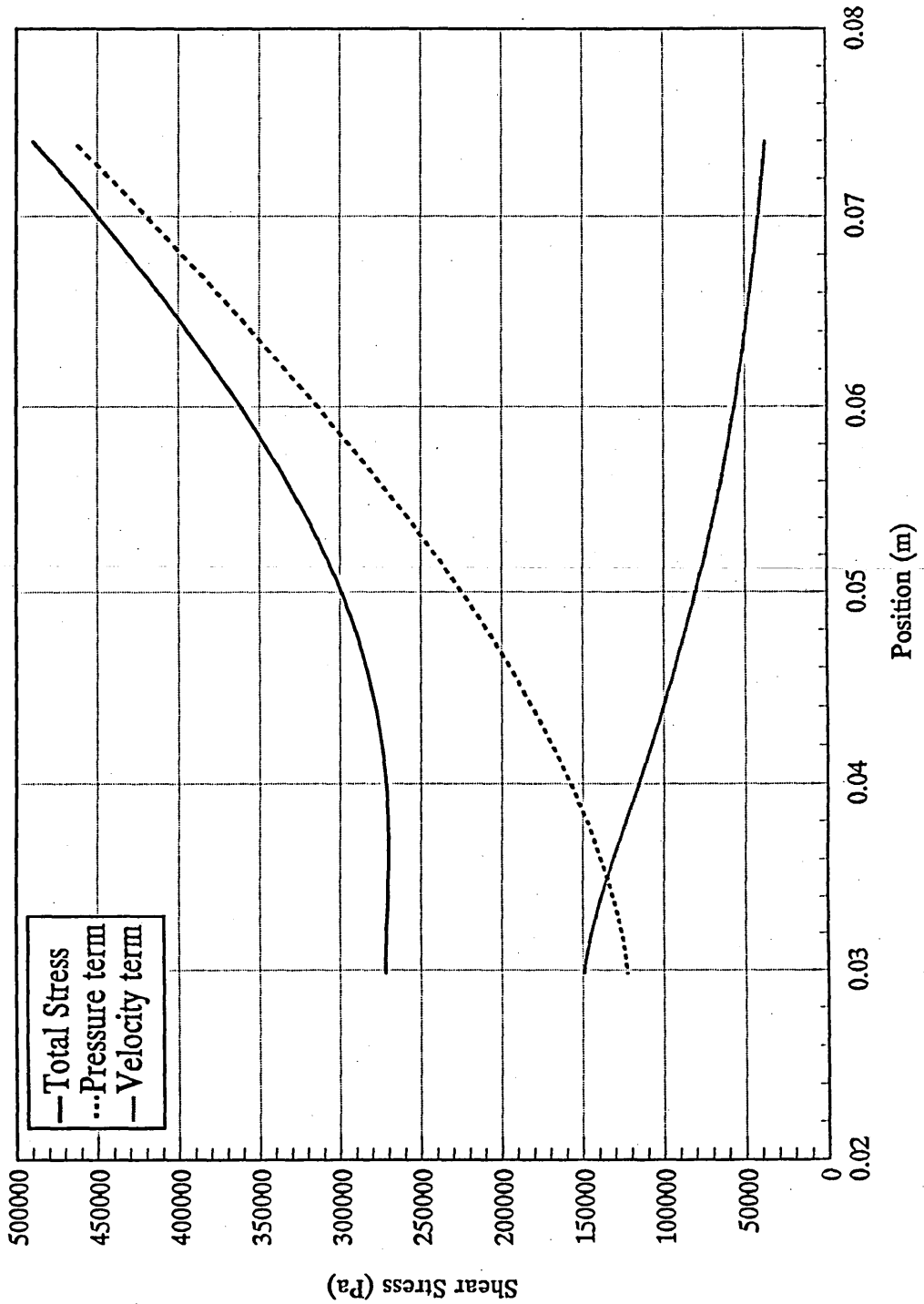

Figure 8.6 - Shear stress (τ_3) components for a h_3/h_2 ratio of 3 at a velocity of 0.1 m/s.

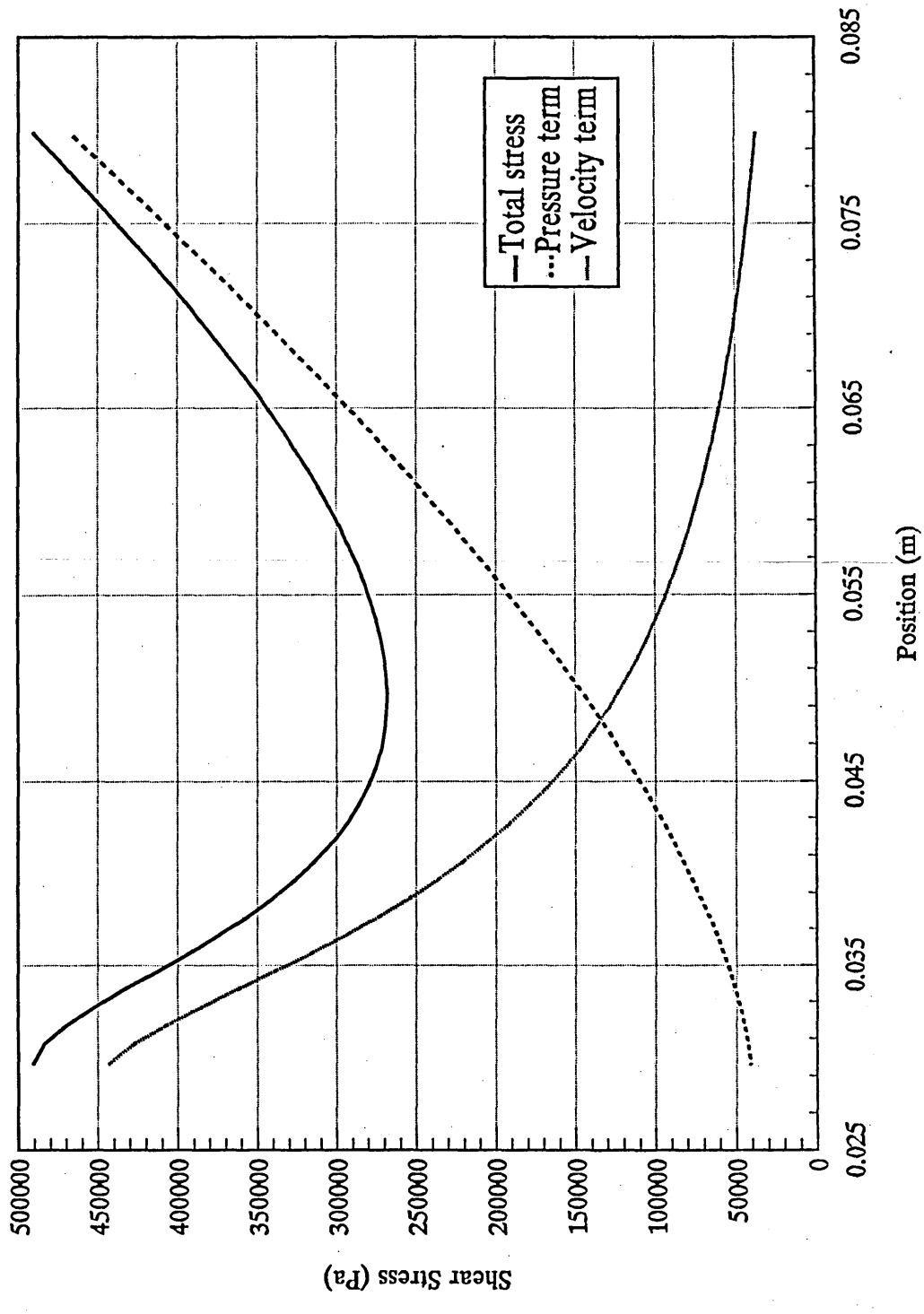

Figure 8.7 - Shear stress (τ_3) components for a h_3/h_2 ratio of 1 at a velocity of 0.1 m/s.

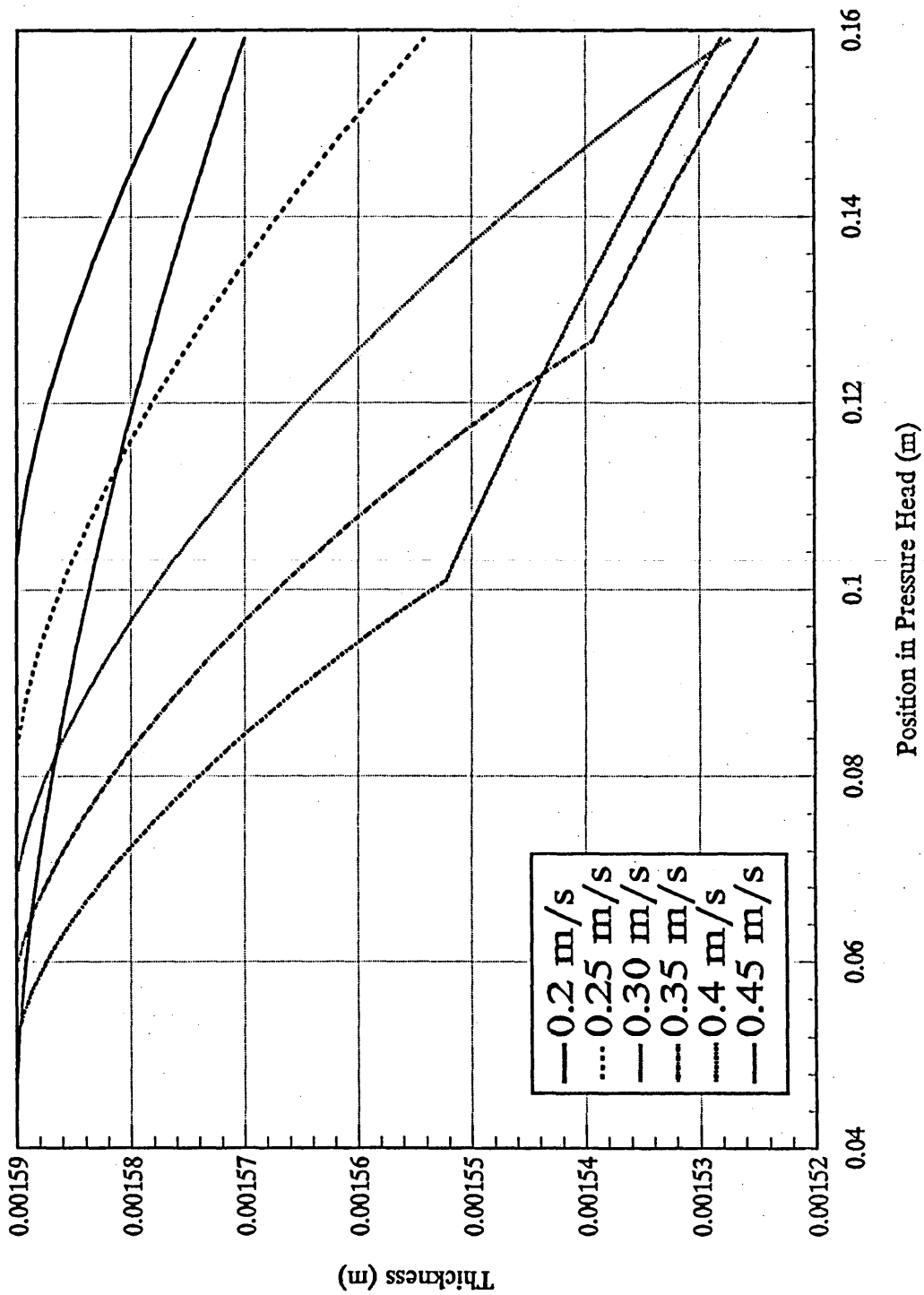

Figure 8.8 - Thickness profiles within the deformation zone showing the change in the slope of deformation when slip occurs.

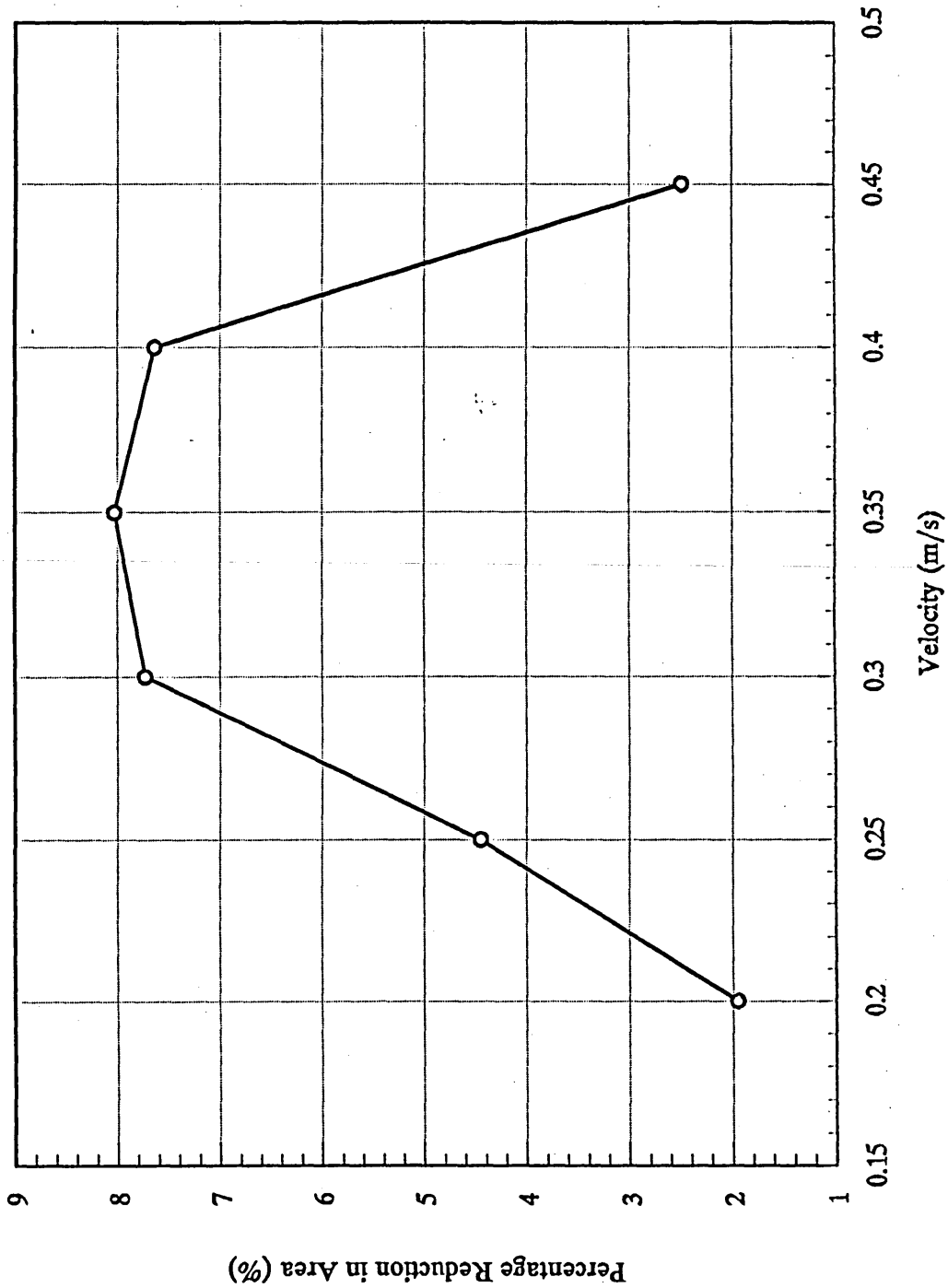

Figure 8.9 - Distinctive bell shaped curve produced by the modified algorithm.

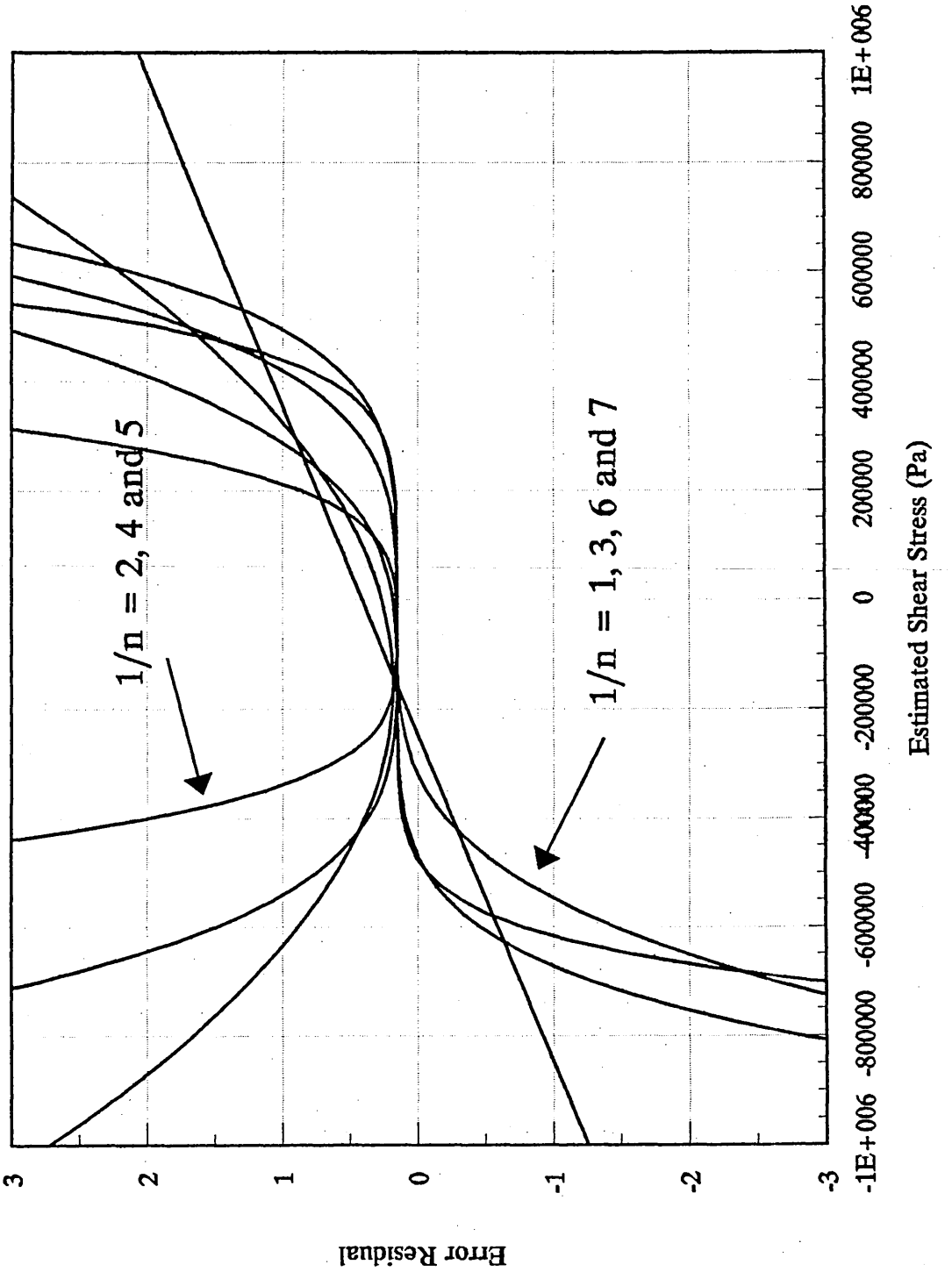

Figure 8.10 - Residual curves for various 1/n values.

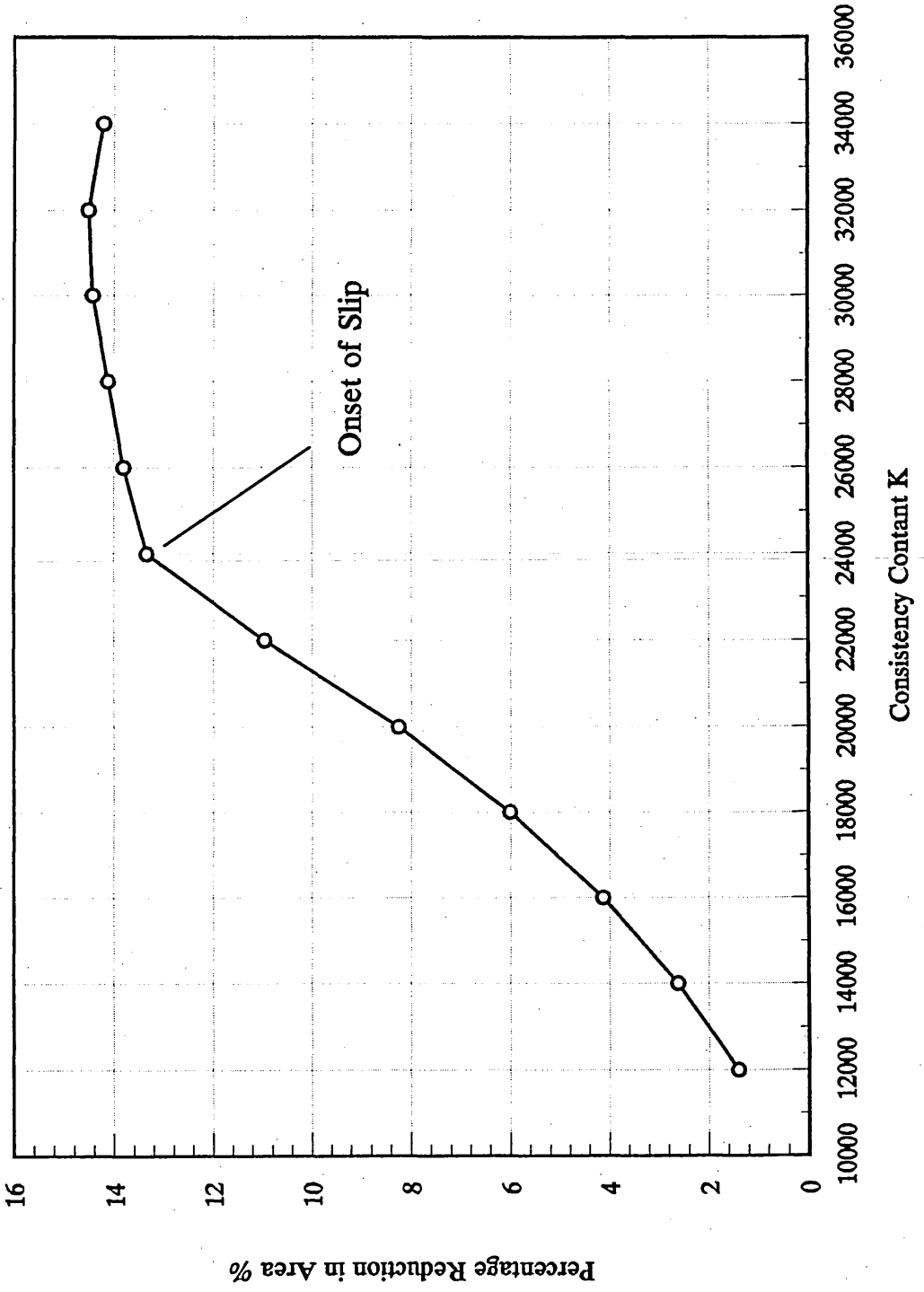

Figure 8.11 - The effect of the consistency constant K on predicted performance.

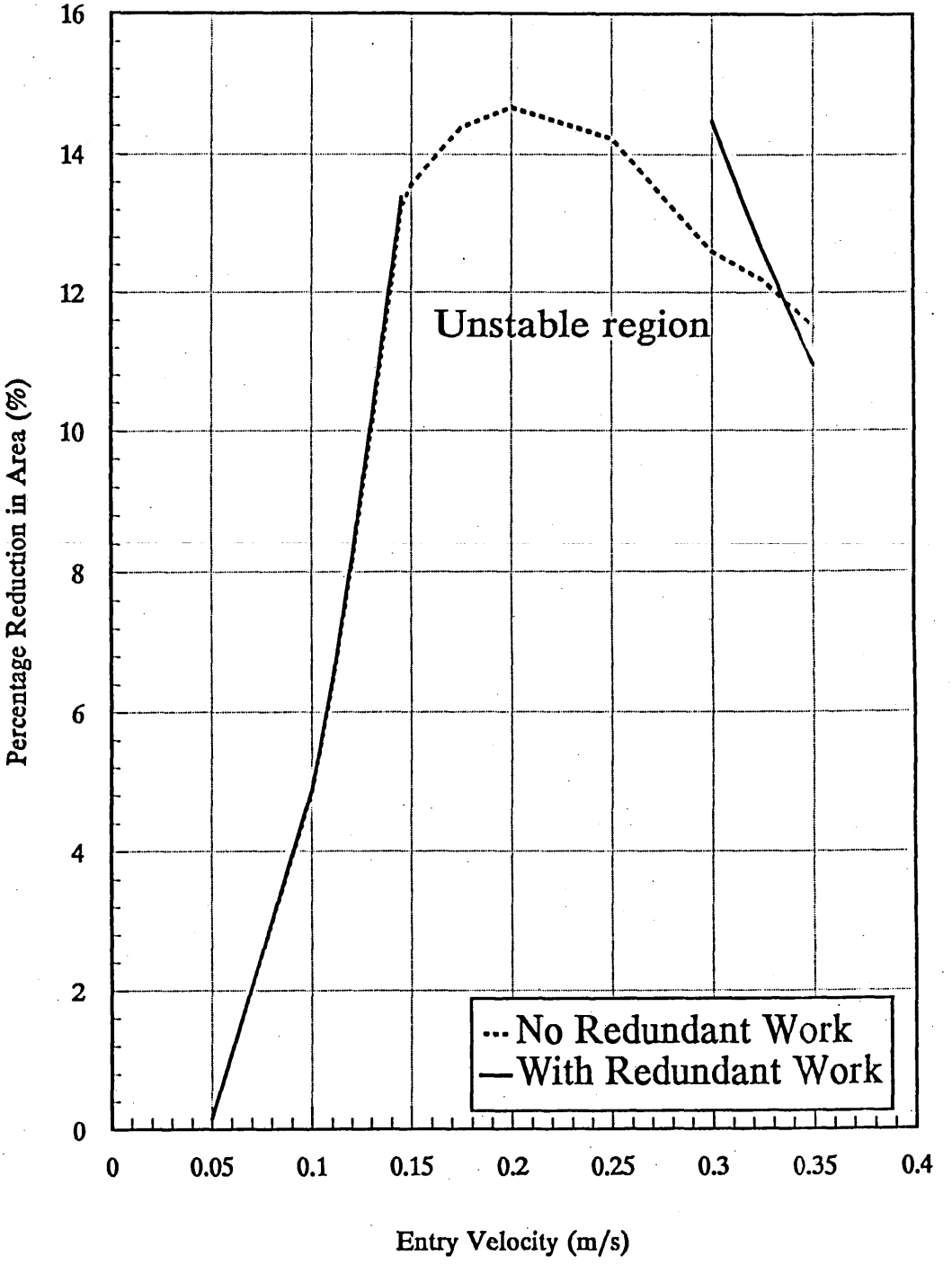

Figure 8.12 - schematic of the effect of redundant work on model predictions and the extent of the unstable zone

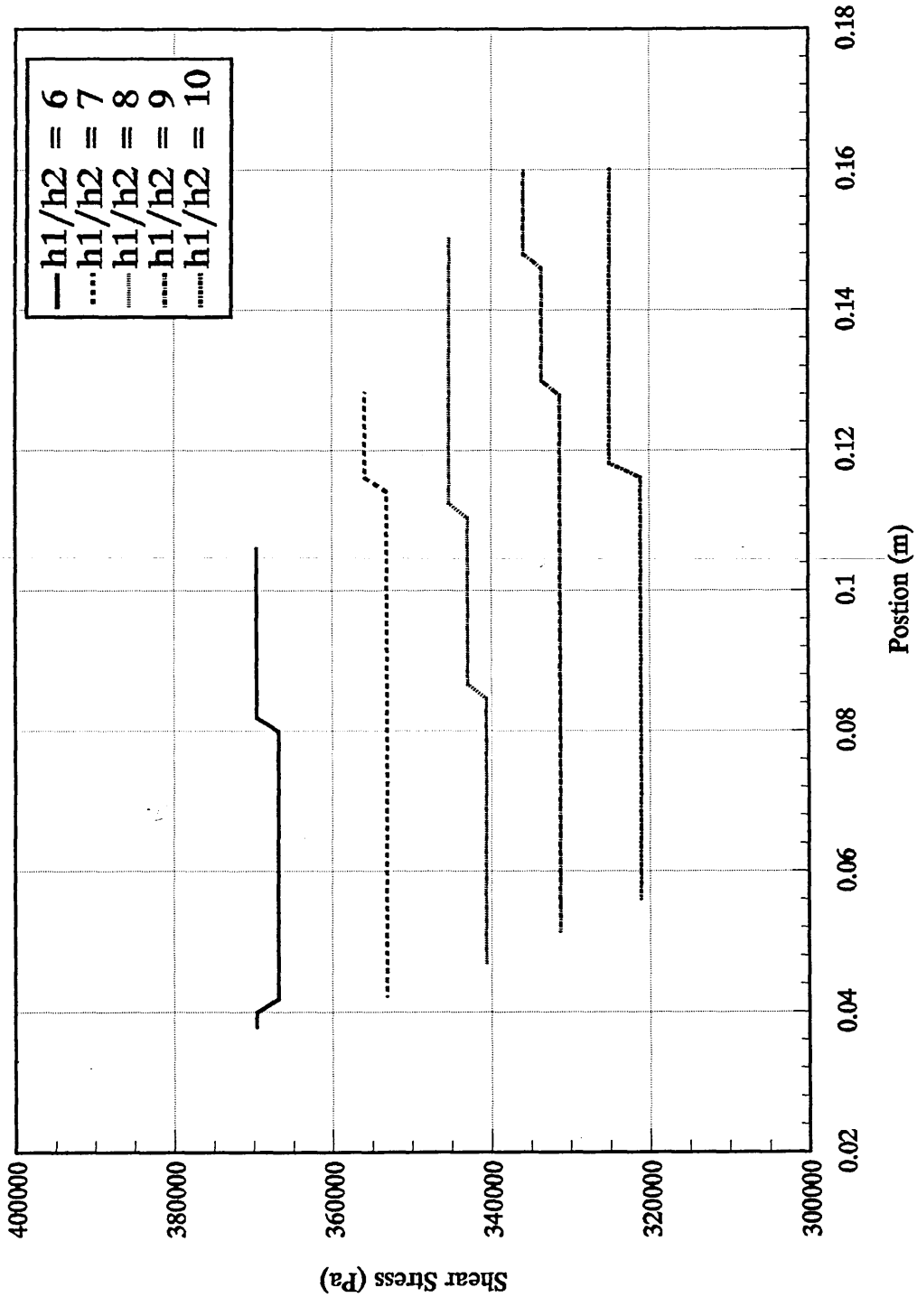

Figure 8.13 - The effect of h_1/h_2 ratio on τ_1.

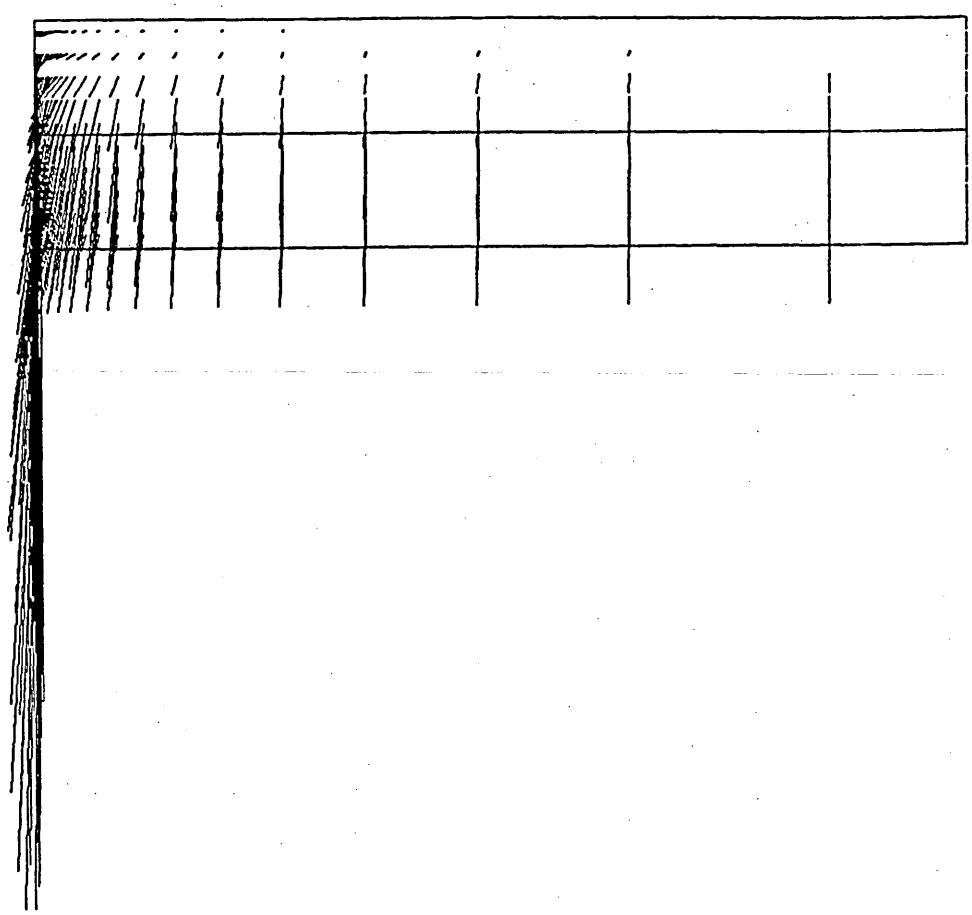

Figure 8.14 - End view of the 32:1 model showing the v and w components of the velocity field in vector form.

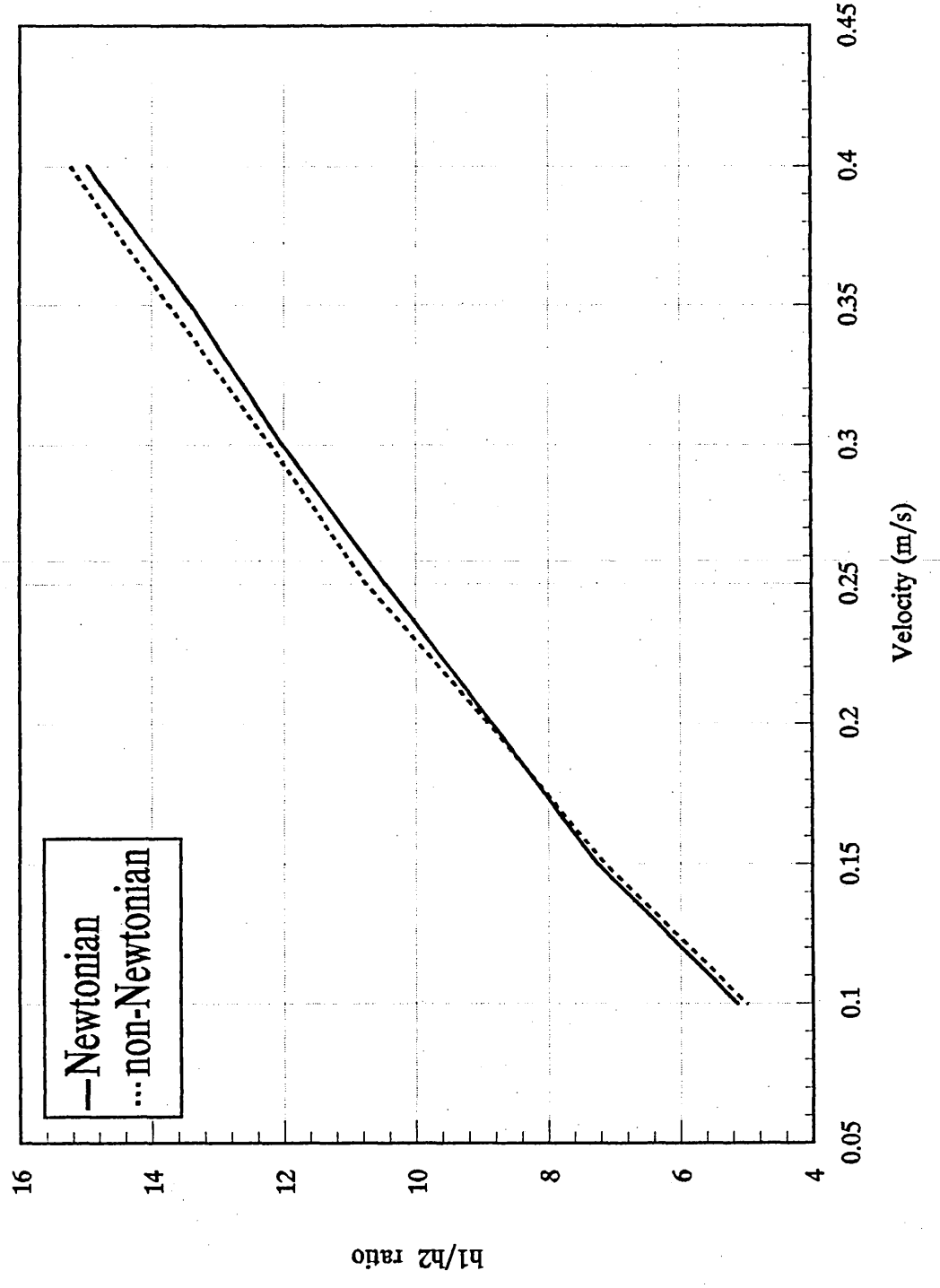

Figure 8.15 - A comparison of the predicted optimum h_1/h_2 ratio for the Newtonian and non-Newtonian (n=1.0) merit functions.

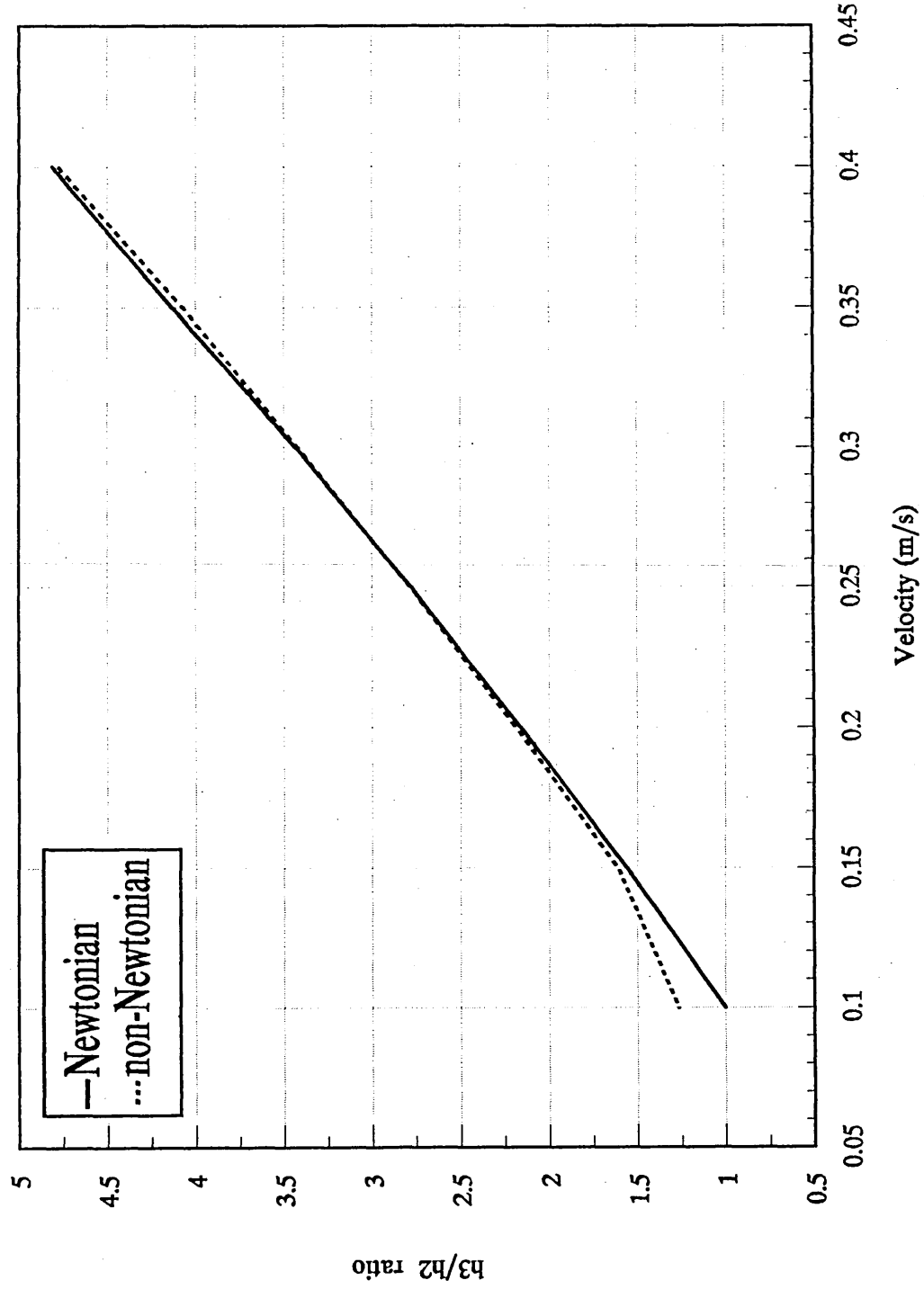

Figure 8.16 - A comparison of the predicted optimum h_3/h_2 ratio for the Newtonian and non-Newtonian (n=1.0) merit functions.

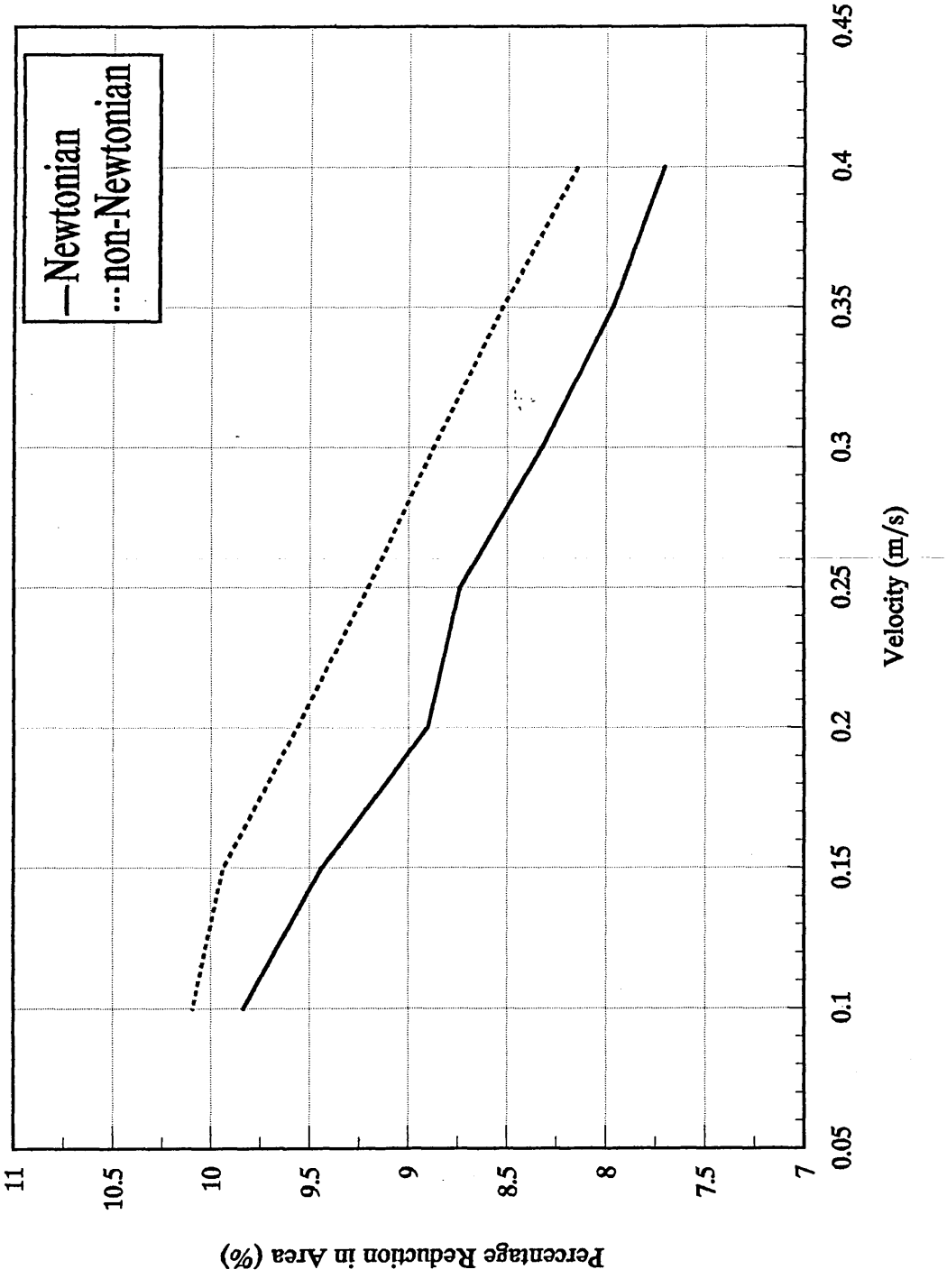

Figure 8.17 - A comparison of the predicted P.R.A. ratio for the Newtonian and non-Newtonian (n=1.0) merit functions.

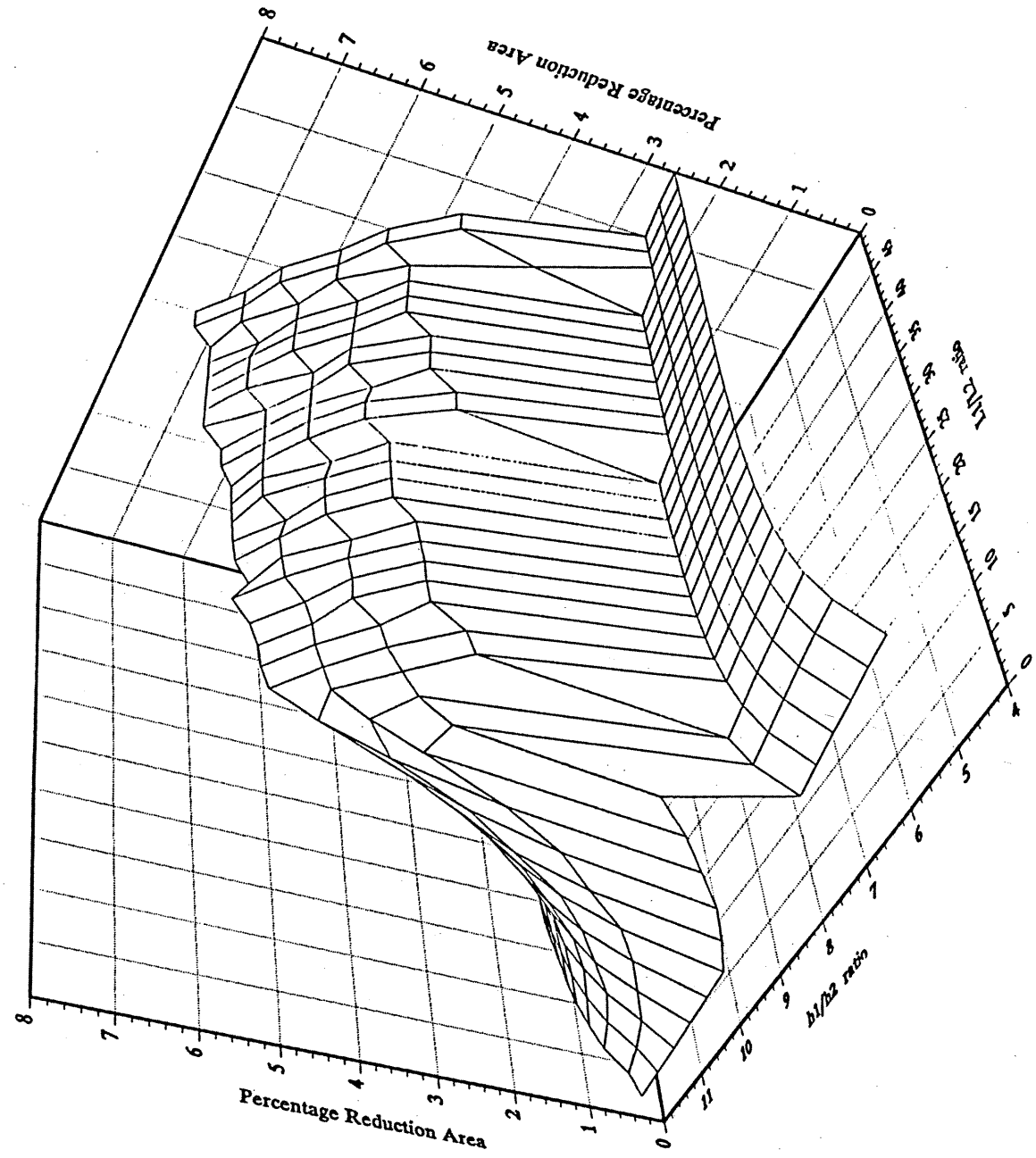

Figure 8.18 - Frame 1: performance surface development for the Newtonian merit function at a velocity of 0.2 m/s and $h_3/h_2 = 1.5$.

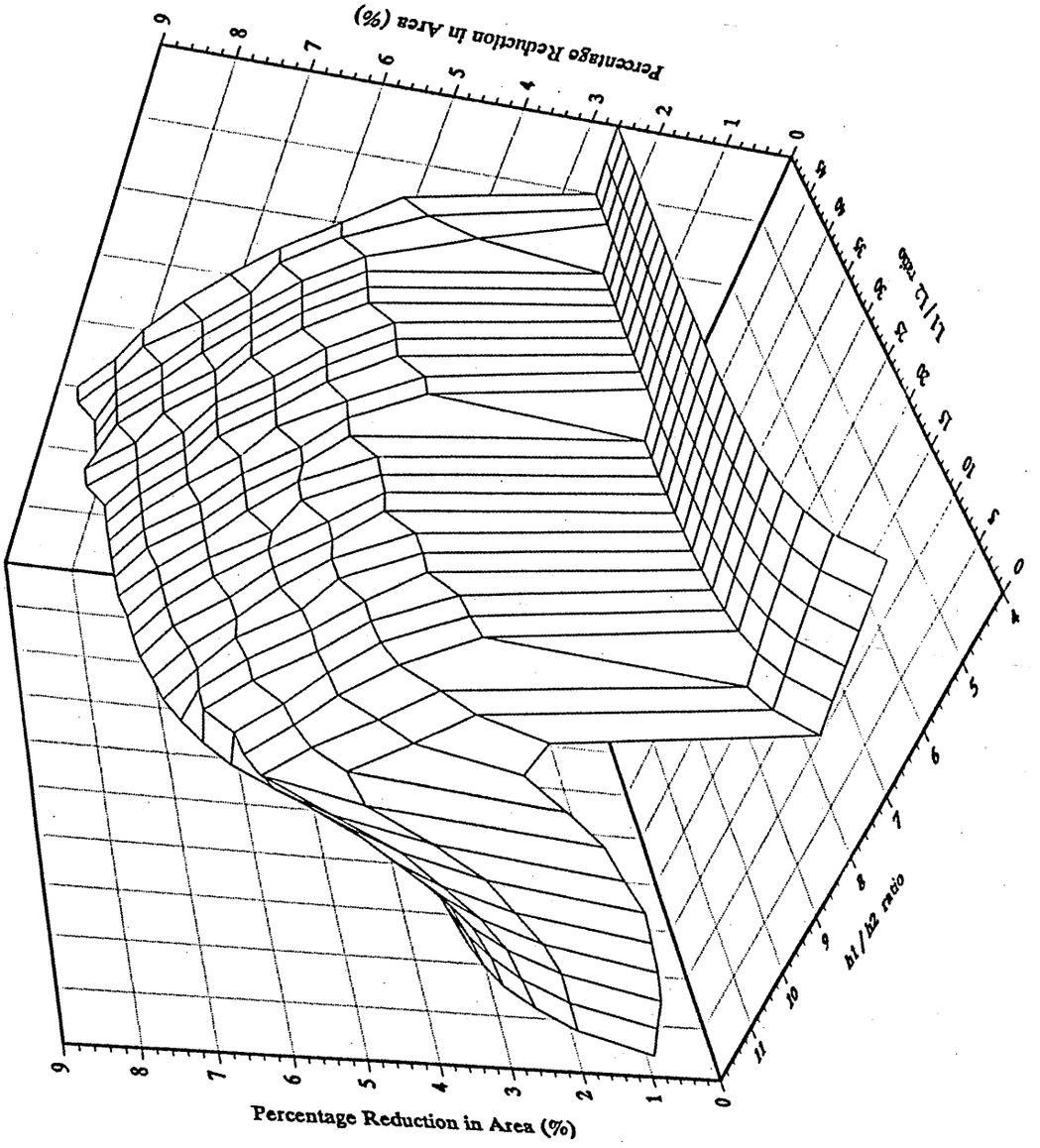

Figure 8.19 - Frame 2: performance surface development for the Newtonian merit function at a velocity of 0.2 m/s and $h_3/h_2 = 2$.

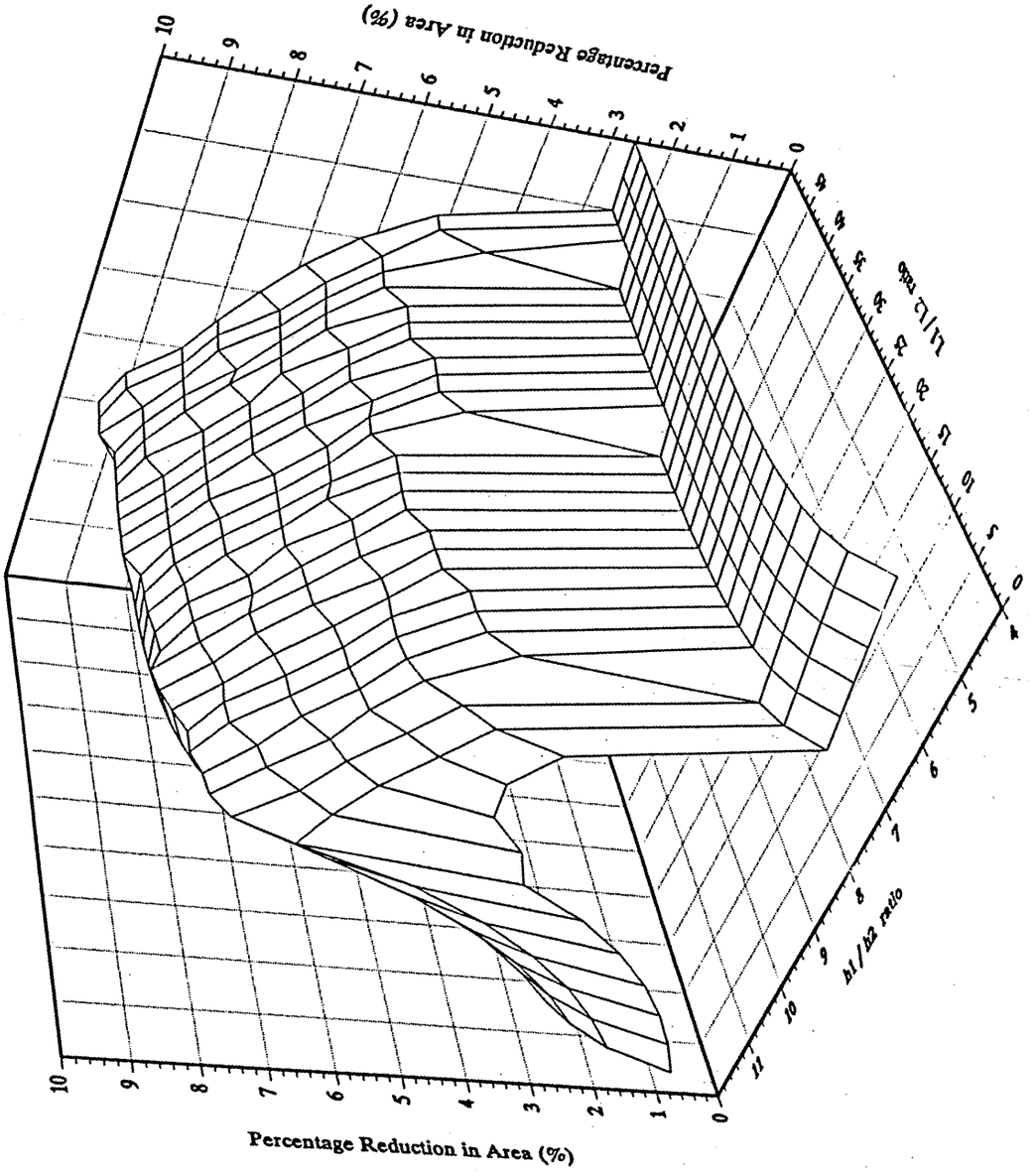

Figure 8.20 - Frame 3: performance surface development for the Newtonian merit function at a velocity of 0.2 m/s and $h_3/h_2 = 2.16$ (optimum).

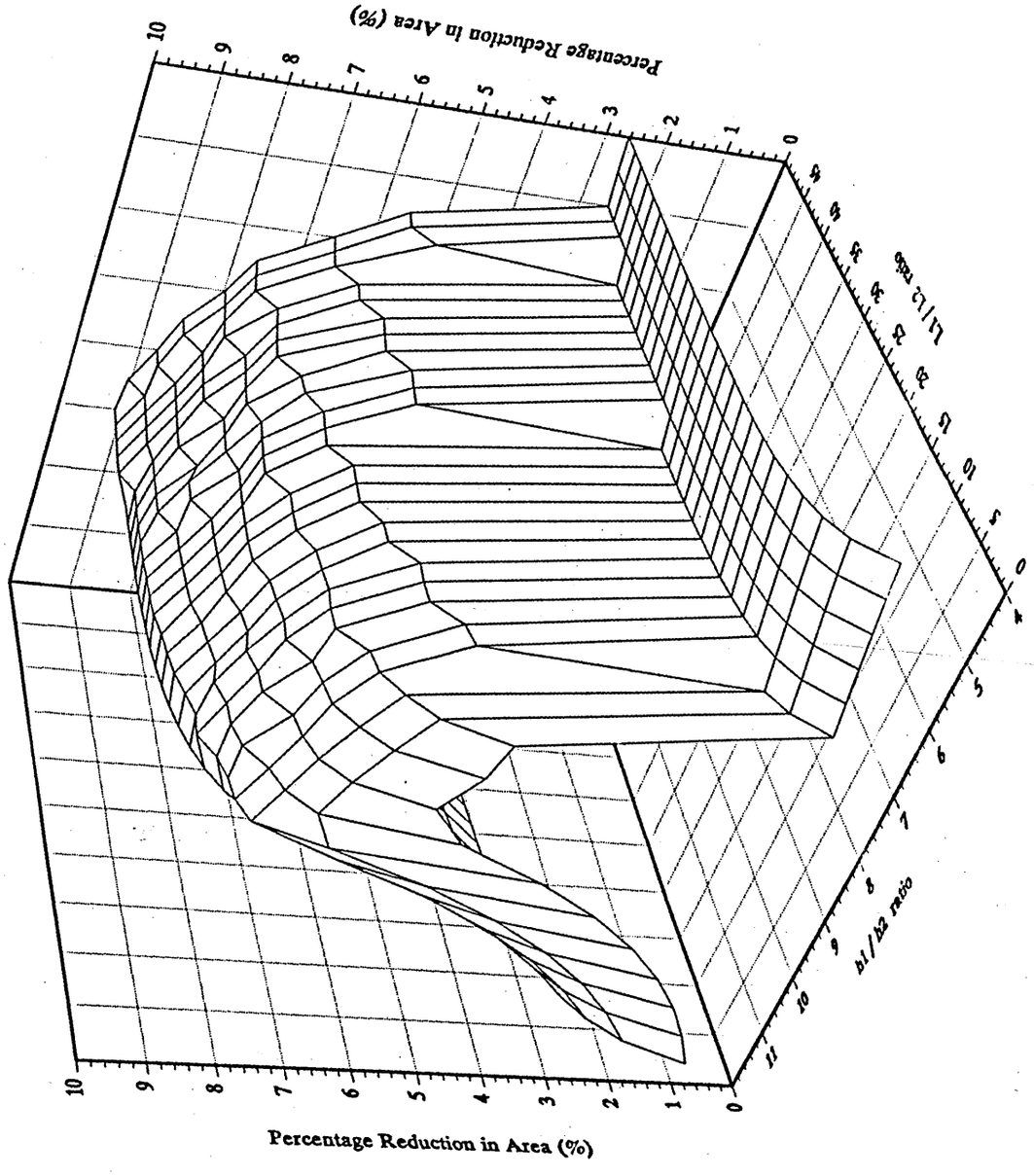

Figure 8.21 - Frame 4: performance surface development for the Newtonian merit function at velocity a of 0.2 m/s and $h_3/h_2 = 2.5$.

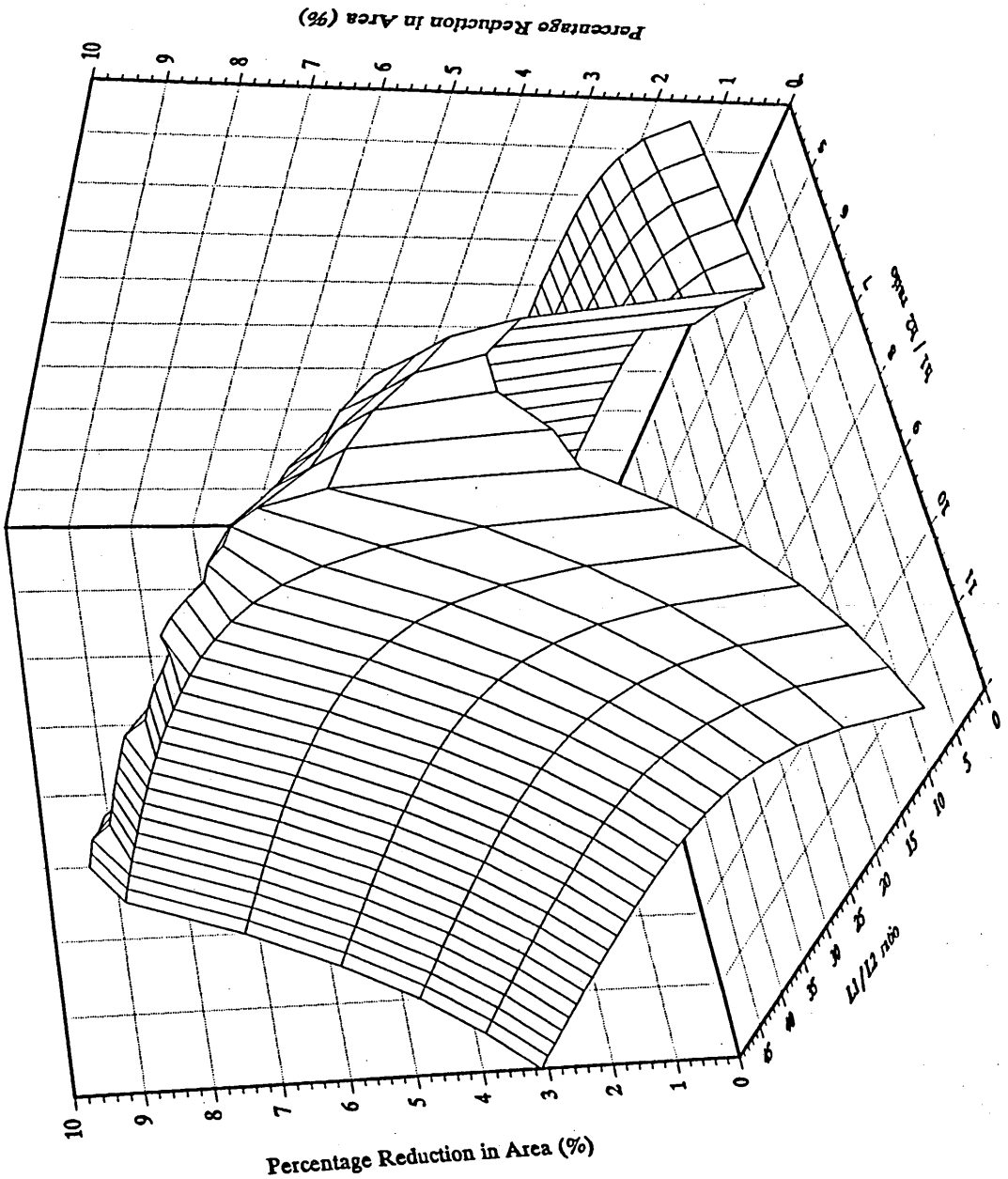

Figure 8.22 - Alternate view of figure 8.20.

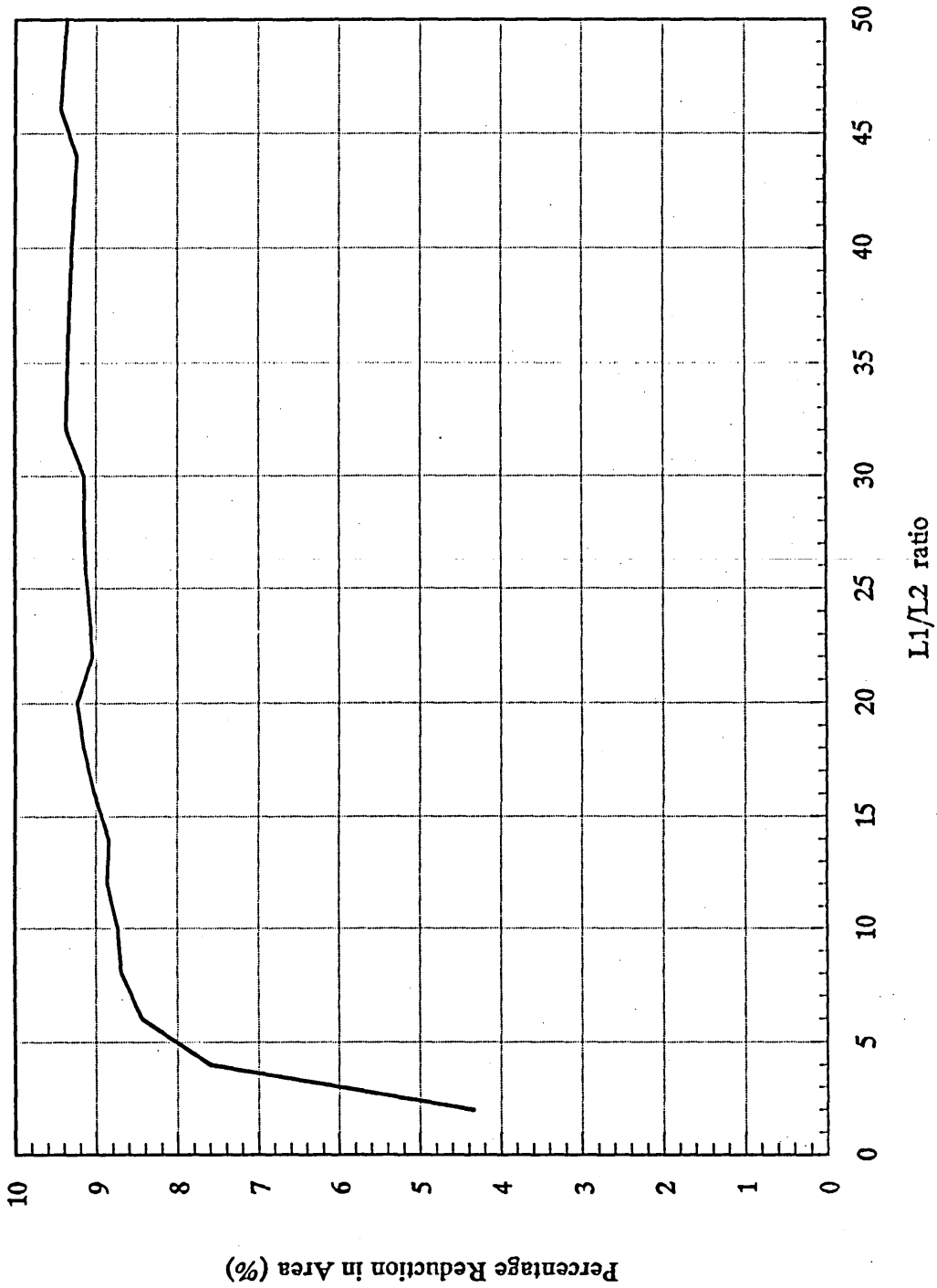

Figure 8.23 - Cross-section of figure 8.20 at h_1/h_2 ratio = 9.

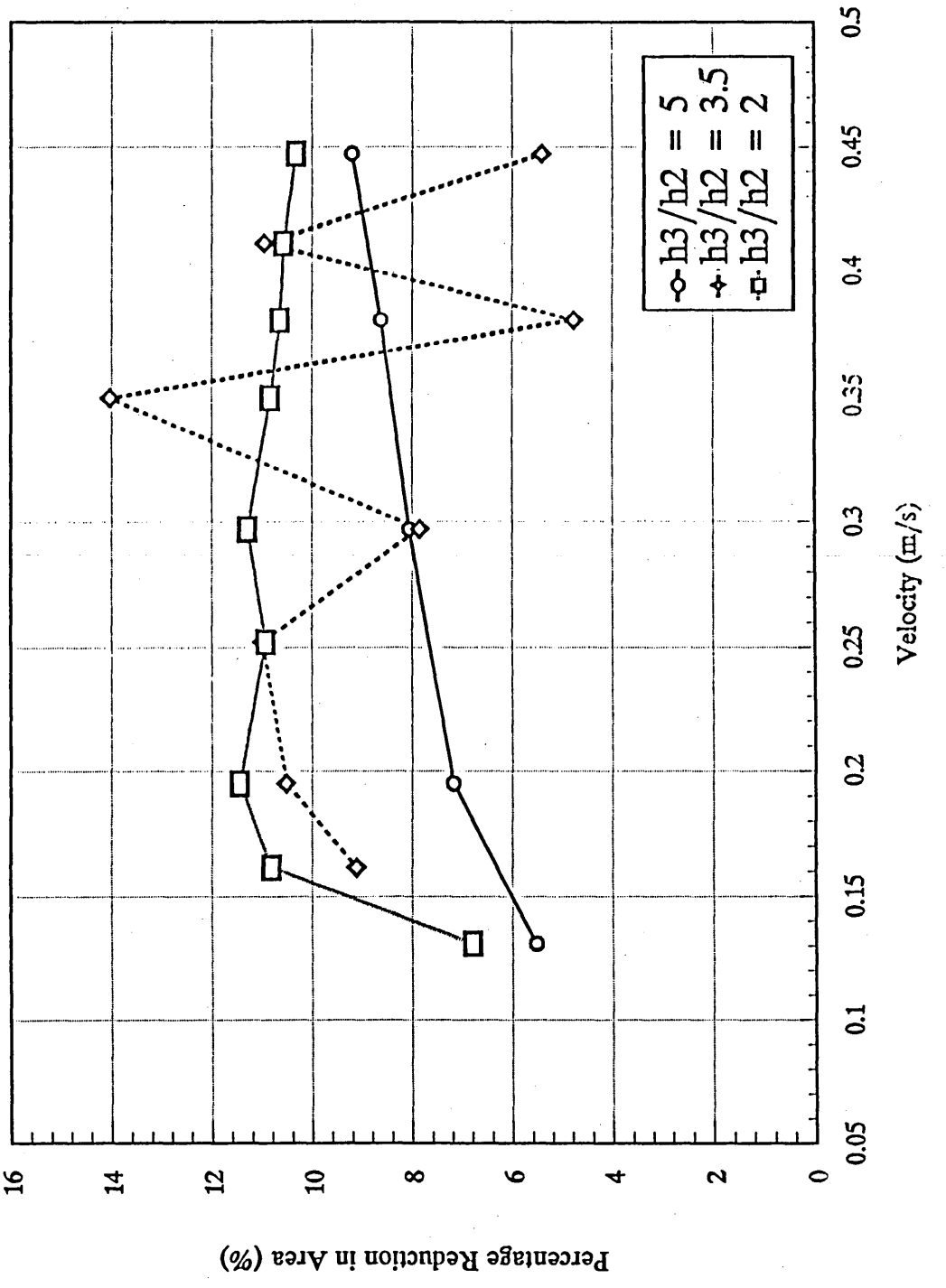

Figure 8.24 - Percentage Reduction in Area for various h_3/h_2 ratio at 195°C.

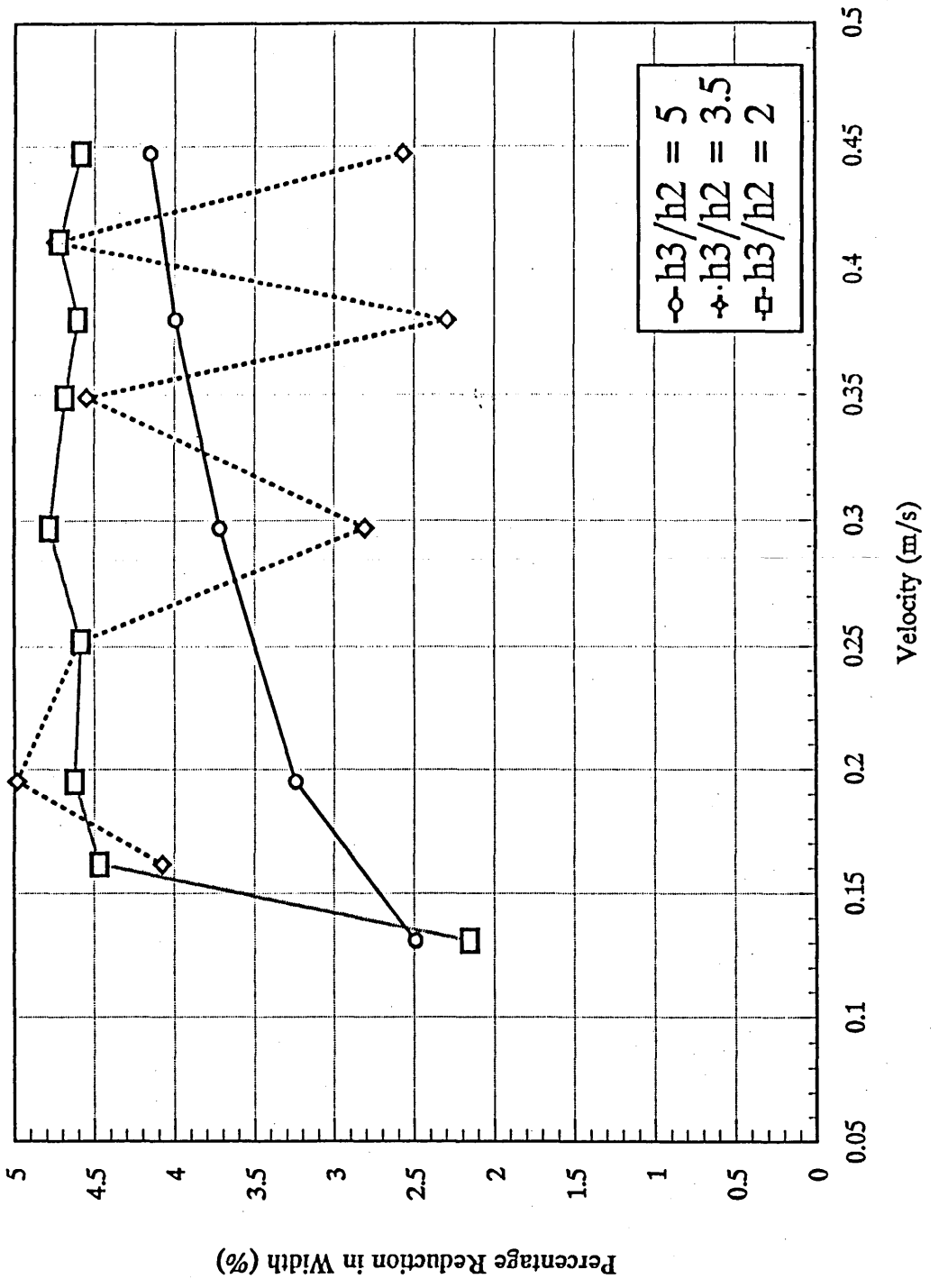

Figure 8.25 - Percentage Reduction in Width for various h_3/h_2 ratio at 195°C.

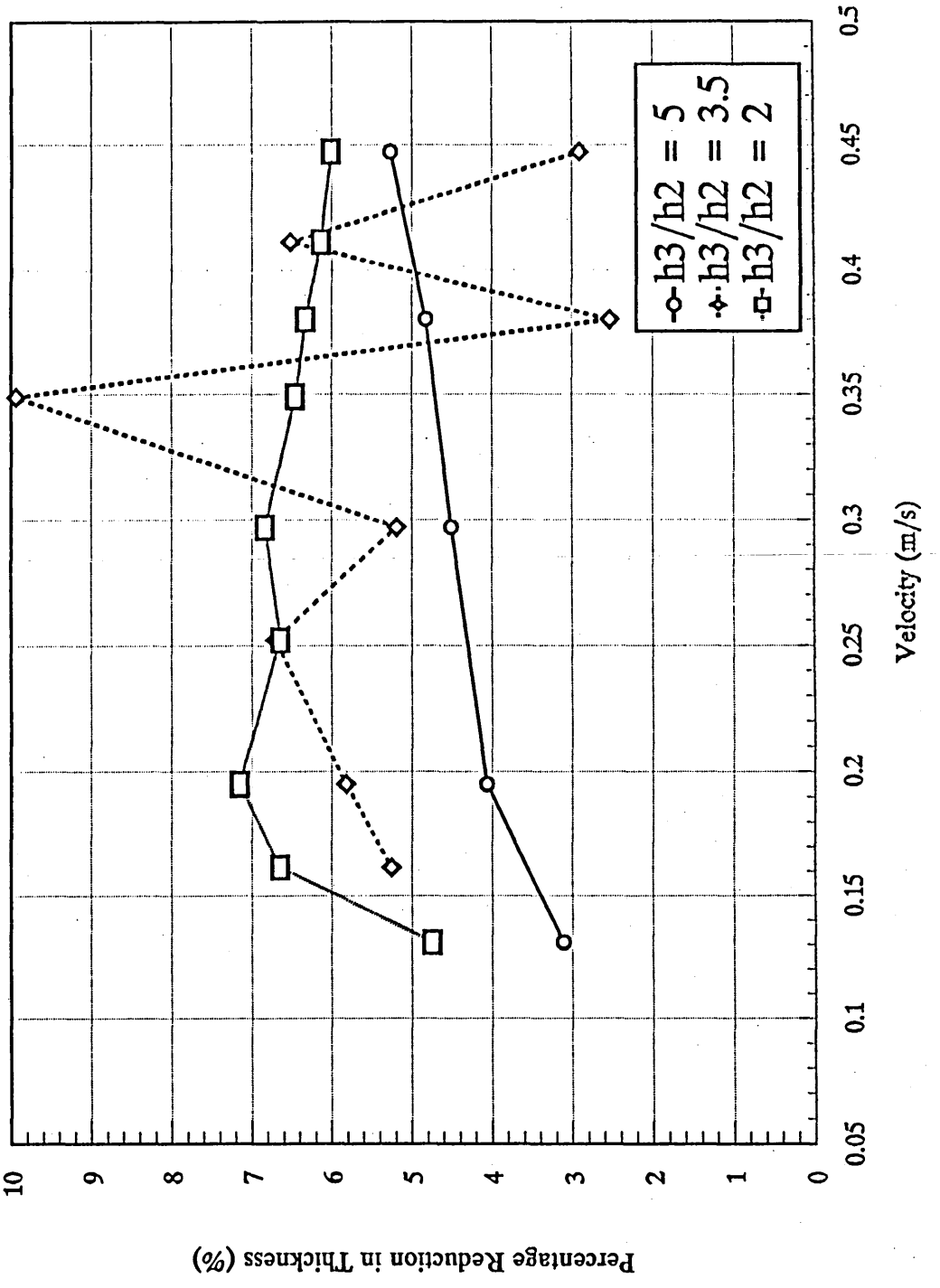

Figure 8.26 - Percentage Reduction in Thickness for various h_3/h_2 ratio at 195°C.

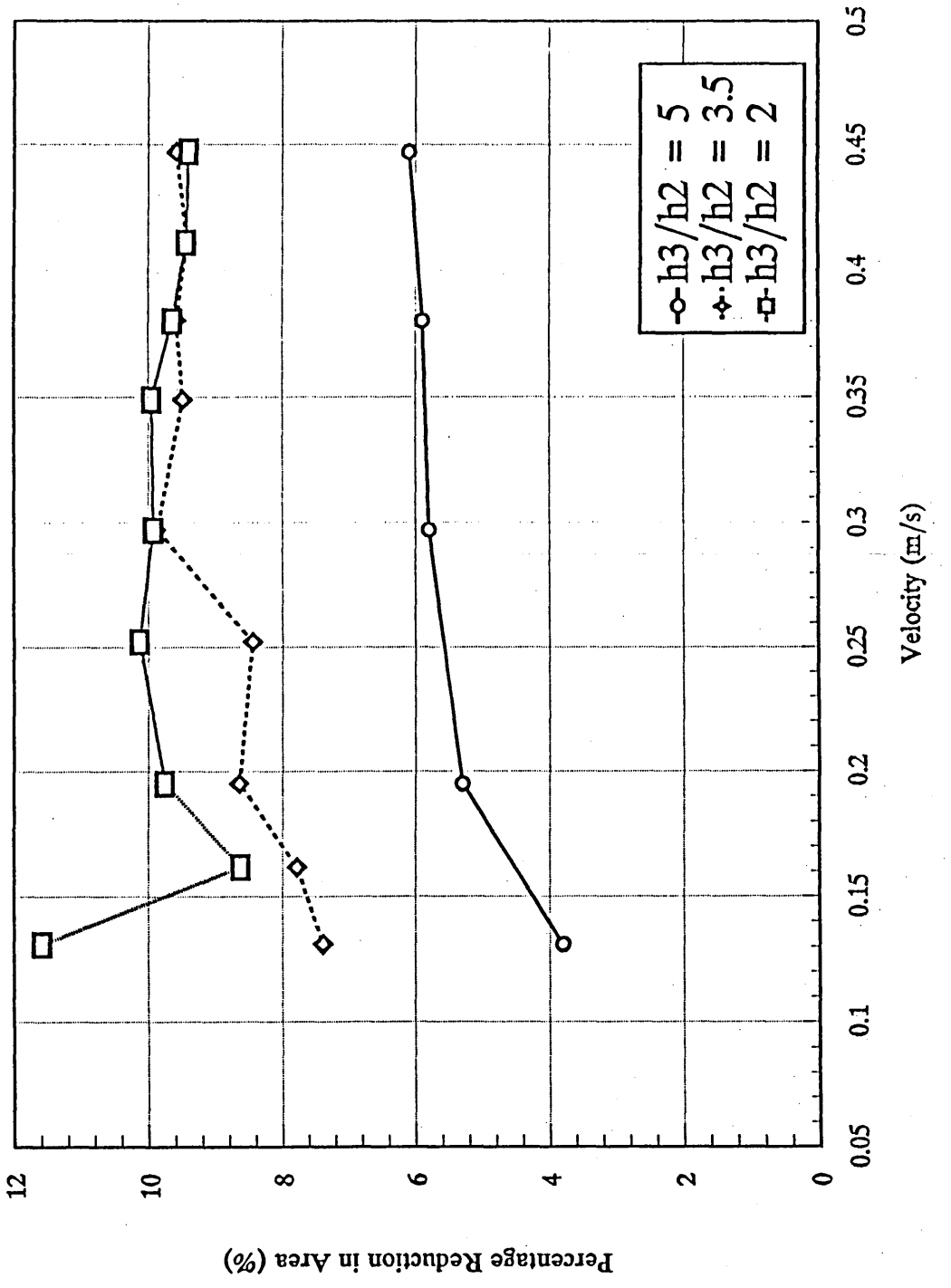

Figure 8.27 - Percentage Reduction in Area for various h_3/h_2 ratio at 215°C.

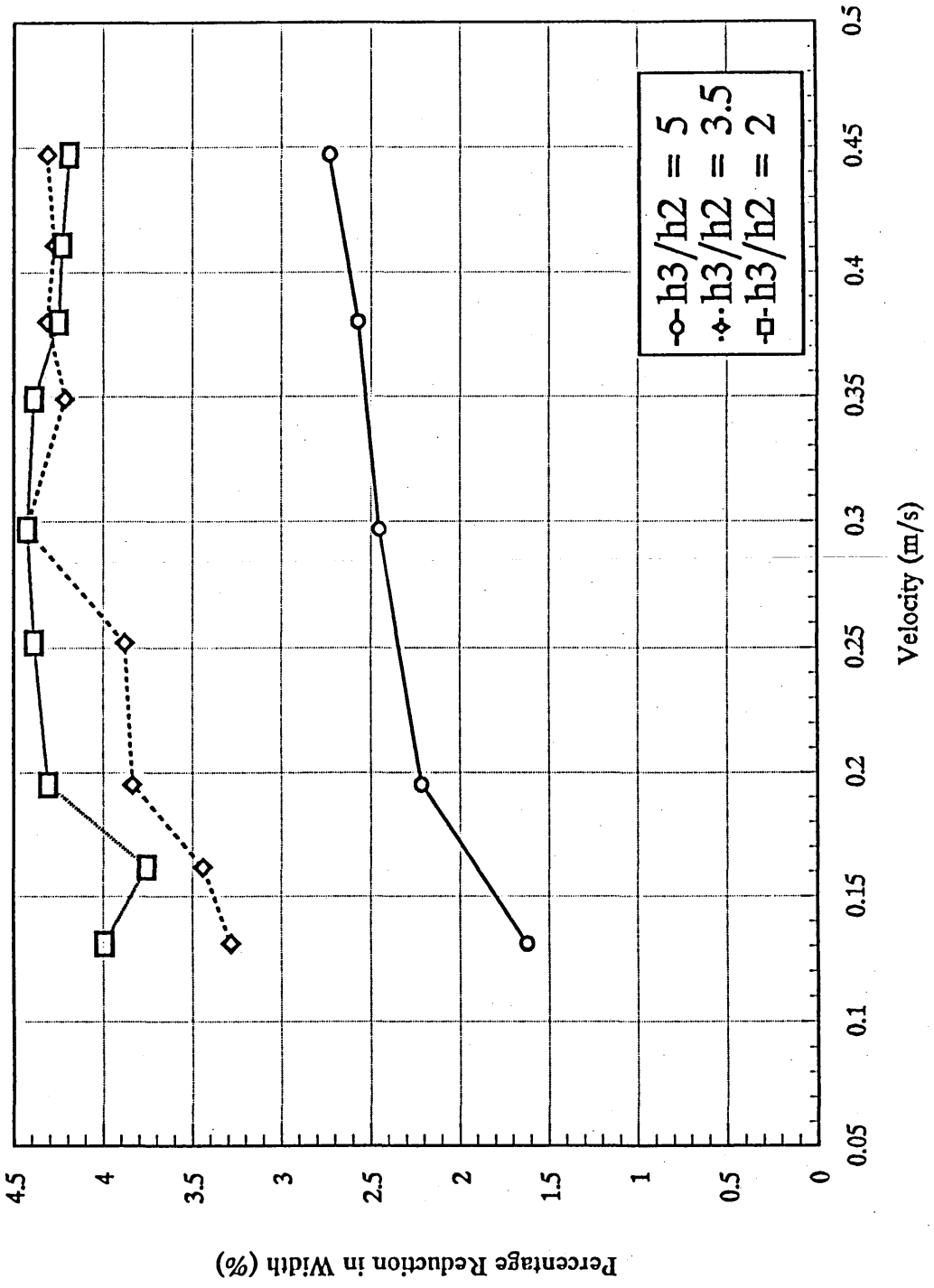

Figure 8.28 - Percentage Reduction in Width for various h_3/h_2 ratio at 215°C.

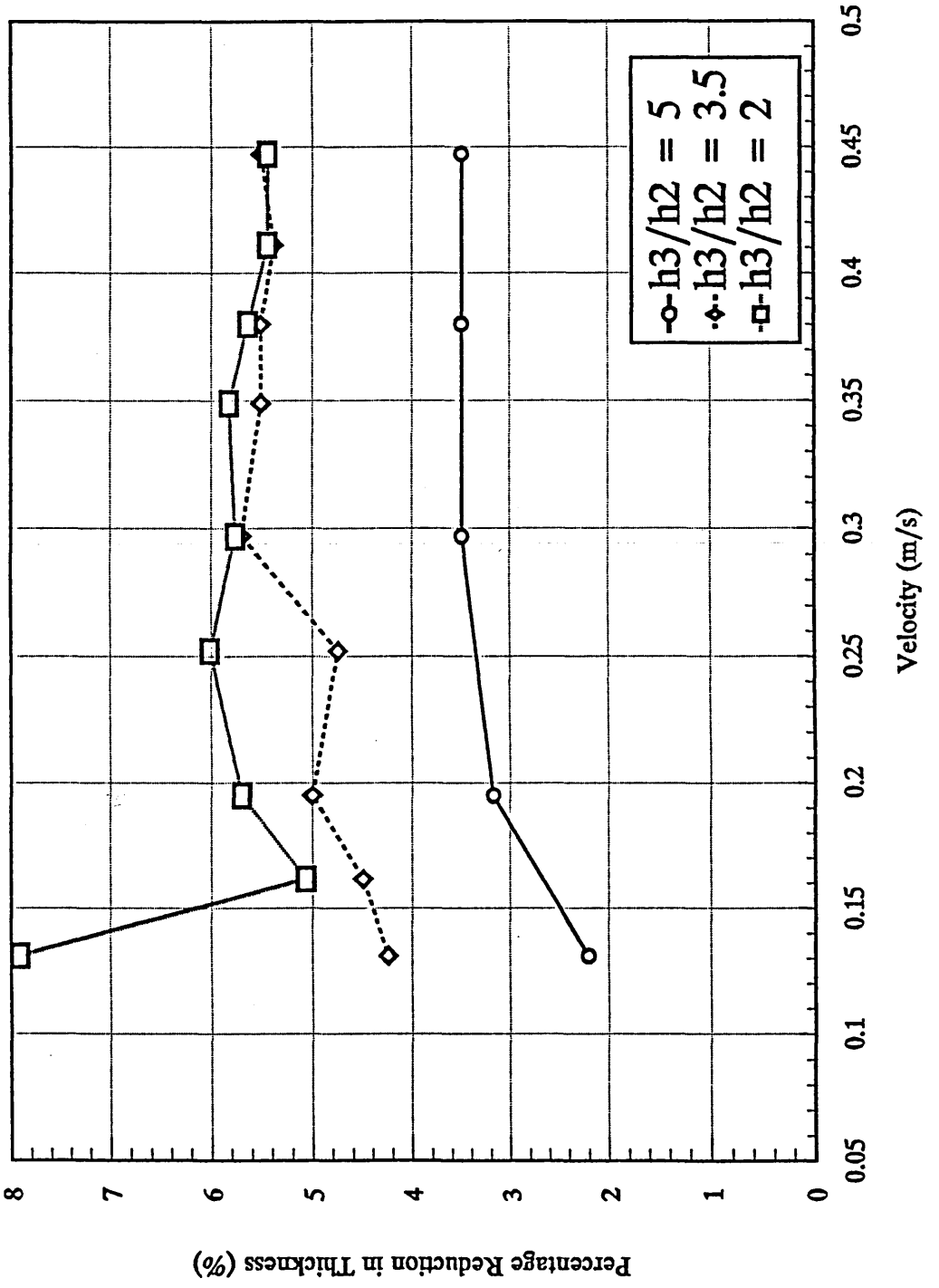

Figure 8.29 - Percentage Reduction in Thickness for various h_3/h_2 ratio at 215°C.

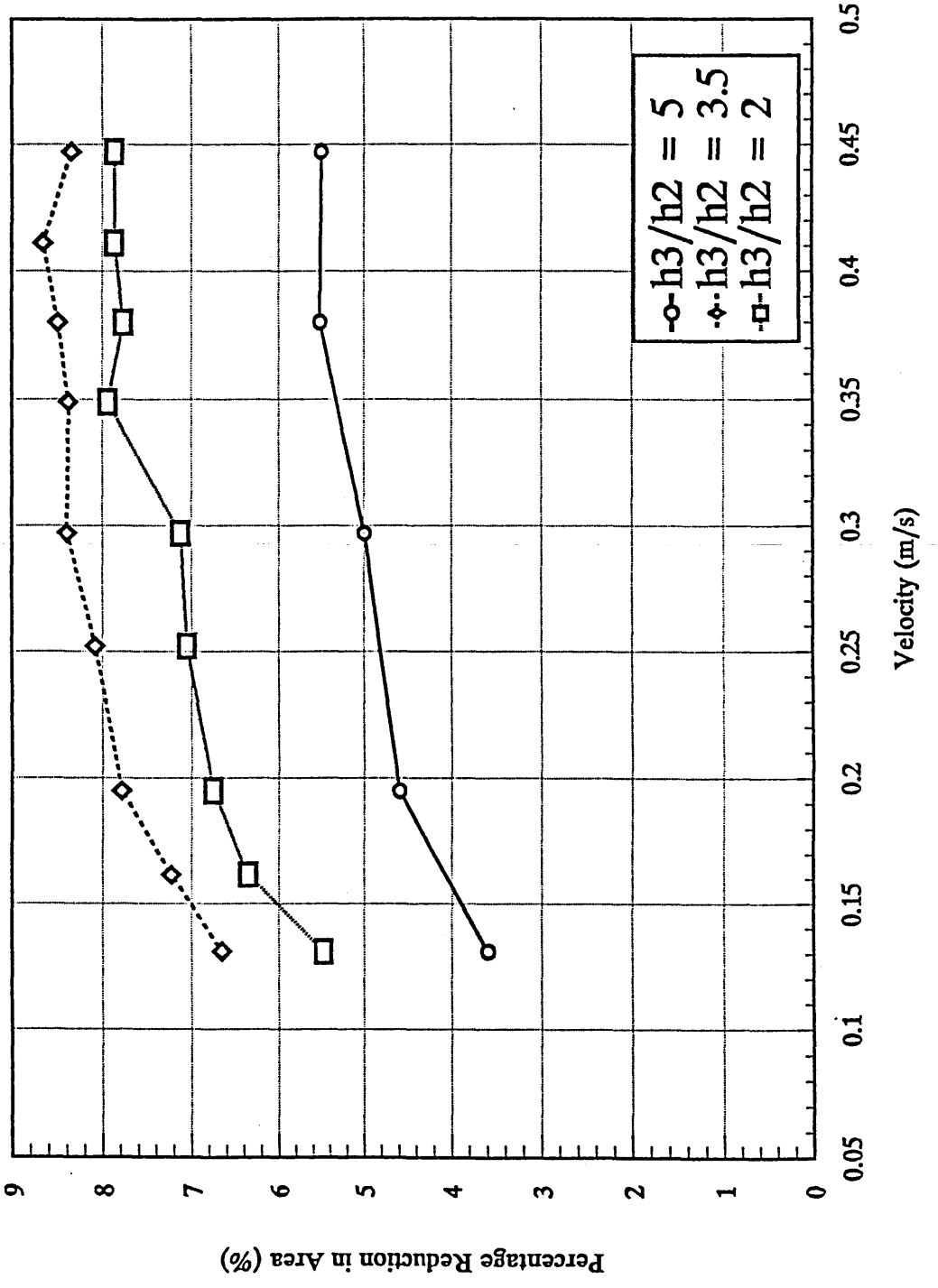

Figure 8.30 - Percentage Reduction in Area for various h_3/h_2 ratio at 235°C.

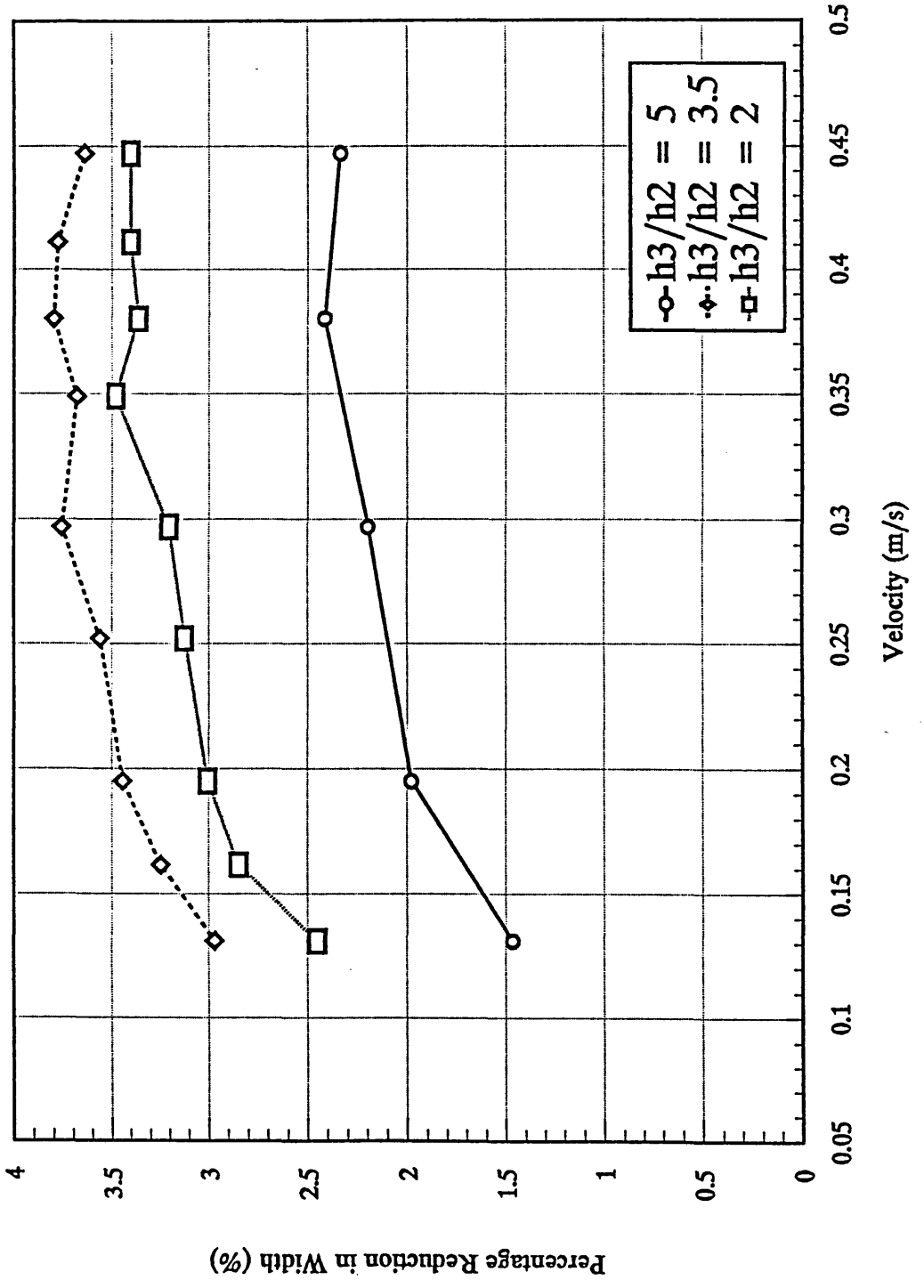

Figure 8.31 - Percentage Reduction in Width for various h_3/h_2 ratio at 235°C.

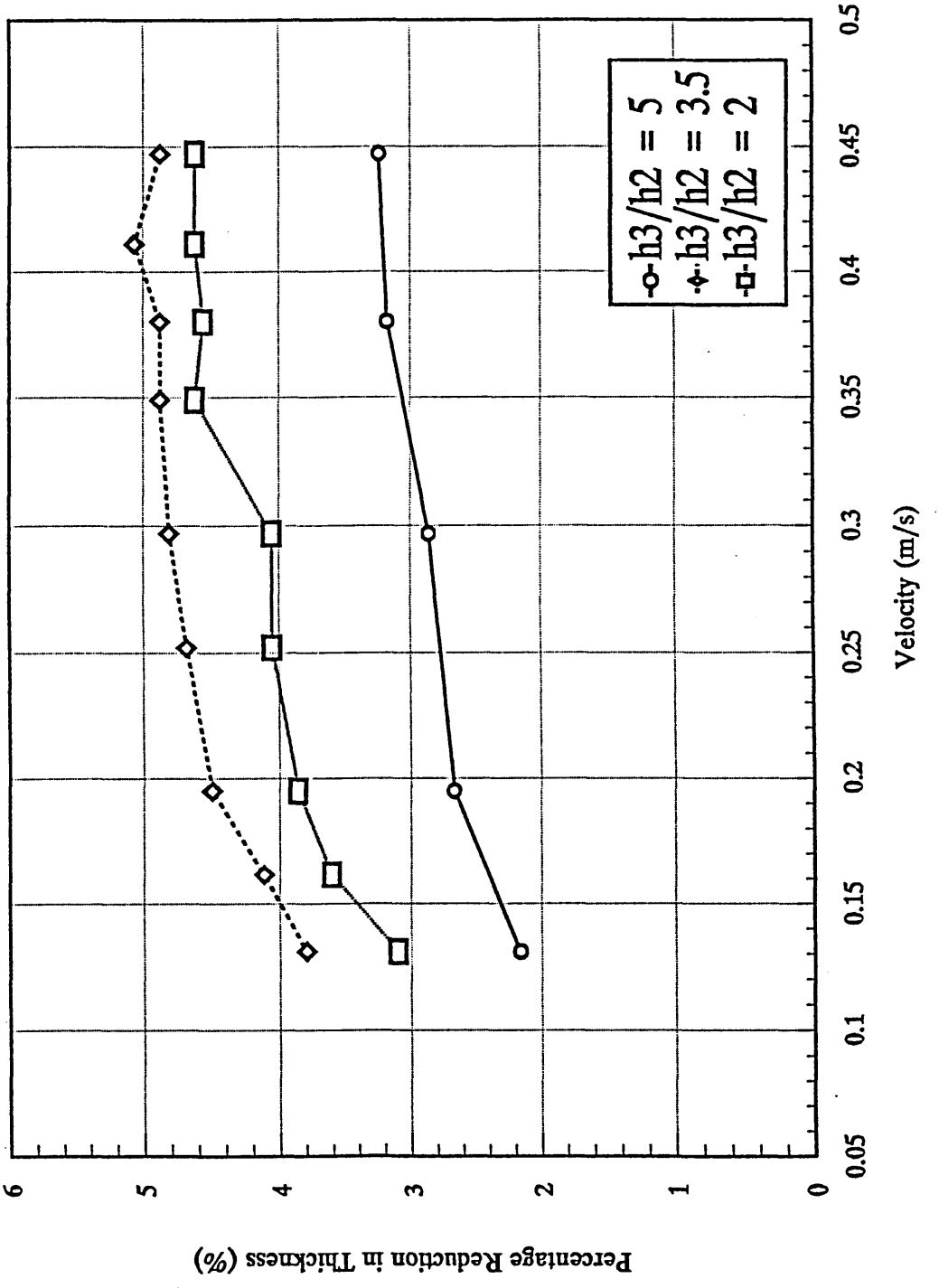

Figure 8.32 - Percentage Reduction in Thickness for various h_3/h_2 ratio at 235°C.

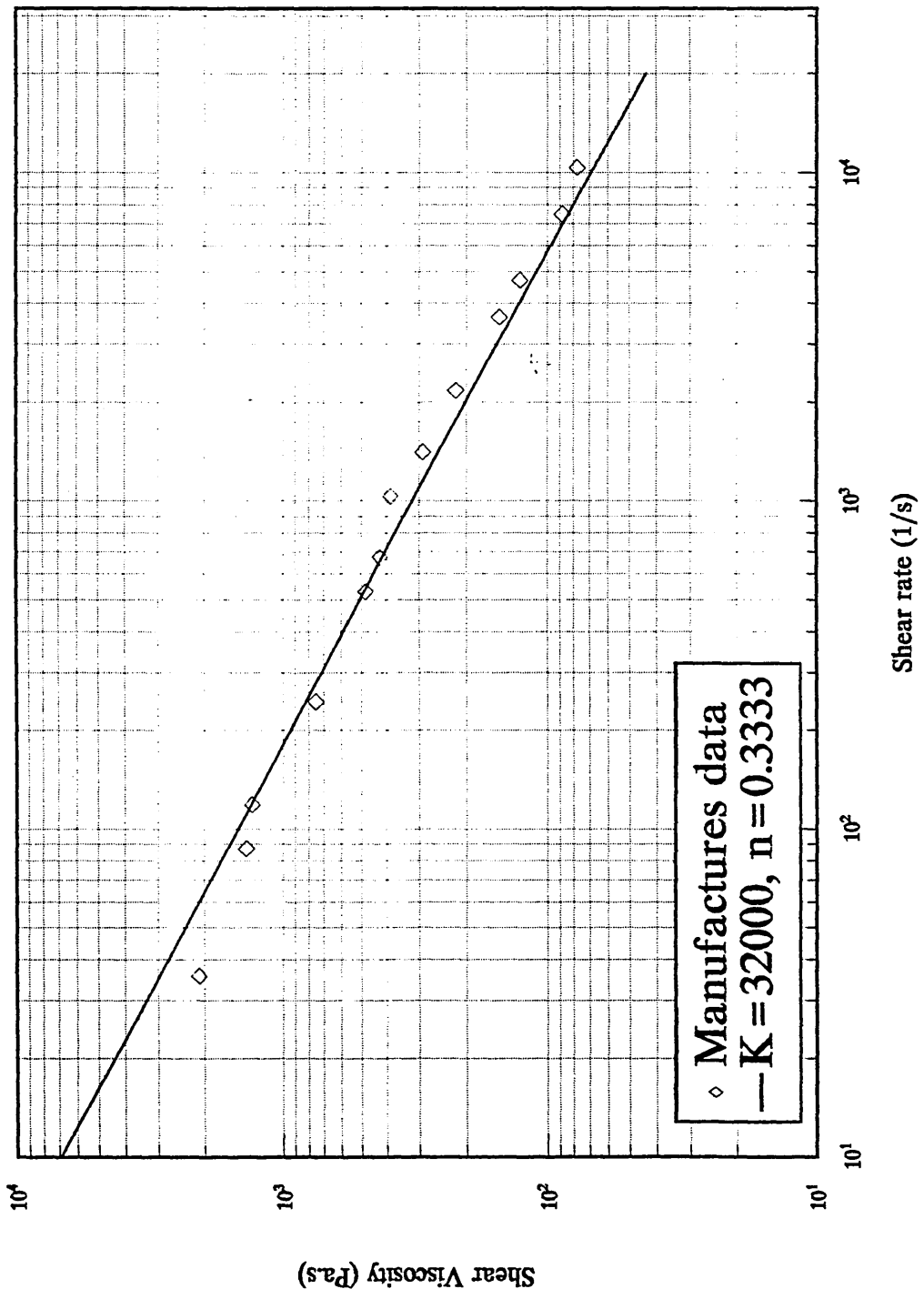

Figure 8.33 - Manufactures viscosity data for Grilamid L25 and curve fitted power law approximation.

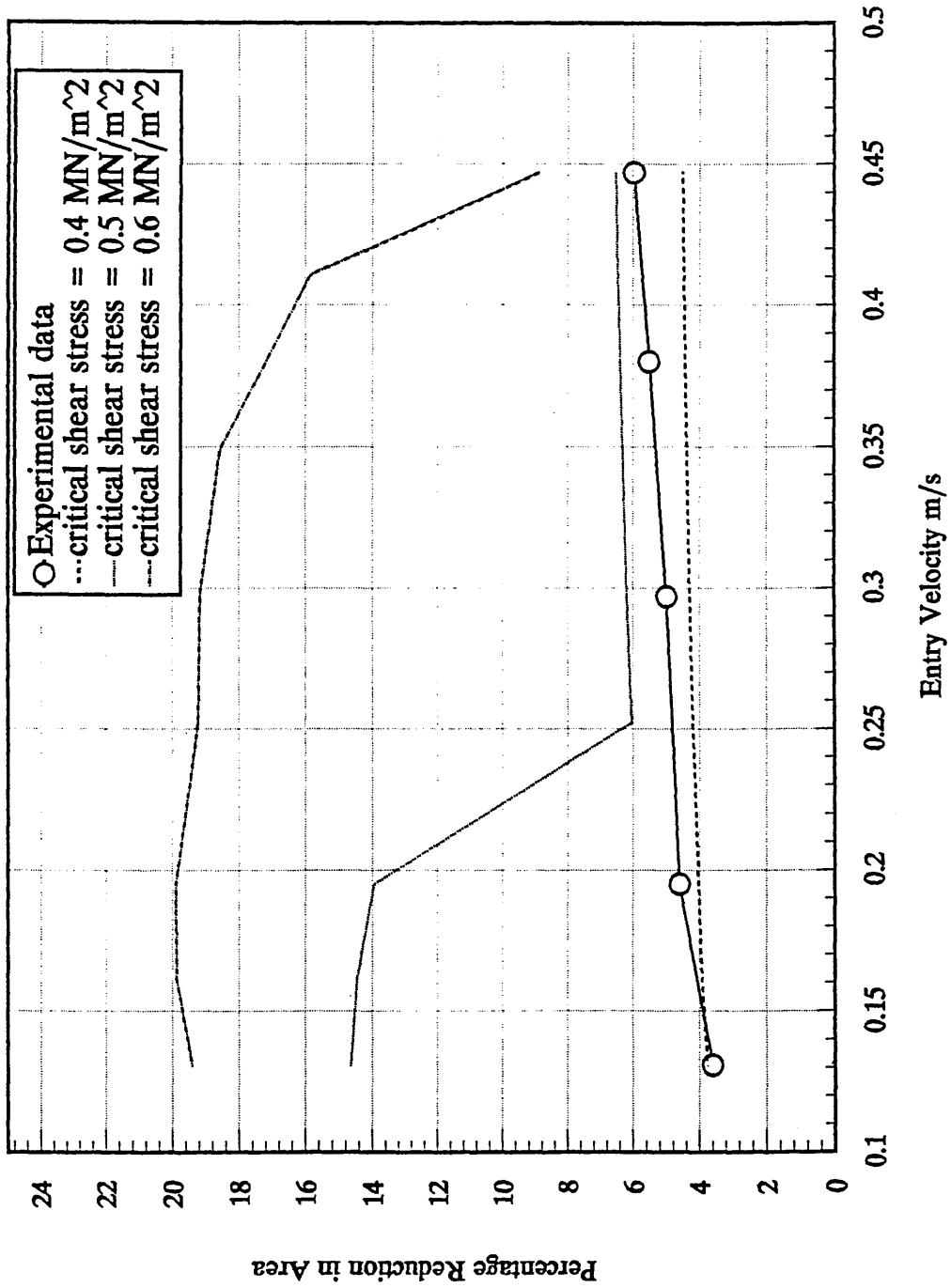

Figure 8.34 - Comparison of experimental and power law model predicted performance with a h_3/h_2 ratio of 5.

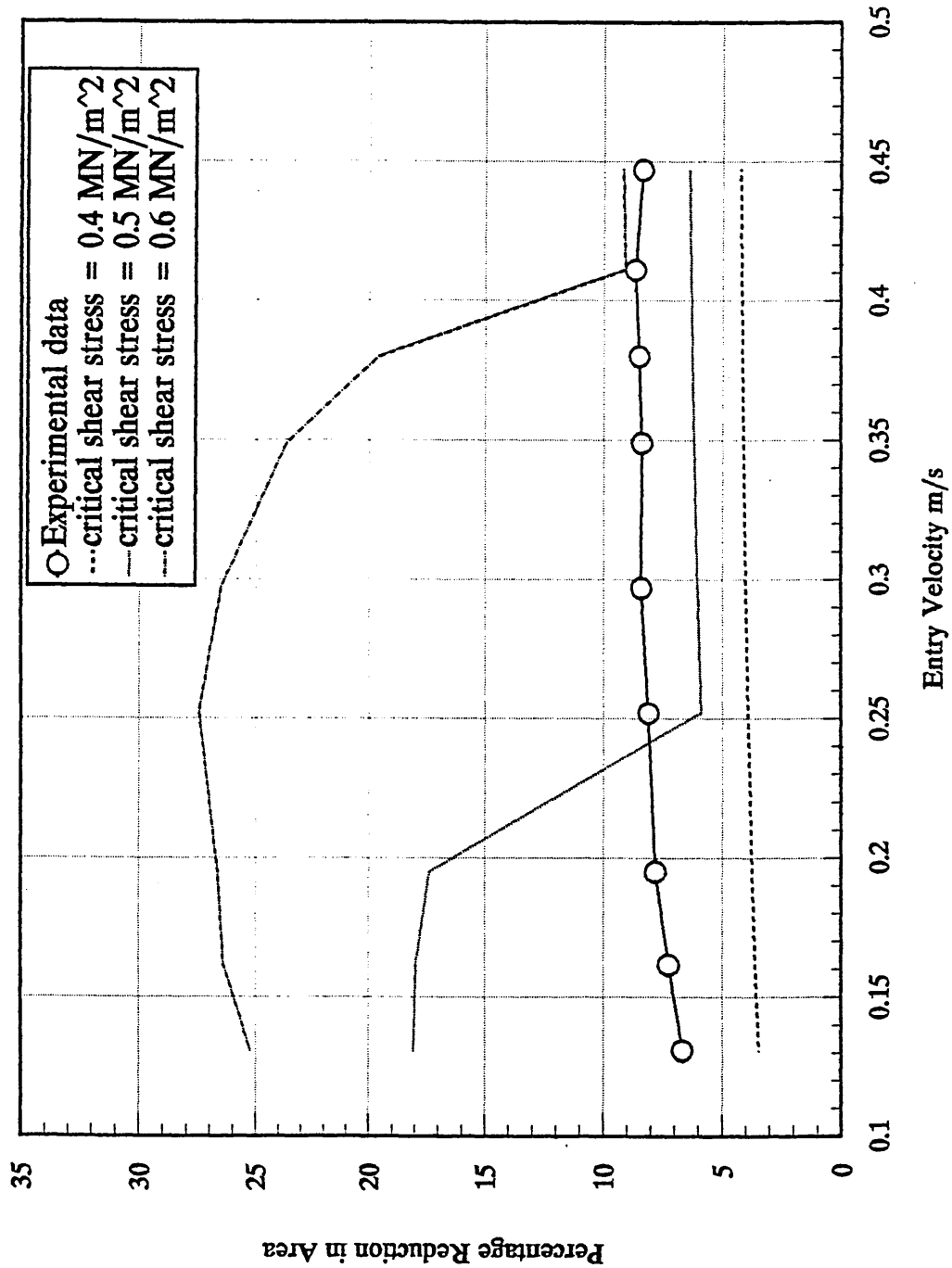

Figure 8.35 - Comparison of experimental and power law model predicted performance with a h_3/h_2 ratio of 3.5.

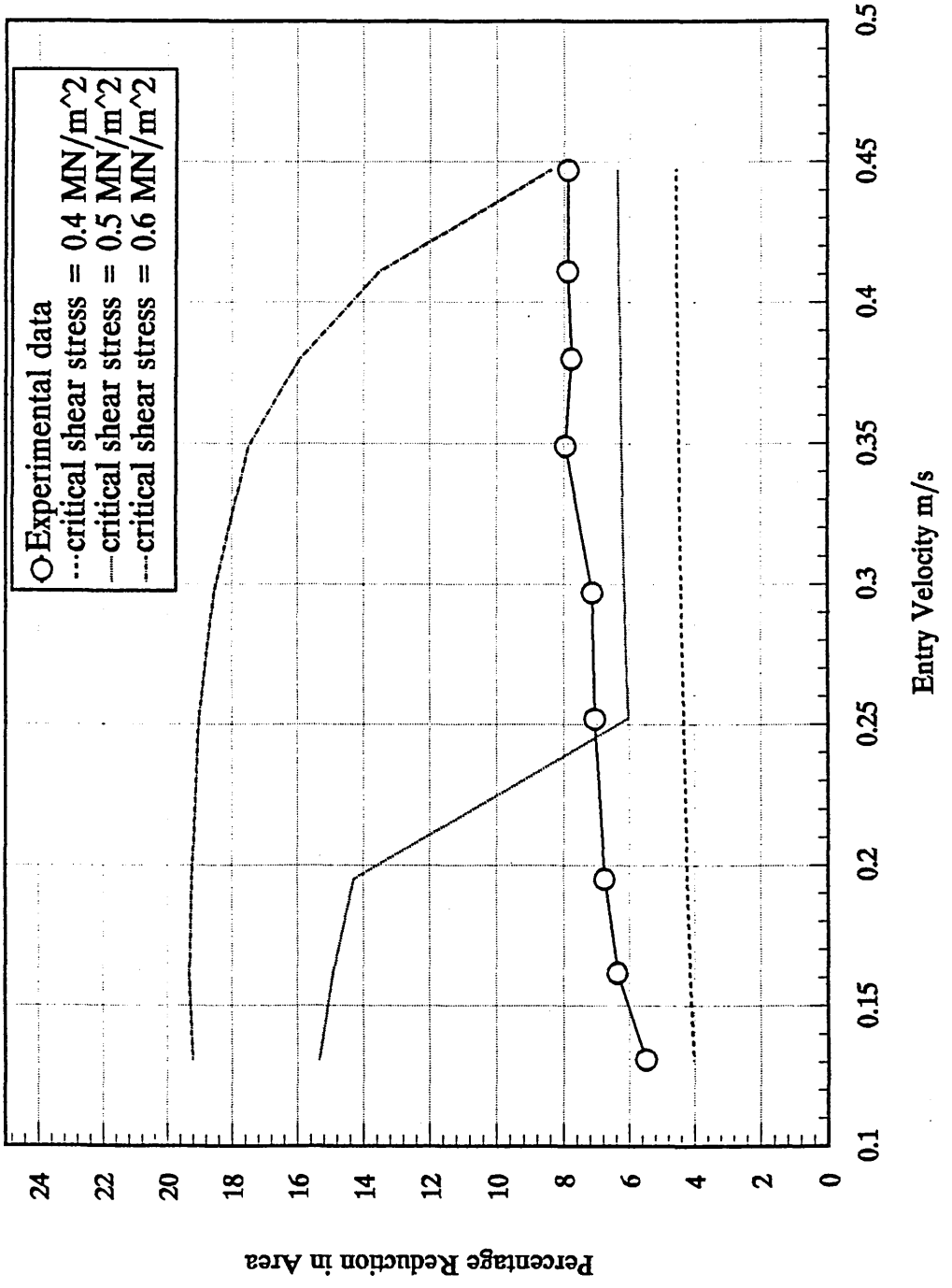

Figure 8.36 - Comparison of experimental and power law model predicted performance with a h_3/h_2 ratio of 2.

CHAPTER 9

9.0 Conclusions

The current work has addressed various issues with regards to the Plasto-hydrodynamic drawing process for rectangular strips; because of this the conclusions will be drawn for each issue separately.

9.1 Experimental

Wide copper strip (16-1 aspect ratio) has been successfully reduced using the plasto-hydrodynamic process, the working fluid being Grilamid L25.

An analysis was conducted of the output shape of the drawn material. It was found that the shape of the cross-section of the feed material was preserved with all levels of deformation achieved, and that no smoothing is incurred during the deformation process.

The corner radius of the section was also analysed using a graphical method; the data was highly scattered and no correlation could be made with reduction other than to say the corner radius is reduced in the plasto-hydrodynamic process.

9.2 Mathematical Modelling

A new treatment of the modelling of the condition of slip was introduced with modifications to the solution algorithm, an improved dynamic response to the slip condition was then demonstrated.

A new non-Newtonian model of the plasto-hydrodynamic process has been developed. It utilises a constitutive equation of the power law form, which allows greater flexibility in the range of non-Newtonian fluids which may be modelled. It has been demonstrated that the dominant term in the onset of slip is the edge

shear stress τ_3. This term consists of pressure and velocity driven components. The pressure driven component is proven to be dominant in the creation of τ_3, and hence the onset of slip. A comparison of the experimental data and the model showed the following: i) a good correlation in the form of the model prediction and the experimental data, ii) the model under-predicts the performance of the process.

9.3 Computational Fluid Dynamic analysis of the Hydrostatic assumption

A Computational Fluid Dynamic (CFD) analysis was made of a plasto-hydrodynamic pressure head at various aspect ratios and velocities. The pressure fields were compared with the hydrostatic assumption. It was found that: i) the hydrostatic assumption is reasonable for all aspect ratio and velocities, ii) a reduced overall pressure from that predicted by the theoretical analysis was found and identified as a significant mechanism for error, and iii) the reduction in overall pressure is shown to be inversely proportional to the aspect ratio of the material.

9.4 Numerical Optimisation

The technique of Numerical Optimisation has been successfully applied to both Newtonian and non-Newtonian models of the plasto-hydrodynamic drawing process. A good correlation between the Newtonian and the non-Newtonian model simulating Newtonian conditions is demonstrated providing an increased confidence in the accurate coding of the two mathematical models. The optimum h_1/h_2 and h_3/h_2 ratios are shown to be proportional to velocity and a linear function of velocity. A mechanism for the insensitivity of the system to the land ratio L_1/L_2 was identified, using sequences of performance surfaces to show the performance of the system in 3 dimensional space.

9.5 Suggestions for further work

The plasto-hydrodynamic drawing process has been proven to be successful in the deformation of rectangular section material. Improvements have been introduced to the solution algorithm for models of the process, and a new non-Newtonian model has been produced of the process. However, the current work has revealed two main issues for further work.

Firstly, experimental data shows the importance of h_3/h_2 ratio on the performance of the process. The model does not exhibit the same degree of sensitivity to h_3/h_2 ratio as the experimental data. The CFD analysis predicted lower overall pressures in the pressure head, which will have a significant impact on the plasto-hydrodynamic equation. Leakage of fluid away from the step through the side clearance has been identified as a possible source of the reduction in overall pressure in the pressure head. The volume of this flow would logically depend upon the side clearance, and hence the h_3/h_2 ratio. An attempt should be made to include the effect of any such leakage on the overall pressure within the mathematical model of the process, coupled with an experimental programme with differing aspect ratio and h_3/h_2 ratio to provide data to assess the accuracy of the predictions.

Secondly, an attempt was made to introduce an expression for the redundant work induced during the deformation process. The analysis proved to be unstable in areas of high reduction, on the performance curve. This instability was attributed to two factors: i) the over prediction of deformation performance when not in a condition of total slip in the pressure head, placing the model in an unstable region, and ii) the inability of the hardening law to allow for differential hardening across the section. A programme could then be instigated to develop a 3 dimensional plasticity model of the process, using the present model as the boundary of the solution of the plasticity equations.

References

1) Fukui S, Ohi T, Kudo H, Takila I and Senio J, Some aspects of friction in metal strip drawing, Int J Mech Sci, Vol 4, pp 297-312, 1962.

2) Lancaster PR, Rowe GW, Experimental study of the influence of lubrication upon cold drawing under approximately plane-strain conditions at low speeds, Proc Instn Mech Engrs, Vol 178, Pt 1, No 3, pp 69-88, 1963-1964.

3) Green AP, Hill R, Calculations of the influence of friction and die geometry in sheet drawing, J Mech Phys Solids 1, 31, 1952.

4) Hoffman O, Sachs G, Introduction to the theory of plasticity for engineers, McGraw-Hill, New York and London, 1953.

5) Green AP, Plane strain theories of drawing, Proc Instn Mech Engrs, London, 174, No 31, pp 847-864, 1960.

6) Kudo H, Tanaka S, Imamura K, and Suzuki K, Investigation of cold forming friction and lubrication with a sheet drawing test, Annals of CIRP, Vol 25/1, pp 179-184, 1976.

7) Wilson WRD, Cazeault P, Measurement of frictional conditions in lubricated strip drawing, NARMAC - IV, pp 165-171, 1976.

8) Rao RS, Devenpeck ML, Wright PK, Appleby EJ, Lu CY and Richmond O, New strip drawing experiments using transparent sapphire dies, Int J Mech Sci, Vol 27, No 11/12, pp 725-740, 1985.

9) Appleby EJ, Lu CY, Rao RS, Devenpeck ML, Wright PK and Richmond O, Strip drawing : A theoretical-experimental comparison, Int J Mech Sci, Vol 26, No 5, pp 351-362, 1984.

10) Parsons B, Taylor R and Cole BN, High speed drawing of metals : A first report, Proc Instn Mech Engrs, Vol 180, Pt 31, pp 230-240, 1965-1966.

11) Baxter RS, High speed drawing of metals, PhD thesis, University of Leeds, 1968.

12) Devenpeck ML, Rigo JH, Research apparatus for simulating high speed drawing of thin strip, Procs 7th North American Manufacturing Research Conf, Univ of Michigan, pp 81-88, 1979.

13) Christopherson DG, Naylor H, Promotion of fluid lubrication in wire drawing, Proc Inst Mech Engrs

14) Tattersal GH, Hydrodynamic lubrication in wire drawing, J Mech Eng Sci, No 4 P 378, 1961.

15) Osterle JF Dixon JR, Viscous lubrication in wire drawing, ASLE transactions 5, 233-241, 1962.

16) Cheng HS, Plasto-hydrodynamic lubrication, Proc Symp Friction & Lubrication in Metal Processing, New York, pp 69-89, 1966.

17) Bedi DS, A hydrodynamic model for wire drawing, The Int Jr Prod Res, Vol 6, No 4, pp 329-343, 1968.

18) Bloor SM, Dowson D, and Parson B, An elasto-plasto-hydrodynamic lubrication analysis of the plane strain drawing process. Jr Mech Eng Sci, Vol 12, pp 178-190, 1970.

19) Dowson D, Parsons B and Lidgitt PJ, An elasto-plasto-hydrodynamic lubrication analysis of the wire drawing process, Inst Mech Engrs, C 16, pp 97-106, 1972.

20) Lancaster PR, A study of lubrication in the high speed drawing process, Wire Industry, pp 294-297, 1972.

21) Avitzur B, The application of hydrodynamic lubrication in wire drawing and extrusion, Wire Journal, pp 74-79, 1976.

22) Kudo H, Tsubouchi M, Takadha H and Okamura K, An investigation into plasto-hydrodynamic lubrication with a cold sheet drawing test, Annals of CIRP, Vol 31/1, pp 175-180, 1982.

23) Wilson WRD, Mahdavian SM, A thermal Reynolds equation and its application in the analysis of plasto-hydrodynamic inlet zones, Transactions of the ASME, pp 572-578, 1974.

24) Dow TA, Kannel JW and Bupara SS, A hydrodynamic lubrication theory for rolling including thermal effects, Transactions of the ASME, pp 4-13, 1975.

25) Mahdavian SM, Wilson WRD, Lubricant flow in a plasto-hydrodynamic work zone, Transactions of the ASME, pp 16-21, 1976.

26) Thompson PJ, Symmons GR, A plasto-hydrodynamic analysis of the lubricating and coating of wire using a polymer melt during drawing, Proc Inst Mech Engr 13, 191, 1977.

27) Symmons GR, Stevens AJ and Thompson PJ, Hydrodynamic lubrication and coating of wire using a polymer melt during the drawing operation, Wire Industry, pp 469-473, 1978.

28) Crampton R, Hydrodynamic lubrication and coating of wire using a polymer melt during drawing process, PhD Thesis, Sheffield City Polytechnic, 1980.

29) Crampton R, Symmons GR and Hashmi MSJ, A non-Newtonian plasto-hydrodynamic analysis of the lubrication and coating of wire using a polymer melt during drawing, Int Symp Metal Working Lubrication, San Francisco, USA, p 107, 1980.

30) Hashmi MSJ, Crampton R and Symmons GR, Effects of strain hardening and strain rate sensitivity of the wire material during drawing under non-Newtonian lubrication conditions, Int J Mach Tool Des Res, Vol 21, No 1, pp 71-86, 1981.

31) Hashmi MSJ, Symmons GR and Parvinmehr H, A novel technique of wire drawing, Jr Mech Eng Sci (c) I Mech E, Vol 24, No 1, pp 1-4, 1982.

32) Symmons GR, Hashmi MSJ, and Parvinmehr H, Plasto-hydrodynamic die-less wire drawing : Theoretical treatment and experimental results, Proc Int Conf on developments in drawing of metals, Metal Society, London, pp 54-61, 1983.

33) Parvinmehr H, Optimisation of plasto-hydrodynamic system of wire drawing using polymer melts, PhD Thesis, Sheffield City Polytechnic, 1983.

34) Hashmi MSJ, Symmons GR, A mathematical model for the drawing of a solid continuum through Newtonian fluid filled tubular orifice, Proc 4th Int Conf on Mathematical Modelling, Zurich, 1983.

35) Hashmi MSJ, Symmons GR, A numerical solution for the plasto-hydrodynamic drawing of a rigid non-linearly strain hardening continuum through a conical orifice, 2nd Int Conf on Numerical Methods for Non-linear Problems, Spain, 1984.

36) Parvinmehr H, Symmons GR and Hashmi MSJ, A non-Newtonian plasto-hydrodynamic analysis of die-less wire drawing process using a stepped bore unit, Int Jr Mech Sci, Vol 29, No 4, pp 239-257, 1987.

37) Panhwar MI, Crampton R and Hashmi MSJ, Die-less tube sinking : A plasto-hydrodynamic analysis based on Newtonian fluid characteristics, Proc of 5th Polytechnic Symp on Manufacturing Engineering, Brighton Polytechnic, 1986.

38) Panhwar MI, A novel technique for tube sinking, Phd Thesis, Sheffield City Polytechnic, 1986.

39) Symmons GR, Hashmi MSJ and Xie YD, The optimisation of a plasto-hydrodynamic wire drawing process, IASTED Conference, Paris, June 1987.

40) Xie YD, Modelling and control of die-less wire drawing, PhD Thesis, Sheffield City Polytechnic, 1987.

41) Symmons GR, Xie YD and Hashmi MSJ, Thermal effect on a plasto hydrodynamic wire drawing process using a polymer melt, Xth Int Con on Rheology, Sydney, Australia, August 1988.

42) Memon AH, Plasto-hydrodynamic die-less strip drawing, PhD Thesis, Sheffield City Polytechnic, 1988.

43) Symmons GR, Memon AH and Hashmi MSJ, A mathematical model for plasto-hydrodynamic drawing of narrow strips, Mathl Comput Modelling, Vol 11, pp 926-931, 1988.

44) Symmons GR, Memon AH and Hashmi MSJ, A Newtonian model of a plasto-hydrodynamic drawing process of a rectangular cross-sectional continuum, IASTED Conf, Switzerland, 1988.

45) Symmons GR, Memon AH, Crampton R and Hashmi MSJ, Thermal effect on a plasto-hydrodynamic strip drawing process using a polymer melt, Xth Int congress on Rheology, Univ Sydney, Australia, 1988.

46) Symmons GR, Memon AH, Zhang Ming and Hashmi MSJ, Polymer coating of wire using a die-less drawing process, Journal of Materials Processing Technology, 26, pp 173-180, 1991.

47) Symmons GR, Zhang Ming, Die-less wire drawing using Borosiloxane as a pressure medium, Proc of 7th Conf of the Irish Manufacturing Committee, pp 466-475, 1990.

48) Hashmi MSJ, Al-Natour, Development of a complex geometry pressure unit for hydrodynamic coating applications, Proc of 6th Conf of the Irish Manufacturing Committee, pp 280-297, 1989.

49) Panhwar MI, Hashmi MSJ, A mathematical model for drawing of solid continuum through Newtonian fluid filled conical orifice, Mehran Univ Rese Jnl of Engi & Tech, Vol 7, No 2, pp 5-12, 1988.

50) Skellend AHP, Non-Newtonian flow and heat transfer, Wiley, New York, 1967.

51) Williams ML, Landel RF and Ferry JD, The temperature dependence of relaxation mechanisms in amorphous polymers and other glass-forming liquids, Journal of the American Chemical Society, 77, 3701, 1955.

52) Westover RF, Effect of hydrostatic pressure on polyethylene melt rheology, Society of Plastics Engineers Transactions, 1, 14, 1961.

53) Semjonov V, Über ein Rotationsviskosimeter zur Messung der Druckabhängigabhängigkeit der Vislosität einiger Polyolefinschmelzen, Rheologica Acta, 2, 138, 1965.

54) Cogswell FN, The influence of pressure on the viscosity of polymer melts, Plastics and Polymers, 41, 39, 1973.

55) Benbow JJ, Lamb P, New aspects of melt fracture, SPE transactions pp 7-17, 1963.

56) Bagley EB, Schreiber HP, Effect of die entry geometry on polymer melt fracture and extrudate distortion, Transactions of the Society of Rheology, pp 341-353, 1961.

57) Howells ER, Benbow JJ, Flow defects in polymer melts, Transactions of the Plastics Institute, 30, pp 240-253, 1962.

58) Metzger AP, Hamilton CW, The oscillating shear phenomenon in high density polyethylenes, Society of plastics engineers pp 107-112, 1964.

59) Metzger AP, Hamilton CW and Merz EH, Anomalous flow behaviour of high density polyethylene melts, Society of Plastics Engineering Transactions, pp 21-26, 1963.

60) Cogswell FN, Lamb P, The mechanism of melt distortion, Trans J Plastics Inst, 35, pp 809-813, 1967.

61) Tordella JP, Unstable flow of molten polymers, A second site of melt fracture, Journal of Applied Polymer Science, 7, pp 215-229, 1963.

62) Stokes GG, On the theories of the internal friction of fluids in motion, Procs Camb Phil Society, Vol 1, No 2, pp 16-18, 1845.

63) Jianming W, Gaobing J, The optimum design of the Rayleigh slider bearing with a power law fluid, Wear, 129, pp 1 - 11, 1989.

64) Körber F, Eichinger A, Die grundlagen der bildsamen Verformung, Mitt K-Wilhelm-Inst Eisenforsch, Düsseld, 22, 57, 1940.

65) Sachs G, Plasticity problems in metals, Trans Faraday Soc, 24, 84, 1928.

66) Rayleigh Lord OM, Notes on the theory of lubrication, Philosophical Magazine, 35, 1-12, 1918.

67) Rohde SM, Finite element optimisation of finite stepped slider bearing profiles, ASLE transactions, 17, 105-110, 1974.

68) Kettleborough CF, An electrolytic tank investigation into stepped thrust bearings, Proc Instit of Mech Eng, 169, 679, 1955.

69) Kettleborough CF, The stepped thrust bearing - a solution by relaxation methods, Trans ASME, 76, 19, 1954.

70) Elkouh AF, Yang Der-Fa, Flow of a power law fluid in a Rayleigh step, Trans ASME 113, 428-433, 1991.

71) Wang J, Jin G, The optimum design of the Rayleigh slider bearing with a power law fluid, Wear, 129, 1-11, 1989.

72) Bourgin P, Gay B, The optimum Rayleigh bearing in terms of load capacity or friction for Non-Newtonian lubricants, Trans ASME, 107, 59-67, 1985.

73) Stokes MR, Symmons GR, Numerical optimisation of the plasto-hydrodynamic drawing of narrow strips, Proc Int Conf on Advances in Materials and Processing Technologies, Dublin, 1993.

74) Bunday BD, Basic Optimisation Methods, Edward Arnold, USA, 1984.

75) Dantzig GB, Linear programming and extensions, Princeton Univ Press, 1963.

76) Nelder JA, Mead R, A simplex method for function minimisation, Computer Journal, 7, pp 308-313, 1965.

77) Hooke R, Jeeves TA, Direct search solution of numerical and statistical problems, Jnl Assn Comp Mach, 8, pp 212-229, 1961.

78) Fletcher R, Powell MJD, A rapidly convergent descent method for minimisation, Comp Journal, 6, 163-168, 1963.

79) Fletcher R, Reeves CM, Function minimisation by conjugate gradients, Computer Journal, 7, 149-154, 1964.

80) Rosenbrock HH, An automatic method for finding the greatest or least value of a function, Computer Journal, 3, 175-184, 1960.

81) Stokes MR, Symmons GR, A 3D computational fluid dynamic analysis of the pressure distribution in the plasto-hydrodynamic drawing of rectangular sections, Proc of 10th Conf of the Irish Manufacturing Committee, Vol 1, pp 226-237, 1993.

82) Hashmi MSJ, Crampton R and Symmons GR, Effects of strain hardening and strain rate sensitivity of the wire material during drawing under non-Newtonian plasto-hydrodynamic lubrication conditions, Int J Mach Des Res, Vol 21, No 1, pp 71-86, 1981.

Appendix 1

It should be noted that within the following FORTRAN code, calls are made to various graphical subroutines from the Extend Graphics Library. Due to copyright restrictions further details cannot be given in this work. Information on the form and scope of the library may be obtained from the manufacturers.

Design Decisions Inc
P.O. Box 12884
Pittsburgh
Pennsylvania 15241
(415) 941-4525

```
C*********************************************************************C
C  NUMERICAL MODEL MENU SYSTEM MOD6                                   C
C                                                                     C
C  M   M    OOO    DDDD    6666                                      C
C  MM MM   O   O   D   D  6                                          C
C  M M M   O   O   D   D  66666                                      C
C  M M M   O   O   D   D  6    6                                     C
C  M   M    OOO    DDDD    6666                  M.R. STOKES         C
C*********************************************************************C
      REAL*8 H1,H2,H3,L1,L2,VIS,YS,K,N,W,T,TAUCRI,VEL,PRT,PRW,PRA,NN,
     &T1,VEXE,OTEMP,DIA,PLC,PLI,DFINAL
      LOGICAL FL1,SLIP,EFLAG
      SLIP=.FALSE.
      FL1=.FALSE.
      EFLAG=.FALSE.
C
C GET DEFAULTS FROM DISC
C
      OPEN(7,FILE='DEFAULT.DAT')
      READ(7,*) H1,H2,H3,L1,L2,VIS,YS,K,N,W,T,TAUCRI,NN,T1,VEL,OTEMP,
     &DIA,PLC,PLI
      CLOSE(7)
C
C CLEAR SCREEN
C
      CALL SETCRT(3)
      CALL CLEARS(0,23)
  1   CALL CLS
C
C DISPLAY MENU
C
      WRITE(6,170)
 170  FORMAT(36('*'),2X,'MENU',2X,36('*'))
      WRITE(6,180)
 180  FORMAT(4X,'1    CHANGE SET PARAMETERS',14X,'6    NEWTONIAN WIRE')
      WRITE(6,190)
 190  FORMAT(4X,'2    NEWTONIAN STRIP',20X,'7    NON NEWTONIAN WIRE')
      WRITE(6,200)
 200  FORMAT(4X,'3    NON NEWTONIAN STRIP',16X,'8')
      WRITE(6,210)
 210  FORMAT(4X,'4',39X,'9    DATA FILE')
      WRITE(6,220)
 220  FORMAT(4X,'5',39X,'10   EXIT')
      WRITE(6,230)
 230  FORMAT(79('*'))
      WRITE(6,240)
 240  FORMAT(32X,'MODEL PARAMETERS')
      WRITE(6,230)
C
C  PARAMTER DISPLAY
C
      WRITE(6,100) L1,YS
  100 FORMAT(4X,'1    L1=',F6.4,23X,'10   SIG yield=',F12.0)
      WRITE(6,110)L2,NN
  110 FORMAT(4X,'2    L2=',F6.4,23X,'11   STRAIN RATE CONST=',F8.0)
      WRITE(6,115) T1
  115 FORMAT(41X,'12   STRAIN RATE INDEX=',F5.2)
      WRITE(6,117)H1,K
  117 FORMAT(4X,'3    H1=',F7.6,22X,'13   STRAIN HARD-G CONST',F11.0)
      WRITE(6,120)H2,N
  120 FORMAT(4X,'4    H2=',F7.6,22X,'14   STRAIN HARD-G INDEX',F7.4)
      WRITE(6,130)H3
  130 FORMAT(4X,'5    H3=',F7.6)
      WRITE(6,140)VIS
  140 FORMAT(41X,'15   INITIAL VISCOSITY=',F9.4)
      WRITE(6,145) W,PLC
  145 FORMAT(4X,'6    WIDTH=',F7.4,19X,'16   POWER LAW CONST=',F7.3)
      WRITE(6,150) T,PLI
  150 FORMAT(4X,'7    THICKNESS=',F7.5,15X,'17   POWER LAW INDEX=',F7.3)
      WRITE(6,160) DIA,OTEMP
  160 FORMAT(4X,'8    DIAMETER=',F7.5,16X,'18   INITIAL TEMP=',F5.1)
      WRITE(6,163) TAUCRI
  163 FORMAT(41X,'19   CRITICAL SHEAR STRESS=',F9.0)
      WRITE(6,165) VEL
  165 FORMAT(4X,'9    INITIAL VELOCITY=',F7.3)
      WRITE(6,230)
      WRITE(6,*)' '
      WRITE(6,*)'ENTER OPTION REQUIRED'
      READ(5,*) IOPT
C
C TAKE ACTION ON IOPT
C
      IF(IOPT.EQ.1) CALL DEFAULTS(H1,H2,H3,L1,L2,VIS,YS,K,N,W,T,TAUCRI
     &,NN,T1,VEL,OTEMP,DIA,PLC,PLI)
C
C
      IF(IOPT.EQ.2) THEN
        CALL SOLVE(H1,H2,H3,L1,L2,VIS,YS,K,N,W,T,TAUCRI,VEL,PRT,PRA,PRW
     &,T1,NN,VEXE,FL1,SLIP)
C
        IF(FL1) THEN
         CLOSE(1)
         CLOSE(2)
         CLOSE(3)
         CLOSE(4)
         CLOSE(7)
         FL1=.FALSE.
        ENDIF
C
        CALL OUTPUT(H1,H2,H3,L1,L2,VIS,YS,K,N,W,T,TAUCRI,VEL,PRT
     &,PRA,PRW,T1,NN,VEXE,SLIP)
      ENDIF
C
C
      IF(IOPT.EQ.3) THEN
C
        CALL PLAW(W,T,H1,H2,H3,L1,L2,YS,VEL,PLC,PLI,TAUCRI,FL1,N,
     &K,PRT,PRW,PRA,VEXE)
C
      CALL ENDPLT(1,1)
      CALL GSTOP(3,23)
      CALL CLS
      WRITE(6,*) ' PRT= ',PRT
      WRITE(6,*) ' PRW= ',PRW
      WRITE(6,*) ' PRA= ',PRA
      WRITE(6,*) ' VEXE= ',VEXE
      READ(5,*)
```

```
C
      ENDIF
C
C
      IF(IOPT.EQ.4) THEN
       CALL CLS
       WRITE(6,*)'                    FUNCTION NOT AVAILABLE'
       DO 4 I=1,10
         WRITE(6,*) ' '
   4   CONTINUE
       READ(*,*)
       ENDIF
C
C
      IF(IOPT.EQ.5) THEN
       CALL CLS
       WRITE(6,*)'                    FUNCTION NOT AVAILABLE'
       DO 5 I=1,10
         WRITE(6,*) ' '
   5   CONTINUE
       READ(*,*)
       ENDIF
C
C
      IF(IOPT.EQ.6) THEN
C
        CALL NEWWIRE (L1,L2,H1,H2,DIA,VIS,VEL,YS,TAUCRI,NN,T1,K,N,SLIP,
     &VEXE,DFINAL,FL1,PRA,EFLAG)
C
        IF(FL1) THEN
         CLOSE(1)
         CLOSE(2)
         CLOSE(3)
         CLOSE(4)
         CLOSE(7)
         FL1=.FALSE.
        ENDIF
C
        IF(.NOT.EFLAG) CALL OUT6(H1,H2,L1,L2,VIS,YS,K,N,TAUCRI,VEL,
     &DFINAL,PRA,T1,NN,VEXE,SLIP,DIA)
C
      ENDIF
C
C
      IF(IOPT.EQ.7) THEN
       CALL CLS
       WRITE(6,*)'                    FUNCTION NOT AVAILABLE'
       DO 7 I=1,10
         WRITE(6,*) ' '
   7   CONTINUE
       READ(*,*)
       ENDIF
C
C
      IF(IOPT.EQ.8) THEN
       CALL CLS
       WRITE(6,*)'                    FUNCTION NOT AVAILABLE'
       DO 8 I=1,10
         WRITE(6,*) ' '
   8   CONTINUE
       READ(*,*)
       ENDIF
C
C
      IF(IOPT.EQ.9) CALL TECHFILE(FL1)
C
C
      IF(IOPT.EQ.10) THEN
       CALL CLS
       STOP 'HAVE A NICE DAY'
      ENDIF
      GOTO 1
C
      END

C*********************************************C
C  CLS                                        C
C*********************************************C
      SUBROUTINE CLS
      DO 2 I=1,25
       WRITE(6,*)' '
   2  CONTINUE
      RETURN
      END



C*****************************************************************************C
C  DEFAULTS                                                                   C
C*****************************************************************************C
      SUBROUTINE DEFAULTS(H1,H2,H3,L1,L2,VIS,YS,K,N,W,T,TAUCRI,NN,T1,VEL
     &,OTEMP,DIA,PLC,PLI)
      REAL*8 H1,H2,H3,L1,L2,VIS,YS,K,N,W,T,TAUCRI,NN,T1,VEL,OTEMP,DIA,
     &PLC,PLI
C
   1  CALL CLS
C
C  PARAMTER DISPLAY
C
      WRITE(6,230)
  230 FORMAT(79('*'))
      WRITE(6,240)
  240 FORMAT(30X,'EDIT MODEL PARAMETERS')
      WRITE(6,230)
      WRITE(6,100) L1,YS
  100 FORMAT(4X,'1    L1=',F6.4,23X,'10   SIG yield=',F12.0)
      WRITE(6,110)L2,NN
  110 FORMAT(4X,'2    L2=',F6.4,23X,'11   STRAIN RATE CONST=',F8.0)
      WRITE(6,115) T1
  115 FORMAT(41X,'12   STRAIN RATE INDEX=',F5.2)
      WRITE(6,117)H1,K
  117 FORMAT(4X,'3    H1=',F7.6,22X,'13   STRAIN HARD-G CONST',F11.0)
      WRITE(6,120)H2,N
  120 FORMAT(4X,'4    H2=',F7.6,22X,'14   STRAIN HARD-G INDEX',F7.4)
      WRITE(6,130)H3
```

```
  130 FORMAT(4X,'5    H3=',F7.6)
      WRITE(6,140)VIS
  140 FORMAT(41X,'15   INITIAL VISCOSITY=',F9.4)
      WRITE(6,145) W,PLC
  145 FORMAT(4X,'6    WIDTH=',F7.4,19X,'16   POWER LAW CONST=',F7.3)
      WRITE(6,150) T,PLI
  150 FORMAT(4X,'7    THICKNESS=',F7.5,15X,'17   POWER LAW INDEX=',F7.3)
      WRITE(6,160) DIA,OTEMP
  160 FORMAT(4X,'8    DIAMETER=',F7.5,16X,'18   INITIAL TEMP=',F5.1)
      WRITE(6,163) TAUCRI
  163 FORMAT(41X,'19   CRITICAL SHEAR STRESS=',F9.0)
      WRITE(6,165) VEL
  165 FORMAT(4X,'9    INITIAL VELOCITY=',F7.3)
      WRITE(6,230)
      WRITE(6,*)' '

C
C
C


      WRITE(6,*)' '
      WRITE(6,*)' '
      WRITE(6,*)' '
      WRITE(6,*)'SELECT #ITEM TO BE CHANGED(ENTER 20 TO EXIT)'
      READ(5,*)IOPT
C
C
C

      IF(IOPT.EQ.20) THEN
       OPEN(7,FILE='DEFAULT.DAT')
       WRITE(7,*) H1,H2,H3,L1,L2,VIS,YS,K,N,W,T,TAUCRI,NN,T1,VEL,OTEMP,
     &DIA,PLC,PLI
       CLOSE(7)
       RETURN
      ENDIF

      IF(IOPT.EQ.1) THEN
       WRITE(0,116)
       READ(0,*) L1
       L1=L1/1000.
      ENDIF
  116 FORMAT(1X,'ENTER L1 IN mm')
C
      IF(IOPT.EQ.2) THEN
       WRITE(6,111)
       READ(5,*)L2
       L2=L2/1000.
      ENDIF
  111 FORMAT(1X,'ENTER L2 IN mm')
C
      IF(IOPT.EQ.3)THEN
       WRITE(0,101)
       READ(0,*) H1
       H1=H1/1000.
      ENDIF
  101 FORMAT(1X,'ENTER H1 IN mm')
C
      IF(IOPT.EQ.4) THEN
       WRITE(6,102)
       READ(5,*)H2
       H2=H2/1000.
      ENDIF
  102 FORMAT(1X,'ENTER H2 IN mm')
C
      IF(IOPT.EQ.5) THEN
       WRITE(6,103)
       READ(5,*) H3
       H3=H3/1000.
      ENDIF
  103 FORMAT(1X,'ENTER H3 IN mm')
C
      IF(IOPT.EQ.6) THEN
       WRITE(6,155)
       READ(5,*) W
       W=W/1000
      ENDIF
  155 FORMAT(1X,'ENTER INITIAL WIDTH IN MM')
C
      IF(IOPT.EQ.7) THEN
       WRITE(6,151)
       READ(5,*) T
       T=T/1000
      ENDIF
  151 FORMAT(1X,'ENTER INITIAL THICKNESS IN MM')
C
      IF(IOPT.EQ.8) THEN
        WRITE(6,42)
        READ(5,*) DIA
        DIA=DIA/1000
      ENDIF
   42 FORMAT (1X,'ENTER INITIAL DIAMETER IN MM')
C
      IF(IOPT.EQ.9) THEN
       WRITE(6,170)
       READ(5,*) VEL
      ENDIF
  170 FORMAT(1X,'ENTER VELOCITY OF MATERIAL M/S ')
C
      IF(IOPT.EQ.10) THEN
       WRITE(6,135)
       READ(5,*) YS
       YS=YS*1000000
      ENDIF
  135 FORMAT(1X,'ENTER YIELD STRESS MN/M^2')
C
      IF(IOPT.EQ.11) THEN
       WRITE(6,365)
       READ(5,*) NN
      ENDIF
  365 FORMAT(1X,'ENTER STRAIN RATE CONSTANT ')
C
      IF(IOPT.EQ.12) THEN
       WRITE(6,161)
       READ(5,*) T1
      ENDIF
  161 FORMAT(1X,'ENTER STRAIN RATE INDEX  ')
C
      IF(IOPT.EQ.13) THEN
```

```
      WRITE(6,345)
      READ(5,*) K
      K=K*1000000
     ENDIF
  345 FORMAT(1X,'ENTER STRAIN HARDENING CONSTANT(MN/M^2) ')
C
      IF(IOPT.EQ.14) THEN
       WRITE(6,141)
       READ(5,*) N
      ENDIF
  141 FORMAT(1X,'ENTER STRAIN HARDENING INDEX')
C
      IF(IOPT.EQ.15) THEN
       WRITE(6,125)
       READ(5,*) VIS
      ENDIF
  125 FORMAT(1X,'ENTER VISCOSITY IN NS/M^2 ')
C
      IF(IOPT.EQ.16) THEN
        WRITE(6,152)
        READ(5,*) PLC
      ENDIF
  152 FORMAT(1X,'ENTER THE POWER LAW CONSTANT TERM ')
C
      IF(IOPT.EQ.17) THEN
        WRITE(6,153)
        READ(5,*) PLI
      ENDIF
  153 FORMAT(1X,'ENTER THE POWER LAW INDEX TERM ')
C
      IF(IOPT.EQ.18) THEN
        WRITE(6,154)
        READ(5,*) OTEMP
      ENDIF
  154 FORMAT(1X,'ENTER ORIGINAL TEMPERATURE ')
C
      IF(IOPT.EQ.19) THEN
       WRITE(6,121)
       READ(5,*) TAUCRI
       TAUCRI=TAUCRI*1000000
      ENDIF
  121 FORMAT(1X,'ENTER CRITICAL SHEAR MN/M^2')
C
      GOTO 1
      END



      SUBROUTINE TECHFILE(FL1)
      LOGICAL FL1
      CHARACTER FCODE*3,FNAME*12
C
      DO 11 I=1,24
      WRITE(6,*)' '
   11 CONTINUE
   10 WRITE(6,*)'ENTER A 3 CHARCTER CODE TO IDENTIFY MODEL RUN (ENCLOSE
     &IN SINGLE QUOTES)'
      READ(5,*,ERR=10) FCODE
      FNAME=FCODE//'PABS.TXT'
      OPEN(1,FILE=FNAME)
      FNAME=FCODE//'PGRAD.TXT'
      OPEN(2,FILE=FNAME)
      FNAME=FCODE//'TDEFO.TXT'
      OPEN(3,FILE=FNAME)
      FNAME=FCODE//'YDOT.TXT'
      OPEN(4,FILE=FNAME)
      FNAME=FCODE//'.DOC'
      OPEN(7,FILE=FNAME)
      WRITE(7,100)
      FL1=.TRUE.
C
  100 FORMAT(2X,'X',11X,'TI',11X,'WI',10X,'TAU1I',8X,'YDOT1',8X,'TAU3I'
     &,8X,'YDOT2',8X,'PI',10X,'DPDXI',9X,'YI1',9X,'SIGXI',10X,'RS',10X,
     &'SIGRW',10X,'B')
C
      RETURN
      END


C*********************************************************************C
C  OUTPUT SUBROUTINE                                                  C
C                                                                     C
C  OUTPUTS GENERAL DATA TO SCREEN                                     C
C                                                                     C
C*********************************************************************C
      SUBROUTINE OUTPUT(H1,H2,H3,L1,L2,VIS,YS,K,N,W,T,TAUCRI,VEL,PRT
     &,PRA,PRW,T1,NN,VEXE,SLIP)
      REAL*8 H1,H2,H3,L1,L2,VIS,YS,K,N,W,T,TAUCRI,VEL,PRT,PRW,PRA,T1,
     &NN,VEXE
      LOGICAL SLIP
C
      WRITE(0,100)
      WRITE(0,110) H1
      WRITE(0,120) H2
      WRITE(0,130) H3
      WRITE(0,140) L1
      WRITE(0,150) L2
      WRITE(0,160)
      WRITE(0,170) W
      WRITE(0,180) T
      WRITE(0,190) YS
      WRITE(0,200) K
      WRITE(0,210) N
      WRITE(0,300) NN
      WRITE(0,310) T1
      READ(0,*)
      WRITE(0,220)
      WRITE(0,230) VIS
      WRITE(0,240) TAUCRI
      WRITE(0,250)
      WRITE(0,*)
      IF(SLIP) WRITE(0,*) ' SLIP PRESENT IN PRESSURE HEAD'
      WRITE(0,260) VEL
```

```
      WRITE(0,350) VEXE
      WRITE(0,270) PRW
      WRITE(0,280) PRT
      WRITE(0,290) PRA
      WRITE(0,*)
      WRITE(0,*)
      READ(5,*)
C
  100 FORMAT(' DIE GEOMETRY')
  110 FORMAT(/' H1== ',F8.6)
  120 FORMAT(' H2== ',F8.6)
  130 FORMAT(' H3== ',F8.6)
  140 FORMAT(' L1== ',F8.6)
  150 FORMAT(' L2== ',F8.6)
  160 FORMAT(/' STRIP DATA')
  170 FORMAT(/' INITIAL WIDTH == ',F8.6)
  180 FORMAT(' INITIAL THICHNESS == ',F8.6)
  190 FORMAT(' YIELD STRESS == ',F10.1)
  200 FORMAT(' STRAIN HARDENING CONSTANT == ',F12.0)
  210 FORMAT(' STRAIN HARDENING INDEX == ',F8.6)
  220 FORMAT(/' POLYMER MELT DATA')
  230 FORMAT(/' INITIAL VISCOSITY == ',F8.2)
  240 FORMAT(' CRITICAL SHEAR STRESS == ',F12.2)
  250 FORMAT(/' REDUCTION DATA')
  260 FORMAT(/' STRIP VELOCITY == ',F8.4)
  350 FORMAT(' STRIP EXIT VELOCITY ==',F8.4)
  270 FORMAT(' PERCENTAGE REDUCTION WIDTH == ',F9.6)
  280 FORMAT(' PERCENTAGE REDUCTION THICKNESS == ',F9.6)
  290 FORMAT(' PERCENTAGE REDUCTION AREA == ',F9.6)
  300 FORMAT(' STRAIN RATE SENSITIVITY CONSTANT == ',F9.2)
  310 FORMAT(' STRAIN RATE SENSITIVITY INDEX == ',F9.4)
C
      RETURN
      END



C*********************************************************************C
C  OUTPUT SUBROUTINE FOR WIRE MODELS                                  C
C                                                                     C
C  OUTPUTS GENERAL DATA TO SCREEN                                     C
C                                                                     C
C*********************************************************************C
      SUBROUTINE OUT6(H1,H2,L1,L2,VIS,YS,K,N,TAUCRI,VEL,DFINAL
     &,PRA,T1,NN,VEXE,SLIP,DORG)
C
      REAL*8 H1,H2,L1,L2,VIS,YS,K,N,TAUCRI,VEL,DFINAL
     &,PRA,T1,NN,VEXE,DORG
C
      LOGICAL SLIP
C
      WRITE(0,100)
      WRITE(0,110) H1
      WRITE(0,120) H2
      WRITE(0,140) L1
      WRITE(0,150) L2
      WRITE(0,190) YS
      WRITE(0,200) K
      WRITE(0,210) N
      WRITE(0,300) NN
      WRITE(0,310) T1
      WRITE(0,220)
      WRITE(0,230) VIS
      WRITE(0,240) TAUCRI
      READ(0,*)
      WRITE(0,*)
      IF(SLIP) WRITE(0,*) ' SLIP PRESENT IN PRESSURE HEAD'
      WRITE(0,260) VEL
      WRITE(0,350) VEXE
      WRITE(0,160)
      WRITE(0,170) DORG
      WRITE(0,180) DFINAL
      WRITE(0,290) PRA
      WRITE(0,*)
      WRITE(0,*)
      READ(5,*)
C
  100 FORMAT(' DIE GEOMETRY')
  110 FORMAT(/' H1== ',F8.6)
  120 FORMAT(' H2== ',F8.6)
  130 FORMAT(' H3== ',F8.6)
  140 FORMAT(' L1== ',F8.6)
  150 FORMAT(' L2== ',F8.6)
  160 FORMAT(/' WIRE DATA')
  170 FORMAT(' ORIGINAL DIA ==',F10.6)
  180 FORMAT(' FINAL DIA    ==',F10.6)
  190 FORMAT(' YIELD STRESS == ',F10.1)
  200 FORMAT(' STRAIN HARDENING CONSTANT == ',F12.0)
  210 FORMAT(' STRAIN HARDENING INDEX == ',F8.6)
  220 FORMAT(/' FLUID DATA')
  230 FORMAT(/' INITIAL VISCOSITY == ',F8.2)
  240 FORMAT(' CRITICAL SHEAR STRESS == ',F12.2)
  260 FORMAT(/' STRIP VELOCITY == ',F8.4)
  350 FORMAT(' STRIP EXIT VELOCITY ==',F8.4)
  290 FORMAT(' PERCENTAGE REDUCTION AREA == ',F9.6)
  300 FORMAT(' STRAIN RATE SENSITIVITY CONSTANT == ',F9.2)
  310 FORMAT(' STRAIN RATE SENSITIVITY INDEX == ',F9.4)
C
      RETURN

      END


C*********************************************************************C
C  SOLVE - SOLVES THE GOVERNING EQUATIONS OF DEFORMATION FOR THE      C
C          DEFORMATION ZONE, THIS IS ACCOMPLISHED USING A FINITE      C
C          DIFFERENCE FORMULATION, A LINEAR DEFORMATION PROFILE IS    C
C          ASSUMED BETWEEN THE SOLUTION POINTS, VARIABLES HAVE THE    C
C          SAME MEANING AS DEFINED PREVIOUSLY                         C
C*********************************************************************C
      SUBROUTINE SOLVE (H1,H2,H3,L1,L2,VIS,YS,K,N,W,T,TAUCRI,VEL,PRT,
     &PRA,PRW,T1,NN,VEXE,FL1,SLIP)
      REAL*8 H1,H2,H3,L1,L2,VIS,YS,K,N,W,T,TAUCRI,VEL,PRT,PRW,PRA,AI,AI1
```

```
     &,BO,RO,B,T1,NN,BB,DPDXI,DX,HI,HI1,HI2,PI,PI1,PM
     &,SI,SIGXI,SIGXI1,TAU1,TAU3,TAUI,TAUI2,TI,TI1,VI,VI1,WI,WI1,
     &X1,YI,HI21,RES,XP,EDOT,AO,STEP,VEXE,NSTEP,YDOT1,YDOT2,
     &TAUI1,TAUI21
      LOGICAL SLIP,FL1,SFLAG
      REAL*4 SXP,PLOTT
C
      SLIP=.FALSE.
      SFLAG=.FALSE.
      PM=((6.*VIS*VEL*(H1-H2))/(((H1**3.)/L1)+((H2**3.)/L2)))
      TAU1=-((H1*PM)/(2.*L1))-(VIS*VEL/H1)
      TAU3=-((H3*PM)/(2.*L1))-(VIS*VEL/H3)
C
      IF((TAU1.GE.TAUCRI).OR.(TAU3.GE.TAUCRI)) THEN
        TAU1=TAUCRI
        TAU3=TAUCRI
      ENDIF
      TAUI1=TAU1
      TAUI21=TAU3
      X1=YS/((PM/L1)+(2.*DABS(TAU1)/T)+(2.*DABS(TAU3)/W))
C
      IF(X1.GT.L1) THEN
        WRITE(0,100)
        READ(0,*)
        RETURN
      ENDIF
C
C INITIALLY CALCULATE THE START CONDITIONS AT X=X1 POINT OF DEFORMATION
C
      PI1=(PM/L1)*X1
      TI1=T
      WI1=W
      VI1=VEL
      HI1=H1
      HI21=H3
      DPDXI=PM/L1
      SIGXI1=(2*DABS(TAU1)*X1/T)+(2*DABS(TAU3)*X1/W)
      XP=X1
C
      WRITE(0,*) ' ENTER NOMINAL STEP SIZE IN mm'
      READ(0,*) DX
      DX=DX/1000.
      NSTEP=INT(((L1-X1)/DX)+0.5)
      DX=(L1-X1)/NSTEP
      WRITE(0,*)' DX IN METRES = ',DX
C
C  CALL PLOTTING ROUTINE
C
      CALL PLOT1
      IF(FL1) THEN
        WRITE(7,*)' MAXIMUM PRESSURE = ',PM
        WRITE(7,*)' X1 = ',X1
        WRITE(7,*)' CALCULATED STEP SIZE =',DX
        WRITE(7,*)
        WRITE(7,140)
      ENDIF
C
C SOLVING EQUATIONS
C
C
      XPD=0.0
      DO 10 ISTEP=1,NSTEP,1
C
C    INCREMENT X VARIABLE XP
C
      XP=XP+DX
      XPD=XPD+DX
C
C FIND B SLOPE OF DEFLECTION
C
  21  BO=0.0
      STEP=.05
  20  BO=BO+STEP
      RO=RES(BO,H1,HI1,HI21,L1,VIS,YS,W,T,WI1,VI1,PM,PI1,DX,VEL,N,K,
     &SIGXI1,T1,NN,TI1,SLIP,DPDXI,TAUI1,TAUI21)
      IF(DABS(RO).LE.500) GOTO 30
      IF(RO.LE.0.0) THEN
        BO=BO-STEP
        STEP=STEP/2.
      ENDIF
      GOTO 20
  30  B=BO

C
C HENCE, HAVING FOUND B CALCULATE STRESSES,PRESURES,ETC OF NEXT STEP
C
      IF(.NOT.SLIP) THEN
      TI=TI1-B*DX
      HI=HI1+0.5*B*DX
      BB=W*B/T
      HI2=HI21+0.5*BB*DX
      WI=WI1-BB*DX
      VI=VI1*((WI1*TI1)/(WI*TI))
      DPDXI=(1/HI**3)*((PM*(H1**3)/L1)+6*VIS*(VI*HI-VEL*H1))
      TAUI=-(HI*DPDXI/2.)-VIS*VI/HI
      TAUI2=-(HI2*DPDXI/2.)-VIS*VI/HI2
C
C TEST FOR CONDITION OF SLIP
C
      IF((DABS(TAUI).GE.TAUCRI).OR.(DABS(TAUI2).GE.TAUCRI)) THEN
        SLIP=.TRUE.
        SFLAG=.TRUE.
        GOTO 21
      ENDIF
      AO=T*W
      AI1=TI1*WI1
      AI=TI*WI
      EDOT=(VI/DX)*DLOG((AI1/AI))
      SI=1+((EDOT/NN))**(1/T1)
      YI=SI*(YS+(K*(DLOG((AO/AI)))**N))
      SIGXI=((TI1/TI)+(WI1/WI)-2)*YI+(2*DABS(TAUI)*DX/TI)+(2*DABS(TAUI2
     &)*DX/WI)+SIGXI1
      PI=(DPDXI*DX)+PI1
C
C  SAVE NEW VALUES TO I-1 STEP
C
      PI1=PI
```

```
        TI1=TI
        WI1=WI
        TAUI1=TAUI
        TAUI21=TAUI2
        VI1=VI
        HI1=HI
        HI21=HI2
        SIGXI1=SIGXI
       ELSE
        TI=TI1-B*DX
        HI=HI1+0.5*B*DX
        BB=W*B/T
        HI2=HI21+0.5*BB*DX
        WI=WI1-BB*DX
        VI=VI1*((WI1*TI1)/(WI*TI))
        AO=T*W
        AI1=TI1*WI1
        AI=TI*WI
        EDOT=(VI/DX)*DLOG((AI1/AI))
        SI=1+((EDOT/NN))**(1/T1)
        YI=SI*(YS+(K*(DLOG((AO/AI)))**N))
        TAUI=TAUI1
        TAUI2=TAUI21
        SIGXI=((TI1/TI)+(WI1/WI)-2)*YI+(2*DABS(TAUI)*DX/TI)+(2*DABS(TAUI2
      &)*DX/WI)+SIGXI1
        PI=PI1
        DPDXI=0.0

C
C  SAVE NEW VALUES TO I-1 STEP
C
        TI1=TI
        WI1=WI
        VI1=VI
        HI1=HI
        HI21=HI2
        SIGXI1=SIGXI
        PI1=PI
        SLIP=.FALSE.
C
       ENDIF
C
       IF(FL1) THEN
        WRITE(1,125) XP,PI
        WRITE(2,125) XP,DPDXI
        WRITE(3,125) XP,TI
        YDOT1=(TAUI/VIS)
        YDOT2=(TAUI2/VIS)
        WRITE(4,125) XP,YDOT1
        WRITE(7,130) (XP*1000),TAUI,YDOT1,TAUI2,YDOT2,PI,YI,SIGXI,B
       ENDIF
C
  125 FORMAT(1X,E16.8,2X,',',2X,E20.8)
  130 FORMAT(/,F10.6,8(1X,E10.4))
  140 FORMAT('  MM           TAUI     (VI1/HI1)     TAUI2     (VI1/HI2)
     &    PI        YI       SIGXI        B ')
C
C       WRITE(0,*) ISTEP,XP
       PLOTT=SNGL(PI*100/PM)
       SXP=SNGL(100.*XPD/(L1-X1))
       CALL PLTSYM(1,1,SXP,PLOTT,0.01,0.01,1)
       PLOTT=ABS(SNGL(100.*TAUI/TAUCRI))
       CALL PLTSYM(2,5,SXP,PLOTT,0.01,0.01,2)
       PLOTT=ABS(SNGL(100.*TAUI2/TAUCRI))
       CALL PLTSYM(2,2,SXP,PLOTT,0.01,0.01,5)
       PLOTT=SNGL(100.*TI/T)
       CALL PLTSYM(3,3,SXP,PLOTT,0.01,0.01,3)
       PLOTT=SNGL(50.*WI/W)
       CALL PLTSYM(3,3,SXP,PLOTT,0.01,0.01,6)
       PLOTT=SNGL(10*YI/YS)
       CALL PLTSYM(4,4,SXP,PLOTT,0.01,0.01,4)
   10 CONTINUE
C
       PRT=(1-(TI/T))*100
       PRW=(1-(WI/W))*100
       PRA=(1-((WI*TI)/(W*T)))*100
       VEXE=VI
C
       IF(FL1) THEN
        WRITE(7,*)
        WRITE(7,*)
        WRITE(7,*)
        WRITE(7,*) ' INITIAL VELOCITY = ',VEL
        WRITE(7,*) ' EXIT VELOCITY = ',VEXE
        WRITE(7,*) ' FINAL THICKNESS = ',TI
        WRITE(7,*) ' FINAL WIDTH = ',WI
       ENDIF

C
  100 FORMAT('*****  X1 IS GREATER THAN L1  *****')
C
       IF(SFLAG) SLIP=.TRUE.
       CALL ENDPLT(1,1)
       CALL GSTOP(3,23)
       RETURN
       END


C*********************************************************************C
C RESiduals RETURN THE VALUE OF THE RESIDUALS FOR THE GIVEN VALUE OF B C
C*********************************************************************C
       REAL*8 FUNCTION RES(B,H1,HI1,HI21,L1,VIS,YS,WO,TO,WI1,VI1,PM,PI1,
      &DX,VEL,N,K,SIGXI1,T1,NN,TI1,SLIP,DPDXI,TAUI1,TAUI21)
       REAL*8 B,HI1,HI2,L1,VIS,YS,WO,TO,WI1,VI1,PM,PI1,DX,AI,AI1,K,N,NN
      &,PI,SI,SIGXI,SIGXI1,T1,TAUI,TAUI2,TI,VEL,VI,WI,YI,HI,TI1,H1,HI21
      &,DPDXI,BB,EDOT,AO,TAUI1,TAUI21
       LOGICAL SLIP
C
       IF(.NOT.SLIP) THEN
        TI=TI1-B*DX
        HI=HI1+0.5*B*DX
        BB=WO*B/TO
        HI2=HI21+0.5*BB*DX
        WI=WI1-BB*DX
        VI=VI1*((WI1*TI1)/(WI*TI))
        DPDXI=(1/HI**3)*((PM*(H1**3)/L1)+6*VIS*(VI*HI-VEL*H1))
        TAUI=-(HI*DPDXI/2)-VIS*VI/HI
```

```
      TAUI2=-(HI2*DPDXI/2)-VIS*VI/HI2
      AO=TO*WO
      AI1=TI1*WI1
      AI=TI*WI
      EDOT=(VI/DX)*DLOG((AI1/AI))
      SI=1+((EDOT/NN))**(1/T1)
      YI=SI*(YS+(K*(DLOG((AO/AI)))**N))
      SIGXI=((TI1/TI)+(WI1/WI)-2)*YI+(2*DABS(TAUI)*DX/TI)+(2*DABS(TAUI2
     &)*DX/WI)+SIGXI1
      PI=(DPDXI*DX)+PI1
     ELSE
      TI=TI1-B*DX
      HI=HI1+0.5*B*DX
      BB=WO*B/TO
      HI2=HI21+0.5*BB*DX
      WI=WI1-BB*DX
      VI=VI1*((WI1*TI1)/(WI*TI))
      TAUI=TAUI1
      TAUI2=TAUI21
      AO=TO*WO
      AI1=TI1*WI1
      AI=TI*WI
      EDOT=(VI/DX)*DLOG((AI1/AI))
      SI=1+((EDOT/NN))**(1/T1)
      YI=SI*(YS+(K*(DLOG((AO/AI)))**N))
      SIGXI=((TI1/TI)+(WI1/WI)-2)*YI+(2*DABS(TAUI)*DX/TI)+(2*DABS(TAUI2
     &)*DX/WI)+SIGXI1
      PI=PI1
C
      ENDIF
C
      RES=PI+SIGXI-YI
C      WRITE(6,142)RES,PI,SIGXI,YI,B,0.0
C      WRITE(6,142)HI,TI,WI,HI2,DPDXI,DX
C      READ(5,*)
  142 FORMAT(6(1X,E12.5))
C
      RETURN
      END


C*********************************************************************C
C  PLAW  - SOLVES THE GOVERNING EQUATIONS OF DEFORMATION FOR THE      C
C          DEFORMATION ZONE, THIS IS ACCOMPLISHED USING A FINITE      C
C          DIFFERENCE FORMULATION, A LINEAR DEFORMATION PROFILE IS    C
C          ASSUMED BETWEEN THE SOLUTION POINTS, VARIABLES HAVE THE    C
C          SAME MEANING AS DEFINED PREVIOUSLY                         C
C*********************************************************************C
      SUBROUTINE PLAW(W,T,H1,H2,H3,L1,L2,YS,VEL,PLK,PLN,TAUCRI,FL1,SHI,
     &SHK,PRT,PRW,PRA,VEXE)
      REAL*8 W,T,H1,H2,H3,L1,L2,YS,VEL,PLK,PLN,TAUCRI,SHI,SHK,PRT
     &,PRW,PRA,VEXE,TAU105,TAU305,HI1,SLOPE,R1,R2,DB,X1,PI1,
     &PLRES,B,HI,H2I,DX,PI,PM,J1,SIGXI,H,TF,P,RLAM,DPDXI1,B1,B2,
     &BOLD,TI,WI,TAU1I,TAU3I,V05,TAU1,TAU3,DPDX,SIGRW,M,TI1,VI1,WI1
     &,YI1,AR,TAUI21,DELB,Z,VI,DPDX1,TAUI1,RS,XP,XPD,BOOLD,
     &YDOT1,YDOT2,H2I1,SIGXI1,PI05,TS
      LOGICAL SLIP,SFLAG,FL1
      INTEGER*2 ISTEP,NSTEP
      CHARACTER*80 CAP
C
      SLIP=.FALSE.
      SFLAG=.FALSE.
C*****************************************C
C  ITERATE FOR TAU1 AND TAU3                C
C*****************************************C
C
      PM=6*PLK*PLN*(H1-H2)*VEL**PLN
      PM=PM/((((H2)**(2+PLN))/L2)+(((H1)**(2+PLN))/L1))
      DPDX=PM/L1
C
C
C      WRITE(6,*) '   PM                DPDX '
C      WRITE(6,*) PM,DPDX
C      READ(5,*)
C      OPEN(4,FILE='N7.DAT')
C      WRITE(4,*) '  TAU               R1'
C      DO 1107 B1=-1000000,1000000, 25000
C        R1=TS(B1,DPDX,H1,VEL)
C        WRITE(4,*) B1, R1
C        WRITE(6,*) B1, R1
C 1107 CONTINUE
C      CLOSE(4)
C      READ(5,*)
C
      CALL SHEAR(TAU1,DPDX,H1,VEL)
      CALL SHEAR(TAU3,DPDX,H3,VEL)
C
      IF((TAU1.GE.TAUCRI).OR.(TAU3.GE.TAUCRI)) THEN
        TAU1=TAUCRI
        TAU3=TAUCRI
      ENDIF
      TAUI1=TAU1
      TAUI21=TAU3
C*********************************************************C
C  CALCULATE X1 THE DISTANCE TO THE ONSET OF DEFORMATION  C
C*********************************************************C
      X1=YS/((PM/L1)+(2.*DABS(TAU1)/T)+(2.*DABS(TAU3)/W))
C      WRITE(6,*) ' X1 = ',X1
      IF(X1.GT.L1) THEN
        WRITE(0,*)' X1 >> L1  ******  ERROR'
        READ(0,*)
        RETURN
      ENDIF
C*********************************************************************C
C  CALCULATE THE INITIAL CONDITIONS AT X=X1  ONSET OF DEFORMATION C
C*********************************************************************C
      PI=(PM/L1)*X1
      TI=T
      WI=W
      VI=VEL
      HI=H1
      H2I=H3
      DPDX=PM/L1
      SIGXI=(2*DABS(TAU1)*X1/T)+(2*DABS(TAU3)*X1/W)
      XP=X1
C
      IRW=0
```

```
      WRITE(6,*) 'INCLUDE REDUNDANT WORK   1=YES   0=NO'
      READ(5,*) IRW
C      WRITE(6,*) 'DO YOU REQUIRE TRACE OUTPUT TO PRINTER  1=YES 0=NO'
C      READ(5,*) ITRA
C      IF(ITRA.EQ.1.0) THEN
C        WRITE(6,*) 'WHAT STEP FOR DETAILED RESIDUAL REPORTING '
C        READ(5,*) NTRA
C      ENDIF
C
      ITRA=0
      NTRA=0
C
      WRITE(6,*) ' Enter Nominal step size in mm '
      READ(5,*) DX
      DX=DX/1000.
      NSTEP=INT(((L1-X1)/DX)+0.5)
      DX=(L1-X1)/NSTEP
      WRITE(6,*) ' DX IN METRES = ',DX
      M=W/T
C*************************C
C CALL PLOTTING ROUTINE   C
C*************************C
      CALL PLOT1
      IF(FL1) THEN
        WRITE(7,*)' MAXIMUM PRESSURE = ',PM
        WRITE(7,*)' X1 = ',X1
        WRITE(7,*)' CALCULATED STEP SIZE =',DX
        WRITE(7,*)
      ENDIF
      CAP='POWER LAW  SIMULATION'
      CALL PLTSTG(2,0,50.,110.,0.0,2,1,CAP,21)
C      CALL KEY
      IF(ITRA.EQ.1) THEN
        OPEN(8,FILE='LPT1')
        WRITE(8,*) '   XP       TI        TAU1I        TAU3I        PI
     &  DPDXI1      YI1      SIGXI     RS      SIGRW       B dB'
      ENDIF
C************************C
C  SOLVING EQUATIONS     C
C************************C
      XPD=0.0
      DO 10 ISTEP=1,NSTEP,1
C*******************************C
C  INCREMENT  X  VARIABLE  XP    C
C*******************************C
      XP=XP+DX
      XPD=XPD+DX
C*******************************C
C  FIND SLOPE OF DEFLECTION    C
C*******************************C
  21  B1=1E-9
      B2=2E-4
      DB=2.5E-6
      R1=PLRES(B1,H1,HI,H2I,PLK,PLN,VEL,W,T,DX,BOLD,PI,PM,SHI,SHK,J1,L1,
     &SIGXI,YS,TI,WI,SLIP,TAU1I,TAU3I,IRW,IMON)
      R2=PLRES(B2,H1,HI,H2I,PLK,PLN,VEL,W,T,DX,BOLD,PI,PM,SHI,SHK,J1,L1,
     &SIGXI,YS,TI,WI,SLIP,TAU1I,TAU3I,IRW,IMON)
  20  CONTINUE
      IF(DABS(R1).LE.20000) THEN
         B=B1
         GOTO 30
      ENDIF
      IF(DABS(R2).LE.20000) THEN
         B=B2
         GOTO 30
      ENDIF
C
C  GET SIGNS OF SEARCH POINTS
C
      IF(R1.GE.0.0) THEN
       ISR1=1
      ELSE
       ISR1=0
      ENDIF
      IF(R2.GE.0.0) THEN
       ISR2=1
      ELSE
       ISR2=0
      ENDIF
C
C MAIN LOOP
C
      IF(ISR1.EQ.ISR2) THEN
        SLOPE=((R2-R1)/(B2-B1))
        IF(SLOPE.GT.0.0) THEN
          IF((ISR1.EQ.1).AND.(ISR2.EQ.1)) THEN
            B1=B1-DB
            IF(B1.LE.0.0) THEN
             B1=B1+DB
             DB=DB/2
             GOTO 20
            ENDIF
          ELSE
            B2=B2+DB
          ENDIF
        ELSE
          IF((ISR1.EQ.1).AND.(ISR2.EQ.1)) THEN
            B2=B2+DB
          ELSE
            B1=B1-DB
            IF(B1.LE.0.0) THEN
             B1=B1+DB
             DB=DB/2
             GOTO 20
            ENDIF
          ENDIF
        ENDIF
      ELSE
        IF(DABS(R1).GE.DABS(R2)) THEN
          B1=B1+(DABS(B1-B2))/2
        ELSE
          B2=B2-(DABS(B1-B2))/2
        ENDIF
        DB=DABS(B2-B1)/3
      ENDIF
      R1=PLRES(B1,H1,HI,H2I,PLK,PLN,VEL,W,T,DX,BOLD,PI,PM,SHI,SHK,J1,L1,
     &SIGXI,YS,TI,WI,SLIP,TAU1I,TAU3I,IRW,IMON)
```

```
      R2=PLRES(B2,H1,HI,H2I,PLK,PLN,VEL,W,T,DX,BOLD,PI,PM,SHI,SHK,J1,L1,
     &SIGXI,YS,TI,WI,SLIP,TAU1I,TAU3I,IRW,IMON)
      GOTO 20
  30  CONTINUE
C*********************************************************************C
C HENCE HAVING FOUND B,  EVALUATE SIG'S AND PRESSURES OF N+1 STEP C
C*********************************************************************C
      IF(.NOT.SLIP) THEN
C
       HI1=H(HI,B,DX)
       H2I1=H(H2I,B*M,DX)
       TI1=TF(TI,B,DX)
       WI1=TF(WI,B*M,DX)
       AR=W*T/(WI1*TI1)
       VI1=VEL*AR
       VO5=VEL*W*T/(TF(WI,B*M,DX/2.)*TF(TI,B,DX/2.))
C**********************C
C FOR THE PRESSURES    C
C**********************C
       DPDXI1=(6*PLN*PLK*(VI1/HI1)**(PLN-1))/(HI1**3)
       DPDXI1=DPDXI1*((VI1*HI1-VEL*H1)+((PM*H1**(2+PLN))/
     &(6*L1*PLN*PLK*VEL**(PLN-1))))
       PI1=P(PI,DPDXI1,DX)
       PIO5=P(PI,DPDXI1,DX/2)
C**************************C
C FOR MATERIAL PROPERTIES   C
C**************************C
       YI1=YS+SHK*((DLOG(AR)**SHI))
C***********************C
C  FOR THE STRESSES      C
C***********************C
       CALL SHEAR(TAU1O5,DPDXI1,H(HI,B,DX/2.0),VO5)
       CALL SHEAR(TAU3O5,DPDXI1,H(H2I,B,DX/2.0),VO5)

C       WRITE(6,*) 'H1= ',H1
C       WRITE(6,*) 'HI= ',H(HI,B,DX/2.0)
C       WRITE(6,*) 'HI2= ',H(H2I,B,DX/2.0)
C       WRITE(6,*) 'PM= ',PM
C       WRITE(6,*) 'L1= ',L1
C       WRITE(6,*) 'VEL= ',VEL
C       WRITE(6,*) 'VI1= ',VI1
C       WRITE(6,*) 'VO5= ',VO5
C       WRITE(6,*) 'PLK= ',PLK
C       WRITE(6,*) 'PLN= ',PLN
C       WRITE(6,*) 'DPDXI1= ',DPDXI1
C       WRITE(6,*) 'TAU1O5= ',TAU1O5
C       WRITE(6,*) 'TAU3O5= ',TAU3O5
C       READ(5,*)

       IF((DABS(TAU1O5).GE.TAUCRI).OR.(DABS(TAU3O5).GE.TAUCRI)) THEN
         SLIP=.TRUE.
         SFLAG=.TRUE.
         TAU3I=TAUCRI
         TAU1I=TAUCRI
         GOTO 21
       ENDIF
      RS=DABS(BOOLD-B)*(1+M)
      SIGXI1=(SIGXI*WI*TI/(WI1*TI1))+(2.0*PIO5*DX*DTAN(B)/TI1)+
     &(2.0*PIO5*DX*DTAN(M*B)/WI1)+(2.0*DABS(TAU1O5)*DX/TI1)+
     &(2*DABS(TAU3O5)*DX/WI1)
      SIGRW=YI1*RS/4.0
      IF(IRW.EQ.1)  SIGXI1=SIGXI1+SIGRW
C***********************************C
C SAVE NEW VALUES TO THE  ith  STEP C
C***********************************C
        PI=PI1
        TI=TI1
        WI=WI1
        VI=VI1
        VI=VI1
        HI=HI1
        H2I=H2I1
        SIGXI=SIGXI1
        TAU1I=TAU1O5
        TAU3I=TAU3O5
        DELB=B-BOOLD
        BOOLD=B
C
      ELSE
C
       HI1=H(HI,B,DX)
       H2I1=H(H2I,B*M,DX)
       TI1=TF(TI,B,DX)
       WI1=TF(WI,B*M,DX)
       AR=W*T/(WI1*TI1)
       VI1=VEL*AR
       VO5=VEL*W*T/(TF(WI,B*M,DX/2.)*TF(TI,B,DX/2.))
C**********************C
C FOR THE PRESSURES    C
C**********************C
       Z=RLAM(PLN,DBLE(2.0))
       PI1=PI
       PIO5=PI
C**************************C
C FOR MATERIAL PROPERTIES   C
C**************************C
       YI1=YS+SHK*((DLOG(AR)**SHI))
C***********************C
C  FOR THE STRESSES      C
C***********************C
       TAU1O5=TAU1I
       TAU3O5=TAU3I
       RS=DABS(BOOLD-B)*(1+M)
C       SIGXI1=(SIGXI*WI*TI/(WI1*TI1))+(2.0*PIO5*DX*DTAN(B)/TI1)+
C     &(2.0*PIO5*DX*DTAN(M*B)/WI1)+(2.0*DABS(TAU1O5)*DX/TI1)+
C     &(2*DABS(TAU3O5)*DX/WI1)
       SIGXI1=(SIGXI*WI*TI/(WI1*TI1))+(2.0*PIO5*DX*DTAN(B)/TI1)+
     &(2.0*PIO5*DX*DTAN(M*B)/WI1)+(2.0*DABS(TAU1O5)*DX/TI1)+
     &(2*DABS(TAU3O5)*DX/WI1)

       SIGRW=YI1*RS/4.0
C
C  INCLUDE THIS TERM FOR REDUNDENT WORK
C
      IF(IRW.EQ.1) SIGXI1=SIGXI1+SIGRW
C***********************************C
C SAVE NEW VALUES TO THE  ith  STEP C
```

```
C*********************************C
        PI=PI1
        DPDXI1=0.0
        TI=TI1
        WI=WI1
        VI=VI1
        VI=VI1
        HI=HI1
        H2I=H2I1
        SIGXI=SIGXI1
        SLIP=.FALSE.
        DELB=B-BOOLD
        BOOLD=B
C
      ENDIF
C************************C
C OPTIONAL DATA FILE CODE C
C************************C
      IF(FL1) THEN
       WRITE(1,125) XP,PI
       WRITE(2,125) XP,DPDXI1
       WRITE(3,125) XP,TI
       YDOT1=0.0
       YDOT2=0.0
       WRITE(4,125) XP,TAU1I
       WRITE(7,130) XP,TI,WI,TAU1I,YDOT1,TAU3I,YDOT2,PI,DPDXI1,
     &YI1,SIGXI,RS,SIGRW,B
       ENDIF
C
       IF(ITRA.EQ.1) THEN
       WRITE(8,150) ISTEP,TI,TAU1I,TAU3I,PI,DPDXI1,YI1,SIGXI,RS,SIGRW,B
      &,DELB
       ENDIF
C
       PLOTT=SNGL(PI*50/PM)
       SXP=SNGL(100.*XPD/(L1-X1))
       CALL PLTSYM(1,1,SXP,PLOTT,0.001,0.001,1)
       PLOTT=ABS(SNGL(100.*TAU1I/TAUCRI))
       CALL PLTSYM(2,5,SXP,PLOTT,0.001,0.001,2)
       PLOTT=ABS(SNGL(100.*TAU3I/TAUCRI))
       CALL PLTSYM(2,2,SXP,PLOTT,0.001,0.001,3)
       PLOTT=SNGL(100.*TI/T)
       CALL PLTSYM(3,3,SXP,PLOTT,0.001,0.001,4)
       IF(ISTEP.EQ.1) DPDX1=DPDXI1
       IF (DPDX1.EQ.0.0) DPDX1=1.0
       PLOTT=SNGL(50.*DPDXI1/DPDX1)
       CALL PLTSYM(3,3,SXP,PLOTT,0.001,0.001,13)
       PLOTT=SNGL(10*YI1/YS)
       CALL PLTSYM(4,4,SXP,PLOTT,0.001,0.001,14)
C
   10 CONTINUE
C
       PRT=(1-(TI/T))*100
       PRW=(1-(WI/W))*100
       PRA=(1-((WI*TI)/(W*T)))*100
       VEXE=VI
C
       IF(ITRA.EQ.1) CLOSE(8)
       RETURN
  100 FORMAT(3(1X,E10.4),2(F10.0),2(1X,L4))
  125 FORMAT(1X,E12.6,',',1X,E12.6)
  130 FORMAT(F7.6,1X,13(1X,E10.4))
  150 FORMAT(I4,11(1X,E10.4))
       END


C*********************************************************************C
C  POWER LAW RESIDUAL FUNCTION                                        C
C*********************************************************************C
       REAL*8 FUNCTION PLRES(B,H1,HI,H2I,PLK,PLN,VEL,W,T,DX,BO,PI,PM,
      &SHI,SHK,J1,L1,SIGXI,YS,TI,WI,SLIP,TAU1I,TAU3I,IRW,IMON)
       REAL*8 H,TF,P,M,H2I1,TI1,WI1,B,H1,HI,PLK,PLN,VI1,TAU105,
      &TAU305,W,T,DX,AR,VEL,Z,DPDXI1,PI05,PI1,RLAM,TI,WI,H2I,PI,V05,
      &YI1,PM,J1,L1,SIGXI,HI1,BO,YS,RS,SIGXI1,SHI,SHK,SIGRW,TAU1I,TAU3I
       LOGICAL SLIP
C
       M=W/T
C
       IF(.NOT.SLIP) THEN
        HI1=H(HI,B,DX)
        H2I1=H(H2I,B*M,DX)
        TI1=TF(TI,B,DX)
        WI1=TF(WI,B*M,DX)
        AR=W*T/(WI1*TI1)
        VI1=VEL*AR
        V05=VEL*W*T/(TF(WI,B*M,DX/2.)*TF(TI,B,DX/2.))
C**********************C
C FOR THE PRESSURES    C
C**********************C
        Z=RLAM(PLN,DBLE(2.0))
        DPDXI1=(6*PLN*PLK*(VI1/HI1)**(PLN-1))/(HI1**3)
        DPDXI1=DPDXI1*((VI1*HI1-VEL*H1)+((PM*H1**(2+PLN))/
      &(6*L1*PLN*PLK*VEL**(PLN-1))))
        PI1=P(PI,DPDXI1,DX)
        PI05=P(PI,DPDXI1,DX/2)
C*****************************C
C FOR MATERIAL PROPERTIES   C
C*****************************C
        YI1=YS+SHK*((DLOG(AR)**SHI))
C**********************C
C  FOR THE STRESSES      C
C**********************C
        CALL SHEAR(TAU105,DPDXI1,H(HI,B,DX/2.0),V05)
        CALL SHEAR(TAU305,DPDXI1,H(H2I,B,DX/2.0),V05)
C
        RS=DABS(BO-B)*(1+M)
        SIGXI1=(SIGXI*WI*TI/(WI1*TI1))+(2.0*PI05*DX*DTAN(B)/TI1)+
      &(2.0*PI05*DX*DTAN(M*B)/WI1)+(2.0*DABS(TAU105)*DX/TI1)+
      &(2*DABS(TAU305)*DX/WI1)
        SIGRW=YI1*RS/4.0
        IF(IRW.EQ.1.0) SIGXI1=SIGXI1+SIGRW
C
       ELSE
C
        HI1=H(HI,B,DX)
        H2I1=H(H2I,B*M,DX)
```

```
      TI1=TF(TI,B,DX)
      WI1=TF(WI,B*M,DX)
      AR=W*T/(WI1*TI1)
      VI1=VEL*AR
      V05=VEL*W*T/(TF(WI,B*M,DX/2.)*TF(TI,B,DX/2.))
C**********************C
C FOR THE PRESSURES    C
C**********************C
      PI1=PI
      PI05=PI
C***************************C
C FOR MATERIAL PROPERTIES   C
C***************************C
      YI1=YS+SHK*((DLOG(AR)**SHI))
C**********************C
C  FOR THE STRESSES      C
C**********************C
      TAU105=TAU1I
      TAU305=TAU3I
      RS=DABS(BO-B)*(1+M)
      SIGXI1=(SIGXI*WI*TI/(WI1*TI1))+(2.0*PI05*DX*DTAN(B)/TI1)+
     &(2.0*PI05*DX*DTAN(M*B)/WI1)+(2.0*DABS(TAU105)*DX/TI1)+
     &(2*DABS(TAU305)*DX/WI1)
      SIGRW=YI1*RS/2.0
      IF(IRW.EQ.1.0) SIGXI1=SIGXI1+SIGRW
C
      ENDIF
C*****************************C
C SET FUNCTION RETURN VALUE   C
C*****************************C
C      WRITE(6,*) '      P              SIG                 Y'
C      WRITE(6,*)PI1,SIGXI1,YI1
      PLRES=PI1+SIGXI1-YI1
C      WRITE(6,*) B,PLRES
C
C      WRITE(6,*) 'RES      PI1,     SIGXI1,     YI1,      B          ,RW'
      IF(IMON.EQ.1) WRITE(6,101) PLRES,PI1,SIGXI1,YI1,B,SIGRW,SLIP
C      WRITE(6,101) HI1,TI1,WI1,H2I1,DPDXI1,DX
C
 101  FORMAT(6(1X,E11.5),L4)
C
      RETURN
      END

C*********************************************************************C
C SHEAR - SHEAR SUBROUTINE ITERATIVE FINDS THE REQUIRED SHEAR STRESS C
C         DURING SOLUTION OF THE PLASTO-HYDRODYNAMIC DRAWING OF      C
C         RECTANGULAR SECTIONS                                       C
C*********************************************************************C
      SUBROUTINE SHEAR(T,DPDX,HA,V)
      IMPLICIT DOUBLE PRECISION (A-Z)

C      WRITE(6,*) ' OPENING FILE'
C      OPEN(3,FILE='TS.DAT')
C      DO 1919 B1=-1000000,1000000,20000
C       R=TS(B1,PM)
C      WRITE(3,*) B1,R
C 1919 CONTINUE
C      CLOSE(3)
C      WRITE(6,*) ' CLOSING FILE'

      B1=-300000
      B2=-200000
      DB=25000
      ERR=0.005
      R1=TS(B1,DPDX,HA,V)
      R2=TS(B2,DPDX,HA,V)
   22 IF(DABS(R1).LE.ERR) THEN
         T=B1
         GOTO 33
      ENDIF
      IF(DABS(R2).LE.ERR) THEN
         T=B2
         GOTO 33
      ENDIF
C
C  GET SIGNS OF SEARCH POINTS
C
      IF(R1.GE.0.0) THEN
       ISR1=1
      ELSE
       ISR1=0
      ENDIF
      IF(R2.GE.0.0) THEN
       ISR2=1
      ELSE
       ISR2=0
      ENDIF
C
C MAIN LOOP
C
      IF(ISR1.EQ.ISR2) THEN
        SLOPE=((R2-R1)/(B2-B1))
        IF(SLOPE.GT.0.0) THEN
          IF((ISR1.EQ.1).AND.(ISR2.EQ.1)) THEN
            B1=B1-DB
          ELSE
            B2=B2+DB
          ENDIF
        ELSE
          IF((ISR1.EQ.1).AND.(ISR2.EQ.1)) THEN
            B2=B2+DB
          ELSE
            B1=B1-DB
          ENDIF
        ENDIF
      ELSE
        IF(DABS(R1).GE.DABS(R2)) THEN
          B1=B1+(DABS(B1-B2))/2
        ELSE
          B2=B2-(DABS(B1-B2))/2
        ENDIF
        DB=DABS(B2-B1)/3
      ENDIF
      R1=TS(B1,DPDX,HA,V)
      R2=TS(B2,DPDX,HA,V)
```

```
      GOTO 22
   33 CONTINUE
      RETURN
      END


C*******************************C
C SHEAR FUNCTION T              C
C*******************************C
      REAL*8 FUNCTION TS(A,DPDX,HA,V)
      IMPLICIT DOUBLE PRECISION (A-Z)
      COMMON /F1C/ W,T,H1,H2,H3,L1,L2,VEL,PLK,PLN
C
      C1=DPDX*(1/PLK)
      C2=A/PLK
      C3=C1*HA+C2
C
      TEMP=(C3**RLAM(PLN,DBLE(1.0)))- (C2**RLAM(PLN,DBLE(1.0)))
      TS=(TEMP/(C1*RLAM(PLN,DBLE(1.0)))) + V
C
      RETURN
      END

C*******************************C
C  GAP FUNCTION                 C
C*******************************C
      REAL*8 FUNCTION H(HN,SLOPE,DELX)
      REAL*8 HN,SLOPE,DELX
C
      H=HN+SLOPE*DELX
C
      RETURN
      END


C************************C
C THICKNESS FUNCTION     C
C************************C
      REAL*8 FUNCTION TF(TN,SLOPE,DELX)
      REAL*8 TN,SLOPE,DELX
C
      TF=TN-2.0*SLOPE*DELX
C
      RETURN
      END


C************************C
C PRESSURE FUNCTION    C
C************************C
      REAL*8 FUNCTION P(PN,DPDX,DELX)
      REAL*8 PN,DPDX,DELX
C
      P=PN+DPDX*DELX
C
      RETURN
      END

C*******************************C
C  LAMDA FUNCTION               C
C*******************************C
      REAL*8 FUNCTION RLAM(N,M)
      REAL*8 N,M
C
      RLAM=DFLOAT(IDINT((1.0/N)+DFLOAT(M)))
C
      RETURN
      END

C*******************************C
C JAY SUBROUTINE                C
C*******************************C
      SUBROUTINE JAY(J,N)
      REAL*8 A,B,J,N,R1,R2,RLAM
C
      R1=RLAM(N,DFLOAT(1.0))
      R2=RLAM(N,DFLOAT(2.0))
      A=1/(R1*R2)
      B=1/(R1*2.0)
      J=A-B
C
      RETURN
      END


C************************************************C
C   PLOT1 - GRAPH INITIALISATION                 C
C                                                C
C     STARTS USER GRAPHICS MODE                  C
C     STARTS A NEWPLOT                           C
C     VGA MODE 18                                C
C     X AND Y POINTS ARE NORMALIZED TO A RANGE   C
C     0-1.0                                      C
C************************************************C
      SUBROUTINE PLOT1
      IMPLICIT INTEGER*2 (I-N)
      DIMENSION IERR(2)
      CHARACTER*8 SAV,DXF
      CHARACTER*80 CAP
C
      IDEV=1
      MODE=18
      IPORT=0
      IUNIT=0
      VHR=1.0
      SAV='    '
      DXF='    '
      IERR(1)=0
      IERR(2)=0
      CALL GSTART(IDEV,MODE,IPORT,IUNIT,VHR,SAV,DXF,IER)
      CALL NEWPLT(0,1,-30.0,130.0,-80.0,120.0)
C
C DRAW GRID
C
```

```
      CALL PLTDSH(1,1,0.,0.,100.,0.,7)
      CALL PLTDSH(1,1,0.,0.,0.,100.,7)
      CALL PLTDSH(1,1,100.,0.,100.,100.,7)
      CALL PLTDSH(1,1,100.,100.,0.,100.,7)
      CALL PLTDSH(1,50,0.0,25.0,100.0,25.0,7)
      CALL PLTDSH(1,50,0.0,50.0,100.0,50.0,7)
      CALL PLTDSH(1,50,0.0,75.0,100.0,75.0,7)
      CALL PLTDSH(1,50,25.0,0.,25.0,100.,7)
      CALL PLTDSH(1,50,50.0,0.,50.,100.,7)
      CALL PLTDSH(1,50,75.0,0.,75.,100.,7)
C
C  DRAW CAPTIONS
C
      CAP='0.0'
      CALL PLTSTG(2,1,-5.,-2.5,0.0,15,0,CAP,3)
      CAP='25'
      CALL PLTSTG(2,1,-3.,26.,0.0,15,0,CAP,2)
      CALL PLTSTG(2,1,25.0,-3.,0.0,15,0,CAP,2)
      CAP='50'
      CALL PLTSTG(2,1,-3.,51.,0.0,15,0,CAP,2)
      CALL PLTSTG(2,1,50.0,-3.,0.0,15,0,CAP,2)
      CAP='75'
      CALL PLTSTG(2,1,-3.,76.,0.0,15,0,CAP,2)
      CALL PLTSTG(2,1,75.,-3.,0.0,15,0,CAP,2)
      CAP='100'
      CALL PLTSTG(2,1,-3.,100.,0.0,15,0,CAP,3)
      CALL PLTSTG(2,1,100.,-3.,0.0,15,0,CAP,3)
C
C  DRAW LABELS
C
      CAP='Dimensionless Scale'
      CALL PLTSTG(2,1,-15.0,50.,90.0,2,0,CAP,19)
      CAP=' Deformation  Zone '
      CALL PLTSTG(2,0,50.0,-15.,0.0,2,0,CAP,19)
C
      RETURN
      END
```

Appendix 2

It should be noted that within the following FORTRAN code, calls are made to various graphical subroutines from the Extend Graphics Library. Due to copyright restrictions further details cannot be given in this work. Information on the form and scope of the library may be obtained from the manufacturers.

Design Decisions Inc
P.O. Box 12884
Pittsburgh
Pennsylvania 15241
(415) 941-4525

2.1 Newtonian Optimisation code

```
C*************************************************************************C
C OPTIMISATION TWO - PLASTO HYDRO-DYNAMICS                                C
C                                                                         C
C     X(1)=L1                                                             C
C     X(2)=H1/h2                                                          C
C     X(3)=H3/h2                                                          C
C*************************************************************************C
      PROGRAM OPT2
      IMPLICIT DOUBLE PRECISION (A-Z)
      DIMENSION X(3),H(3),P(3),BT(3),ROW(100)
      INTEGER N
      CHARACTER LIN
      CHARACTER*25 FILNAM
      COMMON VEL
C*************************C
C INITIALISE VARIABLES    C
C*************************C
      N=3
      LIN='='
      DO 10 I=1,N
       P(I)=0
   10 CONTINUE
C*************************C
C  MENU SYSTEM            C
C*************************C
  1   CALL CLS
      CALL HEADER
      WRITE(6,*) '1#    MULTI START OPTIMISATION SEQUENCE '
      WRITE(6,*) '2#    SINGLE OPTIMISATION '
      WRITE(6,*) '3#    SURFACE GENERATION '
      WRITE(6,*) '4#    EXIT'
      CALL BLANK(3)
      WRITE(6,*) ' ENTER OPTION REQUIRED '
      READ(5,*) MOPT
      IF((MOPT.GT.4).OR.(MOPT.LT.1)) GOTO 1
C*************************************************************C
C MULTI START OPT CODE BLOCK                                  C
C*************************************************************C
      IF(MOPT.EQ.1) THEN
C
  2   CALL HEADER
      WRITE(6,*) '1#    L1/L2= ',X1L,'  TO  ',X1T,' IN ',X1NSTEP
      WRITE(6,*) '2#    H1/H2= ',X2L,'  TO  ',X2T,' IN ',X2NSTEP
      WRITE(6,*) '3#    H3/H2= ',X3L,'  TO  ',X3T,' IN ',X3NSTEP
      WRITE(6,*) '4#    PROPORTION OF H(1) AS SEARCH VECTOR ',H1T
      WRITE(6,*) '5#    PROPORTION OF H(2) AS SEARCH VECTOR ',H2T
      WRITE(6,*) '6#    PROPORTION OF H(3) AS SEARCH VECTOR ',H3T
      WRITE(6,*) '7#    MINIMUM SIZE OF EUCLIDEAN SEARCH VECTOR',MINSTEP
      WRITE(6,*) ' '
      WRITE(6,*) '8#    RUN'
      CALL BLANK(10)
 11   WRITE(6,*) ' ENTER OPTION REQUIRED '
      READ(5,*) IOPT
C
      IF(IOPT.EQ.42) GOTO 1
      IF((IOPT.GT.8).OR.(IOPT.LT.1)) GOTO 11
C
C
      IF(IOPT.EQ.1) THEN
       WRITE(6,*) ' ENTER INITIAL L1/L2 RATIO  '
       READ(5,*) X1L
       WRITE(6,*) ' ENTER FINAL L1/L2 RATIO  '
       READ(5,*) X1T
       WRITE(6,*) ' ENTER NUMBER OF STEPS '
       READ(5,*) X1NSTEP
       X1STEP=(X1T-X1L)/X1NSTEP
      ENDIF
C
C
      IF(IOPT.EQ.2) THEN
       WRITE(6,*) ' ENTER INITIAL H1/H2 RATIO  '
       READ(5,*) X2L
       WRITE(6,*) ' ENTER FINAL H1/H2 RATIO  '
       READ(5,*) X2T
       WRITE(6,*) ' ENTER NUMBER OF STEPS '
       READ(5,*) X2NSTEP
       X2STEP=(X2T-X2L)/X2NSTEP
      ENDIF
C
C
      IF(IOPT.EQ.3) THEN
       WRITE(6,*) ' ENTER INITIAL H3/H2 RATIO  '
       READ(5,*) X3L
       WRITE(6,*) ' ENTER FINAL H3/H2 RATIO  '
       READ(5,*) X3T
       WRITE(6,*) ' ENTER NUMBER OF STEPS '
       READ(5,*) X3NSTEP
       X3STEP=(X3T-X3L)/X3NSTEP
      ENDIF
C
C
      IF(IOPT.EQ.4) THEN
       WRITE(6,*) 'ENTER PROPORTION FOR SEARCH VECTOR X(1) {L1/L2}'
       READ(5,*) H1T
      ENDIF
C
C
      IF(IOPT.EQ.5) THEN
       WRITE(6,*) 'ENTER PROPORTION FOR SEARCH VECTOR X(2) {H1/H2}'
       READ(5,*) H2T
      ENDIF
C
C
      IF(IOPT.EQ.6) THEN
       WRITE(6,*) 'ENTER PROPORTION FOR SEARCH VECTOR X(3) {H3/H2} '
       READ(5,*) H3T
      ENDIF
C
C
      IF(IOPT.EQ.7) THEN
 42    WRITE(6,*) 'ENTER MINIMUM SIZE OF SEARCH VECTOR '
       READ(5,*) MINSTEP
```

```
       IF(MINSTEP.LE.0) THEN
         WRITE(6,*) ' INVALID SEARCH VECTOR MINIMUM '
         GOTO 42
       ENDIF
      ENDIF
      IF(IOPT.EQ.8) GOTO 12
C
      GOTO 2
C
  12  CALL CLS
      WRITE(6,*) 'Enter file name for data  (enclose in single quotes)'
      READ(5,*) FILNAM
      OPEN(3,FILE=FILNAM)                          '
C
C
      WRITE(6,*) 'ENTER VELOCITY FOR OPTIMISATION '
      READ(5,*) VEL
C
C
      WRITE(3,*) 'FILE = ',FILNAM
      WRITE(3,*) '==========='
      WRITE(3,*) 'PARAMETERS'
      WRITE(3,*) '==========='
      WRITE(3,*) 'MINIMUM SEARCH VECTOR= ',MINSTEP
      WRITE(3,*) 'L1/L2= ',X1L,'  TO  ',X1T,' IN ',X1NSTEP
      WRITE(3,*) 'H1/H2= ',X2L,'  TO  ',X2T,' IN ',X2NSTEP
      WRITE(3,*) 'H3/H2= ',X3L,'  TO  ',X3T,' IN ',X3NSTEP
      WRITE(3,*) 'PROPORTION SEARCH VECTOR H(1)  ',H1T
      WRITE(3,*) 'PROPORTION SEARCH VECTOR H(2)  ',H2T
      WRITE(3,*) 'PROPORTION SEARCH VECTOR H(3)  ',H3T
      WRITE(3,*) ' '
      WRITE(3,100) 'VEL= ',VEL
      WRITE(3,1010)
      WRITE(3,*) 'L1/L2    H1/H2     H3/H2       |     L1/L2     H1/H2
     &H3/H2         MERIT'
      WRITE(3,1010)
 1010 FORMAT(79('='))
C
      DO 15 X1=X1L,X1T,X1STEP
      DO 16 X2=X2L,X2T,X2STEP
      DO 17 X3=X3L,X3T,X3STEP
C
      X(1)=X1
      X(2)=X2
      X(3)=X3
C
      H(1)=H1T*X1
      H(2)=H2T*X2
      H(3)=H3T*X3
C
      CALL HJ(X,BT,H,N,P,MINSTEP,FUNVAL)
C
      WRITE(3,110) X1,X2,X3,X(1),X(2),X(3),FUNVAL
C
C SCREEN ECHO
C
      WRITE(6,110) X1,X2,X3,X(1),X(2),X(3),FUNVAL
  17  CONTINUE
  16  CONTINUE
  15  CONTINUE
C
 100  FORMAT(1X,A5,E13.7)
 110  FORMAT(7(1X,F10.6))
      CLOSE(3)
C
C
      CALL CLS
      WRITE(6,*) 'OPTIMISATION SEQUENCE COMPLETED (press ret)'
      READ(5,*)
      ENDIF
C*********************************************************************C
C                                                                     C
C SINGLE START CODE BLOCK                                             C
C                                                                     C
C*********************************************************************C
      IF(MOPT.EQ.2) THEN
   4  CALL CLS
      CALL HEADER
      WRITE(6,*) '1#    L1/L2= ',X1L
      WRITE(6,*) '2#    H1/H2= ',X2L
      WRITE(6,*) '3#    H3/H2= ',X3L
      WRITE(6,*) '4#    SEARCH VECTOR H(1)  ',H1T
      WRITE(6,*) '5#    SEARCH VECTOR H(2)  ',H2T
      WRITE(6,*) '6#    SEARCH VECTOR H(3)  ',H3T
      WRITE(6,*) '7#    SIZE OF MINIMUM SEARCH VECTOR',MINSTEP
      WRITE(6,*) ' '
      WRITE(6,*) '8#    RUN'
      CALL BLANK(10)
  14  WRITE(6,*) ' ENTER OPTION REQUIRED '
      READ(5,*) IOPT
C
      IF(IOPT.EQ.42) GOTO 1
      IF((IOPT.GT.8).OR.(IOPT.LT.1)) GOTO 14
C
C
      IF(IOPT.EQ.1) THEN
       WRITE(6,*) ' ENTER INITIAL L1/L2 RATIO  '
       READ(5,*) X1L
      ENDIF
C
C
      IF(IOPT.EQ.2) THEN
       WRITE(6,*) ' ENTER INITIAL H1/H2 RATIO  '
       READ(5,*) X2L
      ENDIF
C
C
      IF(IOPT.EQ.3) THEN
       WRITE(6,*) ' ENTER INITIAL H3/H2 RATIO  '
       READ(5,*) X3L
      ENDIF
C
C
      IF(IOPT.EQ.4) THEN
       WRITE(6,*) 'ENTER PROPORTION FOR SEARCH VECTOR X(1) (L1/L2)'
       READ(5,*) H1T
      ENDIF
```

```
C
C
      IF(IOPT.EQ.5) THEN
       WRITE(6,*) 'ENTER PROPORTION FOR SEARCH VECTOR X(2) {H1/H2}'
       READ(5,*) H2T
      ENDIF
C
C
      IF(IOPT.EQ.6) THEN
       WRITE(6,*) 'ENTER PROPORTION FOR SEARCH VECTOR X(3) {H3/H2}'
       READ(5,*) H3T
      ENDIF
C
       IF(IOPT.EQ.7) THEN
 43     WRITE(6,*) 'ENTER MINIMUM SIZE OF SEARCH VECTOR '
       READ(5,*) MINSTEP
       IF(MINSTEP.LE.0) THEN
         WRITE(6,*) ' INVALID SEARCH VECTOR MINIMUM '
         GOTO 43
       ENDIF
      ENDIF
C
C
      IF(IOPT.EQ.8) GOTO 25
C
      GOTO 4
C
  25  CALL CLS
      WRITE(6,*) 'ENTER VELOCITY FOR OPTIMISATION '
      READ(5,*) VEL
C
C
      WRITE(6,*) 'PARAMETERS'
      WRITE(6,*) '=========='
      WRITE(6,*) 'MIN STEP= ',MINSTEP
      WRITE(6,*) 'L1/L2= ',X1L
      WRITE(6,*) 'H1/H2= ',X2L
      WRITE(6,*) 'H3/H2= ',X3L
      WRITE(6,*) 'PROPORTION OF SEARCH VECTOR H(1)  ',H1T
      WRITE(6,*) 'PROPORTION OF SEARCH VECTOR H(2)  ',H2T
      WRITE(6,*) 'PROPORTION OF SEARCH VECTOR H(3)  ',H3T
      WRITE(6,*) ' '
      WRITE(6,100) 'VEL= ',VEL
      WRITE(6,*)'-------------------------------------------------------'
      WRITE(6,*) '  X(1)          X(2)          X(3)       |    MERIT '
      WRITE(6,*)'-------------------------------------------------------'
C
      X(1)=X1L
      X(2)=X2L
      X(3)=X3L
C
      H(1)=H1T*X(1)
      H(2)=H2T*X(2)
      H(3)=H3T*X(3)
C
      CALL HJ(X,BT,H,N,P,MINSTEP,FUNVAL)
      CALL BLANK(3)
      WRITE(6,110) X1L,X2L,X3L,X(1),X(2),X(3),FUNVAL
      CALL BLANK(3)
C
      WRITE(6,*) 'OPTIMISATION SEQUENCE COMPLETED {press ret}'
      READ(5,*)
C
      ENDIF
C
C*********************************************************************C
C  SURFACE GENERATION CODE BLOCK                                      C
C                                                                     C
C*********************************************************************C
      IF(HOPT.EQ.3) THEN
  72    CALL HEADER
        WRITE(6,791)     X1L,X1T,X1NSTEP
        WRITE(6,792)     X2L,X2T,X2NSTEP
        WRITE(6,793)     X3L
        WRITE(6,*) ' '
        WRITE(6,*) '4#    RUN'
        CALL BLANK(10)
 791 FORMAT('  1#    L1/L2=',F12.4,' TO ',F12.4,' IN ',F8.3)
 792 FORMAT('  2#    H1/H2=',F12.4,' TO ',F12.4,' IN ',F8.3)
 793 FORMAT('  3#    CONSTANT VALUE OF H3/H2 RATIO= ',F12.6)
 711    WRITE(6,*) ' ENTER OPTION REQUIRED '
        READ(5,*) IOPT
C
        IF(IOPT.EQ.42) GOTO 1
        IF((IOPT.GT.4).OR.(IOPT.LT.1)) GOTO 711
C
C
        IF(IOPT.EQ.1) THEN
         WRITE(6,*) ' ENTER INITIAL L1/L2 RATIO  '
         READ(5,*) X1L
         WRITE(6,*) ' ENTER FINAL L1/L2 RATIO  '
         READ(5,*) X1T
         WRITE(6,*) ' ENTER NUMBER OF STEPS '
         READ(5,*) X1NSTEP
         X1STEP=(X1T-X1L)/X1NSTEP
        ENDIF
C
C
        IF(IOPT.EQ.2) THEN
         WRITE(6,*) ' ENTER INITIAL H1/H2 RATIO  '
         READ(5,*) X2L
         WRITE(6,*) ' ENTER FINAL H1/H2 RATIO  '
         READ(5,*) X2T
         WRITE(6,*) ' ENTER NUMBER OF STEPS '
         READ(5,*) X2NSTEP
         X2STEP=(X2T-X2L)/X2NSTEP
        ENDIF
C
C
        IF(IOPT.EQ.3) THEN
         WRITE(6,*) ' ENTER CONSTANT VALUE FOR H3/H2 RATIO  '
         READ(5,*) X3L
        ENDIF
C
C
        IF(IOPT.EQ.4) THEN
          GOTO 712
```

```
        ENDIF
C
        GOTO 72
C
  712   CALL CLS
        WRITE(6,*) 'Enter file name for data  {enclose in single quotes}'
        READ(5,*) FILNAM
        OPEN(3,FILE=FILNAM)
        CALL CLS
C
C
        WRITE(6,*) 'ENTER VELOCITY FOR OPTIMISATION '
        READ(5,*) VEL
        CALL CLS
        CALL HEADER

C
C
        X3=X3L
C
        COUNT=0.0
        DO 799 ZXN=X2L,X2T,X2STEP
        COUNT=COUNT+1
        ROW(COUNT)=ZXN
 799    CONTINUE
C
        WRITE(3,718) IDINT(X1NSTEP+2),IDINT(COUNT+1)
  718   FORMAT(I4,2X,I4)
        WRITE(3,717) 0.0,(ROW(ZXN),ZXN=1,COUNT,1)
C
        DO 715 X1=X1L,X1T,X1STEP
          C2=0
        DO 716 X2=X2L,X2T,X2STEP
C
          X(1)=X1
          X(2)=X2
          X(3)=X3
          FUNVAL=MERIT(X)
          C2=C2+1
          ROW(C2)=DABS(FUNVAL)
C
  716   CONTINUE
        WRITE(3,717) X1,(ROW(ZXN),ZXN=1,COUNT,1)
  717   FORMAT(F10.6,100(2X,F10.6))
  715   CONTINUE
C
        CLOSE(3)
C
C
        CALL CLS
        WRITE(6,*) 'SURFACE GENERATION COMPLETED {press ret}'
        READ(5,*)
C
      ENDIF
C
      IF(MOPT.EQ.4) THEN
       CALL CLS
       STOP 'HAVE A NICE DAY'
      ENDIF
C
      GOTO 1
      END


C**********************C
C  CLEAR SCREEN        C
C**********************C
      SUBROUTINE CLS
      DO 10 I=1,28
       WRITE(6,*) ' '
  10  CONTINUE
      RETURN
      END


C**************************************C
C       WRITES THE HEADER TITLE        C
C**************************************C
      SUBROUTINE HEADER
C
      WRITE(6,*) '******************************************************'
      WRITE(6,*) 'NEWTONIAN HYDRO-DYNAMIC DRAWING OPTIMISATION PROG'
      WRITE(6,*) '******************************************************'
      WRITE(6,*) ' '
C
      RETURN
      END


C**************************************C
C  BLANK - GENERATES N BLANK LINES     C
C**************************************C
      SUBROUTINE BLANK(N)
      INTEGER N,I
C
      DO 10 I=1,N
        WRITE(6,*) ' '
  10  CONTINUE
      RETURN
      END
```

```
C*********************************************************************C
C  MERIT - SOLVES THE GOVERNING EQUATIONS OF DEFORMATION FOR THE      C
C          DEFORMATION ZONE, THIS IS ACCOMPLISHED USING A FINITE      C
C          DIFFERENCE FORMULATION, A LINEAR DEFORMATION PROFILE IS    C
C          ASSUMED BETWEEN THE SOLUTION POINTS, VARIABLES HAVE THE    C
C          SAME MEANING AS DEFINED IN THE MOD6 MODELLING SYSTEM       C
C          VARIABLES HAVE BEEN REMOVED FROM THE NMF5 VER TO AID       C
C          MERIT FUNCTION CODING                                      C
C*********************************************************************C
      DOUBLE PRECISION FUNCTION MERIT(X)
      IMPLICIT DOUBLE PRECISION (A-Z)
      LOGICAL SLIP,SFLAG
      INTEGER ITERNUM,IMINIT
      DIMENSION X(3)
      COMMON  VEL
C
C CONSTANTS
C
      OL=0.1785
      H2=0.00004
      ONEPART=OL/(X(1)+1)
      L1=X(1)*ONEPART
      L2=0.1785-L1
      H1=X(2)*H2
      H3=X(3)*H2
      IF((L1.LE.0).OR.(L2.LE.0).OR.(H1.LE.0).OR.(H3.LE.0)) THEN
        MERIT=0.0
        SLIP=.TRUE.
        WRITE(6,200) X(1),X(2),X(3),MERIT,SLIP
        RETURN
      ENDIF
C
      VIS=120
      YS=70000000
      K=600000000
      N=0.6
      W=0.0253
      T=0.001575
      TAUCRI=320000
      T1=3.8
      NN=55000
C
      SLIP=.FALSE.
      SFLAG=.FALSE.
      PM=((6.*VIS*VEL*(H1-H2))/(((H1**3.)/L1)+((H2**3.)/L2)))
      TAU1=-((H1*PM)/(2.*L1))-(VIS*VEL/H1)
      TAU3=-((H3*PM)/(2.*L1))-(VIS*VEL/H3)
C
      IF((TAU1.GE.TAUCRI).OR.(TAU3.GE.TAUCRI)) THEN
        TAU1=TAUCRI
        TAU3=TAUCRI
      ENDIF
      X1=YS/((PM/L1)+(2.*DABS(TAU1)/T)+(2.*DABS(TAU3)/W))
C
      IF(X1.GT.L1) THEN
        MERIT=0.0
        WRITE(6,200) X(1),X(2),X(3),MERIT,SLIP
        RETURN
      ENDIF
C
C INITIALLY CALCULATE THE START CONDITIONS AT X=X1 POINT OF DEFORMATION
C
      PI1=(PM/L1)*X1
      TI1=T
      WI1=W
      VI1=VEL
      HI1=H1
      HI21=H3
      DPDXI=PM/L1
      SIGXI1=(2*DABS(TAU1)*X1/T)+(2*DABS(TAU3)*X1/W)
      XP=X1
C
      DX=0.002
      NSTEP=INT(((L1-X1)/DX)+0.5)
      DX=(L1-X1)/NSTEP
C
C SOLVING EQUATIONS
C
      DO 10 ISTEP=1,NSTEP,1
C
C     INCREMENT X VARIABLE XP
C
      XP=XP+DX
C
C FIND B SLOPE OF DEFLECTION
C
  21  BO=0.0
      ITERNUM=0
      STEP=.1
  20  BO=BO+STEP
      RO=RES(BO,H1,HI1,HI21,L1,VIS,YS,W,T,WI1,VI1,PM,PI1,DX,VEL,N,K,
     &SIGXI1,T1,NN,TI1,SLIP,TAUCRI,DPDXI)
      ITERNUM=ITERNUM+1
      IF (ITERNUM.EQ.500) THEN
        MERIT=0.0
        WRITE(6,210)
        RETURN
      ENDIF
C
      IF(DABS(RO).LE.5000) GOTO 30
      IF(RO.LE.0.0) THEN
        BO=BO-STEP
        STEP=STEP/10.
      ENDIF
      GOTO 20
   30 B=BO
C
C HENCE, HAVING FOUND B CALCULATE STRESSES,PRESURES,ETC OF NEXT STEP
C
      IF(.NOT.SLIP) THEN
       TI=TI1-B*DX
       HI=HI1+0.5*B*DX
       BB=W*B/T
       HI2=HI21+0.5*BB*DX
       WI=WI1-BB*DX
       VI=VI1*((WI1*TI1)/(WI*TI))
```

```
      DPDXI=(1/HI**3)*((PM*(H1**3)/L1)+6*VIS*(VI*HI-VEL*H1))
      TAUI=-(HI*DPDXI/2.)-VIS*VI/HI
      TAUI2=-(HI2*DPDXI/2.)-VIS*VI/HI2
C
C TEST FOR CONDITION OF SLIP
C
      IF((DABS(TAUI).GE.TAUCRI).OR.(DABS(TAUI2).GE.TAUCRI)) THEN
        SLIP=.TRUE.
        SFLAG=.TRUE.
        GOTO 21
      ENDIF
      AO=T*W
      AI1=TI1*WI1
      AI=TI*WI
      EDOT=(VI/DX)*DLOG((AI1/AI))
      SI=1+((EDOT/NN))**(1/T1)
      YI=SI*(YS+(K*(DLOG((AO/AI)))**N))
      SIGXI=((TI1/TI)+(WI1/WI)-2)*YI+(2*DABS(TAUI)*DX/TI)+(2*DABS(TAUI2
     &)*DX/WI)+SIGXI1
      PI=(DPDXI*DX)+PI1
C
C  SAVE NEW VALUES TO I-1 STEP
C
      PI1=PI
      TI1=TI
      WI1=WI
      VI1=VI
      HI1=HI
      HI21=HI2
      SIGXI1=SIGXI
     ELSE
      TI=TI1-B*DX
      HI=HI1+0.5*B*DX
      BB=W*B/T
      HI2=HI21+0.5*BB*DX
      WI=WI1-BB*DX
      VI=VI1*((WI1*TI1)/(WI*TI))
      AO=T*W
      AI1=TI1*WI1
      AI=TI*WI
      EDOT=(VI/DX)*DLOG((AI1/AI))
      SI=1+((EDOT/NN))**(1/T1)
      YI=SI*(YS+(K*(DLOG((AO/AI)))**N))
      TAUI=TAUCRI
      TAUI2=TAUCRI
      SIGXI=((TI1/TI)+(WI1/WI)-2)*YI+(2*DABS(TAUI)*DX/TI)+(2*DABS(TAUI2
     &)*DX/WI)+SIGXI1
      PI=PI1
      DPDXI=0.0

C
C  SAVE NEW VALUES TO I-1 STEP
C
      TI1=TI
      WI1=WI
      VI1=VI
      HI1=HI
      HI21=HI2
      SIGXI1=SIGXI
      PI1=PI
      SLIP=.FALSE.
C
      ENDIF
C
   10 CONTINUE
C
      MINIT=((1-((WI*TI)/(W*T)))*100)
      IMINIT=IDINT(MINIT*1E8)
      MERIT=-1*DFLOAT(IMINIT/1E8)
      WRITE(6,200) X(1),X(2),X(3),MERIT,SFLAG
C
  200 FORMAT(4(E19.12),L3)
  210 FORMAT(' **** ITERATION LIMIT EXCEEDED ****')
C
C  100 FORMAT('*****  X1 IS GREATER THAN L1  *****')
C
      RETURN
      END


C*********************************************************************C
C RESiduals RETURN THE VALUE OF THE RESIDUALS FOR THE GIVEN VALUE OF B C
C*********************************************************************C
      DOUBLE PRECISION FUNCTION RES(B,H1,HI1,HI21,L1,VIS,YS,WO,TO,WI1,
     &VI1,PM,PI1,DX,VEL,N,K,SIGXI1,T1,NN,TI1,SLIP,TAUCRI,DPDXI)
      IMPLICIT DOUBLE PRECISION (A-Z)
      LOGICAL SLIP
C
      IF(.NOT.SLIP) THEN
       TI=TI1-B*DX
       HI=HI1+0.5*B*DX
       BB=WO*B/TO
       HI2=HI21+0.5*BB*DX
       WI=WI1-BB*DX
       VI=VI1*((WI1*TI1)/(WI*TI))
       DPDXI=(1/HI**3)*((PM*(H1**3)/L1)+6*VIS*(VI*HI-VEL*H1))
       TAUI=-(HI*DPDXI/2)-VIS*VI/HI
       TAUI2=-(HI2*DPDXI/2)-VIS*VI/HI2
       AO=TO*WO
       AI1=TI1*WI1
       AI=TI*WI
       EDOT=(VI/DX)*DLOG((AI1/AI))
       SI=1+((EDOT/NN))**(1/T1)
       YI=SI*(YS+(K*(DLOG((AO/AI)))**N))
       SIGXI=((TI1/TI)+(WI1/WI)-2)*YI+(2*DABS(TAUI)*DX/TI)+(2*DABS(TAUI2
     &)*DX/WI)+SIGXI1
       PI=(DPDXI*DX)+PI1
      ELSE
       TI=TI1-B*DX
       HI=HI1+0.5*B*DX
       BB=WO*B/TO
       HI2=HI21+0.5*BB*DX
       WI=WI1-BB*DX
       VI=VI1*((WI1*TI1)/(WI*TI))
       TAUI=TAUCRI
       TAUI2=TAUCRI
       AO=TO*WO
```

```
       AI1=TI1*WI1
       AI=TI*WI
       EDOT=(VI/DX)*DLOG((AI1/AI))
       SI=1+((EDOT/NN))**(1/T1)
       YI=SI*(YS+(K*(DLOG((AO/AI))))**N))
       SIGXI=((TI1/TI)+(WI1/WI)-2)*YI+(2*DABS(TAUI)*DX/TI)+(2*DABS(TAUI2
     &)*DX/WI)+SIGXI1
       PI=PI1
C
      ENDIF
C
      RES=PI+SIGXI-YI
C
      RETURN
      END


C*********************************************************************C
C HOOKE AND JEEVES {OPTIMISATION}                                     C
C   MULTIVARIATE DIRECT SEARCH METHOD                                 C
C                                                                     C
C*********************************************************************C
      SUBROUTINE HJ(B,BT,H,N,P,MINSTEP,FUNVAL)
      IMPLICIT DOUBLE PRECISION (A-Z)
      INTEGER N,I
      DIMENSION B(N),H(N),P(N),BT(N)
C
      BASVAL=MERIT(B)
      FMIN=BASVAL
  10  CALL EXPLO(B,H,BT,N,FMIN,BASVAL)
C
      IF(FMIN.LT.BASVAL) THEN
C
C   SET BASE SWOPS B2 FOR BASE POINT AND FMIN FOR BASVAL, IF SUCESS
C   PATCALC CALULATES THE POSTION OF THE THE PATTERN MOVE
C
  20    CALL PATCALC(B,P,N,BT)
        CALL SETBASE(B,BT,N,BASVAL,FMIN)
        CALL EXPLO(P,H,BT,N,FMIN,BASVAL)
        IF(FMIN.LT.BASVAL) THEN
          GOTO 20
        ELSE
          CALL DECH(H,N)
          GOTO 10
        ENDIF
C
      ELSE
C
        ERRVEC=0.0
        DO 45 I=1,N
         ERRVEC=H(I)*H(I)+ERRVEC
  45    CONTINUE
        ERRVEC=DSQRT(ERRVEC)
        IF(ERRVEC.LT.MINSTEP) THEN
        FUNVAL=FMIN
        RETURN
      ELSE
        CALL DECH(H,N)
        GOTO 10
        ENDIF
      ENDIF
C
      END

C*********************************************************************C
C EXPLORATORY MOVE SUBROUTINE                                         C
C  ARGS  B=BASE POINT VECTOR                                          C
C        N=DIMENSION OF VECTORS                                       C
C        H=STEP LENGTH VECTOR                                         C
C        BT=BASE POINT TEMPORARY VECTOR                               C
C        FMIN=FUNCTION MINIMUM                                        C
C        FBASE=FUNCTION VALUE AT BASE POINT                           C
C*********************************************************************C
      SUBROUTINE EXPLO(B,H,BT,N,FMIN,FBASE)
      IMPLICIT DOUBLE PRECISION (A-Z)
      INTEGER N,K
      DIMENSION B(N),H(N),BT(N)
C
      FMIN=FBASE
      BLANK=1.0
      CALL SETBASE(BT,B,N,BLANK,BLANK)
      DO 10 K=1,N
      BT(K)=B(K)+H(K)
      FVAL=MERIT(BT)
      IF(FVAL.GE.FMIN) THEN
      BT(K)=B(K)-H(K)
      FVAL=MERIT(BT)
       IF(FVAL.GE.FMIN) THEN
        BT(K)=B(K)
       ELSE
         FMIN=FVAL
       ENDIF
      ELSE
       FMIN=FVAL
      ENDIF
 10   CONTINUE
      RETURN
      END


C*********************************************************************C
C  DECREMENT STEP VECTOR                                              C
C*********************************************************************C
      SUBROUTINE DECH(H,N)
      IMPLICIT DOUBLE PRECISION (A-Z)
      INTEGER N,I
      DIMENSION H(N)
C
      DO 10 I=1,N
        H(I)=0.5*H(I)
  10  CONTINUE
C
      RETURN
      END
```

```
C*********************************************************************C
C CALCULATES                                                          C
C         P  = B   +  2(B    - B  )                                   C
C          i    i        i+1    i                                     C
C*********************************************************************C
      SUBROUTINE PATCALC(B,P,N,BT)
      IMPLICIT DOUBLE PRECISION (A-Z)
      INTEGER N,I
      DIMENSION B(N),P(N),BT(N)
C
      DO 10 I=1,N
        P(I)=2*BT(I)-B(I)
  10  CONTINUE
      RETURN
      END

C*********************************************************************C
C  SET BASE SWOPS B2 IN TO B, AND FMIN INTO BASVAL                      C
C*********************************************************************C
      SUBROUTINE SETBASE(B,BT,N,BASVAL,FMIN)
      IMPLICIT DOUBLE PRECISION (A-Z)
      INTEGER N,I
      DIMENSION B(N),BT(N)
C
      BASVAL=FMIN
C
      DO 10 I=1,N
        B(I)=BT(I)
  10  CONTINUE
C
      RETURN
      END
```

2.2 Non-Newtonian Optimisation code

```
C*********************************************************************C
C OPTIMISATION THREE - PLASTO HYDRO-DYNAMICS                          C
C                                                                     C
C     X(1)=L1                                                         C
C     X(2)=H1/h2                                                      C
C     X(3)=H3/h2                                                      C
C*********************************************************************C
      PROGRAM OPT2
      IMPLICIT REAL (A-Z)
      DIMENSION X(3),H(3),P(3),BT(3),ROW(100)
      INTEGER N
      CHARACTER LIN
      CHARACTER*25 FILNAM
      COMMON VEL,PLN
C*************************C
C INITIALISE VARIABLES     C
C*************************C
      N=3
      LIN='='
      DO 10 I=1,N
       P(I)=0
   10 CONTINUE
C      X(1)=15
C      X(2)=8
C      X(3)=6
C      H(1)=1.5
C      H(2)=0.8
C      H(3)=0.6
C      MINSTEP=0.01
C      VEL=0.15
C      PLN=1.0
C      GOTO 777
C*****************************C
C  MENU SYSTEM               C
C*****************************C
  1   CALL CLS
      CALL HEADER
      WRITE(6,*) '1#    MULTI START OPTIMISATION SEQUENCE '
      WRITE(6,*) '2#    SINGLE OPTIMISATION '
      WRITE(6,*) '3#    SURFACE GENERATION '
      WRITE(6,*) '4#    EXIT'
      CALL BLANK(3)
      WRITE(6,*) ' ENTER OPTION REQUIRED '
      READ(5,*) MOPT
      IF((MOPT.GT.4).OR.(MOPT.LT.1)) GOTO 1
C*************************************************************C
C MULTI START OPT CODE BLOCK                                  C
C*************************************************************C
      IF(MOPT.EQ.1) THEN
C
  2   CALL HEADER
      WRITE(6,*) '1#    L1/L2= ',X1L,'  TO  ',X1T,' IN ',X1NSTEP
      WRITE(6,*) '2#    H1/H2= ',X2L,'  TO  ',X2T,' IN ',X2NSTEP
      WRITE(6,*) '3#    H3/H2= ',X3L,'  TO  ',X3T,' IN ',X3NSTEP
      WRITE(6,*) '4#    PROPORTION OF H(1) AS SEARCH VECTOR ',H1T
      WRITE(6,*) '5#    PROPORTION OF H(2) AS SEARCH VECTOR ',H2T
      WRITE(6,*) '6#    PROPORTION OF H(3) AS SEARCH VECTOR ',H3T
      WRITE(6,*) '7#    MINIMUM SIZE OF EUCLIDEAN SEARCH VECTOR',MINSTEP
      WRITE(6,*) ' '
      WRITE(6,*) '8#    RUN'
      CALL BLANK(10)
 11   WRITE(6,*) ' ENTER OPTION REQUIRED '
      READ(5,*) IOPT
C
      IF(IOPT.EQ.42) GOTO 1
      IF((IOPT.GT.8).OR.(IOPT.LT.1)) GOTO 11
C
C
      IF(IOPT.EQ.1) THEN
       WRITE(6,*) ' ENTER INITIAL L1/L2 RATIO  '
       READ(5,*) X1L
       WRITE(6,*) ' ENTER FINAL L1/L2 RATIO  '
       READ(5,*) X1T
       WRITE(6,*) ' ENTER NUMBER OF STEPS '
```

```
      READ(5,*) X1NSTEP
      X1STEP=(X1T-X1L)/X1NSTEP
     ENDIF
C
C
     IF(IOPT.EQ.2) THEN
      WRITE(6,*) ' ENTER INITIAL H1/H2 RATIO  '
      READ(5,*) X2L
      WRITE(6,*) ' ENTER FINAL H1/H2 RATIO  '
      READ(5,*) X2T
      WRITE(6,*) ' ENTER NUMBER OF STEPS '
      READ(5,*) X2NSTEP
      X2STEP=(X2T-X2L)/X2NSTEP
     ENDIF
C
C
     IF(IOPT.EQ.3) THEN
      WRITE(6,*) ' ENTER INITIAL H3/H2 RATIO  '
      READ(5,*) X3L
      WRITE(6,*) ' ENTER FINAL H3/H2 RATIO  '
      READ(5,*) X3T
      WRITE(6,*) ' ENTER NUMBER OF STEPS '
      READ(5,*) X3NSTEP
      X3STEP=(X3T-X3L)/X3NSTEP
     ENDIF
C
C
     IF(IOPT.EQ.4) THEN
      WRITE(6,*) 'ENTER PROPORTION FOR SEARCH VECTOR X(1) {L1/L2}'
      READ(5,*) H1T
     ENDIF
C
C
     IF(IOPT.EQ.5) THEN
      WRITE(6,*) 'ENTER PROPORTION FOR SEARCH VECTOR X(2) {H1/H2}'
      READ(5,*) H2T
     ENDIF
C
C
     IF(IOPT.EQ.6) THEN
      WRITE(6,*) 'ENTER PROPORTION FOR SEARCH VECTOR X(3) {H3/H2} '
      READ(5,*) H3T
     ENDIF
C
C
     IF(IOPT.EQ.7) THEN
 42   WRITE(6,*) 'ENTER MINIMUM SIZE OF SEARCH VECTOR '
      READ(5,*) MINSTEP
      IF(MINSTEP.LE.0) THEN
        WRITE(6,*) ' INVALID SEARCH VECTOR MINIMUM '
        GOTO 42
      ENDIF
     ENDIF
     IF(IOPT.EQ.8) GOTO 12
C
     GOTO 2
C
 12  CALL CLS
     WRITE(6,*) 'Enter file name for data  (enclose in single quotes)'
     READ(5,*) FILNAM
     OPEN(3,FILE=FILNAM)
C
C
     WRITE(6,*) 'ENTER VELOCITY FOR OPTIMISATION '
     READ(5,*) VEL
C     WRITE(6,*) 'ENTER NON-NEWTONIAN INDEX '
C     READ(5,*) PLN
C
C
     PLN=0.33333
     WRITE(3,*) 'FILE = ',FILNAM
     WRITE(3,*) '==========='
     WRITE(3,*) 'PARAMETERS'
     WRITE(3,*) '==========='
     WRITE(3,*) 'MINIMUM SEARCH VECTOR= ',MINSTEP
     WRITE(3,*) 'L1/L2= ',X1L,'  TO  ',X1T,' IN ',X1NSTEP
     WRITE(3,*) 'H1/H2= ',X2L,'  TO  ',X2T,' IN ',X2NSTEP
     WRITE(3,*) 'H3/H2= ',X3L,'  TO  ',X3T,' IN ',X3NSTEP
     WRITE(3,*) 'PROPORTION SEARCH VECTOR H(1)  ',H1T
     WRITE(3,*) 'PROPORTION SEARCH VECTOR H(2)  ',H2T
     WRITE(3,*) 'PROPORTION SEARCH VECTOR H(3)  ',H3T
     WRITE(3,*) ' '
     WRITE(3,100) 'VEL= ',VEL
     WRITE(3,100) 'PLN= ',PLN
     WRITE(3,1010)
     WRITE(3,*) 'L1/L2    H1/H2     H3/H2      |     L1/L2     H1/H2
    &H3/H2         MERIT'
     WRITE(3,1010)
1010 FORMAT(79('='))
C
     DO 15 X1=X1L,X1T,X1STEP
     DO 16 X2=X2L,X2T,X2STEP
     DO 17 X3=X3L,X3T,X3STEP
C
     X(1)=X1
     X(2)=X2
     X(3)=X3
C
     H(1)=H1T*X1
     H(2)=H2T*X2
     H(3)=H3T*X3
C
     CALL HJ(X,BT,H,N,P,MINSTEP,FUNVAL)
C
C     IF(EMODE.EQ.2.) THEN
C       WRITE(3,*) '********  SEARCH VECTOR EXCESS DETECTED  ********'
C       WRITE(6,*) '********  SEARCH VECTOR EXCESS DETECTED  ********'
C       EMODE=1.0
C     ENDIF
C
     WRITE(3,110) X1,X2,X3,X(1),X(2),X(3),FUNVAL
C
C SCREEN ECHO
C
     WRITE(6,110) X1,X2,X3,X(1),X(2),X(3),FUNVAL
 17  CONTINUE
```

```
  16  CONTINUE
  15  CONTINUE
C
 100  FORMAT(1X,A5,E13.7)
 110  FORMAT(7(1X,F10.6))
      CLOSE(3)
C
C
      CALL CLS
      WRITE(6,*) 'OPTIMISATION SEQUENCE COMPLETED (press ret)'
      READ(5,*)
      ENDIF
C*****************************************************************C
C                                                                 C
C SINGLE START CODE BLOCK                                         C
C                                                                 C
C*****************************************************************C
      IF(MOPT.EQ.2) THEN
   4  CALL CLS
      CALL HEADER
      WRITE(6,*) '1#    L1/L2= ',X1L
      WRITE(6,*) '2#    H1/H2= ',X2L
      WRITE(6,*) '3#    H3/H2= ',X3L
      WRITE(6,*) '4#    SEARCH VECTOR H(1)  ',H1T
      WRITE(6,*) '5#    SEARCH VECTOR H(2)  ',H2T
      WRITE(6,*) '6#    SEARCH VECTOR H(3)  ',H3T
      WRITE(6,*) '7#    SIZE OF MINIMUM SEARCH VECTOR',MINSTEP
      WRITE(6,*) ' '
      WRITE(6,*) '8#    RUN'
      CALL BLANK(10)
  14  WRITE(6,*) ' ENTER OPTION REQUIRED '
      READ(5,*) IOPT
C
      IF(IOPT.EQ.42) GOTO 1
      IF((IOPT.GT.8).OR.(IOPT.LT.1)) GOTO 14
C
C
      IF(IOPT.EQ.1) THEN
       WRITE(6,*) ' ENTER INITIAL L1/L2 RATIO  '
       READ(5,*) X1L
      ENDIF
C
C
      IF(IOPT.EQ.2) THEN
       WRITE(6,*) ' ENTER INITIAL H1/H2 RATIO  '
       READ(5,*) X2L
      ENDIF
C
C
      IF(IOPT.EQ.3) THEN
       WRITE(6,*) ' ENTER INITIAL H3/H2 RATIO  '
       READ(5,*) X3L
      ENDIF
C
C
      IF(IOPT.EQ.4) THEN
       WRITE(6,*) 'ENTER PROPORTION FOR SEARCH VECTOR X(1) (L1/L2)'
       READ(5,*) H1T
      ENDIF
C
C
      IF(IOPT.EQ.5) THEN
       WRITE(6,*) 'ENTER PROPORTION FOR SEARCH VECTOR X(2) (H1/H2)'
       READ(5,*) H2T
      ENDIF
C
C
      IF(IOPT.EQ.6) THEN
       WRITE(6,*) 'ENTER PROPORTION FOR SEARCH VECTOR X(3) (H3/H2)'
       READ(5,*) H3T
      ENDIF
C
       IF(IOPT.EQ.7) THEN
  43    WRITE(6,*) 'ENTER MINIMUM SIZE OF SEARCH VECTOR '
       READ(5,*) MINSTEP
       IF(MINSTEP.LE.0) THEN
         WRITE(6,*) ' INVALID SEARCH VECTOR MINIMUM '
         GOTO 43
       ENDIF
      ENDIF
C
C
      IF(IOPT.EQ.8) GOTO 25
C
      GOTO 4
C
  25  CALL CLS
      WRITE(6,*) 'ENTER VELOCITY FOR OPTIMISATION '
      READ(5,*) VEL
      PLN=0.3333333
C      WRITE(6,*) 'ENTER NON-NEWTONIAN INDEX '
C      READ(5,*) PLN
C
C
      WRITE(6,*) 'PARAMETERS'
      WRITE(6,*) '=========='
      WRITE(6,*) 'MIN STEP= ',MINSTEP
      WRITE(6,*) 'L1/L2= ',X1L
      WRITE(6,*) 'H1/H2= ',X2L
      WRITE(6,*) 'H3/H2= ',X3L
      WRITE(6,*) 'PROPORTION OF SEARCH VECTOR H(1)  ',H1T
      WRITE(6,*) 'PROPORTION OF SEARCH VECTOR H(2)  ',H2T
      WRITE(6,*) 'PROPORTION OF SEARCH VECTOR H(3)  ',H3T
      WRITE(6,*) ' '
      WRITE(6,100) 'VEL= ',VEL
      WRITE(6,100) 'PLN= ',PLN
      WRITE(6,*)'-------------------------------------------------'
      WRITE(6,*) '  X(1)          X(2)          X(3)       |    MERIT '
      WRITE(6,*)'-------------------------------------------------'
C
      X(1)=X1L
      X(2)=X2L
      X(3)=X3L
C
      H(1)=H1T*X(1)
      H(2)=H2T*X(2)
      H(3)=H3T*X(3)
```

```
C
      WRITE(6,*) X(1),X(2),X(3)
      WRITE(6,*) H(1),H(2),H(3)
      WRITE(6,*) BT(1),BT(2),BT(3)
      WRITE(6,*) P(1),P(2),P(3)
      WRITE(6,*) N,MINSTEP
      WRITE(6,*) VEL,PLN
      READ(5,*)
      WRITE(6,*) 'CALLING HJMAIN'

      CALL HJ(X,BT,H,N,P,MINSTEP,FUNVAL)

      CALL BLANK(3)
      WRITE(6,110) X1L,X2L,X3L,X(1),X(2),X(3),FUNVAL
      CALL BLANK(3)
C
      WRITE(6,*) 'OPTIMISATION SEQUENCE COMPLETED {press ret}'
      READ(5,*)
C
      ENDIF
C
C*********************************************************************C
C  SURFACE GENERATION CODE BLOCK                                      C
C                                                                     C
C*********************************************************************C
      IF(MOPT.EQ.3) THEN
  72    CALL HEADER
        WRITE(6,791)     X1L,X1T,X1NSTEP
        WRITE(6,792)     X2L,X2T,X2NSTEP
        WRITE(6,793)     X3L
        WRITE(6,*) ' '
        WRITE(6,*) '4#    RUN'
        CALL BLANK(10)
  791 FORMAT('  1#    L1/L2=',F12.4,' TO ',F12.4,' IN ',F8.3)
  792 FORMAT('  2#    H1/H2=',F12.4,' TO ',F12.4,' IN ',F8.3)
  793 FORMAT('  3#    CONSTANT VALUE OF H3/H2 RATIO= ',F12.6)
 711    WRITE(6,*) ' ENTER OPTION REQUIRED '
        READ(5,*) IOPT
C
        IF(IOPT.EQ.42) GOTO 1
        IF((IOPT.GT.4).OR.(IOPT.LT.1)) GOTO 711
C
C
        IF(IOPT.EQ.1) THEN
         WRITE(6,*) ' ENTER INITIAL L1/L2 RATIO  '
         READ(5,*) X1L
         WRITE(6,*) ' ENTER FINAL L1/L2 RATIO  '
         READ(5,*) X1T
         WRITE(6,*) ' ENTER NUMBER OF STEPS '
         READ(5,*) X1NSTEP
         X1STEP=(X1T-X1L)/X1NSTEP
        ENDIF
C
C
        IF(IOPT.EQ.2) THEN
         WRITE(6,*) ' ENTER INITIAL H1/H2 RATIO  '
         READ(5,*) X2L
         WRITE(6,*) ' ENTER FINAL H1/H2 RATIO  '
         READ(5,*) X2T
         WRITE(6,*) ' ENTER NUMBER OF STEPS '
         READ(5,*) X2NSTEP
         X2STEP=(X2T-X2L)/X2NSTEP
        ENDIF
C
C
        IF(IOPT.EQ.3) THEN
         WRITE(6,*) ' ENTER CONSTANT VALUE FOR H3/H2 RATIO  '
         READ(5,*) X3L
        ENDIF
C
C
        IF(IOPT.EQ.4) THEN
          GOTO 712
        ENDIF
C
        GOTO 72
C
  712   CALL CLS
        WRITE(6,*) 'Enter file name for data  {enclose in single quotes}'
        READ(5,*) FILNAM
        OPEN(3,FILE=FILNAM)
        CALL CLS
C
C
      WRITE(6,*) 'ENTER VELOCITY FOR OPTIMISATION '
      READ(5,*) VEL
      WRITE(6,*) 'ENTER NON-NEWTONIAN INDEX '
      READ(5,*) PLN
C
        CALL CLS
        CALL HEADER
C
C
        X3=X3L
C
        COUNT=0.0
        DO 799 ZXN=X2L,X2T,X2STEP
        COUNT=COUNT+1
        ROW(COUNT)=ZXN
 799    CONTINUE
C
        WRITE(3,718) IDINT(X1NSTEP+2),IDINT(COUNT+1)
  718   FORMAT(I4,2X,I4)
        WRITE(3,717) 0.0,(ROW(ZXN),ZXN=1,COUNT,1)
C
        DO 715 X1=X1L,X1T,X1STEP
          C2=0
        DO 716 X2=X2L,X2T,X2STEP
C
          X(1)=X1
          X(2)=X2
          X(3)=X3
          FUNVAL=MERIT(X)
          C2=C2+1
          ROW(C2)=DABS(FUNVAL)
C
  716   CONTINUE
```

```
        WRITE(3,717) X1,(ROW(ZXN),ZXN=1,COUNT,1)
  717   FORMAT(F10.6,100(2X,F10.6))
  715   CONTINUE
C
        CLOSE(3)
C
C
        CALL CLS
        WRITE(6,*) 'SURFACE GENERATION COMPLETED {press ret}'
        READ(5,*)
C
      ENDIF
C
      IF(MOPT.EQ.4) THEN
       CALL CLS
       STOP 'HAVE A NICE DAY'
      ENDIF
C
      GOTO 1
      END


C**********************C
C  CLEAR SCREEN        C
C**********************C
      SUBROUTINE CLS
      DO 10 I=1,28
       WRITE(6,*) ' '
  10  CONTINUE
      RETURN
      END

C**************************************C
C       WRITES THE HEADER TITLE        C
C**************************************C
      SUBROUTINE HEADER
C
      WRITE(6,*) '***********************************'
      WRITE(6,*) 'POWER LAW - MODEL OPTIMISATION PROG'
      WRITE(6,*) '***********************************'
      WRITE(6,*) ' '
C
      RETURN
      END


C**************************************C
C  BLANK - GENERATES N BLANK LINES     C
C**************************************C
      SUBROUTINE BLANK(N)
      INTEGER N,I
C
      DO 10 I=1,N
        WRITE(6,*) ' '
  10  CONTINUE
      RETURN
      END


C*************************************************************************C
C  PLAW  - SOLVES THE GOVERNING EQUATIONS OF DEFORMATION FOR THE        C
C          DEFORMATION ZONE, THIS IS ACCOMPLISHED USING A FINITE        C
C          DIFFERENCE FORMULATION, A LINEAR DEFORMATION PROFILE IS      C
C          ASSUMED BETWEEN THE SOLUTION POINTS, VARIABLES HAVE THE      C
C          SAME MEANING AS DEFINED PREVIOUSLY                           C
C*************************************************************************C
      REAL FUNCTION MERIT(X)
      IMPLICIT REAL (A-Z)
      LOGICAL SLIP,SFLAG
      INTEGER IMINIT,ISTEP
      DIMENSION X(3)
      COMMON  VEL,PLN
      COMMON /F1C/ W,T,H1,H2,H3,L1,L2,PLK
      SLIP=.FALSE.
C
C CONSTANTS
C
      OL=0.1785
      H2=0.00004
      ONEPART=OL/(X(1)+1)
      L1=X(1)*ONEPART
      L2=0.1785-L1
      H1=X(2)*H2
      H3=X(3)*H2
      IF((L1.LE.0).OR.(L2.LE.0).OR.(H1.LE.0).OR.(H3.LE.(1*H2))) THEN
        MERIT=0.0
        WRITE(6,200) X(1),X(2),X(3),MERIT,SLIP
        RETURN
      ENDIF
C
      VIS=120
      YS=70000000
      SHK=600000000
      SHI=0.6
      W=0.0253
      T=0.001575
      TAUCRI=320000
      PLK=25000
C      PLK=120
C      PLN=1.0
C*****************************************C
C  ITERATE FOR TAU1 AND TAU3               C
C*****************************************C
C
      PM=6*PLK*PLN*(H1-H2)*VEL**PLN
      PM=PM/((((H2)**(2+PLN))/L2)+(((H1)**(2+PLN))/L1))
C
      DPDX=PM/L1
      CALL SHEAR(TAU1,DPDX,H1,VEL)
      CALL SHEAR(TAU3,DPDX,H3,VEL)
C
      IF((TAU1.GE.TAUCRI).OR.(TAU3.GE.TAUCRI)) THEN
        TAU1=TAUCRI
```

```
        TAU3=TAUCRI
        SLIP=.TRUE.
      ENDIF
      TAUI1=TAU1
      TAUI21=TAU3
C*************************************************************C
C  CALCULATE X1 THE DISTANCE TO THE ONSET OF DEFORMATION  C
C*************************************************************C
      X1=YS/((PM/L1)+(2.*ABS(TAU1)/T)+(2.*ABS(TAU3)/W))
      IF(X1.GT.L1) THEN
        WRITE(0,*)' X1 >> L1  ******  ERROR'
        MERIT=0.0
        RETURN
      ENDIF
C*********************************************************************C
C  CALCULATE THE INITIAL CONDITIONS AT X=X1  ONSET OF DEFORMATION C
C*********************************************************************C
      PI=(PM/L1)*X1
      TI=T
      WI=W
      VI=VEL
      HI=H1
      H2I=H3
      DPDX=PM/L1
      SIGXI=(2*ABS(TAU1)*X1/T)+(2*ABS(TAU3)*X1/W)
      XP=X1
C
      IRW=0
      DX=2.0
      DX=DX/1000.
      NSTEP=INT(((L1-X1)/DX)+0.5)
      DX=(L1-X1)/NSTEP
      M=W/T
C************************C
C  SOLVING EQUATIONS      C
C************************C
      XPD=0.0
      DO 10 ISTEP=1,NSTEP,1
C*******************************C
C  INCREMENT  X  VARIABLE  XP    C
C*******************************C
      XP=XP+DX
      XPD=XPD+DX
C*******************************C
C  FIND SLOPE OF DEFLECTION    C
C*******************************C
  21  B1=1E-9
      B2=2E-4
      DB=1E-5
      R1=PLRES(B1,H1,HI,H2I,PLK,PLN,VEL,W,T,DX,BOLD,PI,PM,SHI,SHK,J1,L1,
     &SIGXI,YS,TI,WI,SLIP,TAU1I,TAU3I)
      R2=PLRES(B2,H1,HI,H2I,PLK,PLN,VEL,W,T,DX,BOLD,PI,PM,SHI,SHK,J1,L1,
     &SIGXI,YS,TI,WI,SLIP,TAU1I,TAU3I)
  20  CONTINUE
      IF(ABS(R1).LE.20000) THEN
         B=B1
         GOTO 30
      ENDIF
      IF(ABS(R2).LE.20000) THEN
         B=B2
         GOTO 30
      ENDIF
C
C  GET SIGNS OF SEARCH POINTS
C
      IF(R1.GE.0.0) THEN
       ISR1=1
      ELSE
       ISR1=0
      ENDIF
      IF(R2.GE.0.0) THEN
       ISR2=1
      ELSE
       ISR2=0
      ENDIF
C
C MAIN LOOP
C
      IF(ISR1.EQ.ISR2) THEN
        SLOPE=((R2-R1)/(B2-B1))
        IF(SLOPE.GT.0.0) THEN
          IF((ISR1.EQ.1).AND.(ISR2.EQ.1)) THEN
            B1=B1-DB
           IF(B1.LE.0.0) THEN
            B1=B1+DB
            DB=DB/2
            GOTO 20
           ENDIF
          ELSE
            B2=B2+DB
          ENDIF
        ELSE
          IF((ISR1.EQ.1).AND.(ISR2.EQ.1)) THEN
            B2=B2+DB
          ELSE
            B1=B1-DB
            IF(B1.LE.0.0) THEN
             B1=B1+DB
             DB=DB/2
             GOTO 20
            ENDIF
          ENDIF
        ENDIF
      ELSE
        IF(ABS(R1).GE.ABS(R2)) THEN
          B1=B1+(ABS(B1-B2))/2
        ELSE
          B2=B2-(ABS(B1-B2))/2
        ENDIF
        DB=ABS(B2-B1)/3
      ENDIF
      R1=PLRES(B1,H1,HI,H2I,PLK,PLN,VEL,W,T,DX,BOLD,PI,PM,SHI,SHK,J1,L1,
     &SIGXI,YS,TI,WI,SLIP,TAU1I,TAU3I)
      R2=PLRES(B2,H1,HI,H2I,PLK,PLN,VEL,W,T,DX,BOLD,PI,PM,SHI,SHK,J1,L1,
     &SIGXI,YS,TI,WI,SLIP,TAU1I,TAU3I)
      GOTO 20
  30  CONTINUE
```

```
C*****************************************************************C
C HENCE HAVING FOUND B,  EVALUATE SIG'S AND PRESSURES OF N+1 STEP C
C*****************************************************************C
      IF(.NOT.SLIP) THEN
C
       HI1=H(HI,B,DX)
       H2I1=H(H2I,B*M,DX)
       TI1=TF(TI,B,DX)
       WI1=TF(WI,B*M,DX)
       AR=W*T/(WI1*TI1)
       VI1=VEL*AR
       VO5=VEL*W*T/(TF(WI,B*M,DX/2.)*TF(TI,B,DX/2.))
C**********************C
C FOR THE PRESSURES    C
C**********************C
       DPDXI1=(6*PLN*PLK*(VI1/HI1)**(PLN-1))/(HI1**3)
       DPDXI1=DPDXI1*((VI1*HI1-VEL*H1)+((PM*H1**(2+PLN))/
     &(6*L1*PLN*PLK*VEL**(PLN-1))))
       PI1=P(PI,DPDXI1,DX)
       PIO5=P(PI,DPDXI1,DX/2)
C**************************C
C FOR MATERIAL PROPERTIES   C
C**************************C
       YI1=YS+SHK*((LOG(AR)**SHI))
C**********************C
C  FOR THE STRESSES      C
C**********************C
       CALL SHEAR(TAU1O5,DPDXI1,H(HI,B,DX/2.0),VO5)
       CALL SHEAR(TAU3O5,DPDXI1,H(H2I,B,DX/2.0),VO5)
C
       IF((ABS(TAU1O5).GE.TAUCRI).OR.(ABS(TAU3O5).GE.TAUCRI)) THEN
         SLIP=.TRUE.
         TAU3I=TAUCRI
         TAU1I=TAUCRI
         GOTO 21
       ENDIF
      RS=ABS(BOOLD-B)*(1+M)
      SIGXI1=(SIGXI*WI*TI/(WI1*TI1))+(2.0*PIO5*DX*TAN(B)/TI1)+
     &(2.0*PIO5*DX*TAN(M*B)/WI1)+(2.0*ABS(TAU1O5)*DX/TI1)+
     &(2*ABS(TAU3O5)*DX/WI1)
      SIGRW=YI1*RS/4.0
      IF(IRW.EQ.1)  SIGXI1=SIGXI1+SIGRW
C************************************C
C SAVE NEW VALUES TO THE  ith  STEP C
C************************************C
        PI=PI1
        TI=TI1
        WI=WI1
        VI=VI1
        VI=VI1
        HI=HI1
        H2I=H2I1
        SIGXI=SIGXI1
        TAU1I=TAU1O5
        TAU3I=TAU3O5
        DELB=B-BOOLD
        BOOLD=B
C
      ELSE
C
       HI1=H(HI,B,DX)
       H2I1=H(H2I,B*M,DX)
       TI1=TF(TI,B,DX)
       WI1=TF(WI,B*M,DX)
       AR=W*T/(WI1*TI1)
       VI1=VEL*AR
       VO5=VEL*W*T/(TF(WI,B*M,DX/2.)*TF(TI,B,DX/2.))
C**********************C
C FOR THE PRESSURES    C
C**********************C
       Z=RLAM(PLN,2.0)
       PI1=PI
       PIO5=PI
C**************************C
C FOR MATERIAL PROPERTIES   C
C**************************C
       YI1=YS+SHK*((LOG(AR)**SHI))
C**********************C
C  FOR THE STRESSES      C
C**********************C
       TAU1O5=TAU1I
       TAU3O5=TAU3I
       RS=ABS(BOOLD-B)*(1+M)
C       SIGXI1=(SIGXI*WI*TI/(WI1*TI1))+(2.0*PIO5*DX*TAN(B)/TI1)+
C     &(2.0*PIO5*DX*TAN(M*B)/WI1)+(2.0*ABS(TAU1O5)*DX/TI1)+
C     &(2*ABS(TAU3O5)*DX/WI1)
       SIGXI1=(SIGXI*WI*TI/(WI1*TI1))+(2.0*PIO5*DX*TAN(B)/TI1)+
     &(2.0*PIO5*DX*TAN(M*B)/WI1)+(2.0*ABS(TAU1O5)*DX/TI1)+
     &(2*ABS(TAU3O5)*DX/WI1)

       SIGRW=YI1*RS/4.0
C
C  INCLUDE THIS TERM FOR REDUNDENT WORK
C
      IF(IRW.EQ.1) SIGXI1=SIGXI1+SIGRW
C************************************C
C SAVE NEW VALUES TO THE  ith  STEP C
C************************************C
        PI=PI1
        DPDXI1=0.0
        TI=TI1
        WI=WI1
        VI=VI1
        VI=VI1
        HI=HI1
        H2I=H2I1
        SIGXI=SIGXI1
C        SLIP=.FALSE.
        DELB=B-BOOLD
        BOOLD=B
C
      ENDIF
C
   10 CONTINUE
C
      MINIT=((1-((WI*TI)/(W*T)))*100)
      IMINIT=INT(MINIT*1E6)
```

```
      MERIT=-1*FLOAT(IMINIT/1E6)
      WRITE(6,200) X(1),X(2),X(3),MERIT,SLIP
C
      RETURN
C
C  100 FORMAT(3(1X,E10.4),2(F10.0),2(1X,L4))
  125 FORMAT(1X,E12.6,',',1X,E12.6)
  130 FORMAT(F7.6,1X,13(1X,E10.4))
  150 FORMAT(I4,11(1X,E10.4))
  200 FORMAT(4(E19.12),L3)
      END


C*********************************************************************C
C  POWER LAW RESIDUAL FUNCTION                                        C
C*********************************************************************C
      REAL FUNCTION PLRES(B,H1,HI,H2I,PLK,PLN,VEL,W,T,DX,BO,PI,PM,
     &SHI,SHK,J1,L1,SIGXI,YS,TI,WI,SLIP,TAU1I,TAU3I)
      REAL H,TF,P,M,H2I1,TI1,WI1,B,H1,HI,PLK,PLN,VI1,TAU105,
     &TAU305,W,T,DX,AR,VEL,Z,DPDXI1,PI05,PI1,RLAM,TI,WI,H2I,PI,V05,
     &YI1,PM,J1,L1,SIGXI,HI1,BO,YS,RS,SIGXI1,SHI,SHK,SIGRW,TAU1I,TAU3I
      LOGICAL SLIP
C
      M=W/T
C
      IF(.NOT.SLIP) THEN
       HI1=H(HI,B,DX)
       H2I1=H(H2I,B*M,DX)
       TI1=TF(TI,B,DX)
       WI1=TF(WI,B*M,DX)
       AR=W*T/(WI1*TI1)
       VI1=VEL*AR
       V05=VEL*W*T/(TF(WI,B*M,DX/2.)*TF(TI,B,DX/2.))
C**********************C
C FOR THE PRESSURES    C
C**********************C
       Z=RLAM(PLN,2.0)
       DPDXI1=(6*PLN*PLK*(VI1/HI1)**(PLN-1))/(HI1**3)
       DPDXI1=DPDXI1*((VI1*HI1-VEL*H1)+((PM*H1**(2+PLN)))/
     &(6*L1*PLN*PLK*VEL**(PLN-1))))
       PI1=P(PI,DPDXI1,DX)
       PI05=P(PI,DPDXI1,DX/2)
C****************************C
C FOR MATERIAL PROPERTIES    C
C****************************C
       YI1=YS+SHK*((LOG(AR)**SHI))
C**********************C
C  FOR THE STRESSES      C
C**********************C
       CALL SHEAR(TAU105,DPDXI1,H(HI,B,DX/2.0),V05)
       CALL SHEAR(TAU305,DPDXI1,H(H2I,B,DX/2.0),V05)
C
       RS=ABS(BO-B)*(1+M)
       SIGXI1=(SIGXI*WI*TI/(WI1*TI1))+(2.0*PI05*DX*TAN(B)/TI1)+
     &(2.0*PI05*DX*TAN(M*B)/WI1)+(2.0*ABS(TAU105)*DX/TI1)+
     &(2*ABS(TAU305)*DX/WI1)
       SIGRW=YI1*RS/4.0
C       IF(IRW.EQ.1.0) SIGXI1=SIGXI1+SIGRW
C
      ELSE
C
       HI1=H(HI,B,DX)
       H2I1=H(H2I,B*M,DX)
       TI1=TF(TI,B,DX)
       WI1=TF(WI,B*M,DX)
       AR=W*T/(WI1*TI1)
       VI1=VEL*AR
       V05=VEL*W*T/(TF(WI,B*M,DX/2.)*TF(TI,B,DX/2.))
C**********************C
C FOR THE PRESSURES    C
C**********************C
       PI1=PI
       PI05=PI
C****************************C
C FOR MATERIAL PROPERTIES    C
C****************************C
       YI1=YS+SHK*((LOG(AR)**SHI))
C**********************C
C  FOR THE STRESSES      C
C**********************C
       TAU105=TAU1I
       TAU305=TAU3I
       RS=ABS(BO-B)*(1+M)
       SIGXI1=(SIGXI*WI*TI/(WI1*TI1))+(2.0*PI05*DX*TAN(B)/TI1)+
     &(2.0*PI05*DX*TAN(M*B)/WI1)+(2.0*ABS(TAU105)*DX/TI1)+
     &(2*ABS(TAU305)*DX/WI1)
       SIGRW=YI1*RS/2.0
C       IF(IRW.EQ.1.0) SIGXI1=SIGXI1+SIGRW
C
      ENDIF
C*****************************C
C SET FUNCTION RETURN VALUE   C
C*****************************C
      PLRES=PI1+SIGXI1-YI1
C
      RETURN
      END


C*********************************************************************C
C SHEAR - SHEAR SUBROUTINE ITERATIVE FINDS THE REQUIRED SHEAR STRESS C
C         DURING SOLUTION OF THE PLASTO-HYDRODYNAMIC DRAWING OF      C
C         RECTANGULAR SECTIONS                                       C
C*********************************************************************C
      SUBROUTINE SHEAR(T,DPDX,HA,V)
      IMPLICIT REAL (A-Z)

C      WRITE(6,*) ' OPENING FILE'
C      OPEN(3,FILE='TS.DAT')
C      DO 1919 B1=-1000000,1000000,20000
C       R=TS(B1,PM)
C      WRITE(3,*) B1,R
C 1919 CONTINUE
C      CLOSE(3)
C      WRITE(6,*) ' CLOSING FILE'
```

```
      B1=-300000
      B2=-200000
      DB=25000
      ERR=0.005
      R1=TS(B1,DPDX,HA,V)
      R2=TS(B2,DPDX,HA,V)
   22 IF(ABS(R1).LE.ERR) THEN
         T=B1
         GOTO 33
      ENDIF
      IF(ABS(R2).LE.ERR) THEN
         T=B2
         GOTO 33
      ENDIF
C
C  GET SIGNS OF SEARCH POINTS
C
      IF(R1.GE.0.0) THEN
       ISR1=1
      ELSE
       ISR1=0
      ENDIF
      IF(R2.GE.0.0) THEN
       ISR2=1
      ELSE
       ISR2=0
      ENDIF
C
C MAIN LOOP
C
      IF(ISR1.EQ.ISR2) THEN
        SLOPE=((R2-R1)/(B2-B1))
        IF(SLOPE.GT.0.0) THEN
          IF((ISR1.EQ.1).AND.(ISR2.EQ.1)) THEN
            B1=B1-DB
          ELSE
            B2=B2+DB
          ENDIF
        ELSE
          IF((ISR1.EQ.1).AND.(ISR2.EQ.1)) THEN
            B2=B2+DB
          ELSE
            B1=B1-DB
          ENDIF
        ENDIF
      ELSE
        IF(ABS(R1).GE.ABS(R2)) THEN
          B1=B1+(ABS(B1-B2))/2
        ELSE
          B2=B2-(ABS(B1-B2))/2
        ENDIF
        DB=ABS(B2-B1)/3
      ENDIF
      R1=TS(B1,DPDX,HA,V)
      R2=TS(B2,DPDX,HA,V)
      GOTO 22
   33 CONTINUE
      RETURN
      END


C*******************************C
C SHEAR FUNCTION T                C
C*******************************C
      REAL FUNCTION TS(A,DPDX,HA,V)
      IMPLICIT REAL (A-Z)
      COMMON  VEL,PLN
      COMMON /F1C/ W,T,H1,H2,H3,L1,L2,PLK
C
      C1=DPDX*(1/PLK)
      C2=A/PLK
      C3=C1*HA+C2
C
      TEMP=(C3**RLAM(PLN,1.0))- (C2**RLAM(PLN,1.0))
      TS=(TEMP/(C1*RLAM(PLN,1.0))) + V
C
      RETURN
      END

C*******************************C
C  GAP FUNCTION                  C
C*******************************C
      REAL FUNCTION H(HN,SLOPE,DELX)
      REAL HN,SLOPE,DELX
C
      H=HN+SLOPE*DELX
C
      RETURN
      END

C************************C
C THICKNESS FUNCTION     C
C************************C
      REAL FUNCTION TF(TN,SLOPE,DELX)
      REAL TN,SLOPE,DELX
C
      TF=TN-2.0*SLOPE*DELX
C
      RETURN
      END


C************************C
C PRESSURE FUNCTION     C
C************************C
      REAL FUNCTION P(PN,DPDX,DELX)
      REAL PN,DPDX,DELX
C
      P=PN+DPDX*DELX
C
      RETURN
      END

C*******************************C
C  LAMDA FUNCTION                C
C*******************************C
```

```
      REAL FUNCTION RLAM(N,M)
      REAL N,M
C
      RLAM=FLOAT(INT((1.0/N)+FLOAT(M)))
C
      RETURN
      END

C*******************************C
C JAY SUBROUTINE                C
C*******************************C
      SUBROUTINE JAY(J,N)
      REAL A,B,J,N,R1,R2,RLAM
C
      R1=RLAM(N,FLOAT(1.0))
      R2=RLAM(N,FLOAT(2.0))
      A=1/(R1*R2)
      B=1/(R1*2.0)
      J=A-B
C
      RETURN
      END


C*************************************************************************C
C HOOKE AND JEEVES (OPTIMISATION)                                         C
C   MULTIVARIATE DIRECT SEARCH METHOD                                     C
C                                                                         C
C*************************************************************************C
      SUBROUTINE HJ(B,BT,H,N,P,MINSTEP,FUNVAL)
      IMPLICIT REAL (A-Z)
      INTEGER N,I
      DIMENSION B(N),H(N),P(N),BT(N)
C
      BASVAL=MERIT(B)
      FMIN=BASVAL
  10  CALL EXPLO(B,H,BT,N,FMIN,BASVAL)
C
      IF(FMIN.LT.BASVAL) THEN
C
C   SET BASE SWOPS B2 FOR BASE POINT AND FMIN FOR BASVAL, IF SUCESS
C   PATCALC CALULATES THE POSTION OF THE THE PATTERN MOVE
C
  20    CALL PATCALC(B,P,N,BT)
        CALL SETBASE(B,BT,N,BASVAL,FMIN)
        CALL EXPLO(P,H,BT,N,FMIN,BASVAL)
        IF(FMIN.LT.BASVAL) THEN
          GOTO 20
        ELSE
          CALL DECH(H,N)
          GOTO 10
        ENDIF
C
      ELSE
C
        ERRVEC=0.0
        DO 45 I=1,N
         ERRVEC=H(I)*H(I)+ERRVEC
  45    CONTINUE
        ERRVEC=DSQRT(ERRVEC)
        IF(ERRVEC.LT.MINSTEP) THEN
          FUNVAL=FMIN
          RETURN
        ELSE
          CALL DECH(H,N)
          GOTO 10
        ENDIF
      ENDIF
C
      END

C*************************************************************************C
C EXPLORATORY MOVE SUBROUTINE                                             C
C  ARGS  B=BASE POINT VECTOR                                              C
C        N=DIMENSION OF VECTORS                                           C
C        H=STEP LENGTH VECTOR                                             C
C        BT=BASE POINT TEMPORARY VECTOR                                   C
C        FMIN=FUNCTION MINIMUM                                            C
C        FBASE=FUNCTION VALUE AT BASE POINT                               C
C*************************************************************************C
      SUBROUTINE EXPLO(B,H,BT,N,FMIN,FBASE)
      IMPLICIT REAL (A-Z)
      INTEGER N,K
      DIMENSION B(N),H(N),BT(N)
C
      FMIN=FBASE
      BLANK=1.0
      CALL SETBASE(BT,B,N,BLANK,BLANK)
      DO 10 K=1,N
        BT(K)=B(K)+H(K)
        FVAL=MERIT(BT)
        IF(FVAL.GE.FMIN) THEN
          BT(K)=B(K)-H(K)
          FVAL=MERIT(BT)
          IF(FVAL.GE.FMIN) THEN
            BT(K)=B(K)
          ELSE
            FMIN=FVAL
          ENDIF
        ELSE
          FMIN=FVAL
        ENDIF
 10   CONTINUE
      RETURN
      END


C*************************************************************************C
C  DECREMENT STEP VECTOR                                                  C
C*************************************************************************C
      SUBROUTINE DECH(H,N)
      IMPLICIT REAL (A-Z)
      INTEGER N,I
      DIMENSION H(N)
C
```

```
      DO 10 I=1,N
        H(I)=0.5*H(I)
   10 CONTINUE
C
      RETURN
      END


C*************************************************************************C
C CALCULATES                                                              C
C          P  = B   +  2(B    - B  )                                      C
C           i    i        i+1    i                                       C
C*************************************************************************C
      SUBROUTINE PATCALC(B,P,N,BT)
      IMPLICIT REAL (A-Z)
      INTEGER N,I
      DIMENSION B(N),P(N),BT(N)
C
      DO 10 I=1,N
        P(I)=2*BT(I)-B(I)
   10 CONTINUE
      RETURN
      END

C*************************************************************************C
C  SET BASE SWOPS B2 IN TO B, AND FMIN INTO BASVAL                        C
C*************************************************************************C
      SUBROUTINE SETBASE(B,BT,N,BASVAL,FMIN)
      IMPLICIT REAL (A-Z)
      INTEGER N,I
      DIMENSION B(N),BT(N)
C
      BASVAL=FMIN
C
      DO 10 I=1,N
        B(I)=BT(I)
   10 CONTINUE
C
      RETURN
      END
```

Numerical Methods in Industrial Forming Processes. Chenot, Wood & Zienkiewicz (eds)
 ISBN 90 5410 087 7

A computer model for plasto-hydrodynamic drawing of narrow strips under flow instabilities

M.R.Stokes & G.R.Symmons
School of Engineering, Sheffield City Polytechnic, UK

ABSTRACT: Plasto-hydrodynamic drawing of circular cross-section wire has been modelled previously. In this technique the deformation to the wire is caused by the combined effect of axial pull and radial pressure generated due to the hydrodynamic action of the viscous fluid. The extent of deformation is such that for a moderately vicous fluid with Newtonian characteristics fracture of the wire is predicted at drawing speeds in excess of about 5m/s even though the smallest bore size of the hydrodynamic pressure unit is larger than the undeformed diameter of the wire. In this study a finite difference computer model has been developed for predicting the reduction in area of a rectangular cross-section narrow strip pulled through a unit having a stepped rectangular cavity which is filled with a viscous Newtonian fluid; the smallest section of the stepped cavity being greater than the section of the undeformed strip. Emphasis has been placed on the modelling of flow instabilities which occur at the elevated shear rates generated by the process and their effects on the deformation profile in the unit.

Key Words Strip drawing, plasto-hydrodynamics, Flow Instabilities, Finite difference, Reduction in area, Melt Fracture.

1 INTRODUCTION

A novel technique of wire drawing has been invented in which no conventional reduction dies are used and polymer melts are introduced as the lubricant in the drawing process. The main feature of this technique is that the conventional dies are replaced by a pressure cylinder which has an internal bore shaped such that hydrodynamic pressure is generated in the polymer melt surrounding the wire. The minimum internal bore size in the pressure cylinder is greater than the incoming wire diameter so no metal to metal contact takes place and there is no need to initially prepare the wire as in conventional wire drawing. The pulling action of the wire through the bore filled with the polymer melt gives rise to drag forces and generates hydrodynamic pressure. The combined effect of the imposed back stress and hydrodynamic pressure can be sufficient to deform the wire with selected sizes of orifice in the pressure chamber and speed of drawing. Wire deformations by this novel process can be varied by change of drawing speed competing with similar percentage reductions in area per pass as with conventional die drawing but offering a more simple flexible output system with no pre-process preparation of the wire.

A number of analytical models have been previously developed in relation to wire drawing and tube sinking. By using a polymer melt as the working fluid, the deformed wire is polymer coated. The choice of polymer used determines the types of coating produced whether an adhered coat or easily removed coat to suit product requirements. The coatings produced on the wire can be used for surface protection against corrosion, electrical insulation or as a preparatory coating for further processing. The thickness of the polymer coat on the wire depends upon the outlet sizes of orifice in the pressure unit. Hence the new process can be designed to suit a variety of wire deformation rates and polymer coating thickness on the wire for a variety of materials and polymers.

Recent research studies have concentrated on applying the die-less drawing process to strip. The above attributes for wire and tube have been applied to the deformation and polymer

coating of strip. Closed form analytical models have been presented for strip drawing (1,2). A numerical solution has been developed for strip drawing (3) using a reduction unit with a rectangular slot of stepped geometry indicating that a reduction in area of the strip in excess of 30% could be achieved in a single pass.

2 PRESENT INVESTIGATION

A new numerical solution for strip drawing is presented using a finite difference method as in (3) and similar model logic and solution of the plasto-hydrodynamic conditions for the stable flow conditions of the working fluid. However, the numerical solution includes a more realistic treatment of the condition where flow instabilities occur. It has been demonstrated that melt fracture takes place at certain critical shear stress in the fluid gaps that are often used in the die-less process to produce high pressure and shear stress. Hence the critical shear stress condition of melt fracture is often met. The previous numerical solution (1) assumed that once the onset of slip at the boundary was reached, the fluid pressure profile remained constant for all further increased velocities. In the present solution, slip is tested for each nodal point, such that, if slip is detected at some position in the deformation region, then the remaining nodal points are calculated using the slip condition.

3 ANALYSIS

The schematic diagram of the process is shown in Fig 1. To formulate expressions the following assumptions were made.

i) the dominant flow is axial and laminar
ii) the fluid pressure acts equally on both faces of the strip
iii) the pressure medium behaves like a Newtonian fluid
iv) isothermal conditions exist

3.1 Onset of plastic yielding of strip

Applying Von Mises Yield criteria, we derive the plasto-hydrodynamic governing equation

$$P_1 + \sigma_{x1} = y_1 \qquad (1)$$

Now let the deformation take place at a point X_1 distant from the entry point. The equilibrium of forces in x-direction at this point gives,

$$\sigma_x = \frac{2\tau_1 X_1}{t_1} + \frac{2\tau_3 X_1}{W_1} \qquad (2)$$

Also $$p_1 = \frac{Pm}{L1} X1 \qquad (3)$$

Substituting value of P_1 and σ_x into equation (1) and simplifying we obtain,

$$X_1 = \left(\frac{Pm}{L_1} + \frac{2\tau_1}{t_1} + \frac{2\tau_3}{W_1}\right)^{Y_1} \qquad (4)$$

3.2 Axial stress and hydrodynamic pressure in the deformation zone.

Consider two points in deformation zone at a distance 'dx' apart, (Fig 2), assuming that deformation between these points takes place linearly so that,

$$\frac{dt}{dx} = \text{Constant} = b \qquad (5)$$

$$\frac{dW}{dx} = \text{Constant} = b^* \qquad (6)$$

Expressing equations (5) and (6) in finite difference form we get,

$$t_i = t_{i-1} - b\ x \qquad (7)$$

$$W_i = W_{i-1} - b\ ^*x \qquad (8)$$

Also from Figure 2 we have, $dh = \frac{1}{2}dt$ and $dh^* = \frac{1}{2}dW$, which in finite difference form gives

$$h_1 = h_{i-1} + \tfrac{1}{2}b\ x \qquad (9)$$

$$h_i^* = h_{i-1} = \tfrac{1}{2}b^*\ x \qquad (10)$$

By considering the continuity of flow of metal, the current velocity is given by,

$$V_i = V_{i-1}\left(\frac{W_{i-1}\ t_{i-1}}{W_i t_i}\right) \qquad (11)$$

And using Levy-Mises flow rule it can be shown that

$$\frac{dW}{W_i} = \frac{dt}{t_i} \text{ and } b^* = mb \qquad (12)$$

where $m = \frac{W_1}{t_1}$

The force equilibrium in x-direction for a

small element, Fig 2, in deformation zone gives,

$$d\sigma_{x_i} = -\frac{dt_{iy_i}}{t_i} - \frac{dW_{iy_i}}{w_i} - \tau_i \cot\theta \frac{dt_i}{t_i} - \tau^* \cot\beta \frac{dW_i}{W_i} \qquad (13)$$

or

$$\sigma_{x_i} = \left(\frac{t_{i-1}}{t_i} + \frac{W_{i-1}}{W_i} - 2\right)y_i + \frac{2\tau_i}{t_i}\frac{x}{} + \frac{2\tau_i^*}{W_i}\frac{x}{} + \sigma_{x_{i-1}} \qquad (14)$$

Equation (14) is an expression to determine the axial stress in the deformation zone. The shear stress terms are given by,

$$\tau_i = -\frac{h_i}{2}p'_i - \frac{\mu V_i}{h_i} \qquad (15)$$

$$\tau_i^* = -\frac{h_i^*}{2}p'_i - \frac{\mu V_i}{h_i} \qquad (16)$$

The flow of polymer melt in the deformation zone will be given by,

$$Q_i = -\frac{h_i^3}{12\mu}\cdot\left(\frac{dp}{dx}\right)_i + \frac{V_i h_i}{2} \qquad (17)$$

And the continuity of the fluid flow will give,

$$Q_i = Q_1 \qquad (18)$$

The equation (18) on simplification gives,

$$p' = \frac{1}{h_1^3}\left[\frac{Pmh_1^3}{L1} + 6\mu(V_i i_h i - Vh_1)\right] \qquad (19)$$

and

$$p_i = p_{i-1} + p_i' \, X \qquad (20)$$

The equation (19) gives the pressure p_i, at any point in the deformation zone.

3.3 Percentage reduction in strip size

The stress-strain relationship of the strip material is given by

$$y = y_1 + K\epsilon^n$$

Therefore,

$$y_i = y_1 + K\left[\ln\left(\frac{W_1 t_1}{W_i t_i}\right)\right]^n \qquad (21)$$

Now the mean strain rate over a small distance may be defined by

$$\bar{\dot{\epsilon}}_m = \frac{1}{x_i - x_{i-1}}\int_{a_{i-1}}^{a_i} \bar{\dot{\epsilon}}.\, dx$$

$$= \frac{1}{x}\int_{a_{i-1}}^{a_i} -\frac{da}{a}\cdot\frac{1}{dt'} \cdot dx$$

thus

$$\bar{\dot{\epsilon}}_m = \frac{V_i}{x}\cdot\ln\left(\frac{a_{i-1}}{a_i}\right) \qquad (22)$$

A flow rule of the form,

$$S = \frac{y_d}{y_s} = 1 + \left(\frac{\bar{\dot{\epsilon}}_m}{N}\right)^{1/T1}$$

where

y_d = dynamic yield stress
N and T_1 are constants

In finite difference form notation the above equation takes the form,

$$S_i = 1 + \left(\frac{\bar{\dot{\epsilon}}_m}{N}\right)^{1/T1}$$

Combining this with equation (21) gives,

$$Y_i = S_i\left[Y_1 + K\left\{\ln\left(\frac{W_1 t_1}{W_i t_i}\right)\right\}^n\right] \qquad (23)$$

Equation (23) gives the current yield stress of the strip material in the deformation zone. Once the plastic yielding is predicted to commence, further permanent deformation should continue to take place as along

$$p_i + \sigma_{x_i} > y_i \qquad (24)$$

The procedure thus involved determination of the point X_1 by using equations (1),(2), and (3) simultaneously. Once the position of onset is determined then the equations in deformation zone were solved by finite difference technique from a point i = X_1 to a point i = L_1-X_1. For any arbitrary value of b, the equation (24) is solved by iteration in conjunction with equations (14), (18), (23) for a small distance x. After determining the value of slope b, the current thickness and the width of the strip may be calculated by using equation (7) and (8). The procedure is repeated in suitable steps up to the step where i = L_1 - X_1 and at that the values of t_i and W_i will give the final dimensions of the strip. The percentage reduction in area of the strip can then be calculated by,

$$PRA = \left(1 - \frac{W_i t_i}{W_{i-1} t_{i-1}}\right) \times 10 \qquad (25)$$

3.4 Condition of slip

Flow instabilities of the pressure medium can take place in the process when high shear of the fluid occurs. Under these circumstances, melt fracture of the polymer melt causes slip at the strip boundary with a loss of performance. Since these flow instabilities are prone at typical practical drawing speeds, the numerical model needs to include this effect to give realistic process performance predictions.

The numerical method tests the shear stress condition for both faces of the strip against a critical shear stress of 0.28 MNm^{-2} for polymer melts. If at any point, in the first land, slip is initiated then this will cause a local discontinuity causing the slip condition to be propagated around the strip section. The changes made i the numerical model, improve the accuracy of process performance prediction.

4 COMPUTER RESULTS AND DISCUSSION

Theoretical results were obtained by using the described plasto-hydrodynamic analysis including the effects of flow instabilities caused by slip. Computer results from the model were used to investigate:

i) effect of slip on deformation process
ii) effect of land length ratios given a constant overall length on percentage reduction in area
iii) effect of gap ratios for three different side gap values on percentage reduction in area
iv) effect of side gap value for various gap ratios on the peak deformation performance

4.1 Effect of slip on deformation

Once slip has been initiated it is assumed that a dynamic equilibrium is achieved, such that the pressure gradient falls to zero and the pressure remains constant at the value at slip initiation. This effectively changes the plasto-hydrodynamic equation to

$$\sigma x - Y + \text{Constant} = 0$$

the effect of this in the solution for B can be seen in the calculated deformation profile, fig 3. At 0.16m/s slip does not occur and with deformation performance, then as the velocity increases through 0.18, 0.19, and 0.2 m/s a distinct in the profile occurs at the onset of slip. This change accounts for fall off in performance for the process after arbitrary peak has been achieved, giving the destinctive shapes shown in Fig 6, 7, and 8.

4.2 Effect of land length ratio's

Fig 4 shows percentage reduction in area (PRA) against entry velocity for various L1/L2 ratio. The drawing performance is seen to improve with an increase in L1/L2 ratio from 3.5 PRA (L1/L2=1) to 11.16 PRA (L1/L2=59). The entry velocity for peak PRA can be seen to decrease from 0.2m/s (L1/L2=1) to 0.15m/s approx (L1/L2=59) with increasing L1/L2 ratio. Fig 5 shows peak PRA for L1/L2 ratio, this demonstrates that increasing L1/L2 ratio above 20 produces diminishing returns with virtually no increase above 50.

4.3 Effect of h1/h2 ratio on deformation performance

Fig shows drawing performance against entry velocity for various h1/h2 ratio, given h3 is constant at 0.0001m. Peak performance is seen to decrease with increasing h1/h2 ratio, while the velocity at which peak performance is attained increases with increasing h1/h2 ratio.

Fig 7 shows drawing performance against entry velocity for various h1/h2 ratio, given h3 is constant at 0.0003m. Peak performance is seen to decrease from 12.37241 PRA (h1/h2=5) to 10.237051 PRA (h1/h2=25) with increasing h1/h2 ratio, while the velocity at which peak performance is attained increases from 0.035m/s (h1/h2=5) to 0.3375m/s (h1/h2=25) for increasing h1/h2 ratio.

4.4 Effect of h3 gap on deformation performance

Fig 9 shows the effect of h3 on peak performance for various h1/h2 ratio. It may be seen that for decreasing h3 the peak performance increases. All values of h3 show a decrease in peak performance with increasing h1/h2 ratio,

h3=0.0005m decrease of 6.006%
h3=0.0003m decrease of 17.25%
h3=0.0001m decrease of 74.46%

with h3 equal to 0.0001m showing a much larger decrease than 0.0003m or 0.0005m.

5.0 CONCLUSIONS

The modification made to the modelling of slip directly effects the predicted drawing performance of the process.

The form of drawing performance so predicted qualitively agrees with previously published experimental data (4).

Whilst quantitative predictions cannot accurately be made this modification is an important step towards successful modelling of the process.

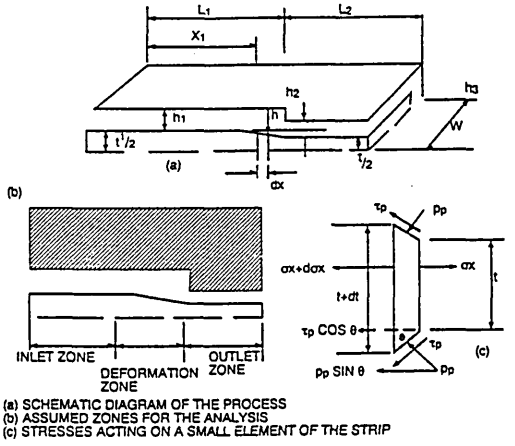

Fig 1 Geometric details of process pressure head.

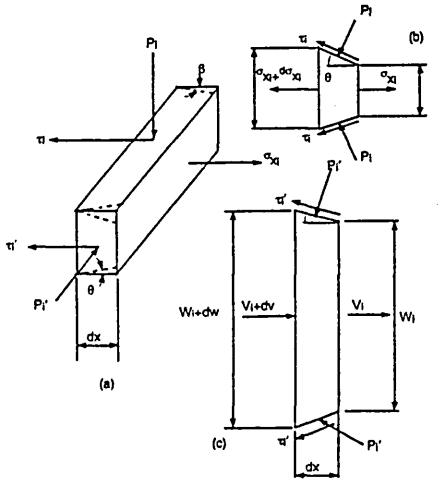

Fig. 2 Stresses acting on a small element.

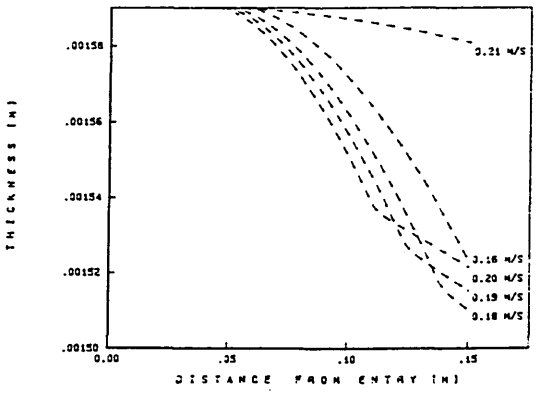

Fig. 3 deformation profiles for the slip region at various velocities.

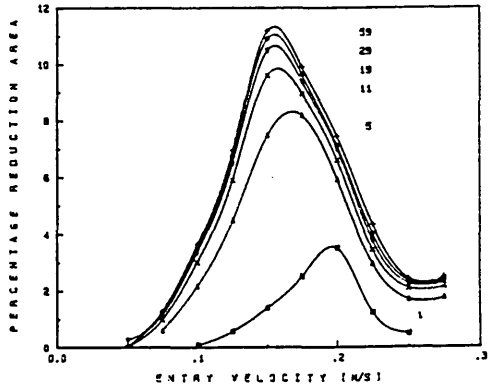

Fig. 4 Drawing performance for various L1/L2 ratio against velocity

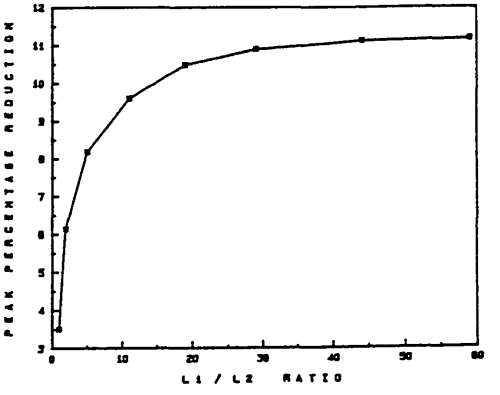

Fig. 5 Peak percentage reduction area for various L1/L2 ratio

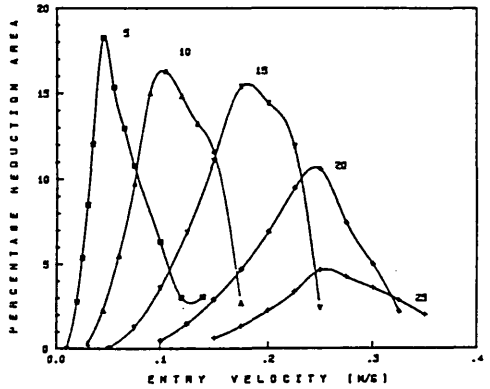

Fig. 6 Drawing performance for various h1/h2 ratio : h3=0.0001m

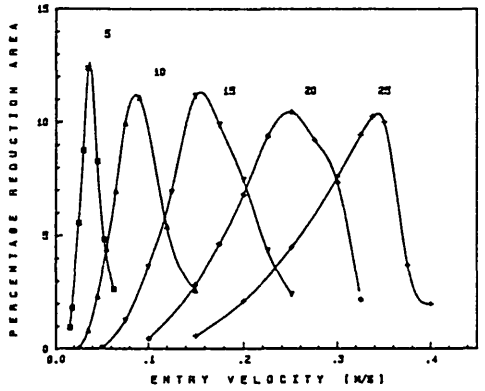

Fig. 7 Drawing performance for various h1/h2 ratio : h3=0.0003m

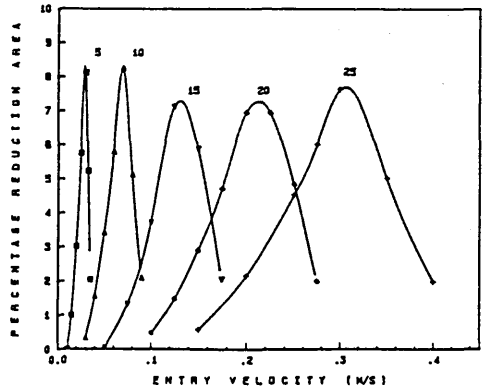

Fig. 8 Drawing performance for various h1/h2 ratio : h3=0.0005m

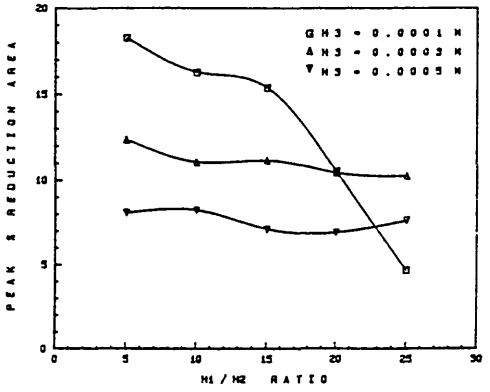

Fig. 9 Effect of h3 on drawing performance against h1/h2 ratio

REFERENCES

1) Symmons, G.R. Hashmi, M.S.J. and Memon, A.H. July 1987. A mathematical model for plasto-hydrodynamic drawing of narrow strips. Paper presented at 6th Int.Conf. on Mathematical Modelling, St Louis, USA.

2) Symmons, G.R. Memon, A.H. and Hashmi, M.S.J. Feb 1988. Newtonian solution for plasto-hydrodynamic drawing of rectangular cross-sectional continuum. Paper presented at IASTED Conf, Switzerland,

3) Symmons G.R. Crampton R. and Hashmi M.S.J. and Parvinmehr, H. June 1989. A Numerical solution for plasto-hydrodynamic drawing of rigid non-linearly strain hardening strip through a stepped rectangular slot. A H Memon, NUMIFORM Conference, Colorado State University USA.

4) Symmons, G.R. Crampton, R. and Hashmi, M.S.J. 1989 An experimental study of a plasto-hydrodynamic strip drawing process. A H Memon, Proceedings of IMech.E. London. Vol 203 Journal of Process Mechanical Engineering.

A 3D computational fluid dynamic analysis of the pressure distribution in the plasto-hydrodynamic drawing of rectangular sections

M.R. Stokes and G.R. Symmons
School of Engineering, Sheffield Hallam University,
Sheffield, UK

Abstract

The process of plasto-hydrodynamic (PH) drawing has previously been modelled for the deformation of circular and rectangular section materials using a polymer melt as a pressure medium. A 3D computational fluid dynamic model with a geometrical configuration analogous to that of a PH pressure head has now been used to examine the pressure distribution around the strip. The computed pressure field is compared with that assumed in the previous models and conclusions drawn as to its possible impact on future models and practical consequences for the drawing of strip.

Key Words Strip drawing, plasto-hydrodynamics, Finite difference, Computational fluid dynamic.

1.0 INTRODUCTION

A novel technique of wire drawing has been invented in which no conventional reduction dies are used and polymer melts are introduced as the lubricant in the drawing process. The main feature of this technique is that the conventional dies are replaced by a pressure unit which has an internal bore shaped such that hydrodynamic pressure is generated in the polymer melt surrounding the wire. The minimum internal bore size in the pressure cylinder is greater than the incoming wire diameter so no metal to metal contact takes place and there is no need to initially prepare the wire as in conventional drawing. The pulling action of the wire through the bore filled with polymer melt gives rise to drag forces and generates hydrodynamic pressure. The combined effect of the

imposed back stress and hydrodynamic pressure can be sufficient to deform the wire with selected sizes of orifice in the pressure unit and speed of drawing. Wire deformations by this novel process can be varied by change of drawing speed competing with similar percentage reductions in area per pass as with conventional die drawing but offering a more simple flexible output system with no pre-process preparation of the wire.

By using a polymer melt as the working fluid, the deformed wire is polymer coated. The choice of polymer used determines the types of coating produced whether an adhered coat or easily removed coat to suit requirements. The coatings produced on the wire can be used for surface protection against corrosion, electrical insulation or a preparatory coating for further processing. The thickness of the polymer coat on the wire depends upon the outlet sizes of orifice in the pressure unit. Hence the new process can be designed to suit a variety of deformation rates and polymer coating thickness on the wire for a variety of materials and polymers.

A number analytical models have been previously developed in relation to wire drawing and tube sinking notably Parvinmehr(1983) and Panhwar(1986). Recent research studies have concentrated on applying the die-less drawing process and analysis to rectangular strip. The progress of which has been reported by Symmons (1989, 1988).

2.0 PRESENT INVESTIGATION

A review is given of a numerical solution for plasto-hydrodynamic strip drawing using a finite difference method as proposed by Parvinmehr (1983) , with the boundary conditions and assumptions proposed by Memon (1988) and modifications made by Stokes (1992) for the treatment of melt instabilities.

An in depth examination will be made of a primary simplifying assumptions used in the derivation of the current model, this being that the fluid pressure acts equally on both faces of the strip. This assumption allows the dimension of the fluid model to be reduced from 3 to 2, with its inherent reduction in complexity.

The examination will take the form of a 3 dimensional computational fluid dynamic model duplicating the internal geometry of a pressure unit prior to the onset of deformation. Two models are used representing pressure units with strip aspect ratios of approximately 16:1 and 32:1.

3.0 ANALYSIS

The internal geometry of a plasto-hydrodynamic pressure unit is given schematically in figure 1. The following simplifying assumptions were made in the derivation of the model.

i) the dominant flow is axial and laminar
ii) the fluid pressure acts equally on both faces of the strip
iii) the pressure medium behaves like a Newtonian fluid
iv) isothermal conditions exist

3.1 Onset of plastic yielding of strip

Application of assumptions (i) and (ii) to Von Mises yield criterion allows the derivation of the plasto-hydrodynamic governing equation.

$$P_1 + \sigma_{xl} = \sigma_{yl} \tag{1}$$

Let x_1 denote the distance from entry into the pressure head and the onset of deformation. Equilibrium of forces acting on the strip in the x-direction yields,

$$\sigma_x = \frac{2\tau_1 x_1}{t_1} + \frac{2\tau_3 x_1}{w_1} \tag{2}$$

Also, assuming a linear profile for constant h

$$P_1 = \left(\frac{P_m}{L_1}\right) x_1 \tag{3}$$

Substitution of equations 2 and 3 into equation 1 and simplifying gives an expression for the distance to yielding,

$$x_1 = \frac{\sigma_{yl}}{\left(\frac{P_m}{L_1} + \frac{2\tau_1}{t_1} + \frac{2\tau_3}{w_1}\right)} \tag{4}$$

3.2 Axial stress and hydrodynamic pressure in the deformation zone

Given two contiguous nodes within the deformation zone at a distance 'dx' apart, figure 2, assuming linear deformation between these nodes then,

$$\frac{dt}{dx} = Constant = b \tag{5}$$

$$\frac{dw}{dx} = Constant = b^* \tag{6}$$

Equations 5 and 6 are then placed in finite difference form to give,

$$t_i - t_{i-1} - b\nabla x \tag{7}$$

$$w_i - w_{i-1} - b^*\nabla x \tag{8}$$

From consideration of continuity the current velocity is given by

$$V_i - V_{i-1}\left(\frac{w_{i-1}t_{i-1}}{w_i t_i}\right) \tag{9}$$

and using Levy- Mises flow rule it can be shown that

$$\frac{dW}{W_i} - \frac{dt}{t_i} \quad , \quad b^* - mb \tag{10}$$

$$where\ m - \frac{w_1}{t_1}$$

Applying equilibrium of forces in the x-direction for a small element, figure 2, in the deformation zone yields in difference form,

$$\sigma_{x_i} - \left(\frac{t_{i-1}}{t_i} + \frac{W_{i-1}}{W_i}\right)Y_i + \frac{2\tau_i x}{t_i} + \frac{2\tau_i^* x}{W_i} + \sigma_{x_i-1} \tag{11}$$

Equation 11 is an expression to determine the axial stress in the deformation zone. The shear stress terms are given by,

$$\tau_i - -\frac{h_i}{2}\frac{\partial p}{\partial x} - \frac{\mu V_i}{h_i} \tag{12}$$

$$\tau_i^* - -\frac{h_i^*}{2}\frac{\partial p}{\partial x} - \frac{\mu V_i}{h_i} \tag{13}$$

Assuming a steady-state condition with consideration of continuity the following expression for the pressure gradient in the deformation zone may be derived,

$$\frac{\partial p}{\partial x} = \frac{1}{h_1^3}\left[\frac{P_m h_1^3}{L_1} + 6\mu(V_i h_i - V h_1)\right] \tag{14}$$

and

$$P_i = P_{i-1} + \left(\frac{\partial p}{\partial x}\right)\nabla x \tag{15}$$

Equation 15 allows the evaluation of the hydrodynamic pressure within the deformation zone

3.3 Plasticity considerations

The working material is assumed to be rigid plastic and straining hardening according to the function below,

$$Y_i = Y_o + k\varepsilon^n \tag{16}$$

in difference form for the i_{th} point in the deformation zone,

$$Y_i = Y_o + k\left(\frac{W_1 t_1}{W_i t_i}\right)^n \tag{17}$$

Previously Hashmi (1981) presented an extension to the hardening law so as to include strain rate sensitivity S_i, which when combined with equation 17 yields,

$$Y_i = S_i\left[Y_o + k\left(\ln\left(\frac{W_1 t_1}{W_i t_i}\right)\right)^n\right] \tag{18}$$

Equation 18 evaluates the current yield stress of the strip material in the deformation zone. Once deformation occurs, it should continue whilst the plasto-hydrodynamic equation is satisfied, that is,

$$P_i + \sigma_{x_i} > Y_i \qquad (19)$$

3.4 Solution procedure

The solution procedure is then;

1) Determine the position of initial yielding
2) Solve the plasto-hydrodynamic equation iteratively for the slope of deformation b at the current node.
3) Determine the process conditions for the current node using the result of two.
4) Move through the calculated deformation zone repeating step 2 and 3.

4 COMPUTATIONAL FLUID DYNAMIC MODEL

The Computational Fluid Dynamic (CFD) models were generated using Fluent, a commercially available CFD modelling system. This system allows the analysis of complex 3 dimensional problems using a wide variety of boundary conditions and solution algorithms. The hardware platform used, was a 486 based IBM compatible computer.

The system in this case was required to solve the incompressible form of the Navier-Stokes equations, given below in vector form,

$$\rho\frac{DV}{Dt} = \rho B + (-\nabla p + \mu\nabla^2 V) \qquad (20)$$

The SIMPLE algorithm as outlined by Patankar (1980) was used to solve for the pressure and velocity fields. The results of which are given in section 5.

4.1 The model

Inspection of figure 1 reveals that a plasto-hydrodynamic pressure head has two planes of symmetry, these were used in defining the problem to reduce the number of nodes required. Figure 3 gives sectional views of one of the meshes used for the analysis, they essentially differ only in the width dimension so as to achieve the required aspect ratio. Graduated mesh spacing was used to attain an as accurate a solution as possible.

5 COMPUTER RESULTS AND DISCUSSION

The pressure fields generated by the models are shown in figures 4 and 5 as a 3 dimensional surface, the height of which specifies the pressure acting on the strip surface. It should be noted that for the presentation of this data, the edge face section of the pressure field has been moved through 90 degrees to form a single view. The change in the form of the peak pressure denotes the edge of the strip and the beginning of the edge face.

It may be seen that the general form of the pressure fields generated by the models agrees with the assumption made in equation 3, that of a linear pressure profile in the x direction. ie.

$$\frac{\partial p}{\partial x} - \left(\frac{P_m}{L_1}\right) - Constant$$

The assumption of pressure propagation around the periphery of the strip is in error as the form of the pressure field varies in the z {width} direction. The percentage pressure difference between the centre of the width face and the centre of the edge face is shown in figure 6.

A peak pressure difference of 9.2% was calculated by the 16:1 ratio model and occurs at the step {x=0.05m}. Changes in pressure are restricted to the immediate area of the step and in to the second land. The model assumes that no deformation takes place in the second land as the direction of the pressure gradient is reversed thus greatly reducing the shear stress generated and effectively halting deformation. Accordingly for the 16:1 model the remaining error may be within reasonable bounds, as deformation may be initiated as early as 30 % of overall L_1 length and as such its effect should be minimised to some degree.

A peak pressure difference of 9.9% was calculated by the 32:1 ratio model and occurs at the step {x=0.05m}. The pressure difference is more general in nature, not restricted to the second land and step region of the pressure unit as with the 16:1 ratio model. Correspondingly the effect of this more general error along the pressure unit should be much greater, although by how much is not quantifiable with the current model.

Both models are incapable of quantifying the effect of the pressure loss on deformation performance as they are fluid models of the instant before deformation begins and propagates back along the pressure unit with increasing draw velocity. The testing of this point is considered valid as all successful experiments using this technique must pass through this point and can only succeed if reasonable negotiated.

6 CONCLUSIONS

The plasto-hydrodynamic drawing process has been successfully modelled at the instant before the onset of deformation.

The assumption of a linear pressure profile in the x direction for both of the pressure unit lands is shown to be accurate.

The assumption of pressure propagation appears to be an accurate assumption for strip aspect ratios up to 16:1. The accuracy of the pressure propagation assumption for aspect ratios above 16:1 is questioned qualitatively, with no quantifiable data available for drawing performance.

FIGURES

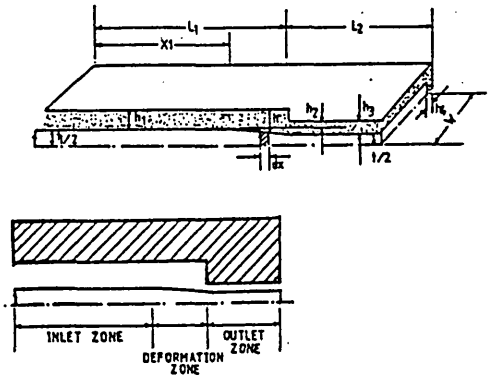

Figure 1 - Schematic diagram of a plasto-hydrodynamic pressure unit

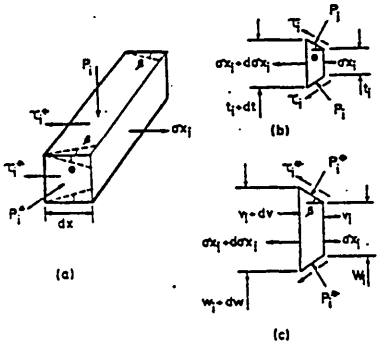

Figure 2 - Strip element within the deformation zone

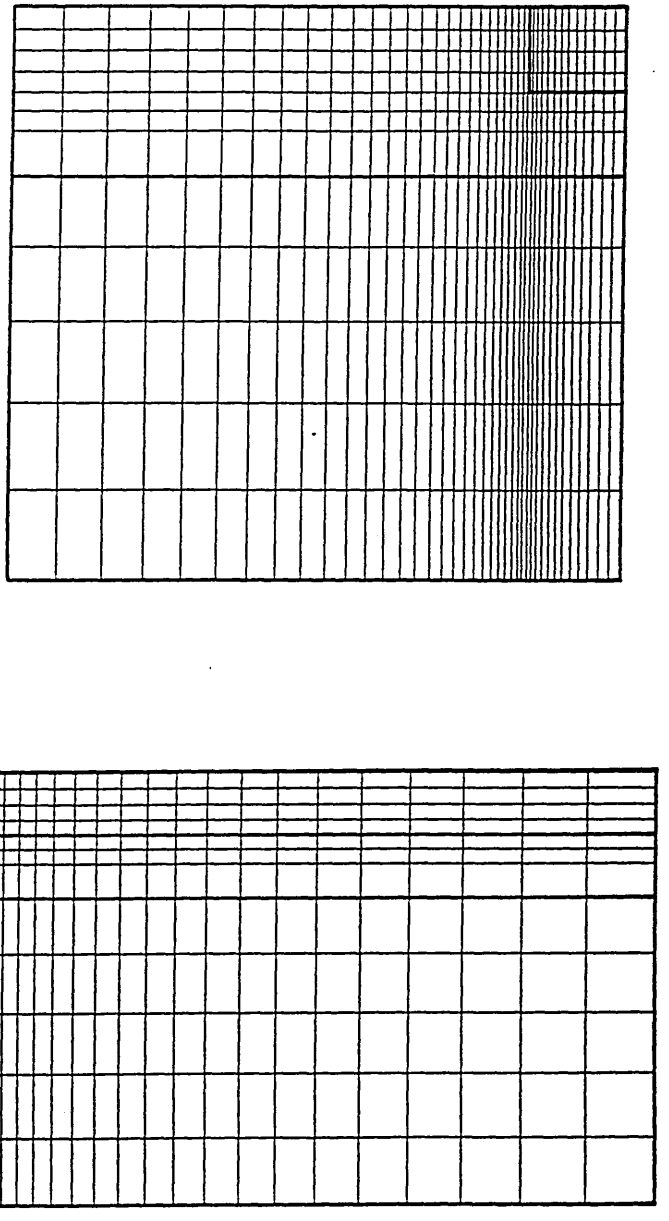

Figure 3 - Example computational mesh, 16:1 ratio model multiple cross sections.

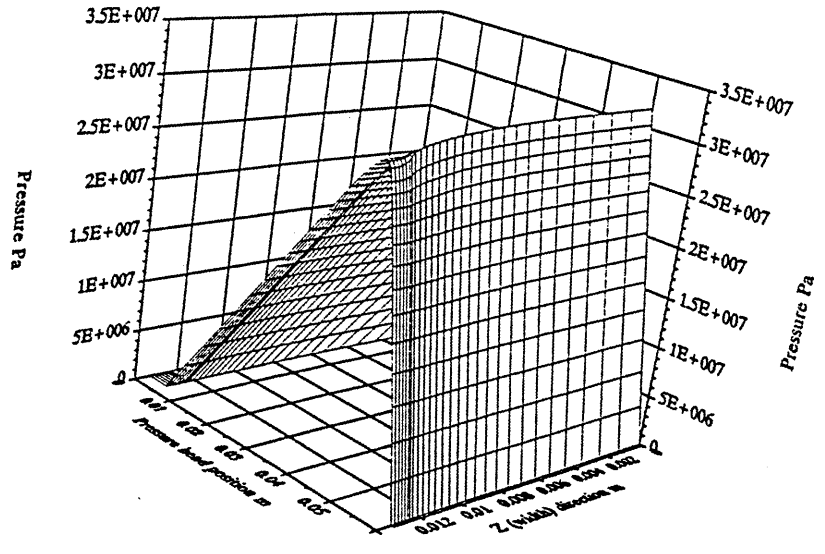

Figure 4 - Pressure field generated by the 16:1 ratio model

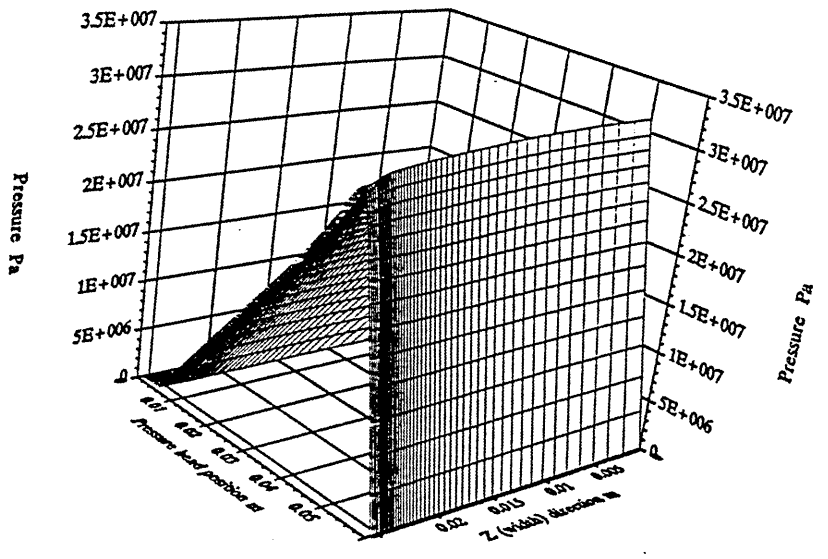

Figure 5 - Pressure field generated by the 32:1 ratio model

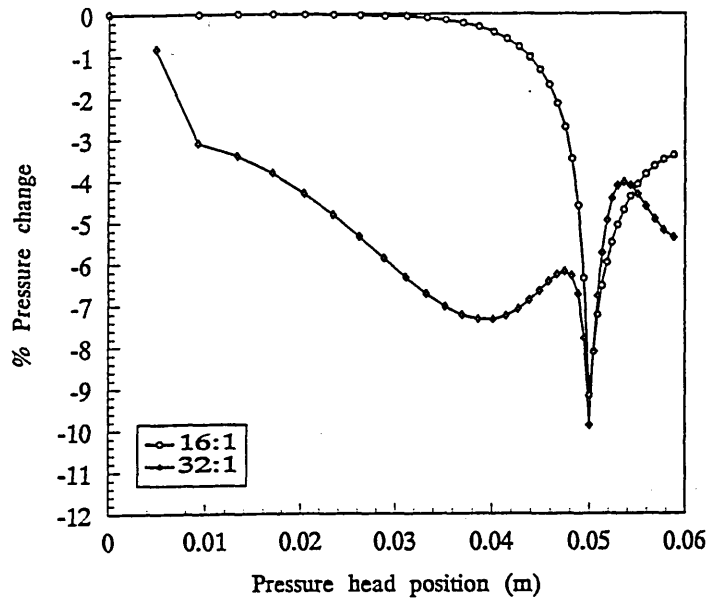

Figure 6 - Pressure change over propagation length against pressure head position

REFERENCES

Hashmi MSJ, Crampton R and Symmons GR (1981). Effects of strain hardening and strain rate sensitivity of the wire material during drawing under non-Newtonian lubrications conditions. Int J Mach Tool Des Res, Vol 21, No 1, 71-86.

Memon AH, Plasto-hydrodynamic die-less strip drawing (1988). Phd Thesis, Sheffield City Polytechnic.

Panhwar MI, Crampton R and Hashmi MSJ (1986). Die-less Tube Sinking : A plasto-hydrodynamic analysis based on Newtonian fluid characteristics. 5th Polytechnic symposium on manufacturing Engineering, Brighton.

Parvinmehr H, Optimisation of the plasto-hydrodynamic system of wire drawing using polymer melts (1983). Phd Thesis, Sheffield City Polytechnic.

Patankar SV, Numerical heat transfer and fluid flow. Hemisphere publishing corporation, New York.

Stokes MR and Symmons GR (1992). A computer model for plasto-hydrodynamic drawing of narrow strips under flow instabilities. Numerical methods in industrial forming processes, Balkema, Rotterdam.

Symmons GR, Crampton R, Hashmi MSJ and Parvinmehr H (1989). A numerical solution for plasto-hydrodynamic drawing of rigid non-linearly strain hardening through a stepped rectangular slot. NUMIFORM Conference, Colorado State University USA.

Symmons GR, Memon AH and Hashmi MSJ (1988). A mathematical model for Plasto-hydrodynamic drawing of narrow strips. Mathl Comput. Modelling, Vol 11, 926-931.

Numerical optimisation of the plasto-hydrodynamic drawing of narrow strips

M.R. Stokes and G.R. Symmons

School of Engineering, Sheffield Hallam University, UK

ABSTRACT

Initial developments in plasto-hydrodynamic drawing were for circular cross section wires, which has previously been modelled. In this process the deformation of the wire is achieved by pulling the wire through a stepped cavity filled with a viscous fluid. Hydrodynamic action generates surface shears and compressive stresses in the material of sufficient magnitude to produce plastic deformation, even though the smallest bore size of the hydrodynamic pressure head is larger than the undeformed diameter of the wire. Both process and model have been extended to a rectangular section strip the results of which have previously been published.

In this study a finite difference computer model of the process has been submitted to the process of numerical multi-dimensional optimisation. The Newtonian, strain hardening, computer model of the process is formed into a merit function, the order of the optimisation problem is seen to be reduced by the use of ratio's. This function was then supplied to the optimisation code. The optimisation code uses the direct search algorithm of Hooke and Jeeves [1]. This method uses a pattern vector in n-dimensional Euclidean space to explore the local region about the current search point before moving in the direction of the computed pattern vector. The method has been proven to have good valley following properties. Multiple applications of the optimisation code were made from different initial points in space to overcome any occurrence of multi-modality, which was speculated upon by Rohde [2] in his study of optimum step profiles for stepped slider bearing profiles.

Emphasis has been placed on the geometrical configuration of the stepped cavity. The fluid properties are approximately those of a generic form of polyethylene, with strip properties of commercially available soft copper, fluid and material properties were constant throughout the study. The results show significantly different optimum cavity configurations and performance surfaces for different velocities.

1. INTRODUCTION

The stepped cavity used in the plasto-hydrodynamic strip process may be described by 5 parameters, L_1,L_2 the land lengths and h_1,h_2 first and second land clearances and h_3 the side clearance, these are shown in Fig. 1. The motion of the strip generates surface shear stresses and hydrodynamic pressures of sufficient magnitude to induce plastic deformation in the strip material. A consequence of the hydrodynamic nature of the process is its extreme sensitivity to the land and side clearances, and to a lesser extent on the land lengths.

The first analysis of a stepped configuration was by Rayleigh [3], who proposed that a linear bearing of this form would yield the maximum load bearing capacity assuming an infinite width. More recent work has been concentrated within two main areas

a) the finite width Rayleigh bearing
b) analyses for non-Newtonian lubricants

Rohde [2] used a finite element model with an applied numerical optimisation algorithm to modify the standard orthogonal step into a pocket configuration which predicted an increase in bearing capacity. Kettleborough [4,5] carried out both experimental and numerical work on pocketed step bearing but no attempt was made to optimise the profile. Non-Newtonian analyses have recently been presented for Rayleigh step bearings by Elkouh and Yang [6], Wang and Jin [7] and Bourgin and Gay [8]. A variety of techniques being utilised for the various analyses.

No application of a formal optimisation method to plasto-hydrodynamic drawing has yet been presented. The object of the following work was then to ascertain the optimum geometry of the pressure head which would produce maximum deformation, for a specified process velocity. This being the most important factor as to whether or not the process could be economically viable.

2.0 METHODS OF SOLUTION

Optimisation theory maybe initially separated into linear and nonlinear programming. Linear programming problems are specified by a linear, multi-variate function which is to be maximised or minimised subject to a number of linear constraints. Dantzig [9] developed an algorithm to solve this type of problem, which in modified form is the basis of modern linear programming theory. Problems that are amenable to solution by linear programming include resource allocation problems in government planning, production planning and the management of transportation distribution systems.

In problems where the assumption of linearity cannot be made nonlinear programming techniques must be utilised. Specialised techniques have been developed for some problems but there is no general procedure for nonlinear programming. There are 2 approaches to nonlinear problems classical and numerical.

2.1 Classical methods

The Classical method is to derive expressions for the first and second derivatives of the function and to solve for n unknowns in n equations given the constraints associated with minimisation and maximisation. This requires that the function to be optimised must be differentiable. The present models of the plasto-hydrodynamic drawing process are not of closed form, requiring the solution of the plasto-hydrodynamic equation (PHE) at each nodal point within the region of deformation. For this reason classical methods were deemed unsuitable and a numerical approach pursued.

2.2 Numerical methods

Numerical methods are have two major subdivisions, unconstrained or constrained optimisation and direct search or gradient algorithms, the latter occurs in both of the former.

A function is said to be unconstrained if the are no bounds placed upon the possible values which any of the function variables may take. The inverse defines a constrained function, a possible example would be the optimisation of a hollow shaft with the outside and internal diameters as variables. It would be nonsense for the internal diameter of the shaft to be larger than the outside diameter.

A direct search method uses repeated evaluations of the function to directly search for the minimum. Various methods have been developed to solve multi-dimensional problems examples of which are the Simplex method by Nelder and Mead [10] and the pattern based method of Hooke and Jeeves [1].

A gradient method uses the gradient of the function as well as the function value to search for the minimum. Various methods have been developed for multi-dimensional problems examples of which are the convergent decent method by Fletcher and Powell [11] also the method of conjugate gradients by Fletcher and Reeves [12].

Note that both categories do search for the minimum and as such are search methods. Hooke and Jeeves [1] stated that the advantages of direct search methods over classical are:

a) They can produce solutions to problems which have been unsuccessfully attempted by classical methods.

b) They provide faster solutions for some problems that are solvable by classical methods.

c) They are well adapted to use on electronic computers, since they tend to use repeated identical arithmetic operations with a simple logic. Classical methods, developed for human use, often stress minimisation of arithmetic by increased sophistication of logic.

d) They provide an approximate solution, improving all the while, at all stages of the calculation. This feature can be important when a tentative solution is needed before the calculations are completed.
e) They require (or permit) different kinds of assumptions about the functions involved in various problems, and thus suggest new classifications of functions which may repay study.

Other points of note in the use of numerical methods are, they have a termination criteria or accuracy attached to their use. An assumption of uni-modality is made by the methods. A function is uni-modal if it has only one and thus a global optima. A function with multiple local optima is said to be multi-modal.

2.3 Choice of solution algorithm

The choice of solution algorithm was influenced by the merit function. In that the plasto-hydrodynamic model is not differentiable in its present form, consequently a direct search method was selected. The method chosen for the optimisation was the pattern search method of Hooke and Jeeves, selection was based on two factors,

i) published data for the method demonstrates the methods effectiveness for multi-dimensional problems
ii) the algorithm is computationally robust in operation

2.4 Optimisation code testing

The algorithm was coded into a suitable FORTRAN subroutine. Before application of the code to the plasto-hydrodynamic model the correctness of the code was tested by the use of Rosenbrock's [13] parabolic valley function, below

$$f(x_1,x_2) = 100(x_2-x_1^2)^2 + (1-x_1)^2 \qquad \textit{Rosenbrock's function}$$

which has a global minimum at x=(1,1), the form of the function is given graphically in Fig. 2. The optimisation code successfully found the function minimum in 34 iterations which is comparable to that taken by the conjugate gradient method of Fletcher and Reeves [12].

2.5 The plasto-hydrodynamic merit function

The merit function is an equation, expression or model of a process that is to be subjected to optimisation. It gives a quantitative result to a particular choice of values for an n dimensional function, of the form

$$M = M(x_1, x_2, x_3, \ldots x_n)$$

The merit function in this case is the plasto-hydrodynamic model. The model used in the merit function is that presented by Stokes and Symmons [14]. The material and fluid properties are declared as constants in the optimisation process and are those of pure copper and a generic form of polyethylene, these are detailed in table 1. Five dimensions are required to define a pressure head geometry L_1, L_2, h_1, h_2 and h_3 which forms a 5 dimension problem. The order of the problem was reduced to a 3 dimension problem by the use of ratios, defined as,

$$x_1 = L_1/L_2$$
$$x_2 = h_1/h_2$$
$$x_3 = h_3/h_2$$

given that the overall length of the pressure head and the clearance h_2 were held constant.

2.6 The optimisation procedure

The optimisation program allows the specification of an array of start points and the entry velocity for the drawing process. Multiple applications of the optimisation process are made on the merit function to establish confidence in the result, as it is possible for the shape of the n-dimensional surface to have local minima and/or the optimisation algorithm to detect false minima because of badly chosen search step lengths/initial positions. The procedure was then to start the process away from any expected optimum point in an attempt to force the algorithm to find its own optimum. The start point, end point and the percentage reduction in area achieved

at the end point were saved to a data file for later evaluation.

3.0 RESULTS - NEWTONIAN MODEL OPTIMISATION PREDICTIONS

Fig. 3 is a representative sample of the numerical predictions produced by each application of the optimisation procedure, showing an array of start points and a scattered distribution of end points in 3 dimensional space. Fig. 4 gives 3 orthogonal views of figure 3 allowing a more detailed view of the optimisation results scatter to be obtained. The format of the present work does not allow the presentation of all seven scatter plots in graphical form. Table 2 details the calculated mean values of merit function variables and results for each velocity. Table 3 details the standard deviation of merit function variables and P.R.A. for each velocity. Data from Tables 2 and 3 are shown graphically in Fig. 5 and Fig. 6 respectively.

4.0 DISCUSSION

4.1 Predicted pressure head clearance ratio

The optimum value of h_1/h_2, h_3/h_2 ratio and PRA can be seen to follow an essentially linear relationship with respect to velocity, Fig. 5. With standard deviations typically between 0.366% and 5.03% of the mean value, it is felt that the parameter values found by the process are realistic.

4.2 Predicted pressure head land length ratio

Optimum values for L_1/L_2 ratio vary in an almost exponential manner, however standard deviations are between 13% and 44% of the calculated optimum, with scatter of this magnitude it is probable that the underlying form has been swamped and as such no conclusions should be drawn from the shape of the curve. Further investigations were carried out to account for this large variation.

A series of performance surfaces were generated by holding the h_3/h_2 ratio constant, giving x, y equal to L_1/L_2, h_1/h_2 respectively and z equal to PRA. The h_3/h_2 ratio was then varied by small increments about the optimum such that a sequence of surfaces illustrating the development of the merit function in 3 dimensional space was formed. An example of a performance surface is shown in Fig. 7. The performance surface is for an exit velocity of 0.15 m/s and a constant h_3 value of 1.559 which is the calculated optimum value at that velocity.

Major characteristics of the surface are a ridge form lying parallel to the L_1/L_2 axis with a step in the region of the origin. The ridge form may logically be explained by the application of two competing phenomenon. Firstly it has been shown previously (Stokes and Symmons [14]) that shear stress and hence applied drawing load is inversely proportional to h_1/h_2 ratio giving increasing PRA. Secondly after a specified value of shear stress slip is assumed to have been initiated, this causes the slope of deformation to be reduced (Stokes and Symmons [14]). Reducing h_1/h_2 ratio will introduce this effect earlier in the deformation region of the pressure head reducing PRA. The step close to the origin at small values of h_1/h_2 and L_1/L_2 ratio was found to be formed as a consequence of slip being present over the entire length of the deformation zone in the pressure head.

Close inspection of Fig. 7 reveals small scale ridging of the surface between the origin and an h_1/h_2 ratio of 7.5 (approx), cross-sections of the surface were taken at various values of L_1/L_2 ratio and are given in Fig. 8. The small scale ridging is restricted to those areas of the performance surface where slip is present, h_1/h_2 ratio less than 7.5 approx. Further cross-sections of the surface were taken parallel to the L_1/L_2 axis, Fig. 9. It can be seen that the optimum point of the surface is within the region effected by slip, an explanation for the large scatter of the L_1/L_2 predictions is now possible. The cross-section through the optimum point of the surface reveals that in the L_1/L_2 axis the surface is multi-modal in that it contains many local optima of which one is the global optimum. This violates a fundamental assumption made in all optimisation procedures that of uni-modality, the program can the be assumed to have fallen into a ridge leading to a local optimum and have been unable to escape hence introducing the scatter into the L_1/L_2 axis. This could occur towards the end of the search procedure when the search step is reducing.

The mechanism by which the surface ridging is formed is as yet unknown, but it can be postulated that it is a consequence of the dynamical interaction of the phenomenon being modelled, namely hydrodynamic

deformation and the non-linear slip mechanism.

4.3 Predicted optimum percentage reduction in area

Inspection of Fig. 5 reveals that the optimum percentage reduction in area decreases with increasing entry velocity. The model used in the optimisation procedure takes into account the strain rate sensitivity of the material during calculation of post yield properties using the method given by Symmons et al [15]. Hence the increase of yield stress is not only a function of strip reduction but also a function of entry velocity, the two being compounded. The reduction in drawing performance with velocity can then be attributed to the velocity dependant hardening of the strip material.

5.0 CONCLUSIONS

In light of the work presented, it is possible to draw the following conclusions:

a) The plasto-hydrodynamic process has been successfully optimised to within the limits of experimental error.

b) The pressure head gap ratios have been shown to have a linear relationship with respect to entry velocity as demonstrated in Fig. 5.

c) The plasto-hydrodynamic process has been found to be multi-modal at a scale an order of magnitude less than the gross form of the performance surface.

d) A useful technique has been developed for use in the design of future plasto-hydrodynamic systems.

TABLES

Table 1

Fluid properties

Viscosity 120 Ns/m^2
Critical shear stress = 0.32 MN/m^2

Strip properties

Yield stress = 70 MN/m^2
Strain hardening Constant K = 600 MN/m^2
Strain hardening Index n = 0.6
Strain rate sensitivity constant T = 3.8
Strain rate sensitivity index nn = 55000
Width = 25.4 mm , Thickness = 1.59 mm

Table 2

	Mean values of merit function variables			
Velocity	L_1/L_2	h_1/h_2	h_3/h_2	P.R.A.
0.1	25.0865	5.1245	1.001	9.83449
0.15	21.4429	7.24625	1.559	9.34354
0.2	17.6084	8.8453	2.160	8.90071
0.25	28.3665	10.4587	2.778	8.7391
0.3	28.8697	12.0142	3.428	8.32282
0.35	38.338	13.4056	4.130	7.96573
0.4	65.4311	14.9782	4.80	7.70613

Table 3

	Standard deviations of merit function variables			
Velocity	L_1/L_2	h_1/h_2	h_3/h_2	P.R.A.
0.1	10.8445	0.257952	0.00351355	0.104956
0.15	6.2183	0.153191	0.00790158	0.2000089
0.2	7.81611	0.105956	0.0100012	0.236915
0.25	7.87859	0.125471	0.0151068	0.089066
0.3	11.4469	0.0866103	0.0152876	0.116584
0.35	15.7719	0.134531	0.0314687	0.141113
0.4	8.51273	0.0847327	0.0212222	0.0282338

FIGURES

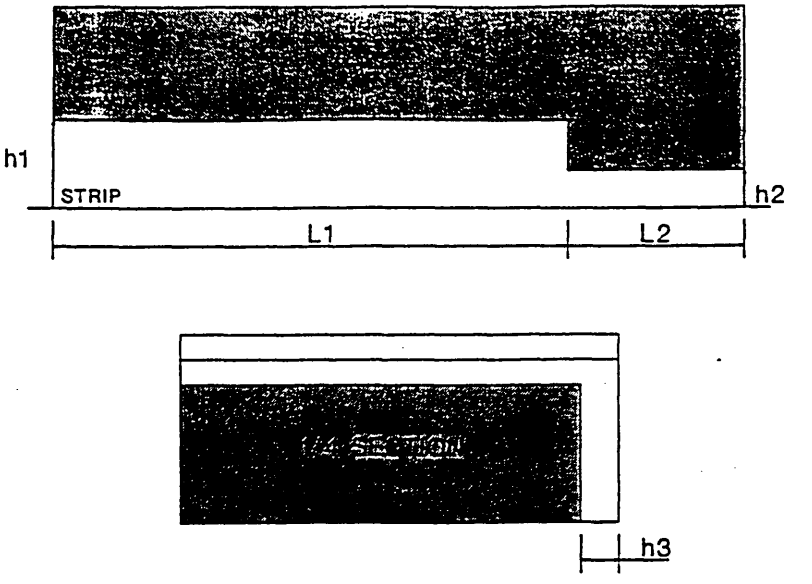

Figure 1 Schematic views of a plasto-hydrodynamic pressure head

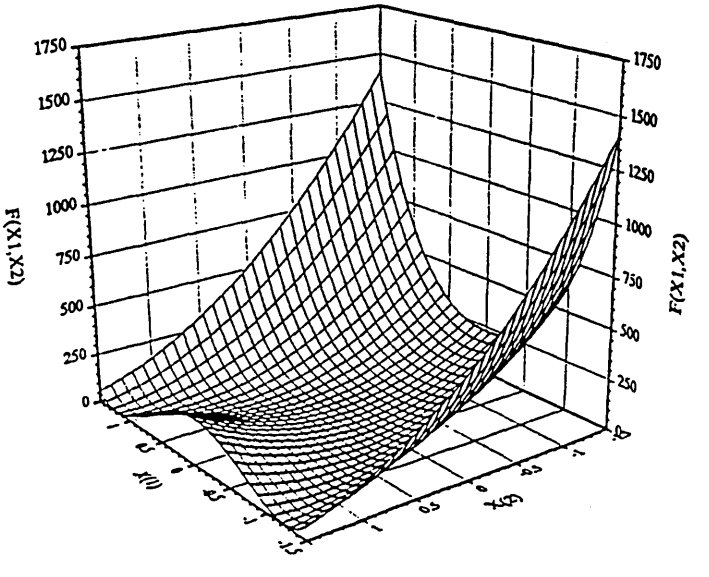

Figure 2 Parabolic valley produced by Rosenbrock's function

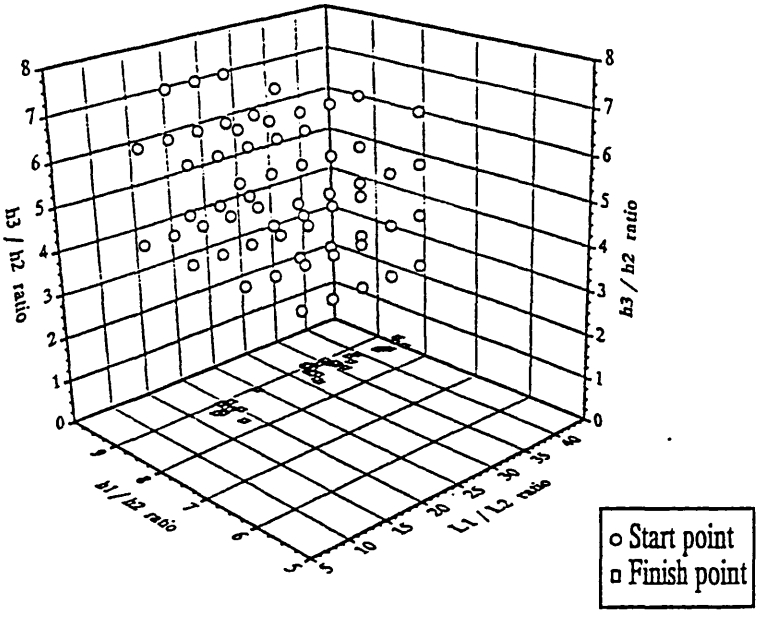

Figure 3 Scatter plot of start and finish points of a multi start optimisation sequence

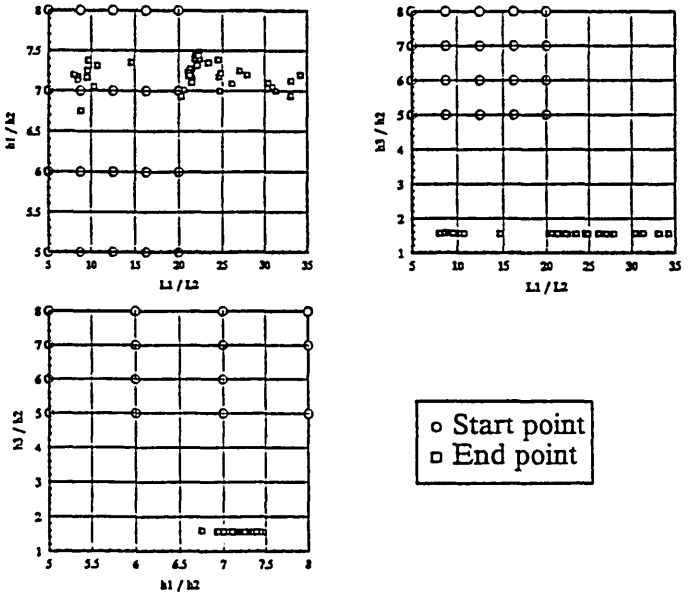

Figure 4 Orthogonal view of a multi start optimisation sequence

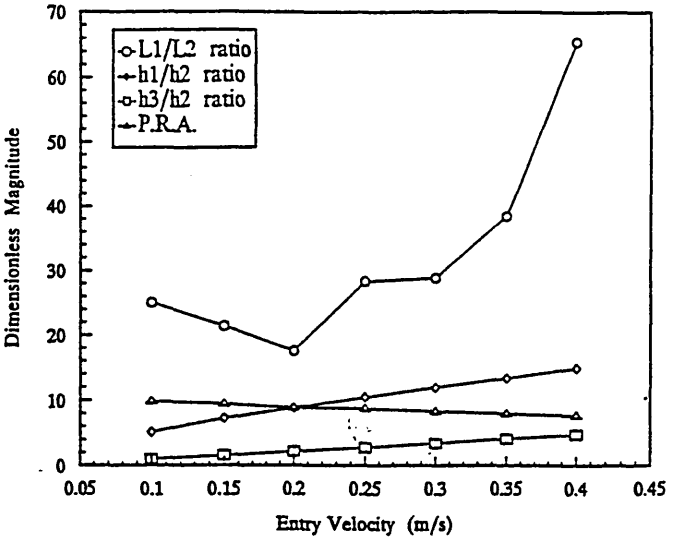

Figure 5 Mean values of optimisation results for a range of entry velocities

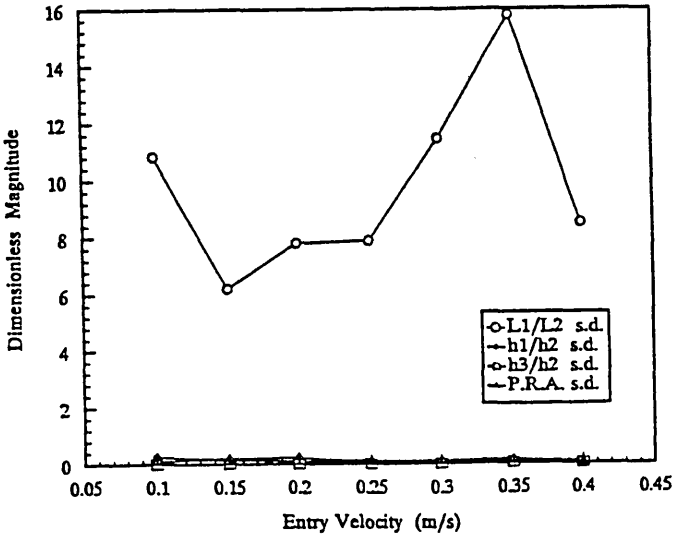

Figure 6 Standard deviations of optimisation results for a range of entry velocities

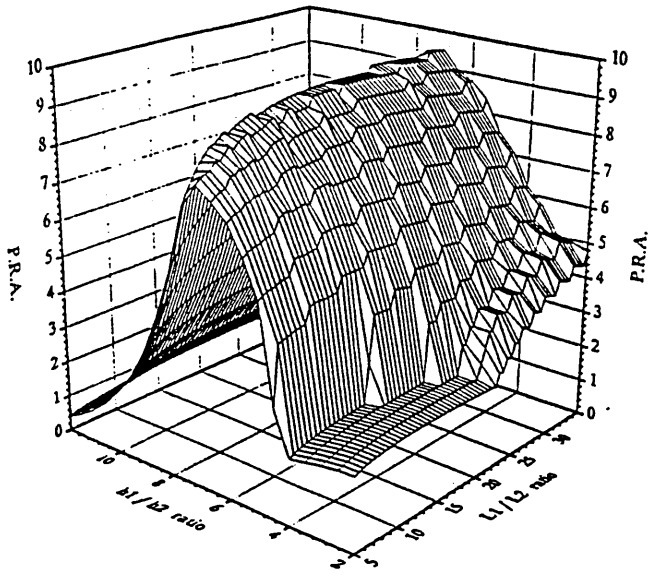

Figure 7 Example performance surface, entry velocity 0.15 m/s

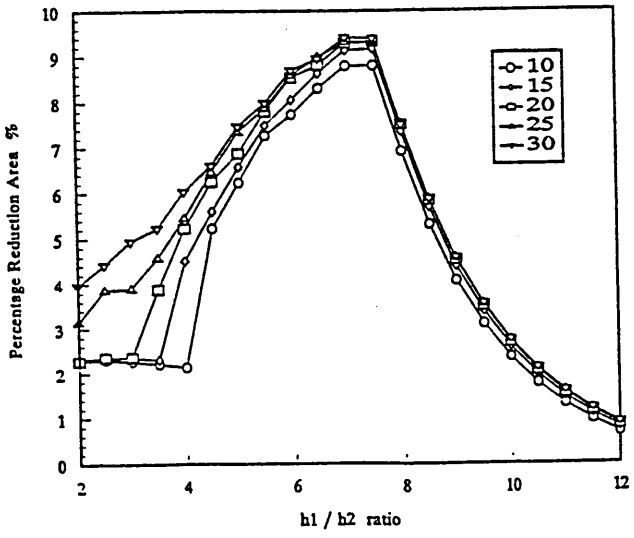

Figure 8 Performance surface cross-sections of constant L_1/L_2 ratio

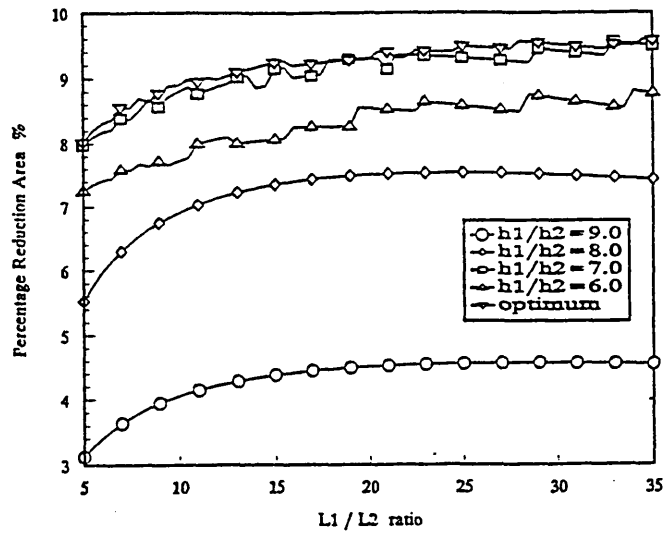

Figure 9 Performance surface cross-sections of constant h_1/h_2 ratio

REFERENCES

[1] R. Hooke T.A. Jeeves, Direct search solution of numerical and statistical problems, Jnl Assn Comp Mach, 8, 1961, 212-229.

[2] S.M. Rohde, Finite element optimisation of finite stepped slider bearing profiles, ASLE transactions, 17, 1974, 105-110.

[3] Lord O.M. Rayleigh, Notes on the theory of lubrication, Philosophical Magazine, 35, 1918, 1-12.

[4] C.F. Kettleborough, An electrolytic tank investigation into stepped thrust bearings, Proc. Instit. of Mech. Eng., 169, 1955, 679.

[5] C.F. Kettleborough, The stepped thrust bearing - a solution by relaxation methods, Trans. ASME, 76, 1954, 19.

[6] A.F. Elkouh Yang Der-Fa, Flow of a power law fluid in a Rayleigh step, ASME transactions, 113, 1991, 428-433.

[7] J. Wang G. Jin, The optimum design of the Rayleigh slider bearing with a power law fluid, Wear, 129,1989, 1-11.

[8] P. Bourgin B. Gay, The optimum Rayleigh bearing in terms of load capacity or friction for Non -Newtonian lubricants, ASME transactions, 107, 1985, 59-67.

[9] G.B. Dantzig, Linear programming and extensions, Princeton Univ. Press, 1963.

[10] J.A. Nelder R. Mead, A simplex method for function minimisation, Computer journal, 7, 1965, 308-313.

[11] R. Fletcher M.J.D. Powell, A rapidly convergent descent method for minimisation. Comp. J., 6, 1963, 163-8.

[12] R. Fletcher C.M. Reeves, Function minimisation by conjugate gradients, The computer journal, 7, 1964, 149-154.

[13] H.H. Rosenbrock, An automatic method for finding the greatest or least value of a function, The computer journal, 3, 1960, 175-184.

[14] M.R. Stokes G.R. Symmons, A computer model for Plasto-hydrodynamic drawing of narrow strips under flow instabilities, Numerical methods in industrial forming processes NUMIFORM 92, Balkema, 1992, p.181.

[15] G.R. Symmons M.S.J. Hashmi A.H. Memon, Newtonian solution for plasto-hydrodynamic drawing of rectangular cross-sectional continuum, paper presented at IASTED conf, Switzerland, 1987.